Universidade de Aveiro Departamento de Física
Ano 2016

Universidade do Porto Faculdade de Ciências

Universidade do Minho Departamento de Física

Adérito Celso Félix Aramuge

Alteração da Sobrelevação do Nível do Mar ao Longo da Costa de Moçambique, para Cenários Climáticos Futuros

Storm Surge Changes Along the Coast of Mozambique for Future Climate Scenarios

Universidade de Aveiro
Ano 2016

Departamento de Física

Adérito Celso Félix Aramuge

Alteração da Sobrelevação do Nível do Mar ao Longo da Costa de Moçambique, para Cenários Climáticos Futuros

Storm Surge Changes Along the Coast of Mozambique for Future Climate Scenarios

Tese apresentada à Universidade de Aveiro para cumprimento dos requisitos necessários à obtenção do grau de Doutor em Física, realizada sob a orientação científica do Prof. Doutor Alfredo Moreira Caseiro Rocha, Professor Associado com Agregação do Departamento de Física da Universidade de Aveiro, e do Prof. Doutor Paulo Manuel Cruz Alves da Silva, Professor Auxiliar do Departamento de Física da Universidade de Aveiro.

Este trabalho foi financiado desde 01-09-2011 a 01-09-2015, por uma bolsa de doutoramento do programa Ciência Global da Fundação Para a Ciência e a Tecnologia, **SFRH/BD/51467/2011.**

PD F FCT PhD PROGRAMMES

This work is dedicated to my family, for their lovingness and moral support, which is my strength inspiring.

o júri

presidente

Prof.º Doutor Artur Manuel Soares da Silva
Professor catedrático da Universidade de Aveiro

Prof.º Doutor Alfredo Moreira Caseiro Rocha
Professor associado com agregação da Universidade de Aveiro

Prof.º Doutor João Carlos Andrade dos Santos
Professor auxiliar com agregação da Universidade de Trás-os-Montes e Alto Douro

Prof.º Doutor João Miguel Sequeira Silva Dias
Professor auxiliar com agregação da Universidade de Aveiro

Doutora Maria Luisa Machado Cerqueira Bastos
Investigadora principal da Faculdade de Ciências da Universidade do Porto

Prof.º Doutor Carlos Manuel Correia Antunes
Professor auxiliar da Faculdade de Ciências da Universidade de Lisboa

agradecimentos/ aknowledgemts:

Completing the PhD thesis has been probably the most challenging activity of my life. During the journey I worked with many people who contributed in different ways to the success of this study and made it unforgettable experience for me. It is a pleasure to convey my gratitude to them.

At first, I would like to express my sincere and respectful gratitude to my advisors, Professors Alfredo Rocha and Paulo Silva, for continuous support, valuable suggestions, constant inspiration, encouragement and proper guidance from the very beginning of the study to the final submission of the thesis.
I express my heartiest thanks to the government of Portugal through the Fundação Para a Ciência e Tecnologia (FCT), for providing the scholarship.

I am also thankful to whole team of Atmosphere's Laboratory at Physics Department of Aveiro University, for their cooperation and companionship.

To all people who directly or indirectly has assisted to bring out this thesis, thank you indeed.

For the last but not least, to all my family members, for their patience in missing me for years long duration, I express to them my heartiest everlasting gratitude.

palavras-chave Costa Moçambicana, mudanças climaticas, sobrelevação do nivel do mar, series temporais.

resumo *Moçambique é afetado por ciclones tropicais que se formam na bacia do Oceano Índico. Cerca de dois terços da população total de Moçambique vive ao longo da costa que se estende por 2700 km e que cuja região, com altitude inferior a 50 m, ocupa várias dezenas de quilómetros em direção ao interior. O aumento do nível médio do mar e um aumento provável da intensidade e/ou frequência de ciclones tropicais, associados a alterações climáticas de origem antropogénica, podem aumentar o risco de cheias ao longo da costa.Neste estudo, estamos principalmente preocupados com a estimativa de alterações das propriedades da sobrelevação do nível do mar ao longo da costa de Moçambique, sob o cenário de mudança do clima RCP8.5. Para atingir tal objetivo, aplicamos um modelo analítico a dados observados de ventos e pressão atmosférica, para estimar a maré meteorológica e a sobrelevação do nível do mar na região. O modelo analítico é validado por comparação dos seus resultados com dados semelhantes obtidos por marégrafos em alguns locais na costa. De seguida, é usado um conjunto de simulações climáticas realizadas pelo modelo climático MPI-ESM-LR. Dados de pressão atmosférica e ventos simulados foram usados no modelo analítico e séries temporais da maré atmosférica foram produzidas para sete locais ao longo da costa. As propriedades estatísticas destas séries e as sobrelevações do nível do mar associadas foram comparadas com aqueles obtidos usando o mesmo modelo analítico e dados meteorológicos observados. Isto foi feito para o período histórico de 1986-2005. Após uma validação com sucesso de ambos os modelos, o analítico e o climático, o modelo analítico foi utilizado com dados meteorológicos simulados pelo MPI-ESM-LR para o cenário RCP8.5, para três períodos distintos nomeadamente, futuros próximo (2016-2035), médio (2046-2065) e distante (2081-2100). As propriedades da sobrelevação do nível do mar para estes períodos foram comparadas com aqueles relativos ao período histórico. Os resultados sugerem um aumento da intensidade da sobrelevação do nível do mar ao longo de toda costa de Moçambique sobretudo devido aos aumento da intensidade dos ciclones tropicais. Com a subida do nível medio do mar, espera-se que aumente a altura do qual o STS inicia a sua propagação. O nivel do mar calculado* (STS+TC+SLR) *para o período historico, futuro proximo, medio e longo são iguais a 0.93 m, 1.19 m, 1.42 m e 1.74 m respectivamente. Esta metodologia é útil porque se recorre a um modelo analítico simples e dados meteorológicos na ausência frequente de dados de nível do mar registados por marégrafos. Permite também a estimativa de alterações futuras de sobrelevação do nível do mar com recurso a variáveis meteorológicas simuladas por modelos climáticos, facilmente disponíveis, em vez de recorrer a modelos físicos ao cálculo da sobrelevação do nível do mar.*

keywords Mozambique coast, climate change, storm surge, time series.

abstract

*Mozambique is affected by tropical cyclones which are formed in the Indian Ocean basin. About two-*thirds *of total population of Mozambique lives along the coast which has 2700 km long and low lying areas (below 50 m height) extend several tens of kilometers inland. Sea level rise and the eventual increase of the intensity and/or frequency of tropical cyclones expected to occur in the future, associated with anthropogenic climate change may increase the risk of coastal flooding. Here, we are mainly concerned with the estimation of changes of storm surge properties along the coast of Mozambique under the RCP8.5 climate change scenario. To achieve this we applied an analytical model which uses observed winds and atmospheric pressure near the surface data to estimate the meteorological tide and storm surges in the region. This model is validated against atmospheric tides obtained from sea level measured by tide gauge observations at some locations along the coast. Next, we used a set of climate simulations performed by the MPI-ESM-LR earth systems model. Simulated winds and atmospheric pressure data were used with the analytical model and atmospheric tide time series were constructed for seven locations along the coast. The statistical properties of these series and the associated storm surges were compared with those obtained by using the same analytical model and meteorological observed data. This was done for the 1986-2005 historical period. After a successful validation of both the analytical and the climate model, the analytical model was used with meteorological data simulated by the MPI-ESM-LR for the RCP8.5 scenario for three distinct periods, namely, near-term (2016-2035), medium-term (2046-2065) and long-term (2081-2100). The storm surge properties for these periods were compared to those from the historical period. The results suggest an enhancement of storm surge intensity along the whole coast of Mozambique mainly due to an increase of tropical cyclone intensity. The SLR will add the point by which the STS starts its propagation. The calculated SL (STS+ TC+SLR) for the historical, near tem, medium and long term are equal to 0.93 m, 1.19 m, 1.42 me 1.74 m respectively. This methodology is very useful since it uses a simple analytical model and meteorological data in the absence of tide gauge records. It can also be used to estimate future storm surge climate changes using meteorological variables easily available rather than using storm surge physical models.*

Table of Contents

List of Figures

List of Tables

List of Acronyms

CDO	Climate Data Online
CMIP5	Coupled Model Intercomparison Project 5
GDACS	Global Disaster Alert and Coordination System
GMSLR	Global Mean Sea Level Rise
IPCC	Intergovernmental Panel on Climate Change
INAM	Instituto Nacional de Meteorologia
INGC	Instituto Nacional de Gestão de Calamidades
ITCZ	Inter-Tropical Convergence Zone
JTWC	Joint Typhoon Warning Center
MC	Mozambique Channel
MPI-ESM-LR	Max Planck Institute-Earth System Model-Low Resolution
MSL	Mean Sea Level
NCDC	National Climate Data Center
NOAA	National Oceanic and Atmospheric Administration
RCP	Representative Concentration Pathway
RMW	Radius of Maximum Wind
RSMC	Regional Specialized Meteorological Centre
SL	Sea Level
SLP	Sea Level Pressure
SLR	Sea Level Rise
SLV	Sea Level Variability
SST	Sea Surface Temperature

STS	Storm Surge
SWIO	South West Indian Ocean
TC	Tropical Cyclone
UA	University of Aveiro
WMO	World Meteorological Organization
ZSF	Zonal Steering Flow

“ANY ONE, WHO HAS NEVER MADE A MISTAKE, HAS NEVER TRIED ANYTHING NEW ".

Albert Einstein

Chapter I – Introduction

1.1 Motivation

In areas affected by Tropical Cyclones (TC), storm surges cause more fatalities than any other natural hazard. Storm surge is one of the main causes of coastal inundation. Another effect is the occurrence of strong currents, which can affect oil rigs and pipelines (Pugh, 1987).

Nowadays, storm surges and coastal flooding pose a threat to 40 million people globally and this Figure could grow to 150 million people by 2070 due to population growth and sea level rise. Storm surge are oscillations of the water level in a coastal or inland body of water in the time range of few hours to a few days, resulting from forcing of atmospheric weather systems (Murty, 1984). Therefore, the simultaneous occurrence of sea level rise associated to a storm surge with TC, may affect parts of the coast, which usually are not, through overtopping and flooding events. Considering that coastal areas and flood plains contain often fertile soils and are generally densely populated, this fact can increases the economic risk of a storm surge (Hinton et al., 2007).

A number of high profile events have raised the awareness of storm surges as the critical factor in coastal hazard, disaster risk reduction and coastal management in a changing climate. The consequences of storm surge associated with climate change, which are in turn related to the mean-sea level rise, are inter-related and are illustrated in Figure 1. According to Turner et al. (1996), the greatest impacts of those consequences will occur on small islands in developing states, followed by low lying deltas in low-income developing states, and coastal lowlands throughout the developing countries.

While storm surges, astronomical tides and tsunamis are all classed as long waves, there are at least two important differences between the former and the two latter types (WMO-N.1067, 2011). First, whereas tides and tsunamis occur on the oceanic scale, storm surges are predominantly a coastal phenomenon. Second, significant tsunamis and tides cannot occur in a completely enclosed small coastal or inland body of water, but storm surges can occur in completely enclosed lakes, canals and rivers.

The scientific evidence indicates that increased surface temperature will intensify cyclone activity and heighten storm surges. These surges will, in turn, create more damaging flood conditions in coastal zones and adjoining low-lying areas. The destructive impact will generally be greater when storm surges are accompanied by strong winds and large onshore waves. The historical evidence highlights the danger associated with storm surges (Dasgupta et al. 2009a).

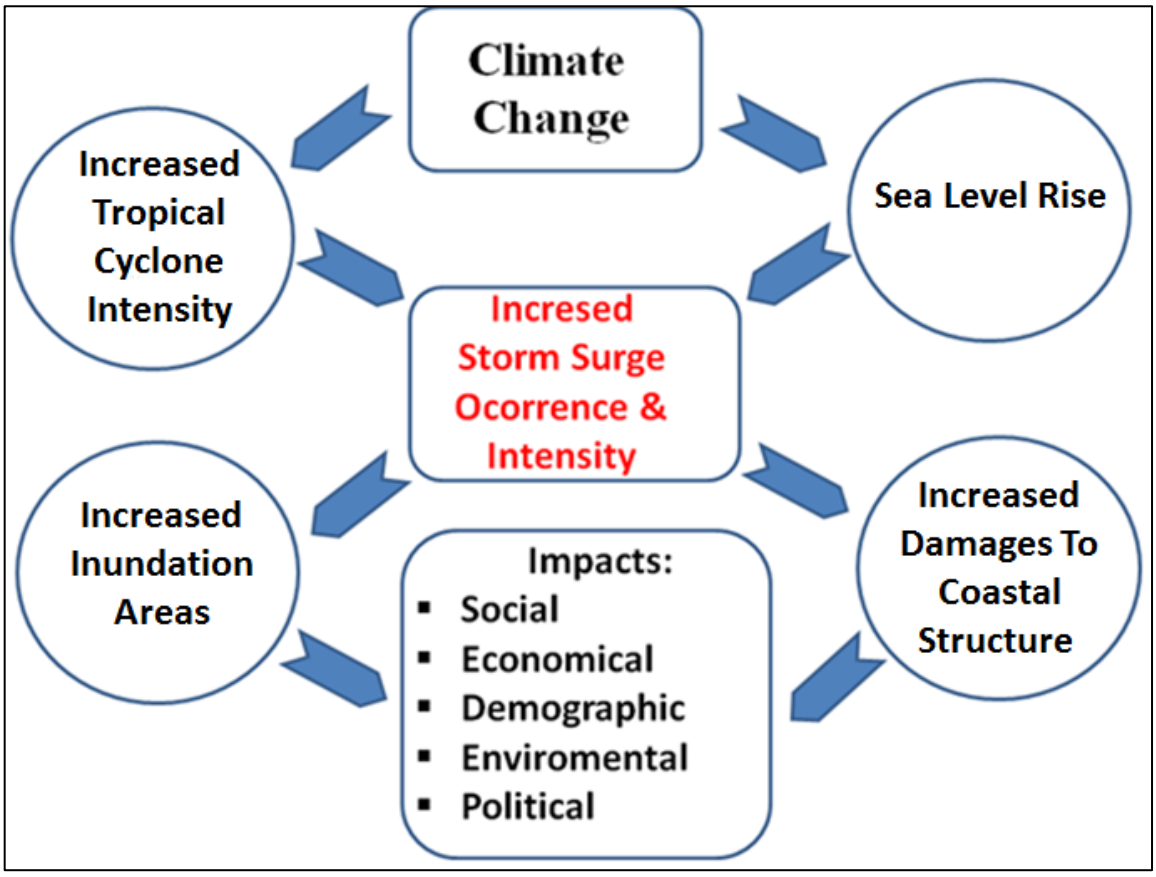

Figure 1. Effects of climate change and their interactions.

Mozambique is an African country located in the east coast of Southern Africa between parallels 10 ° 20'S and 26 ° 50'S. The coast is about 2700 km long and is the third largest coastline in Africa and is intensely occupied by population that gains their livelihood by exploiting the resources existing in the sea.

As it has been mentioned before, the study area lies along the coastal zone of Mozambique (Figure 2). In this figure, the topography features of Mozambique are represented. It is clear that the coastal areas less than 50 m height occupy most of the

coast and extend several tenths of kilometers inland. These features are of great concern in the presence of sea level rise (SLR), particularly if associated to storm surges. The coastal zone is economically characterized by the main cities, services and industries such as tourism, trade and ports. The population gains their livelihood at the expense of the resources existing there. The ports are strategically associated with roads, providing services in transportation with intense movement of loads from national clients as well as for neighboring countries.

The detailed characteristics of the area of study are given in Chapter III and the locations from which the data will be used are given later, in Chapter IV. Regarding to storm surge knowledge, this geographical area is a scientifically mostly unknown area so far and, as such, a study on storm surges is highly recommended.

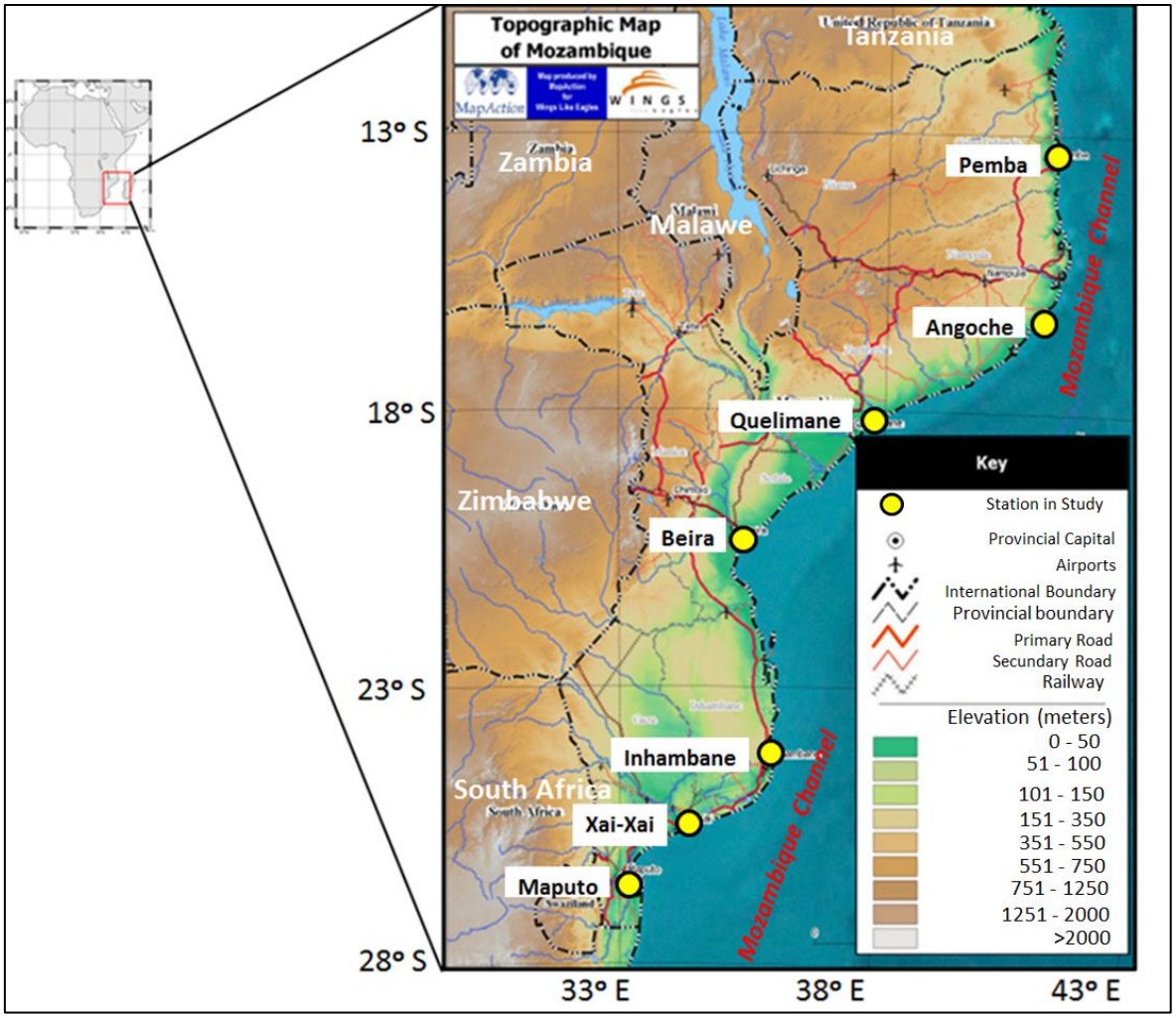

Figure 2. The study area and topography. Source: Reliefweb.int - Adapted.

The low-lying nature of its coastal zone combining with the nearly two-thirds of Mozambique total population which lives along the coast, have made this country one of the most vulnerable to natural disasters (INGC, 2009).

In what concerns vulnerability and natural disasters, Mozambique occupies the 44th place in a rank of 171 countries, with 70.89 % of vulnerability and a World Risk Index of 9.03 % (Mucke et al., 2014). This situation is crucial for Mozambique if compared with other countries. According to the same author, despite the exposure of 12.73 %, the country has got a susceptibility of 65.89 % and a lack of coping capacities and adaptive capacities of 84.15 % and 62.64 % respectively. In turn, the country is located in a favorite path of potentially deadly TCs which eventually causes storm surge where it makes landfall. Their susceptibility to high impact weather like TCs and storm surges, compounds the poverty issues.

From a universe of 80 developing countries studied, one of the top 10 countries at risk from intensification of storm surges is Mozambique, occupying the 10th place with 51.7% due to coastal population, 5th place with 55% due to coastal Gross Domestic Product (GDP) and 8th place with 55.1% due to coastal urban areas (Dasgupta et al. 2009b).

The projections for future climate scenarios, shows that the mean-sea level by 2100 will globally rise to 0.98 m according to Church et al. (2011) and, TCs intensity may increase by +2 to +11% (IPCC, 2013) in general. Therefore, it can be concluded that storm surge intensity in the future climate scenarios will also increase. This situation will represent potential disaster conditions for the population and infrastructures along the coast, taking in consideration that the more intense is the wind, the greater is the amount of water dragged to the coast. The lack of resources for mitigation, or relocation, can cause great political and economic stresses in poorer states.

The South West Indian Ocean (SWIO) cyclonic basin has garnered less attention from the scientific community, in spite of accounting for 10% of cyclone activity worldwide. The same happens for storm surge studies. Nevertheless, important research has been accomplished in the SWIO basin. For example, Dasgupta et al (2009b) and Mavume et al. (2009) studied storm surge in the Mozambican coast. Neumann et al (2013) assessed the risk of cyclone-induced storm surges and sea level rise in Mozambique. The results found from those studies are discussed later in the chapter IV of this thesis.

As concluded by Dasgupta et al. (2009a), Mozambique will experience significant increases in the percentage of their coastal urban extent, falling within surge zones with SLR and intensified storm surges (see Figure 3). According to this author, the results indicate that areas prone to storm surge in Mozambique account for more than 50% of GDP generated in their coastal regions. As far as coastal wetlands are concerned, Mozambique is in the group of countries where the absolute impacts will be largest, encompassing 1.318 km^2. Despite the interested work done, that study does not quantifies the storm surge heights associated with those impacts.

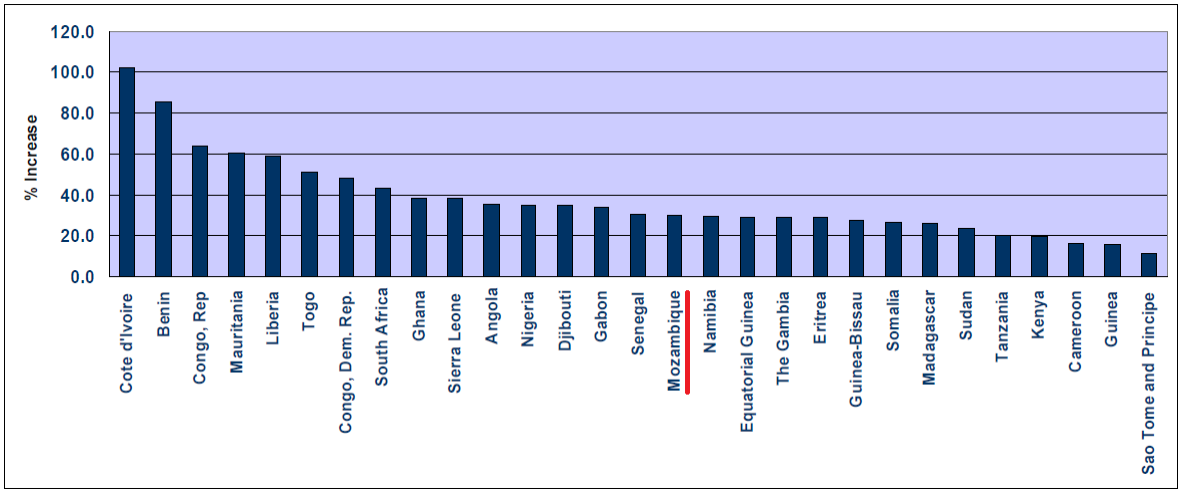

Figure 3. Percentage increase in storm surge zone for Africa region. Source: Dasgupta et al. 2009a - Adapted.

According to INGC (2009), in the period 1980-2007, 56 TCs and tropical storms entered the Mozambique Channel. Fifteen (25%) of them made landfall on the coast of Mozambique. From these, four cyclones hit the North, eight hit the Centre and three hit the South. Only four occurred in the period 1980-1993, whilst the other eleven occurred in the later period from 1994-2007. Two cyclones in the period 1980-1993 were classified as category 3-5 compared to seven in the period 1994-2007. Observations also suggest a recent southward shift in TC trajectories and landfall locations (INGC, 2009). From 2007 to 2014, 21 TCs and tropical storms entered the Mozambique Channel, where ten (47%) of then made landfall on the coast of Mozambique. TCs are more frequent between January and February and cause rains accompanied by thunderstorms, strong winds and stormy, sometimes reaching over 100 km/h.

Although the 4-year average return period of cyclones affecting Mozambique is relatively modest, Vitart et al., (2003), occasional storms moving in unusual directions, such as TC

Favio in February 2007, can cause surprising damage (Klinman and Reason, 2008). The damages of some TCs from the period 1994-2012 are presented in Table 1 (Fitchett and Grab, 2013).

Table 1. Reported damages done by some TC that landed in Mozambique from 1994 to 2012.

TC Month	TC Name	TC Category	TC Deaths	TC Damages	TC Homeless
1994, March.	Nadia	4	204 dead,	$240 million damage	1.5 million homeless,
1996, January.	Bonita	4	11 dead.	-	-
2000, February.	Eline	4	150 dead,	4 ships sunk.	1000 casualties, 300.000 displaced from flooding
2001, March.	Dera	2	100 deaths,	severe flooding.	250.000 displaced,
2003, January.	Delfina	Tropical Storm	47 deaths, 19 deaths from flooding.	several days power outage in Nampula, $3.5 million in damage.	22.000 displaced,
2003, March.	Japhet	4	17 dead.	237.000ha cropland destroyed, livestock losses.	23.000 homeless,
2007, February.	Favio	4	10 dead and 100 injured.	$71 million in damage.	33.000 homeless,
2008, March.	Jokwe	3	16 dead	75% of power lines in Nampula destroyed.	55.000 homeless
2012, January.	Funso	4	15 dead from ship sinking,	70.000 with no access to clean drinking water.	56.000 homeless,

TC Favio made landfall in Vilanculos village, on the coast of southern Mozambique as category 3 cyclones after genesis over a week earlier in the central tropical South Indian Ocean. Compounding an already devastating season of floods, Favio led to the death of 10 people and injuries of 100 more. Schools, businesses and hospitals were destroyed as well as a prison from which 600 inmates escaped (Figure 4). In all, the flooding season up to 2007, had caused the displacement of over 120,000 people in Mozambique (Padgett, 2007). It exhibited a highly unusual track after approaching the southeastern tip of Madagascar because, instead of moving back out into the SWIO as is typical, it turned northwestwards and impacted the Mozambique coast about 300 km further equatorward. For further reading about TC damages, see (du Plessis, 2002; Reason and Keibel, 2004; Reason, 2007; Klinman and Reason, 2008; Malherbe et al., 2012).

In addition to its unusual track, this TC made landfall in Mozambique during an El Nino year, an occurrence that has been reported once. The simultaneous occurrence of TC and El Niño generates higher storm surge heights.

Due to the scarcity and dispersion of tide gauge station localization, most of TC storm surge induced are not registered. This is because either the TC makes its land fall in the city where there is no tide gauge station to register the height reached by storm surge, or the TC makes land fall in the bush area where there is no population nor tide gauge station.

From empirical knowledge, historical storm surges have affected the coast of Mozambique, information about flooded areas or damages are available, however, there are no records about the heights reached.

Despite this fact, no scientific field survey was carried out to register the height of storm surge reached, after a TC passed through a certain region. The surge can move coastal structures and soil several miles inland.

Figure 4. Damages and inundations caused by Tc Favio, 2007. Source: INGC–Adapted.

Coastal storms in Mozambique Channel have highlighted the need for more proactive management of the coastline. The uncertainty of knowledge on effects of a combination of severe sea storms and future climate change in the coast of Mozambique, is the greatest gap of information which creates a barrier to informed decision making.

The motivation for this study comes from the need to raise human preparedness and adaptation to storm surge events, considering the future climate scenarios. Also, motivation comes from the need to provide a series of technical tools to the members of the Government of Mozambique, mainly to the Instituto Nacional de Meteorologia (INAM) and the Instituto Nacional de Gestão de Calamidades (INGC), to better understand the effects of storm surge coupled with sea level rise and increase of Tc intensity in the coast of Mozambique. Additionally, understanding storm surge behavior is important for isolating potentially predictable features of TCs, with benefits for risk assessment and planning in countries lying along their preferred paths. We focus on the distribution of storm surge height and wind, because knowledge of their changes will be useful for local and national planners.

Also, the study may demonstrate that a relatively simple approach on the knowledge about the storm surge in the future, can provide valuable information about the current

and future risk of storm surge and coastal erosion under climate change, to infrastructure as well as natural features along the coast.

1.2 Objectives

The ability to forecast storm surge impacts to those coastal regions severely affected by tropical cyclone flooding, can be greatly improved by a better understanding the behavior or the dynamics of storm surge over the coast.

This study is mainly concerned with the evaluation of the impact of climate change on storm surges along the cost of Mozambique. This is performed by using an analytical model which has to be validated against observed data. Storm surge is calculated by using meteorological forcing data, namely wind speed and sea level pressure (SLP). With this, we may understand the future properties of storm surges along the coast of Mozambique, by estimating the climate change effects on storm surges. This will be done for the near-term (2016-2035), medium-term (2045-2065) and long-term (2081-2100) future climate scenarios, relative to the historical period (1986-2005).

This work regards the risks inherent of the coastal occupation, and is pretended to be an useful tool that may help decision makers in their planning activities in Mozambique. This effort will also improve the knowledge to estimate on how to determine where to invest in designing storm surge applications.

1.3 Thesis Structure

This thesis includes five chapters, which summarize the different aspects of the study:

Chapter 1 – Introduction: Provides a general overview of storm surge, TC and SLR studies information for the area of study, in terms of their generation, causes and consequences.

Chapter 2 – Theoretical Framework: Here it is discussed the existing literature putting the remaining chapters in context with the present knowledge. The processes which contribute to storm surges are described. It also presents the current state of knowledge

of storm surge, TC and sea level variability (SLV) in the world, particularly for SWIO, concretely in the Mozambique Channel.

Chapter 3 – Methodology: This chapter covers the methods and approaches used in this study. It also, explains the data compilation, the building, testing and validation of the model.

Chapter 4 - Results and Discussion: An entirely results are discussed, focused on the storm surge model validation and sensitivity analysis. An intensive analysis of changes in the statistics of storm surges is undertaken, following a robust quality control of the data. Statistical calculations are presented. Storm surge heights for the future climate scenario are calculated and results thoroughly analyzed. Here we compare the effect on storm surge for different future climate scenarios, taking into account both coastal peak surge heights and the direction of wind. Also, it is shown the wind blowing quadrant that has more influence in generating maximum storm surge heights. The influence of future climate scenarios and the dynamics of the storm surge within the stations in Mozambique coast are also described. The storm surge statistical properties are investigated.

Chapter 5 – Summary and Conclusion: This chapter provides the overall achievements of the current work before presenting the general conclusions. Also, it presents a summary of all the work, final conclusions and recommendations for further studies.

Chapter II - Theoretical Framework

2.1 Meteorological Description

The weather in Mozambique is determined by the location of the equatorial low pressure zone, tropical anticyclone cells and Antarctic polar fronts. Anticyclonic cells are located on both sides of the southern Africa over the Atlantic and Indian oceans.

According to Tinley (1971), northern Mozambique is affected by the extension of the East African monsoon system with winds blowing north to northeast during the southern summer and south to southwest during the southern winter. Central and southern Mozambique is affected by the Southeast Trade Wind System and receives easterly prevailing winds throughout the year.

The annual average near-surface atmospheric temperature is about 23°C, but for the coastal zones of southern and northern Mozambique is about 26°C. The climate in the south of the Zambezi River is influenced by subtropical anti-cyclonic zone. North of Sofala along the Zambezi River lays a transitional zone, the Intertropical Convergence Zone (ITCZ), with high rainfall (Saetre and Silva, 1979). The average annual precipitation is about 1200 mm, and occurs mainly during the summer, between the months of November and April. The climate in the region north of the Zambezi River is under the influence of the equatorial low-pressure zone with the NE monsoon in the warm season. The climate is generally tropical humid with two distinct seasons: dry or winter and wet or summer.

2.1.1 Tropical Cyclones

A tropical cyclone is a non-frontal cyclone of synoptic scale developing over tropical waters and having a definite organized wind circulation with average wind of 63 km/h or more, surrounding the center (Elsberry, 1995).

There are three components of a cyclone that combine to make up the total cyclone hazard. Those components are strong winds, intense rainfall and oceanographic features including high energy waves, strong currents, storm surge and resulting storm tide. The destructive force of cyclones, however, is usually expressed in terms of the strongest wind

gusts experienced. Maximum wind gust is related to the central pressure and structure of the system, whilst the storm surge is linked closely to the combination of surface wind speed, central pressure and local bathymetry. Rainfall intensity varies considerably, with the heaviest rain typically associated with the system after it decays into a tropical low, or rain depression, as it loses intensity over land.

The eye of a full matured cyclone is surrounded by a 10-15 km thick wall of convective clouds where the maximum wind occurs. The height of the wall goes up to 15 km and is the most dangerous part of a cyclone storm. The entire TC system moves only at about 20-25 Km/h along with the large-scale atmospheric flow around it, however, it is characterized by strong winds of the order of 100 to 200 Km/h. (Pradhan et al. 2012).

By far, storm surge associated with severe tropical cyclone are the most damaging. The intense winds that are characteristic of tropical cyclone, blowing over a large surface of water where the TC lies cause the sea water to pile up to coastal and lead to the sudden inundation and flooding of coastal regions. According to Valdivia (2004), about 90% of the damage is due to inundation of land by sea water. Most of the world´s greatest human disasters associated with the tropical cyclones have been directly attributed to storm surges and storm waves.

In addition, in river delta areas, flooding can occur from the combined effects of tides and surge from the sea that penetrates into the rivers and the excess of water in the river due to heavy rains from the cyclone that flow down the river into the sea.

Mozambique lies in the favorite path of TCs which are formed in the SWIO basin, Figure 5. According to Palmén (1948) and McBride (1995), TCs are formed in equatorial regions, where SST exceeds 26ºC to 27°C. Rarely this phenomenon is formed within less than 4º to 5° latitude from the Equator (Anthes, 1982). There are several other conditions favoring the genesis of TCs, listed by Henderson-Sellers et al. (1998) namely: The large values of low level relative vorticity, the weak vertical and horizontal wind shear, the conditional instability through a deep atmospheric layer, the large relative humidity in the lower and middle troposphere and the deep oceanic mixed layer. The large relative humidity in the lower and middle troposphere is fulfilled within the ITCZ. The frequency and intensity of a TC may depend on natural cycles such as the El Niño-Southern Oscillation (ENSO), the Quasi-Biennial zonal wind Oscillation (QBO) and the Madden-Julian Oscillation (MJO), according to Pielke and Landsea (1999), Landsea *et al*. (1999) and Madden and Julian (1994), respectively.

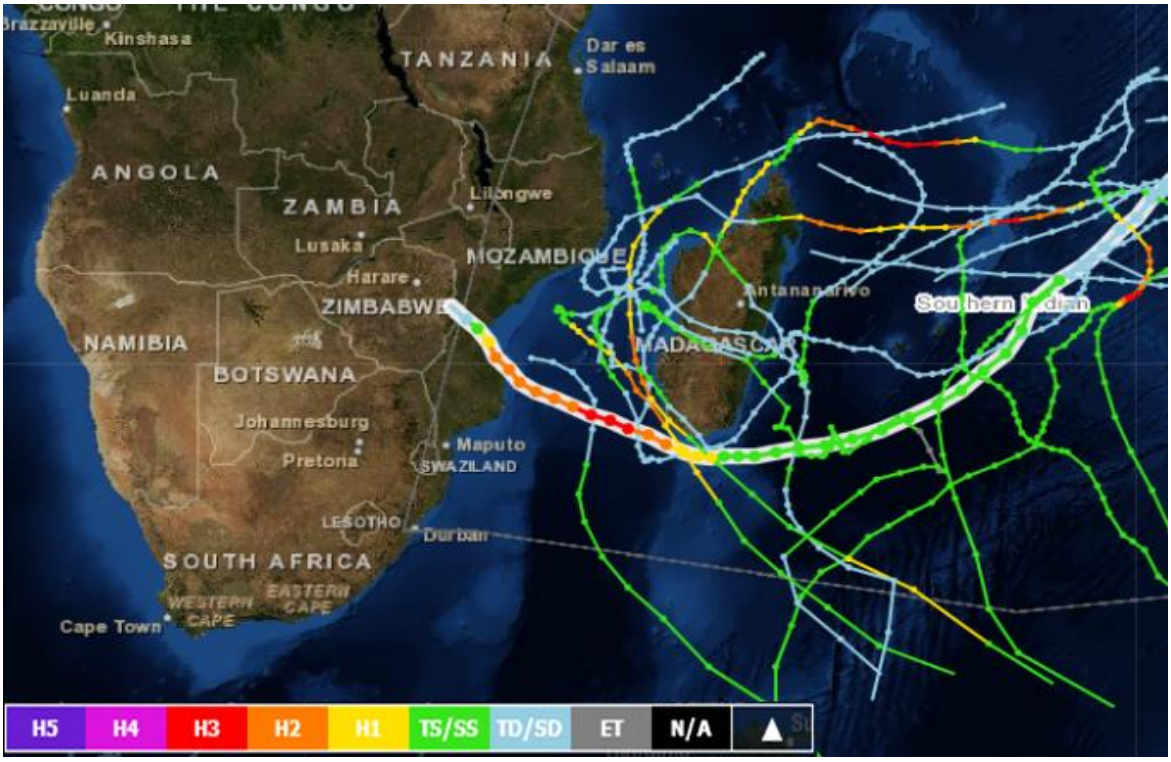

Figure 5. Southern Indian Ocean tropical cyclone tracks, 2004-2007. (Source: NOAA- Adapted)

The country is located in a path of potentially deadly TCs, (INGC, 2009). TCs forming in the SWIO repeatedly affect island nations and countries on the mainland of Africa (Vitart et al., 2003; Malherbe et al., 2012). According to Matyas (2015), in the period of 1948 to 2010, about half of the 94 tropical systems that developed in the small area of water in the SWIO, made landfall. On average, each year, 14% of the global TCs are formed in the SWIO basin (Jury, 1993; Ho et al., 2006; Mavume et al., 2009). The tropical cyclone season in Mozambique starts in October and ends in April. However, they are more frequent between January and February. According to Vitart et al. (2003), storms generated within the Mozambique Channel represent about 10% of the total number of SWIO tropical cyclones and they are generally short lived and weak in comparison to storms generated east of Madagascar.

Several TC such as Eline, Dera, Favio and Funso have devastated the country in the recent years of 2000, 2001, 2007 and 2012 respectively (du Plessis, 2002; Reason and Keibel, 2004; Reason, 2007; Klinman and Reason, 2008; Malherbe et al., 2012). The forecasted maximum storm surge height due to TC Funso in 2012, GDACS (2012), was

1.3 meters, which failed to be confirmed against the observation because of lack of tide gauge. That is why there is a need for a countrywide survey on high water mark collection.

As stated by Knutson et al (2010), some increase in the mean maximum wind speed of tropical cyclones is likely (+2 to +11% globally) with projected twenty-first-century warming, although increases may not occur in all tropical regions. Based on analysis of observations and experiments with the ECMWF atmospheric model, Vitart et al. (2003) suggested that the most important factor in determining the risk of landfall on Mozambique in a given SWIO TC season is the zonal steering current or steering flow.

According to the study of Vitart et al. (2003), the probability of a TC making landfall in Mozambique is five times higher in years with a zonal steering flow of at least one standard deviation below average. These results lead to a conclusion that the increased TC activity in the west site of Madagascar was more likely to increase the risk of landfall over Mozambique.

Fitchett and Grab (2014) in their study concluded that from the total TCs that made its landfall over Mozambique, 34.5% are developed within the Mozambique Channel and the remaining 65.4% developed within the greater SWIO. From those that developed within the SWIO basin, 44.1% pass to the north of Madagascar and subsequently moved in a south-westerly direction to make landfall over Mozambique, 20.6% pass to the south of Madagascar and move in a north-westerly direction toward Mozambique and the remaining 35.3% continue over the island of Madagascar through the Mozambique Channel to make landfall over Mozambique (Appendix A).

The relatively weak easterly vertical wind shear and high sea surface temperatures, averaging 28 ºC during the austral summer, characterize the Mozambique Channel. Those conditions conduct to tropical cyclone formation (Jury and Pathack, 1991; Suzuki *et al.*, 2004; Mavume *et al.*, 2009).

Gray (1968) stated that this area of wind shear, along the ITCZ, provides cyclonic vorticity at low levels and divergent anticyclonic outflow aloft to aid tropical cyclogenesis.

TCs are categorized by its wind intensity, which is defined as the maximum mean wind speed over open flat land or water. This is sometimes referred to as the maximum sustained wind and will be experienced around the eye-wall of the cyclone. The common indicator of the intensity of the storm associated with a tropical cyclone is the maximum sustained wind. The definition of sustained winds recommended by WMO and used by

most weather agencies is that of a 10-minute average at a height of 10 m. It is found within the eyewall at a distance defined as the radius of maximum wind (RMW), within a mature TC. The value of sustained winds are determined via their sampling and averaging the sampled results over a period of time (Matyas, C. J., 2015).

From satellite imagery it is possible to determine the value of the maximum sustained winds within a TC over the ocean. When available, Land, ship, aircraft reconnaissance observations, and radar imagery can also estimate this quantity. This value helps to determine damage expected from a TC, through use of such scales as the Saffir-Simpson scale.

For the SWIO, the intensity scale used to quantify the magnitude of the tropical cyclone is shown in the Table 2.

Table 2. TC Intensity Scale for the SWIO**.**

	Category	**Sustained Winds (Km/h)**
1	Tropical disturbance	< 51
2	Tropical depression	51-63
3	Moderate tropical storm	63-88
4	Severe tropical storm	89-117
5	Tropical cyclone	118-165
6	Intense tropical cyclone	166-212
7	Very intense tropical cyclone	>212

2.2 Oceanographic Description

2.2.1 Sea Surface Temperature - SST

The Mozambique Channel displays a strong seasonal sea surface temperature (SST) contrast of about 5°C between summer and winter. SST minima of about 25°C occurs in late austral winter, from June to September, while maxima of about 30°C occurs in austral summer, from December to February, yielding an annual mean SST of about 27.6°C (Fallet et al., 2010). Following Crimp et al. (1998), an increase in sea surface temperature of 2 °C at the Agulhas current Retroflection can substantially affect the atmospheric circulation over the whole southern African subcontinent. An increase in SST over the South Indian Ocean will statistically lead to an increase in rainfall over regions that form the drainage regions for some of the main rivers of the South African east coast (Walker, 1990).

There is also a distinct wet and dry season in western tropical Indian Ocean, which is concomitant with the sea surface annual cycle and it is associated with cross-equatorial heat and moisture advection (Fallet et al., 2010). During the wet season, prevailing northeasterly winds originating from northern tropics bring moisture from the tropical Indian Ocean to the African continent when SST maxima and its ITCZ are situated in the Southern tropics. In contrast, the dry season is dominated by less humid south easterly winds originating from the southern hemisphere mid latitudes as the sea surface temperature maxima and the intertropical convergence zone are positioned in the northern tropics.

2.2.2 Tides, Waves and Oceanic Currents

Tides are long waves that result from the gravitational attraction of the moon and sun acting on the water bodies on the earth. The mutual attraction between the earth and moon must be balanced by a centrifugal force, which results in a rotating system with an axis of rotation located within the earth (Dean *et al.*, 2002). The rotation of the earth causes the cyclical rise and fall of the ocean levels on a daily (diurnal) and half-daily (semidiurnal) basis. Variations in the relative positions of the earth, moon, and sun cause fluctuations in the strength of the astronomical forcing. The periods of the interactions between the oceans, moon and sun range from a few hours to somewhat more than a day

and their wave lengths, accordingly, vary between a few hundred and a few thousand kilometers (Holthuijsen, 2007).

When the wind starts to blow over a calm sea, as summarized by Miles (1960), the resonance mechanism would come in to action first, producing an initial rate of growth of wave energy linearly with time. As the wave becomes larger, the instability mechanism becomes more effective and the wave energy increases exponentially. The wind set-up is caused by the wind blowing across the surface of the water over hundreds of square kilometers, while wave set-up is caused by the generation and then release of wave momentum in the water column as waves are formed, shoal, and then break.

The continental shelf of Mozambique up to 200 meter isobaths has an area of 104 km^2 (Figure 6). It is narrow in the south and in the North, with two banks of ecological importance (Hoguane and Pereira, 2003). The tides behave like a standing wave, i.e. the tidal current changes direction in high tide and at low tide, and the high currents speeds are observed during intermediate periods. The tides are semi-diurnal with fairly significant diurnal inequality (Hoguane, 1999).

Ocean surface waves are propagating oscillations on the ocean-atmosphere interface. The extent to which tropical cyclones contribute to extreme wave conditions is not much studied in the SWIO. Yet, waves of 10 m are reported hitting the coast of Madagascar, indicating a potential contribution to extreme wave events (Chang-Seng and Jury, 2010).

All Mozambican coastline, is subject to the influence of the warm current of the Mozambique Channel-Agulhas and the corresponding maritime, prevailing East quadrant winds (Muchangos, 1999). The pattern of movement of ocean water along the coast of Mozambique, according to Saetre and Silva (1982), is characterized by three anticyclone cells, which vary its position throughout the year, and by small wind vortices between the large, anti-cyclonic eddies. During the austral summer the vortices, anti-cyclonic eddies seem to be separated by a cyclone and vortex during the austral winter the two vortexes seem to merge into a single, extending in the form of language to the central part of Mozambique.

Over the shelves of the Mozambique Channel, according to Saetre (1985), the nature of the waters is characterized by the average drift patterns at the sea surface, which indicate a strong movement pole ward along the eastern shelf of Mozambique. However, in some places in the channel, the average flow is small and the respective direction is not distinct.

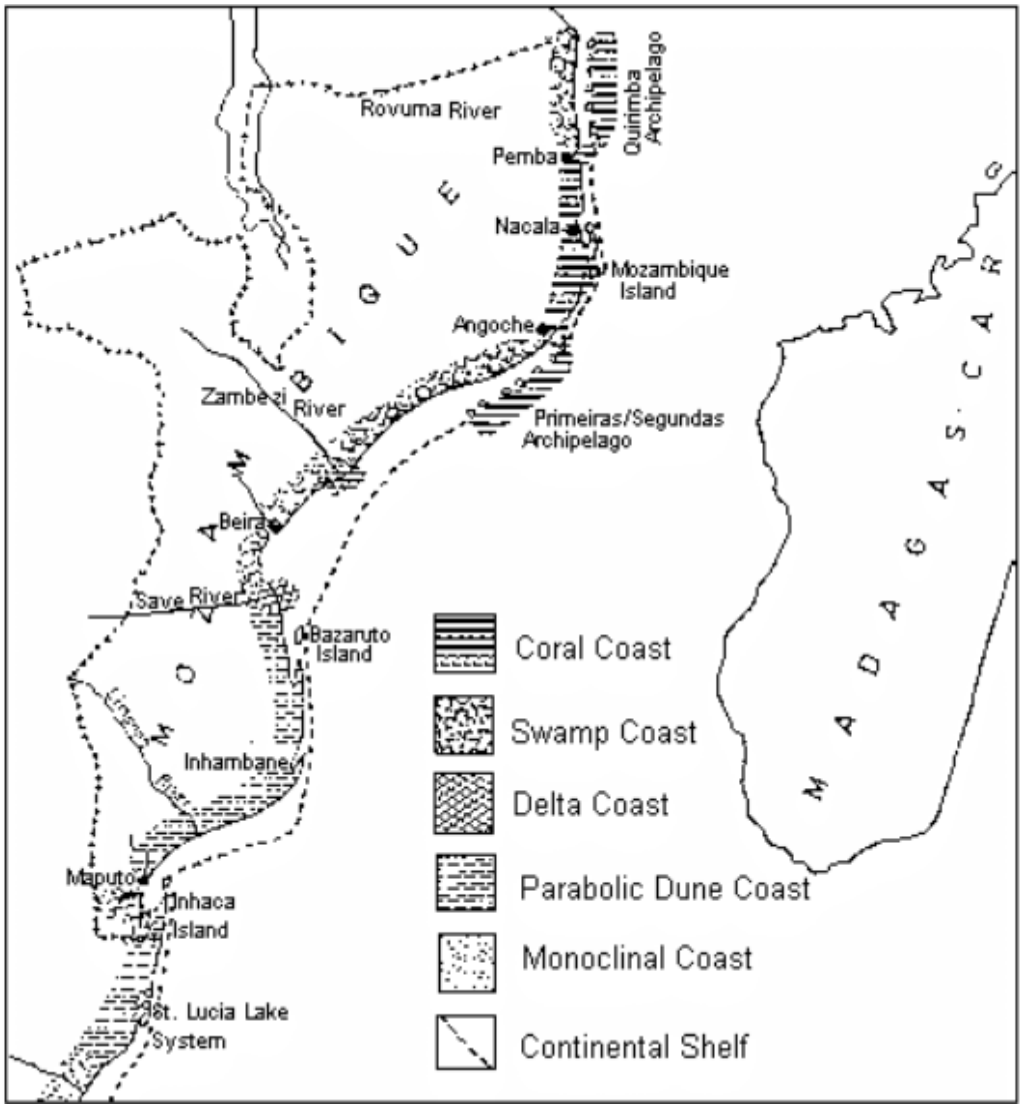

Figure 6. The dashed line represents the 200 m isobaths. Source: Hoguane & Pereira (2003).

The flow has a very high variability in the western side of the channel, but low in the eastern side, which is evident in analyses done from altimetric observations (Lutjeharms et al., 2000b). The Mozambique current is derived from the North East Madagascar current, a branch of South Equatorial current (New et al., 2006). The Mozambique Channel is dominated by the discontinuous surface Mozambique current that mainly constitutes of southward propagating anticyclonic eddies.

2.3 Climate Change

Climate change is defined as a change in the state of the climate that can be identified by changes in the mean and/or the variability of its properties and that persists for an extended period, typically decades or longer (IPCC, 2014). This may be due to natural internal processes or external forcing such as modulations of the solar cycles, volcanic eruptions, and persistent anthropogenic changes in the composition of the atmosphere or in land use.

The coastal flooding is often caused by extreme events, such as storm surges. So, climate change poses risks for human and natural systems. The impacts, adaptation, and vulnerability of climate change span a vast range of topics (Figure 7). With the global warming inducing increases in mean sea level and possible changes to weather patterns that drive extreme of sea level, such as storms surge, are likely to increase the frequency and severity of coastal flooding and erosion in the future (AR5, 2014).

Information about the present threat about the storm surge and how this threat will change in the future is essential to assess the impact of climate change on the coast and to subsequently formulate adaptation responses to changing climate conditions. The United Nations Framework Convention on Climate Change (UNFCCC) thus makes a distinction between climate change attributable to human activities altering the atmospheric composition, and climate variability attributable to natural causes.

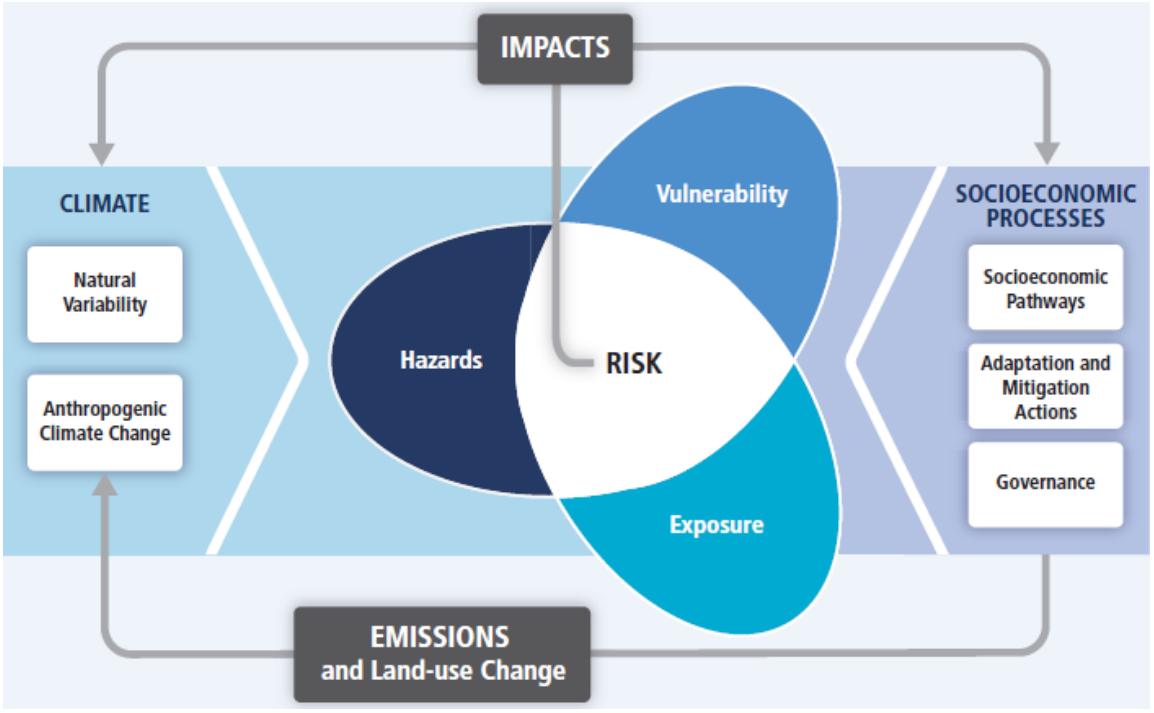

Figure 7. Implication of climate in society. Source: IPCC (2014).

When trying to predict how future global warming will contribute to climate change and develop mitigation strategies, many factors have to be taken into account. The key variable is the amount of future greenhouse gas emissions. Other variables are developments in technology, changes in energy generation and land use, global and regional economic circumstances and population growth (IPCC 2007).

In order to the research between different groups be complementary and comparable, a standard set of scenarios are used to ensure that starting conditions, historical data and projections are employed consistently across the various branches of climate science.

Those scenarios are called Representative Concentration Pathways (RCPs). They are representative in that they are one of several different scenarios that have similar radiative forcing and emissions characteristics. The RCP are based on selected scenarios from four modelling teams/models working on integrated assessment modelling, climate modelling, and modelling and analysis of impacts. There are four RCPs namely RCP8.5, RCP6, RCP4.5 and RCP2.6, which were selected, defined and named according to their total radiative forcing in 2100 (Table 3).

Table 3. The RCP and the related total radiative forcing.

RCP	Total Radiative Forcing
RCP 8.5	Rising radiative forcing pathway leading to 8.5 W/m² in 2100.
RCP 6	Stabilization without overshoot pathway to 6 W/m² at stabilization after 2100
RCP 4.5	Stabilization without overshoot pathway to 4.5 W/m² at stabilization after 2100
RCP 2.6 or 3-PD2	Peak in radiative forcing at ~ 3 W/m² before 2100 and decline

The RCPs form a set of greenhouse gas concentration and emissions pathways designed to support research on impacts and potential policy responses to climate change (Moss et al. 2010; van Vuuren et al. 2011a).

According to Fisher et al. (2007) and IPCC (2008), the RCPs 8.5 corresponds to a high greenhouse gas emissions pathway, the reason why is so-called 'baseline' scenario, that does not include any specific climate mitigation target. It combines assumptions about high population and relatively slow income growth with modest rates of technological change and energy intensity improvements, leading in the long term to high energy demand and GHG emissions in absence of climate change policies. Compared to the total set of RCPs, the RCP8.5 corresponds to the pathway with the highest greenhouse gas emissions (Riahi et al., 2011).

According to Dasgupta, et al. (2009b) and Rahmstorf (2007), the scientific evidence indicates that climate change will intensify storm surges and there are evidences which suggest that sea-level rise could reach 1 meter or more during this century. The IPCC (2013) also reports that change will affect sea levels extremes and ocean waves in two principal ways. First: Due to the extratropical and tropical storms that are one of the key drivers of sea level extremes and waves. So, future changes in intensity, frequency, duration, and path of these storms will impact them. Second: Sea level rise adds to the heights of sea level extremes, regardless of any changes in the storm-related component.

2.3.1 Mean Sea Level Rise

Rising sea level represents a serious hazard for coastal communities. Changes in extreme sea levels occur due to mean sea level rise or changes in storminess. Changes in mean sea level are more or less understood, and there is a consensus that sea level will rise during the 21st Century.

According to Neumann et al (2013), sea level rise as a result of climate change may also have an important effect on the damage that could result from cyclones. Higher sea levels provide a higher launch point for storm surges in the region. This increases both the areal extent of surge and the depth of surge in areas already vulnerable to coastal storms. In addition, future sea level rise, while uncertain, is more reliably forecast to 2050 than future storm activity. In general, the increase in sea level would make existing storms significantly more damaging, even for minimal changes in storm activity. This analysis focuses on the more reliably forecast marginal effect of sea level rise on the extent and effective return period of these already damaging storms.

According to Nicholls and Cazenave (2010), several regions are vulnerable to coast flooding caused by future relative or climate-induced sea level rise. At highest risk are coastal zone with dense populations, low elevations, appreciable rates of subsidence, and or inadequate adaptive capacity. Figure 8 shows the vulnerability of the coast of Mozambique to coast flooding caused by future relative or climate-induced sea level rise.

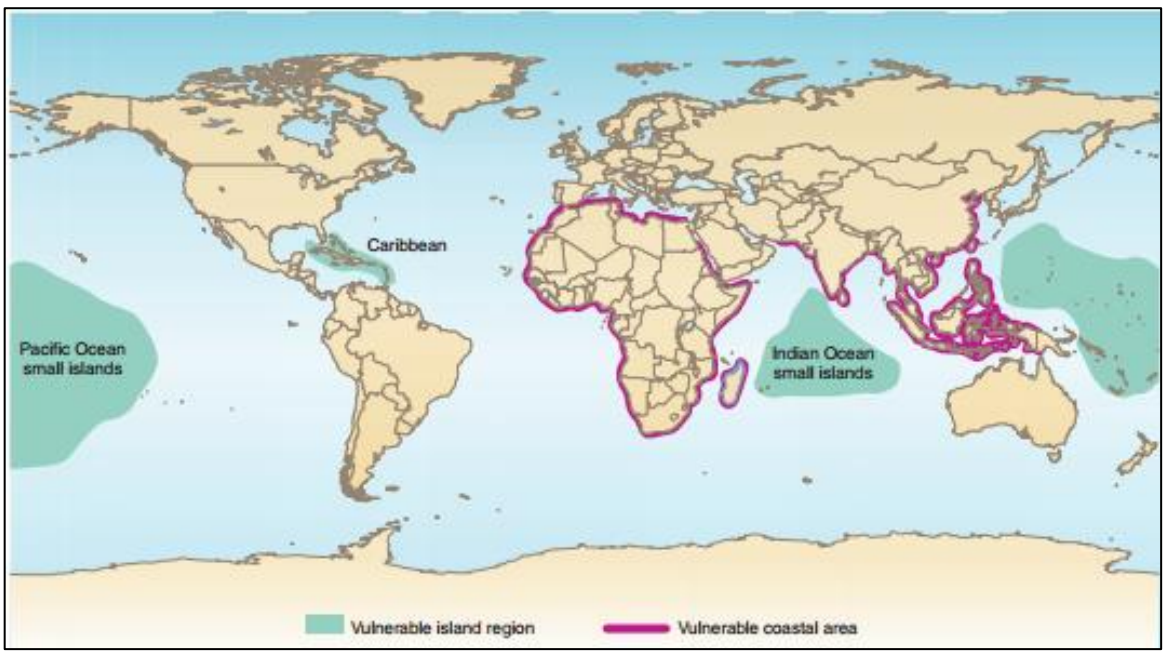

Figure 8. Coastal zones at highest risk of flooding due to SLR. Source: Nicholls and Cazenave (2010).

From the projections of IPCC (2013), is very likely that the rate of global mean sea level rise during the 21st century will exceed the rate observed during 1971–2010 for all RCPs scenarios, due to increases in ocean warming and loss of mass from glaciers and ice sheets. The assessment report five, states that for the period 2081–2100, compared to 1986–2005, global mean sea level rise is likely to be in the 5 to 95% range of projections from process based models, which give 0.26 to 0.55 m for RCP2.6, 0.32 to 0.63 m for RCP4.5, 0.33 to 0.63 m for RCP6.0, and 0.45 to 0.82 m for RCP8.5. For RCP8.5, the rise by 2100 is 0.52 to 0.98 m with a rate during 2081–2100 of 8 to 16 mm yr $^{-1}$ (Figure 9).

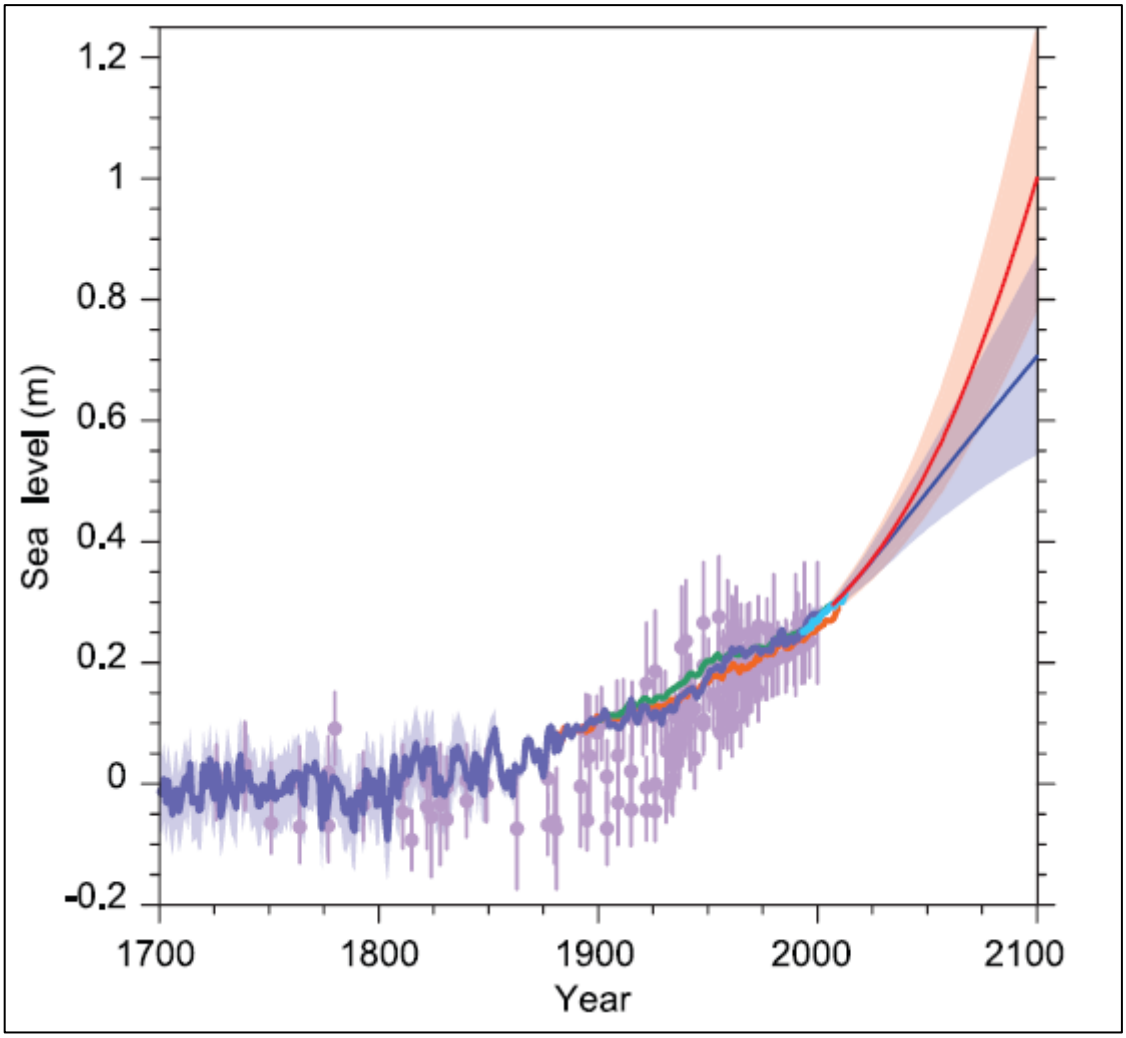

Figure 9. Likely ranges for projection of global mean sea level rise for RCP2.6 (blue) and RCP8.5 (red) Scenarios. Source: IPCC, 2013.

The sum of thermal expansion simulated by Coupled Model Intercomparison Project phase 5 (CMIP5) Atmosphere–Ocean General Circulation Models (AOGCMs), glacier mass loss computed by global glacier models using CMIP5 climate change simulations,

and estimates of land water storage explain 65% of the observed global mean sea level rise for 1901–1990 and 90% for 1971–2010 and 1993–2010.

The results from the study of Church et al.(2011) shows that the global sea level is rising and is expected to continue to rise on a multi-centennial to millennial time scale (Yin 2012, IPCC 2013). However, sea level is not rising at the same rate globally but exhibits significant spatial variations (Cazenave et al., 2008, Cazenave and Llovel, 2010, Stammer et al., 2013).

The latest Assessment Report (IPCC 2013), accounted for the projections of sea level rise (Figure 9), of 0.12, 0.32 and 0.72 m for the periods 2016-2035, 2046-2065 and 2081-2100 respectively, relative to 2000. Those values were obtained through interpolation in the graphic of Figure 9. These SLR values were used in this present study.

2.3.2 Tropical Cyclones

Emanuel (2008) showed that for the Indian Ocean, models results suggest that there is an overall tendency toward a decreasing frequency of tropical cyclones but increasing cyclone intensity. In this context, tropical cyclones will represent potential disaster condition for the population and infrastructures along the coast, taking in consideration that the more intense is the wind, the greater is the amount of water dragged to the coast. Twenty century reanalysis points to an increase in annual wind storms since 1871, (Donat et al. 2011).

The projections based on the SRES A1B scenario, assessed by Knutson et al. (2010), concluded that it is likely that the global frequency of tropical cyclones will either decrease or remain essentially unchanged while mean intensity (as measured by maximum wind speed) increases by +2 to +11% . However, by using available modelling studies that are capable of producing very strong cyclones typical project, other authors projected a substantial increases in the frequency of the most intense cyclones and it is more likely than not that this increase will be larger than 10% in some basins (Emanuel et al., 2008; Bender et al., 2010; Knutson et al., 2010, 2013; Yamada et al., 2010; Murakami et al., 2012).

Projections for the 21st century, IPCC (2013), indicate that it is likely that the global frequency of tropical cyclones will either decrease or remain essentially unchanged,

concurrent with a likely increase in both global mean tropical cyclone maximum wind speed and rain rates. The influence of future climate change on tropical cyclones is likely to vary by region, but there is low confidence in region-specific projections. The frequency of the most intense storms will more likely than not increase in some basins.

2.3.3 Storm Surges

Climate change is expected to accelerate sea level rise and increase storm events, which will subsequently impact the coastlines and their coastal systems. This process will exacerbate the economic and social vulnerability of the growing populations in coastal regions, increasing the pressures that already exist in these environments.

Seneviratne et al., (2012), concluded that it is very likely that mean sea level rise will contribute to an increase in future sea level extremes. Projected changes in storm surges, relative to mean sea level, have been assessed by applying climate–model forcing to storm-surge models. Those results are in concordance with the study by Dasgupta et al. (2009b), that demonstrates that there is a risk of intensification of storm surge impacts in Mozambique by considering coastal occupation, coastal urban areas and coastal gross domestic product. However, this study does not quantifies the future storm surge heights.

Dasgupta et al. (2009a) have considered a 10 percent future intensification of storm surges compared to a 1-in-100-year historical storm surge. They examined the impacts of sea level rise with these intensified storm surges in developing countries, assessing impacts in terms of land area, population, agriculture, urban extent, major cities, wetlands, and local economies.

They concluded that Sub-Saharan African countries will suffer considerably from these changes. For Mozambique alone, the study estimates an incremental impact loss of 3,268 km^2 land area (over 40 percent of coastal land area) of which approximately 291 km^2 is agricultural land (about 24 percent of coastal agricultural land), 78 km^2 is urban (over 55 percent of coastal urban land) and 1,318 km^2 is wetland (over 45 percent of coastal wetlands). In addition, the study estimates that over 380,000 people (51percent of the coastal population) and US$140 million GDP (55 percent of coastal GDP) could be lost.

In sub-Saharan Africa, storm surge zones are concentrated in Madagascar, Mauritania, Mozambique and Nigeria. These countries alone account for about half (53 %) of the total

increase in the region's surge zones resulting from sea level rise and intensified storms (Dasgupta et al., 2009a). According to the same study, Mozambique is between the countries of the Sub-Saharan Africa region that will experience significant increases in the percentage of their coastal urban extent falling within surge zones with SLR and intensified storm surges.

Depending of the research objectives as well as the kind of data available, the methodology for STS calculation differ. For instance, Lee et al. (2009), has used sea level data from the National Oceanographic Research Institute to calculate storm surges along the Korean Peninsula. The STS were obtained by calculating the difference between the observed and predicted sea level. The tide analysis method, harmonic or response, were applied and compared at Masan and Yeosu during Typhoons Maemi and Ewiniar, in order to find the influences of the surface elevation data and tide analysis method on calculated storm surge.

According to the same author, depending on the sea level data and tidal prediction method used, calculated surge heights differed by as much as 70 (50) cm for the maximum surge of 211 (168) cm at Masan (Yeosu) during Typhoon Maemi. They have used the harmonic method with 1 year of data which produced the most reliable surge calculations. However, the extended response method using a 1-month record was almost as accurate as the harmonic method using the 1-year record. The extended response method might offer a good alternative for tidal prediction when a 1-year record is unavailable. They also concluded that the sampling interval of sea level data was more important for surge calculations, especially for sharply peaked surges, than was the sea level record length.

Dasgupta et al. (2009) used another different methodology for STS calculation. They primarily followed the method outlined by Nicholls (2008). Then, with the method in a slightly modified version, surges for the two storm surge scenarios (with and without climate change) were calculated as follows:

Current storm surge = S100

Future storm surge = S100 + SLR + (UPLIFT * 100 yr) / 1000 + SUB + S100 * x

Where:

S100 = 1 in 100 year surge height (m); SLR = 1 m; UPLIFT = continental uplift/subsidence in mm/yr; SUB = 0.5 m (applies to deltas only); x = 0.1, or increase of 10%, applied only in coastal areas currently prone to cyclones or hurricanes. Surges were calculated using data associated with the coastline.

Neuman et al. (2013) by using a simulated dataset of storms and surges along with three alternative forecasts for future SLR in Mozambique, has estimated the effect of climate change induced SLR on surge risk from cyclones. The overall method involves four steps: Simulate storm generation activity over the 21st century; Use wind fields as inputs to a storm surge model; Generate a cumulative distribution function of storm surge heights for selected locations in the SLOSH domain: SLOSH results generated without SLR for each of the simulated events provide a 'base case' of surge heights against which future storms can be evaluated; Estimate the effect of SLR on the return-time of storms: using the distribution of storm surges in the base case, the study estimates how SLR effectively increases the frequency of damaging storm surges; comparing three scenarios of future SLR magnitude in 2050.

The global vulnerability analysis done by Hoozemans et al. (1993) and Nicholls and Tol (2006), shows that East Africa, including small island states and countries with extensive coastal deltas, is one of the more problematic regions and could experience severe loss of land. These studies demonstrate Mozambique's troubling exposure to impacts of tropical cyclones, from the high vulnerability of long stretches of coastline and the low adaptive capacity due to poverty in the country.

2.3.4 Sea Level Pressure

What concern to the response to atmospheric pressure changes, sea level pressure is projected to increase over the subtropics and mid-latitudes (depressing sea level) and decrease over high latitudes (raising sea level), especially over the Arctic, by the end of the 21st century, associated with a poleward expansion of the Hadley Circulation and a poleward shift of the storm tracks of several degrees latitude (Held and Soden, 2006).

Chapter III – Methodology

This chapter briefly discusses the methodology and data sources pertaining to the calculation of storm surge. It starts by summarizing the approaches that have been used to analyze the SLV and atmospheric condition data, obtained for the study. Then, it explains how these data were applied to the different datasets.

In science, a model is a representation of an idea, an object or even a process or a system that is used to describe and explain phenomena that cannot be experienced directly. Analytical models are mathematical models that have a closed form solution, i.e. the solution to the equations used to describe changes in a system can be expressed as a mathematical analytic function.

The difference between an analytical model and numerical model is that, numerical methods use exact algorithms to present numerical solutions to mathematical problems, while analytical methods use exact theorems to present formulas that can be used to present numerical solutions to mathematical problems with or without the use of numerical methods.

In the past, before the computer era, the techniques used for storm surge prediction were analytical, empirical, graphical and statistical. Electrical analog methods were also occasionally used (WMO-N.1076, 2011). With the advent of computers, numerical methods are now used almost exclusively. However, for the sake of simplicity, simple analytical and graphical methods are still used occasionally. For site specific purposes, empirical and statistical methods are also used (WMO-N.1076, 2011).

Analytical models can quite naturally complement empirical data, whether archival or experimental (Dikolli et al., 2012). Combining theoretical and empirical analyses also imposes structure on the reporting of results, which makes the study more focused and clear regarding its main contribution.

.

3.1. Data Source and Collection

Data are essential for scientific research and policy planning. However, there needs to be attention to data quality and the estimates and models based on those data. That is why data is an integral part of research. The results of research and its methods are directly dependent on the collected data and its analysis.

We have to mention that at the outset, we acknowledged the limitations in the availability of data from TG, storm surge heights records, which somehow contributes for limitations when comes the stage of data analysis.

The sea level records database of Mozambique is not continuous since it has many missing data and, the ones that exist, present a lot of gaps in the data time series. These missing data vary from a few hours to more than one month and the corresponding periods of available data differ from station to station. There is also limited network coverage of TG for a long coast with an extension of about 2700 km. The installed TGs are operated by the National Institute of Hydrography and Navigation (INAHINA), with a network which consists of thirteen stations from which, only three (Maputo, Inhambane and Pemba) are operational, despite the irregularity that it works with. The station of Inhambane and Pemba are in the GLOSS network of TG.

The station of Maputo is the only one with nearly completed data for about 13 years, although, there are gaps in the time series which ranges from 1 day to Months. The TG station of Maputo, Beira and Pemba are spaced equally along the coastline of Mozambique Channel with a distance of about 1300 km between then, for a coast of about 2700 km long. Those stations have got at least one year with almost complete time series for 1974, 1996 and 1998 respectively. Those are the TG stations used in this study for the calculation of storm surge from TG time series.

As mentioned in the theoretical framework chapter of this thesis, by using sea level information, storm surge can be calculated by subtracting the observed sea level from the predicted sea level. However, taking in consideration the deficient coverage of TG network as well as the scarcity of TG data availability, has leaded us to use data sets of sea level pressure, wind speed and direction to proceed with this study, following the availability of this type of data.

The observed data of atmospheric pressure, wind direction and intensity of 7 meteorological stations, namely Maputo, Xai-Xai, Inhambane, Beira, Quelimane, Angoche and Pemba were used as input for running the analytical model to calculate storm surge.

The historical atmosphere data, wind and SLP, from 1973 to 2011, was downloaded from the Climate Data Online (CDO) site, at National Climate Data Center (NCDC) of the National Oceanic and Atmospheric Administration (NOAA). The data are hourly observed and despite that, it contains gaps of observation which ranges from 1 (one) to 24 hours. The 1973-2011 period of the data, covers the historical period used for this study which is 1986-2005. The choice of period 1973-2011 atmospheric data was done taking in consideration the period of availability of TG data, which are 1974 for Maputo TG station, 1996 for Beira TG station, 1998 for Pemba TG station, to allow the respective comparison or validation against the TG results. The wind was measured at height of 10 meters.

The hourly sea level records data used to validate the analytical model are from Maputo, Beira and Pemba TG stations for the period of data availability. According to Pugh (1987), the longer is the data period used in the estimation of the harmonic constants, the more accurate will be the results.

For the study of future climate scenarios of storm surge, namely the near term future (2016-2035), medium term future (2046-2065) and long term future (2081-2100), climatological data scenarios of sea level pressure and wind speed and direction, were obtained from the low resolution version of the Max Planck Institute of Meteorology Earth System Model (MPI-ESM-LR) model which participated in the Coupled Model Intercomparison Project Phase 5 (CMIP5) (Taylor et al., 2012). The model has 1.9º horizontal resolution and 47 hybrid sigma-pressure levels (Giorgetta et al., 2013). The time period 1986-2005 is the reference time period for the present-day. All projections in the IPCC AR5 WGI report are given relative to this period. The difference between the average for the period 2081- 2100 and the present-day reference time period constitutes the 21st century projections. The year 2100 is the upper reference time period, long term parameters.

The RCP8.5 scenario was chosen since it is the most widely studied and eventually the most probable future scenario. The downloaded data are daily sampled, in NetCDF format and regards the RCP8.5, which corresponds to the pathway with the highest greenhouse gas emissions (Riahi et al., 2011). The tropical cyclone data, wind intensity and sea level pressure, of each tropical cyclone event were collected from the Regional Specialised

Meteorological Centre (RSMC) in Reunion, which is the tropical cyclone center for the South West Indian Ocean - SWIO. The period that the data refer to is from 1985 to 2015, corresponding to 30 tropical cyclone seasons, in the South West Indian Ocean. The SLR data were calculated based on the IPCC AR5 report.

3.1.1 MPI-ESM-LR Model and CMPI5 Project

The MPI-ESM-LR, is a coupled model from ECHAM atmosphere, JSBACH land and MPIOM ocean (Figure 10).The MPI-ESM-LR is a comprehensive Earth-System Model, in the sense that it couples the ocean, atmosphere and land surface through the exchange of energy, momentum, water and important trace gases such as carbon dioxide. As such it reflects the interests and expertise of the three departments that constitute the MPI-M. The MPI-ESM was used as the basis for the MPI contribution to the fifth phase of the Coupled Model Intercomparison Project (CMIP5), and is the current workhorse of Max Planck Institute Scientists.

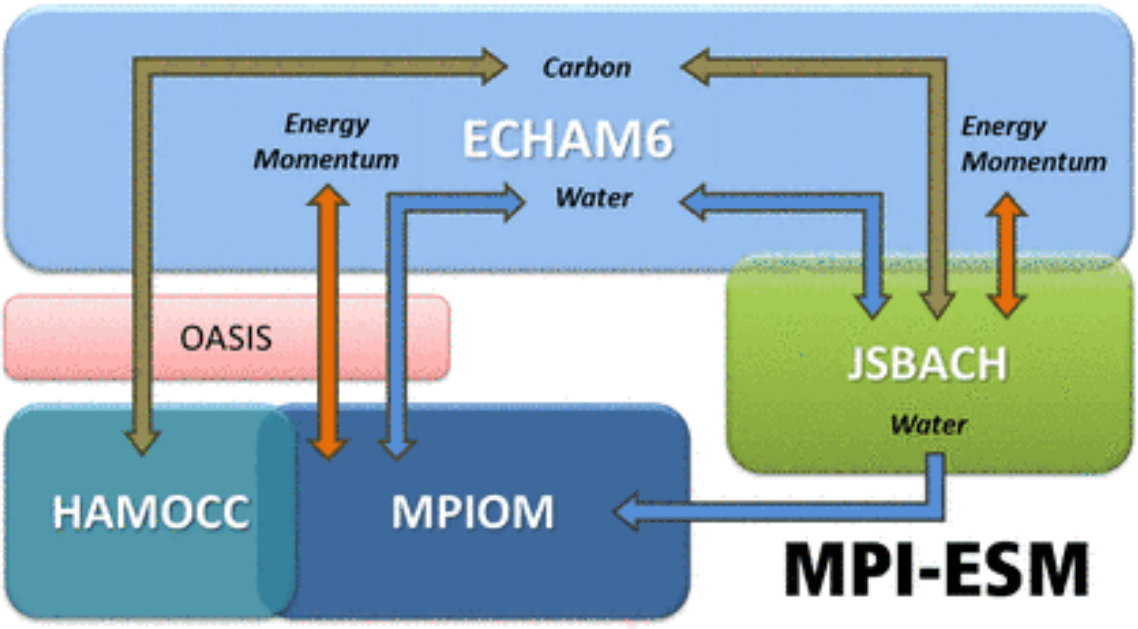

Figure 10. MPI-ESM coupled from ECHAM6, JSBACH and MPIOM. Source: MPI.

The CMIP5 is meant to provide a framework for coordinated climate change experiments and thus includes simulations for assessment in the Fifth Assessment Report (AR5) as

well as others that extend beyond the AR5. It is a project that promotes a standard set of model simulations in order to evaluate how realistic the models are in simulating the recent past, provide projections of future climate change on two time scales, near term (out to about 2035) and long term (out to 2100 and beyond) and, understand some of the factors responsible for differences in model projections, including quantifying some key feedbacks (Taylor et al., 2012).

The study done by Brands et al. (2013) has assessed the ability of seven Earth System Models (ESMs) from the CMIP5 to reproduce present climate conditions in Europe and Africa. These authors analyzed only seven ESMs from CIMP5 that were representative of the full ensemble of the models used in that program. This is done from a downscaling perspective, taking into account the requirements of both statistical and dynamical approaches. They concluded that the MPI-ESM-LR reproduces well the projections of wind and sea level pressure, which are the parameters that are used in this study for the analyze of future climate scenario. According to the same study, the models HadGEM2-ES and MPI-ESM-LR generally outperform the remaining models along the lateral boundaries of the Euro-CORDEX, Med-CORDEX and CORDEX Africa domains, which is in qualitative agreement with the study done by Brands et al. (2011a), who validated the former versions of these models over southwestern Europe. This fact leaded as to use the MPI-ESM-LR model for the present study.

3.2 Storm Surge

The sea level oscillations responds continuously to astronomical, oceanographic and atmospheric (pressure and near-surface winds) interactions over a wide range of periods (Pugh, 1987). The combined effects of atmospheric pressure and wind forcing on sea level produce oscillations known as meteorological tides or low frequency sea level oscillations (storm surge).

Bowden (1983) defines storm surge as a disturbance of sea level, relative to that due to tides alone, produced by meteorological causes. The term storm surge is normally reserved for the excess sea levels generated by severe storm. The surge is strongest where the winds are enhanced by the motion of the tropical cyclone, therefore, the left forward quadrant of the storm is the most dangerous storm surge region.

The general representation of the observed sea level ζ (t) which varies with time may be written as:

$$\zeta(t) = Z_0(t) + T(t) + S(t) \tag{3.1}$$

Where $Z_0(t)$ is the mean sea level which changes slowly with time, $T(t)$ is the tidal part of the variation and $S(t)$ is the meteorological surge component.

From the rearrangement of the equation (3.1), storm surge may be defined as the difference between the observed and predicted levels (Pugh, 1987):

$$S(t) = \zeta(t) - Z_0(t) - T(t) \tag{3.2}$$

The time scale, of storm surge may range from a few hours to several days. A surge of several days duration could be identified by subjecting the sea level data to a low-pass numerical filter which would eliminate oscillations of frequencies within the diurnal, semi-diurnal and high harmonic tidal bands, which are terrestrial harmonic components M4, M6 and M8.

Storm surge is usually considered to be driven by two meteorological processes namely the atmospheric pressure and extreme wind stress (Pugh, 2004). These processes bring the water of the seas into motion. When a high-pressure area moves over a free water surface, it originates an additional weight on it, causing a water out-flow (low meteorological tide), which is a potential shipping hazard (Faggioni et al. 2006). On the contrary, when a perturbed front produces a drop in atmosphere weight, the hydrostatic compensation adjustment will be realized in a bump produced by a flow of incoming tide (high meteorological tide). The second way by which the weather affects the sea level is by wind drag at the water surface. The extent to which they are felt at depths below the surface is determined by the length of time of which they act and by density stratification of water column, which controls the downward transfer of momentum (Pugh, 2004).

For a given site and time, according to Santos and Miranda (2006), the sea level is determined by the combination of two effects: the astronomical and meteorological tide. By neglecting resonances and second-order effects, the storm surge can be determined by wind and atmospheric pressure. While the astronomical tide is deterministic, the meteorological effects have a stochastic nature.

According to Pugh (2004), there is a natural distinction between the effects of storm at low latitude (tropical surges) and those at higher latitudes (extra-tropical surges). The latter are slower to develop and more widely spread in their impact than the intense local impacts of tropical surges. The same author states that, if a time series of the hourly residuals is computed by subtracting the predicted tide and the mean sea level from the observed levels, several useful statistics may be derived. One of those is the standard deviation of the time series from the mean value of zero which is a general measure of the magnitude of the weather effects. It varies from a few centimeters at tropical ocean islands to tens of centimeters in areas of extensive shallow water subject to storm weather.

The motion of water is described by hydrodynamic processes and, the basic dynamical equations are as follow (Bowden, 1983):

$$\frac{Du}{Dt} - fv = -\frac{1}{\rho}\frac{\partial p_a}{\partial x} - g\frac{\partial}{\partial x}(\zeta - \bar{\zeta}) + \frac{1}{\rho}\frac{\partial \tau_x}{\partial z} \tag{3.3}$$

$$\frac{Dv}{Dt} + fu = -\frac{1}{\rho}\frac{\partial p_a}{\partial y} - g\frac{\partial}{\partial y}(\zeta - \bar{\zeta}) + \frac{1}{\rho}\frac{\partial \tau_y}{\partial z} \tag{3.4}$$

For momentum in the *x* and *y* direction, with the continuity equation

$$\frac{\partial u}{\partial x} + \frac{\partial v}{\partial y} + \frac{\partial w}{\partial z} = 0 \tag{3.5}$$

By integrating through a vertical column from the bottom $z = -h$ to the surface $z = \zeta$ and defining components *u, v* of the volume transport by

$$U = \int_{-h}^{\zeta} u\, dz \qquad V = \int_{-h}^{\zeta} v\, dz \tag{3.6}$$

The depth-integrated equations may be written as

$$\frac{\partial U}{\partial t} + \frac{\partial}{\partial x}\left(\frac{U^2}{h+\zeta}\right) + \frac{\partial}{\partial y}\left(\frac{UV}{h+\zeta}\right) - fV = -\frac{(h+\zeta)}{\rho}\frac{\partial p_a}{\partial x} - g(h+\zeta)\frac{\partial}{\partial x}(\zeta - \bar{\zeta}) + \frac{\tau_{sx} - \tau_{bx}}{\rho} \tag{3.7}$$

$$\frac{\partial V}{\partial t} + \frac{\partial}{\partial x}\left(\frac{UV}{h+\zeta}\right) + \frac{\partial}{\partial y}\left(\frac{V^2}{h+\zeta}\right) + fU = -\frac{(h+\zeta)}{\rho}\frac{\partial p_a}{\partial y} - g(h+\zeta)\frac{\partial}{\partial y}(\zeta - \bar{\zeta}) + \frac{\tau_{sy} - \tau_{by}}{\rho} \tag{3.8}$$

$$\frac{\partial U}{\partial x} + \frac{\partial V}{\partial y} + \frac{\partial \zeta}{\partial t} = 0 \tag{3.9}$$

In these equations the elevation ζ, the velocity components *u* and *v* and the transport components *U, V* refer to the resultant values due to tidal constituents and the meteorological effects. In coastal waters of limited extent the direct effects of the tide-generating potential, represent by $\bar{\zeta}$, can often be neglected. The tangential shearing stress of the wind on the sea surface is represented by the components τ_{sx} and τ_{sy} while τ_{bx} and τ_{by} represent the components of bottom stress.

The most important parameter in determining storm surge amplitude Pugh (1987), is the wind speed and the water depth. The surge amplitude is directly proportional to the square of the wind speed. So, if the wind speed doubles, the surge heights increase fourfold. In addition, the surge amplitude is inversely proportional to the water depth. Thus, the shallower is the water, the greater the surge amplitude. This happens because as shallow waters are entered, approximately the same energy is compressed into a shorter, vertical column of water.

Interactions with tides, wind waves or river flow, as well as the effects of precipitation on surges in rivers, lakes and estuaries are among other factors that can increase the storm surge amplitude (WMO-N.1076, 2011).

TC storm surges, respond very strongly to meteorological reinforcement, despite not been freely propagating waves. Nevertheless, in regions outside of intense wind forcing, coastally trapped waves emerge that progress along the shoreline, with crests normal to the coastline.

On the word of Tang et al. (1997), the wave height decreases exponentially from the coast with an e-folding length scale equal to the Rossby radius of deformation *c/f*, in which *f* is the Coriolis parameter and *c* is the phase speed of the wave in the alongshore direction. This feature is important for the storm surge the relaxation phase, after a tropical cyclone makes landfall, or for the case of a TC traveling parallel to the coast in the areas upstream or downstream of the storm's center (Tang et al., 1997).

As said by Flather (2001), storm surge is a long gravity wave with a length scale similar to the size of the generating tropical cyclone, which lasts for several hours depending on the size of the cyclone and speed of movement. The surge usually consists of a single passing wave that elevates or depresses the sea surface height.

When extreme storm winds act over extensive regions of shallow water, as stated by Simpson and Riehl (1981) and Gornitz (2005), major destructive storm surges are known to occur. Since in the governing equations the wind stress term is divided by the total depth whereas the surface pressure gradient force is not, it follows that wind forcing increases importantly in shallower water (Flather, 2001). In other hand, according to Jelesnianski (1972), coastal peak surges created by a given TC over wide continental shelves can be up to three times greater than those created by the same TC over narrower shelves.

Under ideal and steady-state conditions in deep water, the net transport of water by the wind occurs at a 90° angle to the right of the wind vector in the Northern hemisphere, and the alongshore component of wind stress causes a storm surge if the coast is to the right of the wind, following Ekman setup (Shen and Gong, 2009). For the Southern Hemisphere it happen the opposite side, the net transport of water by the wind occurs at a 90° angle to the left of the wind vector, and the alongshore component of wind stress causes a storm surge if the coast is to the left of the wind, Ekman setup (Shen and Gong, 2009).

The across-shore component of wind stress becomes more important as the water depth decreases, since the bottom stress diminishes the Coriolis tendency for transport to be to the right or left of the wind (Northern or Southern Hemisphere). Winds blowing onshore over shallow water will pile water up along the coast (Weisberg and Zheng, 2006b).

By combining the three forcing, the meteorological tide time series can be calculated by using equation (3.10):

$$S = \Delta\zeta + \boldsymbol{\zeta}_z + \boldsymbol{\zeta}_m \tag{3.10}$$

Where *S* is meteorological surge, $\Delta\zeta$ is the displacement of water level from the mean due to pressure disturbance, $\boldsymbol{\zeta}_z$ is the displacement of water level from the mean due to onshore wind and $\boldsymbol{\zeta}_m$ is the displacement of water level from the mean due to alongshore wind.

3.2.1 Inverted Barometer Effect

The inverted barometric effect is the response of sea level to changes in atmospheric pressure perturbation.

According to Wunsch and Stammer (1997), the first serious dynamical discussion may be that of Jeffreys (1916), who was interested in the polar motion problem and who concluded that the oceanic response should be an essentially static one.

If the level in a mercury barometer increases, the sea level is depressed and vice versa (Pugh, 2004). This response is explained through a theoretical model derived from the equations of hydrodynamics, considering an ocean with constant depth (Proudman, 1953). The level of the sea surface, for local variation of atmospheric pressure, will change relative to the mean sea level. The equation representing the inverted barometer effect, can be derivate from the schematic Figure 11 and reads:

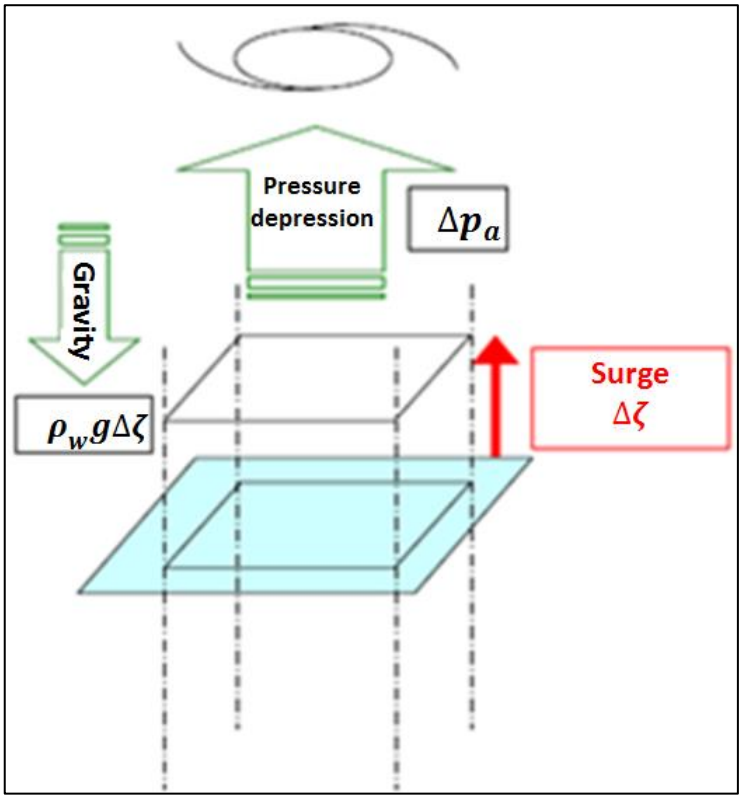

Figure 11. Schematic diagram of the parameters to determine the displacement of water level from the mean, due to inverted barometer effect. Source: Nadao Kono – JCOMM 2012 - adapted.

$$\Delta\zeta = -\frac{1}{g\rho_w}\Delta p_a \quad (3.11)$$

Where $\Delta\zeta$ is the displacement of water level from the mean due to pressure disturbance, $\Delta \boldsymbol{P_a}$ is the atmospheric pressure disturbance relative to a long-term time average at the gauge location, $\boldsymbol{\rho_w}$ the sea water density and **g** the gravitational acceleration.

The inverted barometer effect specifies that a 1 hPa decrease of atmospheric pressure, below a reference pressure, results in approximately 1 cm increase in water level (Kantha and Whitmer, 1994). When a low atmospheric pressure system coincides with a high water spring tide, extreme sea level can be expected.

As argued by Pugh (2004), atmospheric pressure in tropical regions has a much smaller range, their characteristics being a 12-hour cycle with amplitudes around 1 hPa and maximum pressure at 1000 and 2200 hours. The inverted barometer response of the sea levels to these pressure cycles produces a non-gravitational local tide with the same frequency as the gravitational solar diurnal tide, S_2.

3.2.2 Wind Stress

As stated by Pugh (2004), when two layers of moving fluid are in contact, energy and momentum are transferred from the more rapidly moving layer to the slower layer. The physics of this transfer process is very complicated. However, basic functional relationship can be combined with empirical constants to give useful formulae for calculating some of the effects.

In physical oceanography and fluid dynamics, the wind stress is the shear stress exerted by the wind on the surface of large bodies of water. It is the force component parallel to the surface, per unit area and is assumed proportional to the square of the wind speed. The equation of wind stress is mathematically written as:

$$\tau_s = C_D \rho w^2 \quad (3.12)$$

where $\boldsymbol{w}$ is the wind speed measured at a given height, usually taken as 10 m, above the sea surface, $\boldsymbol{C_D}$ is a drag coefficient and $\boldsymbol{\rho}$, the air density.

This means that although wind effects on sea level are small for normal winds, they can become very significant during big storms.

The wind blows either onshore or alongshore. The onshore and alongshore wind stress are represented by equations (3.13) and (3.14) respectively.

$$\tau_{sx} = C_D \rho |w| u \tag{3.13}$$

$$\tau_{sy} = C_D \rho |w| v \tag{3.14}$$

Where $\boldsymbol{\tau_{sx}}$ and $\boldsymbol{\tau_{sy}}$ are the onshore and alongshore wind stresses, ***u*** and ***v*** are wind components in ***i*** and ***j*** directions and ***w*** is the wind speed at height of 10 meters.

3.2.3 Drag Coefficient

As the link between the easily measured wind velocity and the more difficult direct measurement of wind stress, the drag coefficient (C_D) is the key parameter for the determination of the momentum transfer between atmosphere and ocean. The drag coefficient for the ocean surface is found to increase with wind speed (Smith, 1980).

Bowden (1983), stated that the value of C_D depends on the height at which the wind is measured, the stability of the lowest few meters of the atmosphere and the roughness of the sea surface, as affected by waves. The value of C_D also depends on the wind itself, but the dependence of wind stress on wind is not strictly quadratic.

Considering what was mentioned about the relation between the drag coefficient and wind speed, for different range of wind speed the C_D can be calculated in different ways, according to different authors such as:

$C_D = 1.1 * 10^{-3}$ If 1 m s^{-1} ≤|w|< 6 m s^{-1} (Large and Pound, 1981) (3.15)

$C_D = (0.061 + 0.063w)10^{-3}$ If 6 m s^{-1} ≤|w|< 22 m s^{-1} (Smith, 1980) (3.16)

$C_D = 2.5 * 10^{-3}$ If |w|> 22 m s^{-1} (Powell et al., 2003) (3.17)

3.2.4 Alongshore and Onshore Wind

The wind that blows parallel or perpendicular to the coast is called alongshore or onshore wind, respectively. The flow produced by a balance between the pressure gradient force and the Coriolis force, is frictionless flow. However, momentum from the wind field is transferred into the ocean by friction. Due to the interaction between ocean and atmosphere, the drag of the wind in the sea surface moves the water in ways that changes sea levels. The biggest effects are observed when strong wind blows over shallow water (Pugh, 2004). The schematic diagram of the parameters to determine the displacement of water level from the mean due to onshore wind is shown in the Figure 12.

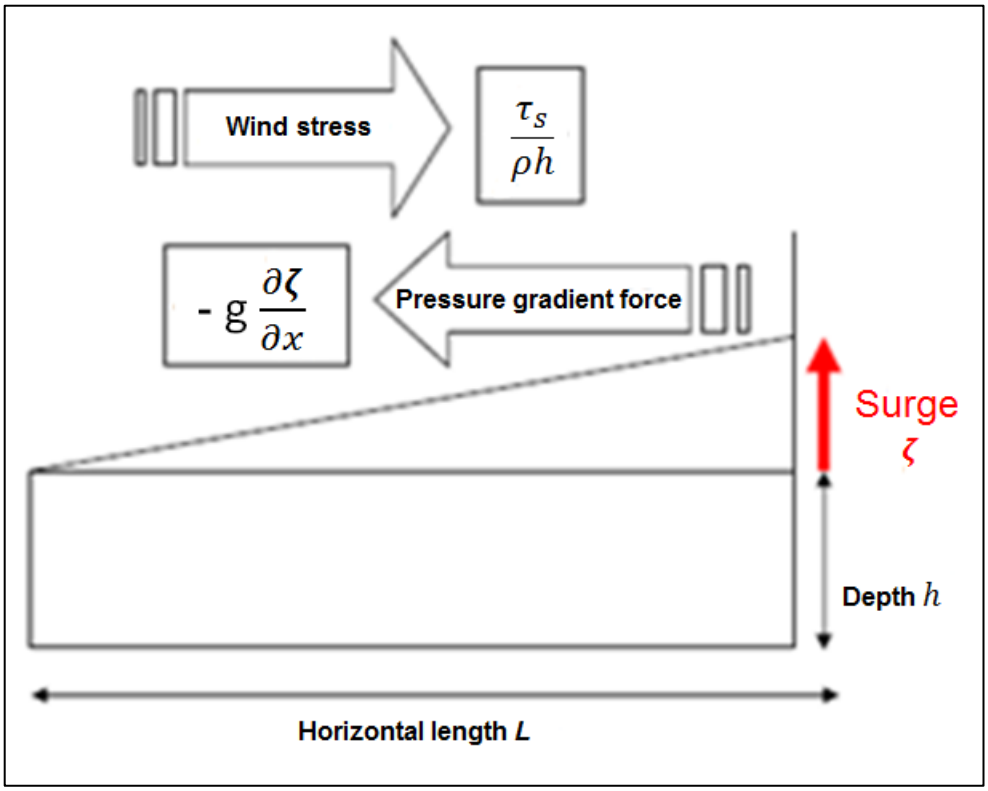

Figure 12. Schematic diagram of the parameters to determine the displacement of water level from the mean due to onshore wind. Source: Nadao Kono – JCOMM 2012 - adapted.

When a component of wind stress acts parallel to a coast line, the onset of Ekman transport is followed by development of water level differences (Pugh and Woodworth, 2014). Those differences have their own influence on the water movements, distorting the simple Ekman transport dynamics. Therefore, a successful storm surge modeling greatly depends on an accurate estimate of the wind stress (Doyle 2002; Moon 2005; Xie et al. 2008).

The parameters which must be known to determine the displacement of water level from the mean, due to alongshore wind, can be seen through the schematic diagram in the Figure 13.

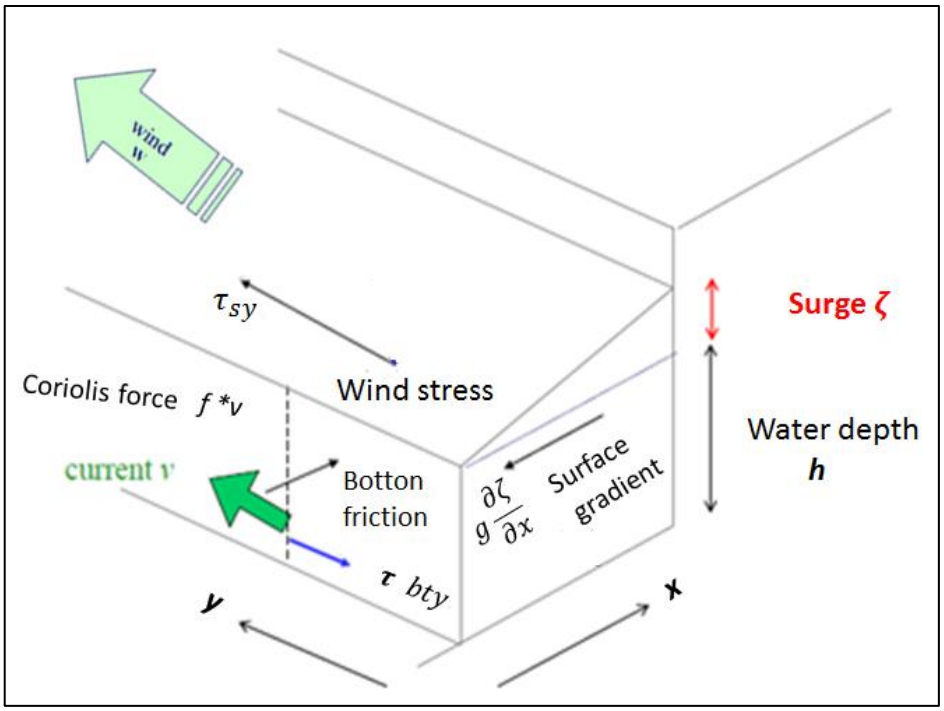

Figure 13. Schematic diagram of the parameters which must be known to determine the displacement of water level from the mean due to alongshore wind. Source: Nadao Kono – JCOMM 2012 – Adapted.

By considering that Mozambique is affected by the southeast trade wind system and receives easterly prevailing winds throughout the year (Tinley, 1971), in conjunction with the clockwise rotation of TC winds, the winds from the South and Southeast quadrants have more influence on storm surge generation, because the wind forcing produces an Ekman current to the left side of the wind propagation (Colling, 2001). This fact leads the water to pile up higher than the ordinary sea level.

From the schematic Figure 12, considering a continental shelf of width L and constant water depth h, no SLP variation and no alongshore wind component, a steady-state balance with null current is quickly established between the surface wind stress ($\frac{\tau_s}{\rho h}$) and

the pressure gradient force ($-g\frac{\partial \zeta}{\partial x}$), due to the slope of the sea surface (Csanady, 1982). This relation can be mathematically written as:

$$g\frac{\partial \zeta}{\partial x} = \frac{\tau_{sx}}{\rho h} \quad \leftrightarrow \frac{\partial \zeta}{\partial x} = \frac{\tau_{sx}}{\rho g h} \tag{3.18}$$

By integrating equation (3.18) through the horizontal length L, leads us to equation (3.19) and the final result is the equation (3.19) which is used for the wind setups due to onshore wind.

$$\zeta = \int_0^L \frac{\tau_{sx}}{\rho g h} dx = \frac{\tau_{sx}}{\rho g h} L \tag{3.19}$$

$$\zeta = \frac{\tau_{sx}}{\rho_w g h} L \quad \leftrightarrow \quad \zeta_z = \frac{\tau_{sx}}{\rho_w g h} L \tag{3.20}$$

From the schematic Figure 13, when the wind blows parallel to the to the coast, it tends to turn the water to the left or right (South Hemisphere or North Hemisphere), due to Coriolis force and Ekman transport. Considering a continental shelf of width L and constant water depth h, no SLP variation and no onshore wind component, the geostrophic balance is established between the pressure gradient force and the Coriolis force. The equation (3.7) is reduced to:

$$g\frac{\partial \zeta}{\partial x} = fV \tag{3.21}$$

At same time, it is assumed equilibrium between the surface shears stress τ_{sy} and the bottom shear stress $\tau_{b\tau y}$ in the Y direction. The equation (3.8) is reduced to (3.22):

$$\tau_{sy} = \tau_{b\tau y} \tag{3.22}$$

$$\tau_{b\tau y} = \rho_w C_D V^2 \tag{3.23}$$

$$\tau_{sy} = \rho_w c_D V^2 \tag{3.24}$$

$$V = \sqrt{\frac{\tau_{sy}}{\rho_w C_D}} \tag{3.25}$$

$$g\frac{\partial \zeta}{\partial x} = f\sqrt{\frac{\tau_{sy}}{\rho_w C_D}} \quad \Rightarrow \quad \frac{\partial \zeta}{\partial x} = \frac{f}{g}\left(\frac{\tau_{sy}}{\rho_w C_D}\right)^{1/2} \tag{3.26}$$

By integrating through the continental shelf from x=0 to x=L, the final result is equation (3.28):

$$\boldsymbol{\zeta} = \int_0^L \frac{f}{g}\left(\frac{\tau_{sy}}{\rho_w C_D}\right)^{1/2} dx \qquad (3.27)$$

.

$$\boldsymbol{\zeta} = \frac{f}{g}\left(\frac{\tau_{sy}}{\rho_w C_D}\right)^{1/2} L \quad \leftrightarrow \quad \boldsymbol{\zeta}_m = \frac{f}{g}\left(\frac{\tau_{sy}}{\rho_w C_D}\right)^{1/2} L \qquad (3.28)$$

Where $\boldsymbol{\zeta}_z$ is the displacement of water level from the mean due to onshore wind, τ_{sx} the onshore surface wind stress, $\boldsymbol{L}$ the platform width, $\boldsymbol{\rho_w}$ the sea water density, $\boldsymbol{g}$ the gravitational acceleration, $\boldsymbol{h}$ the depth of the water column, $\boldsymbol{\zeta}_m$ is the displacement of water level from the mean due to alongshore wind, $\boldsymbol{f}$ the Coriolis parameter, $\boldsymbol{v}$ is the current, τ_{sy} the alongshore surface wind stress and $\boldsymbol{C_D}$ is the bottom drag coefficient considered as 0.002 (Menemenlis et al. 2007).

Santos and Miranda (2006) in their STS study and Menemenlis et al. (2007) have used equations (3.20) and (3.28) to calculate the displacement of water due to on shore and alongshore wind setup.

3.3. Data Processing and Analysis

With a view to reach to a certain conclusion for a given situation or problem, data analysis is used as a process to revise, transform and remodel certain information or data. One of the most important uses of data analysis is that it helps in keeping human bias away from research conclusion with the help of proper statistical treatment. Data analysis helps a researcher to filter both qualitative and quantitative data for an assignment research. Thus, it can be said that the process is of utmost importance for both the research and the researcher.

Due to the scarcity of historical storm surge data in Mozambique, extrapolation of trends in past storm activity is generally not a useful approach. TG stations measure the variation in water level along the coast. Since tidal cycles are predictable, storm surge can be calculated by subtracting what the water level would have been in the absence of the storm from the measured water level.

Atmospheric pressure and extreme wind stress processes are usually considered to be the source of storm surge generation. The combination of astronomical tide and storm surge determines the sea level (Santos and Miranda, 2006). In this study we do not assess the relative likelihoods of inundations zones affected by those storm surge scenarios.

The proposed methodology does not pretend to assess the inundation in the coast due to storm surge. The basic methodology presented here however could be extended to assess a range of different impacts areas or sectors.

3.3.1 Storm Surge Calculation from TG data

Hourly values of 3 TGs distributed along the coast of Mozambique namely in Pemba, Beira and Maputo, the North, Center and South region respectively (Figure4), are used to validate model results, specifically for large and extreme SL anomalies. The period considered for the validation is integrated in the time series of atmospheric data from NOAA which is from 1973 to 2011. However the length of time series differ from station to station, spanning from few years to the whole considered period, as clearly depicted in Appendix B.

Based on storm surge definition, in line with Pugh (1987), the storm surge is calculated by subtracting the harmonic tidal predictions from the observed sea level. This was done by means of a harmonic analysis carried out with the standard program T-Tide (Pawlowicz et al., 2002). The program T_Tide, Harmonic Analysis Toolbox for Matlab, developed by Rich Pawlowicz at UBC, takes a raw tidal time series as input and outputs the amplitude and phase of the harmonic constituents for the time series, along with error estimates. Is a package of routines that can be used to perform classical harmonic analysis with nodal corrections, inference, and a variety of user specified options. Predictions can also be made using the analyzed constituents. The data used in the study were quality checked and the null values (NaN) were used in the gapes of data where it was needed.

In this way, the validation of the meteorological tide data was done by following the steps below:

- To obtain the harmonic constants of each TG;

- To forecast the astronomical tide for the same period, measured by TG through the harmonic constants obtained in step before;
- To calculate the difference between the predicted and the measured value of astronomical tide. This residual value corresponds to the series of meteorological tide;
- To compare the meteorological tide values obtained from reanalysis with those obtained from TG.

Here we have considered meteorological tide as the residual from the observed and predicted tide. The storm surges are identified by considering higher percentiles of the meteorological tide distribution.

Post-processing of the data was accomplished using T_Tide software developed in the Matlab® (http://www.mathworks.com/) programming language. Most Matlab® M-files used for post-processing are available via the World Wide Web (WWW).

3.3.2 Storm Surge calculation from Atmospheric forcing from NOAA

Storm surge is usually considered to be driven by two processes namely the atmospheric pressure and extreme wind stress. An analytical model was used, which consider the atmospheric pressure and wind components. The inverted barometric effect, which is the response of sea level to changes in atmospheric pressure was used with sea level pressure data to estimate the perturbations of the sea level by using equation (3.11) and the result was added to the one obtained from the wind setup effects, which was decomposed into an onshore and alongshore components, equations (3.20) and (3.28) respectively (Santos and Miranda, 2006; Wannawong and Ekkawatpanit, 2012). Those equations represent the three main storm surge forcing used in the study.

For validation of this step, storm surge results from TG and from analytical model were compared, through the statistical analysis by calculating error measures, correlation and an index of agreement. To best evaluate differences of the distributions between the analyzed results of storm surge obtained from TG and from analytical model (by using data from NOAA), the probability density functions (PDFs) have been estimated and compared. The PDFs were estimated using the Kernel method, following Silverman (1986), with a normalized Gaussian as the Kernel function.

A kernel distribution is a nonparametric representation of the PDF of a random variable. It can be used when a parametric distribution cannot properly describe the data, or when is needed to avoid making assumptions about the distribution of the data. This distribution is defined by a smoothing function and a bandwidth value that controls the smoothness of the resulting density curve. In kernel estimation, the choice of the smoothing parameter is much more critical than the choice of the kernel. Yet, for each PDF in this study, a default bandwidth was used which is optimal for normal densities.

The provided wind data from NOAA consists of the wind speed and wind direction. Nevertheless, the calculation of wind components "*u*" and "*v*" had to be done. By having the wind speed and direction, "*u*" and "*v*" wind vector components can be calculated.

The wind components "*u*" and "*v*" used in equations (3.13) and (3.14) were calculated by applying trigonometric equations, taking in consideration the wind direction:

$\varphi met \leq 90°$: wind blowing from Quadrant I to Quadrant III

$$u = -W \sin(180° - \varphi met) \quad v = -W \cos(180° - \varphi met) \tag{3.29}$$

$90° < \varphi met \leq 180°$: wind blowing from Quadrant II to Quadrant IV

$$u = W \cos(\varphi met - 90°) \quad v = -W \sin(\varphi met - 90°) \tag{3.30}$$

$180° < \varphi met \leq 270°$: wind blowing from Quadrant III to Quadrant I

$$u = W \sin(\varphi met - 180°) \quad v = W \cos(\varphi met - 180°) \tag{3.31}$$

$270° < \varphi met \leq 360°$: wind blowing from Quadrant IV to Quadrant II

$$u = -W \cos(\varphi met - 270°) \quad v = W \sin(\varphi met - 270°) \tag{3.32}$$

where φmet is the meteorological wind direction, W is the wind speed, *u* and *v* are the zonal and meridional wind components, respectively.

Cross correlations among the sea level, atmospheric pressure and wind stresses were calculated. The meteorological forcing contains the wind stress and sea level pressure data at specified time intervals. The zonal and meridional wind stress are computed from the wind speed and direction using equations (3.13) and (3.14).

In order to make this conversion, there is a need to decide on the equation to use for the drag coefficient because there are numerous relationships that attempt to parameterize

the drag coefficient. Without further insight into the optimal drag coefficient response to high winds, we accept the formulation from specific author (Large and Pound, 1981; Smith, 1980 and Powell et al., 2003) for specific wind intensity also, as it is simple and seems to capture the middle of the road solution. The drag coefficient is calculated by considering wind intensity according to equations (3.15), (3.16) and (3.17).

3.3.3 Storm Surge calculation from Atmospheric forcing from CIMP5

The analytical model was used with sea level atmospheric pressure and wind data generated by the MPI-ESM-LR model, to evaluate changes in the statistical properties of storm surges for future climate change scenarios along the Mozambican coast. The data for the present climatological period, from 1986-2005, were computed by using the validated analytical model. Then, the results were compared with the one obtained by using data from NOAA, to see whether the MPI-ESM-LR model data can reproduce the NOAA data. The results are shown later for percentiles 95 (P95), 99 (P99) and 99.9 (P99.9) associated with significant, very significant and highly significant storm surges, respectively.

3.3.4 Tropical Cyclone Climate Intensity at SWIO basin

When examining the scientific literature, it is apparent that the frequency, distribution and intensity of cyclones are major fields of interest (Terry, 2007). However, for this study only the intensity is considered because the study concerns the STS height for the future and not the return time of STS with such height.

Considering that climate models do not fully resolve the characteristics of TCs due to their relatively low spatial resolutions (Camargo and Wing, 2016), there is a need to consider this with further calculations.

The calculation is done again, considering the average wind intensity from tropical cyclone. The average intensity of TC in SWIO is calculated based on the historical data of major TC that occurred in SWIO basin. The period is from 1985 to 2015 and the related data are shown in Appendix C.

From here on we assume that the MPI-ESM-LP is not able at all to resolve TC. Indeed, Camargo and Wing (2016) mention that TC-generated STS simulated by climate models constitute a small part of the real STS. Therefore, we added the TC cyclone generated STS to P95, P99 and P99.9 which define the STS in this study, namely, the contribution due to the TC climatological values of a sea-level pressure of 940 hPa and a wind speed of 160 km/h, as mentioned before

Following the projections by Knutson et al. (2010), it is likely that the global frequency of tropical cyclones will either decrease or remain essentially unchanged while the mean intensity (as measured by the maximum wind speed) increases by +2 to +11% . Other authors concluded that the intensity will be larger than 10% in some basins (Emanuel et al., 2008; Bender et al., 2010; Knutson et al., 2010, 2013; Yamada et al., 2010; Murakami et al., 2012). In the study done by Dasgupta et al. (2009a) they also used a range of 10% increase of TC intensity.

For this study were considered the 10% increase on TC intensity. This percentage was added to the average climate TC intensity obtained from 1985-2015. Those TC intensity values were used to aggregate in the calculation of storm surge for future climate scenarios.

3.3.5 Inclusion of Future Sea Level Rise in Storm Surge Calculation

Sea Level Rise, as a result of climate change may also have an important effect on the damage that could result storm surge. In addition, future SLR, while uncertain, is more reliably forecasted to 2050 than future storm activity. In general, the increase in sea level would make existing storms significantly more damaging, even for minimal changes in storm activity. The results from the study of Church et al. (2011) show that the global sea level is rising and is expected to continue to rise on a multi-centennial to millennial time scale (Yin 2012, IPCC 2013).

Taking in consideration this future behavior of the sea, the projections for the future storm surge scenarios have to consider the SLR. Considering the uncertainty on future sea level, this analysis is not based on a single SLR scenario. Instead, three possible amplitudes of SLR are considered and results are presented for all these cases without trying to aggregate results for these possible futures.

The projections scenarios of SLR used in this study to incorporate in a storm surge calculation for near, medium and long term future climate scenarios are 0.12, 0.39 and 0.72 m, respectively.

Dasgupta et al. (2009a), in their study, have considered one unique value of 1 meter for SLR for 2100, while Neumann et al. (2013) have considered three SLR scenarios as low (0.156 meters), medium (0.285 meters), and high (0.378 meter) based on the work of the IPCC (Meehl et al., 2007) and Rahmstorf (2007). Both studies were used in analyses supporting the World Bank's Economics of Adaptation of Climate Change (EACC). Local SLR may differ from global average SLR due to local factors such as change in bed elevation, coastal geometry, glacial isostatic adjustment and land water sources, amongst others. However this represents typically a small variation relative to the global average and are, therefore, not considered here. As such, we have used the global average SLR and not the local SLR. This can be clearly seen in Figure 14 which shows the spatial distribution of SLR in 2081-2100 relative to 1986-2005 for the RCP8.5 scenario. Local SLR along the coast of Mozambique is indeed similar and even greater that the global average of SLR shown in Figure 9 which means that we can even be underestimating the SLR in the region.

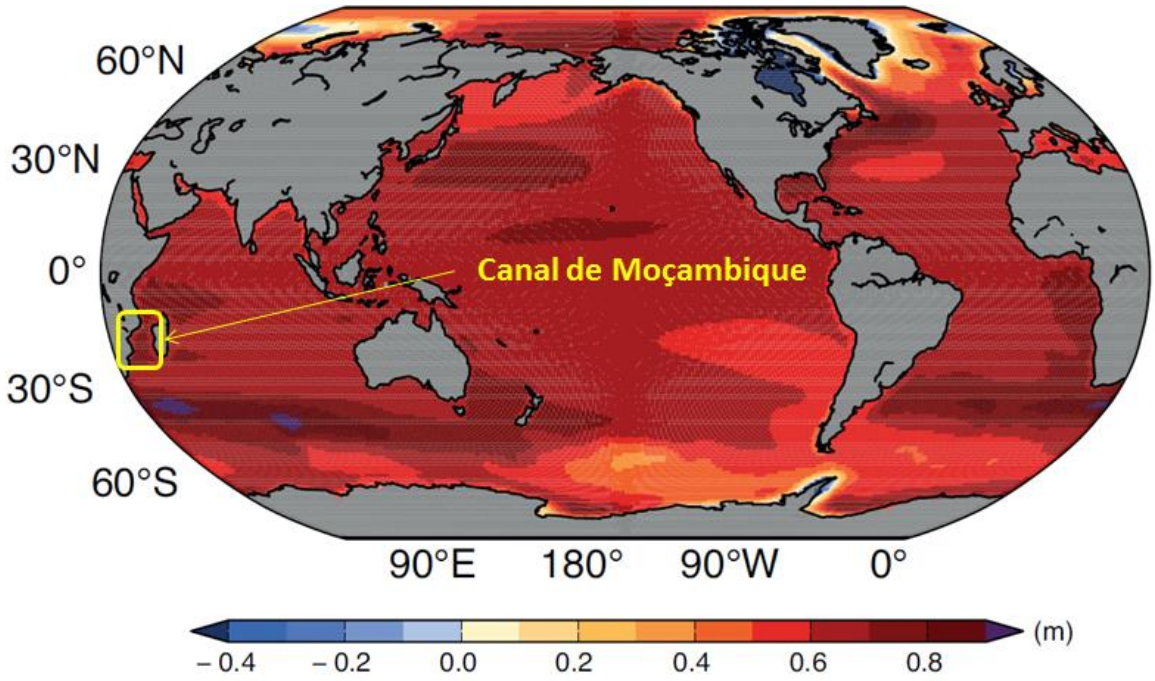

Figure 14. Mean regional relative sea level change evaluated from 21 CMIP5 models for RCP8.5. Source: IPCC, 2013 - Adapted.

3.3.6 Statistical Analyses

As a tool for the classification of storm surge and validation of the analytical model, three classes of storm surges namely significant, very significant and highly significant were defined for sea levels above P95, P99 and P99.9, respectively (Gama et al., 1994; Marcos et al., 2011, Gaslikova et al., 2011). Statistics for the evaluation and comparison of models were done accordingly by using Root Mean Square Error – RMSE, equation (3.33) and index of agreement, equation (3.34)

$$\mathrm{RMSE} = \sqrt{\frac{1}{n}\sum_{i=1}^{n}(f_n - r_n)^2} \tag{3.33}$$

where f is the predicted value, r is the observation value and n is the total number of points in a spatial-temporal combined space.

Following Willmott (2012), the index of agreement *"d"* is used especially for validating prediction models. It represents the ratio of the mean square error and the potential error and is defined by the equation (3.34), where "*o*", "*p", "$\bar{o}$"* and "$\bar{p}$" represents observed, predicted, average of observed and average of predicted data respectively, The index of agreement is a bounded and non-dimensional measure.

$$d = 1 - \frac{\sum_{i=1}^{n}(o_i - p_i)^2}{\sum_{i=1}^{n}(|p_i - \bar{p}| + |o_i - \bar{o}|)^2} \tag{3.34}$$

Chapter IV – Results and Discussion

4.1 Results for the Historical Period

4.1.1 Storm Surge from Sea Level Variability - Tide Gauges.

We analyzed TG data from the three stations namely from Maputo in the south, Beira in the center and Pemba in the north of Mozambique Channel. In the analysis of TG data all events, positive and negative residuals were considered.

The meteorological tides were obtained by applying the T_Tide Software to filter the observed sea level time series at the three stations. Figures 15, 16 and 17, show the results from Maputo, Beira and Pemba stations respectively. The observed sea level are represented in the black, the predicted in green, the meteorological tide in red and the day moving average of meteorological tide in blue color. The calculated difference between the TG observed and predicted time series, resulted in a time series of the sea level due to meteorological forcing. The time series filtered with the moving average of 24 hours, are only shown here for the purpose of identifying more clearly the lower frequency oscillation of the time series. They are not used later in the analysis. This is accomplished using the unfiltered time series (red curves). The harmonic constituents used to predict the tide for Maputo, Beira and Pemba are presented in Appendix D, E and F respectively.

Three classes of storm surges (STS), are defined, namely significant, very significant and highly significant associated with percentiles P95, P99 and P99.9, respectively. The results are shown in Figure 18.

From the meteorological tide calculated with the analytical model for the three TG station, the maximum values obtained are 0.39 m, 1.06 m and 0.58 m for Maputo, Beira and Pemba, respectively. The maximum observed sea levels for the stations were 1.9 m, 3.59 m and 2.25 m, respectively. For the period that the analyses refer to, for Maputo and Pemba stations, there is no tropical cyclone event associated. So we did not expect large variations in the TG registrations for this period.

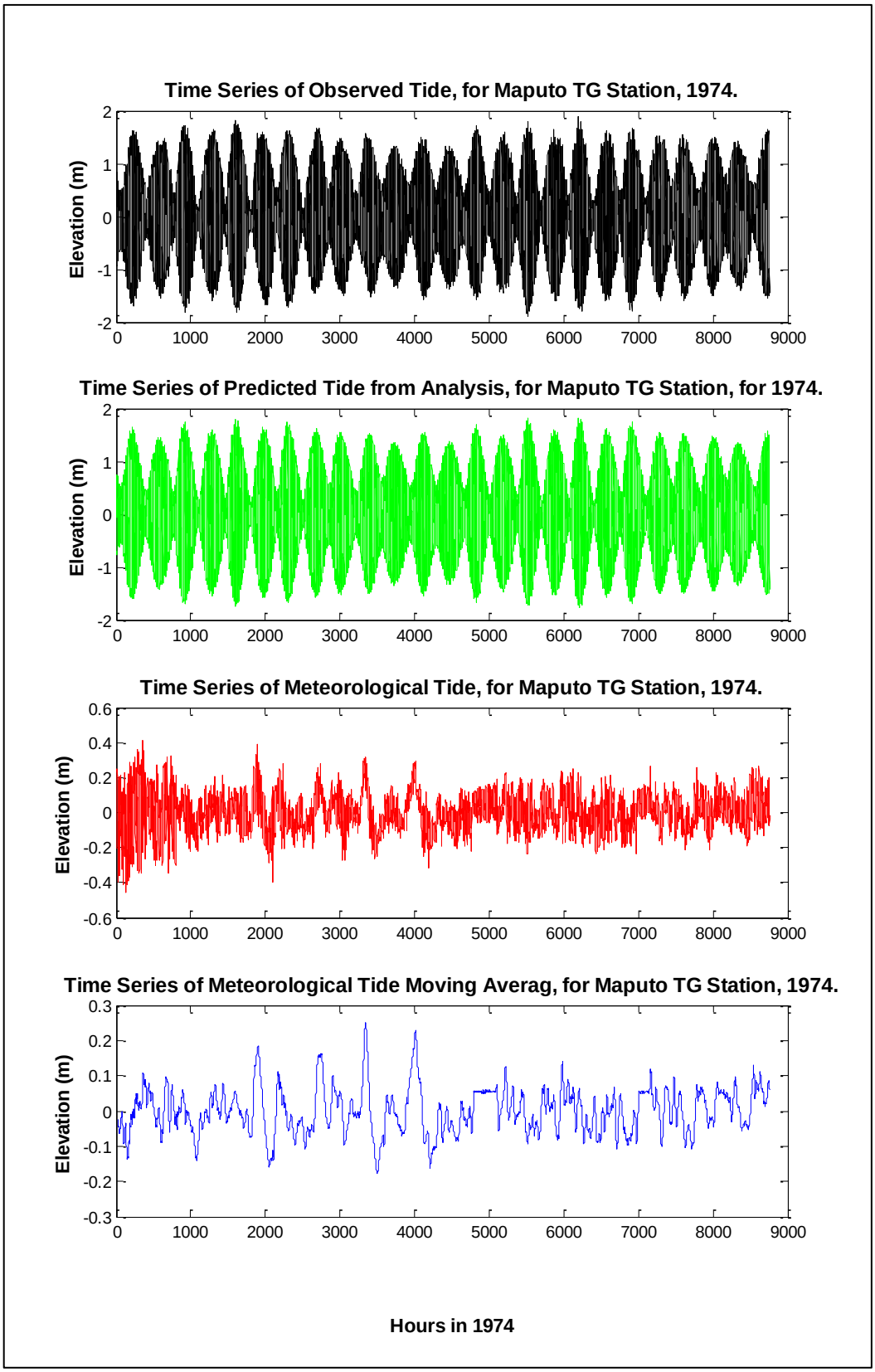

Figure 15. Oscillations of observed (black), predicted (green), filtered (red) and moving average (blue) of sea level time series for Maputo TG station, for 1974**.**

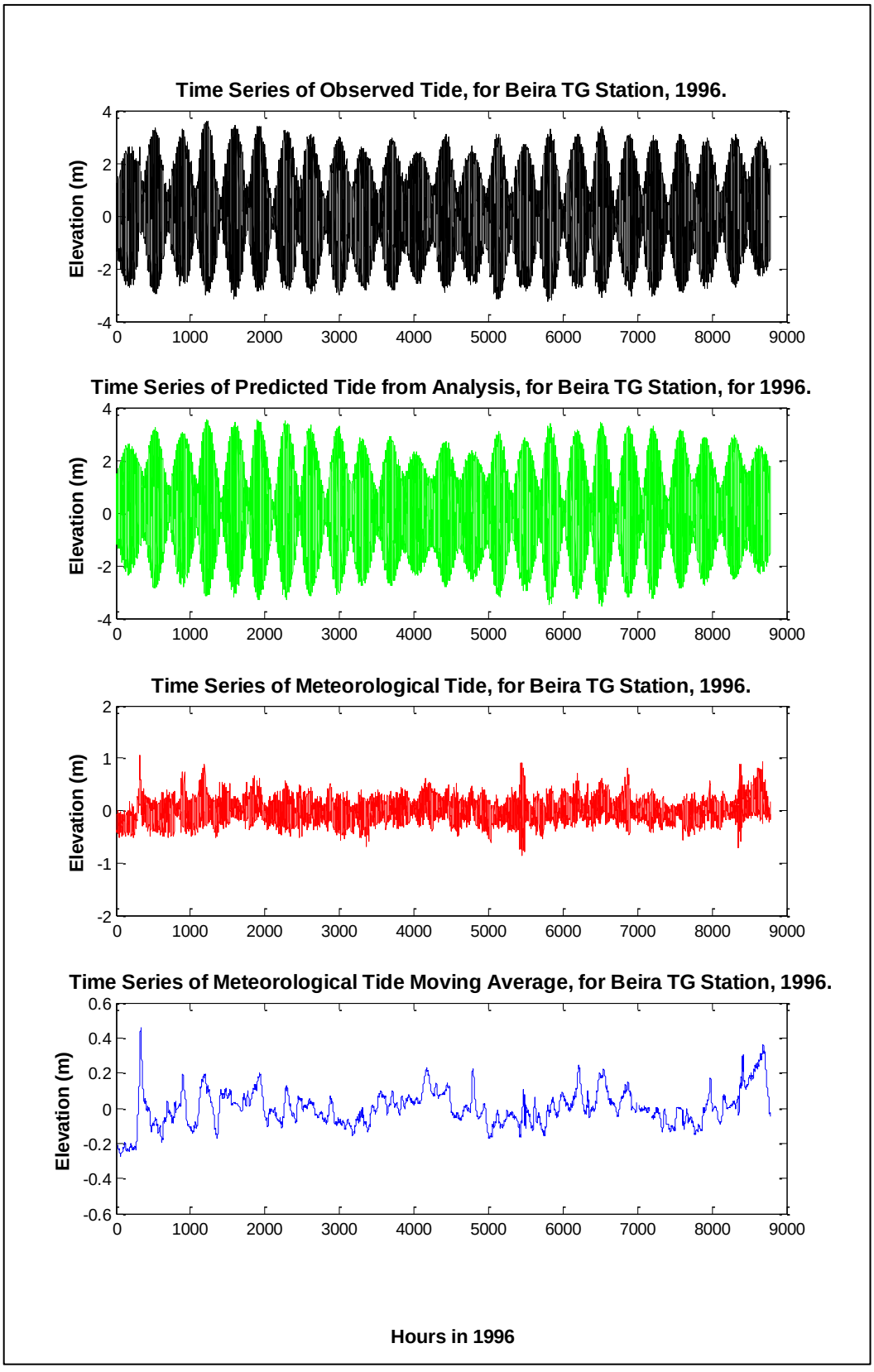

Figure 16. Same as Figure 15, but for Beira Station.

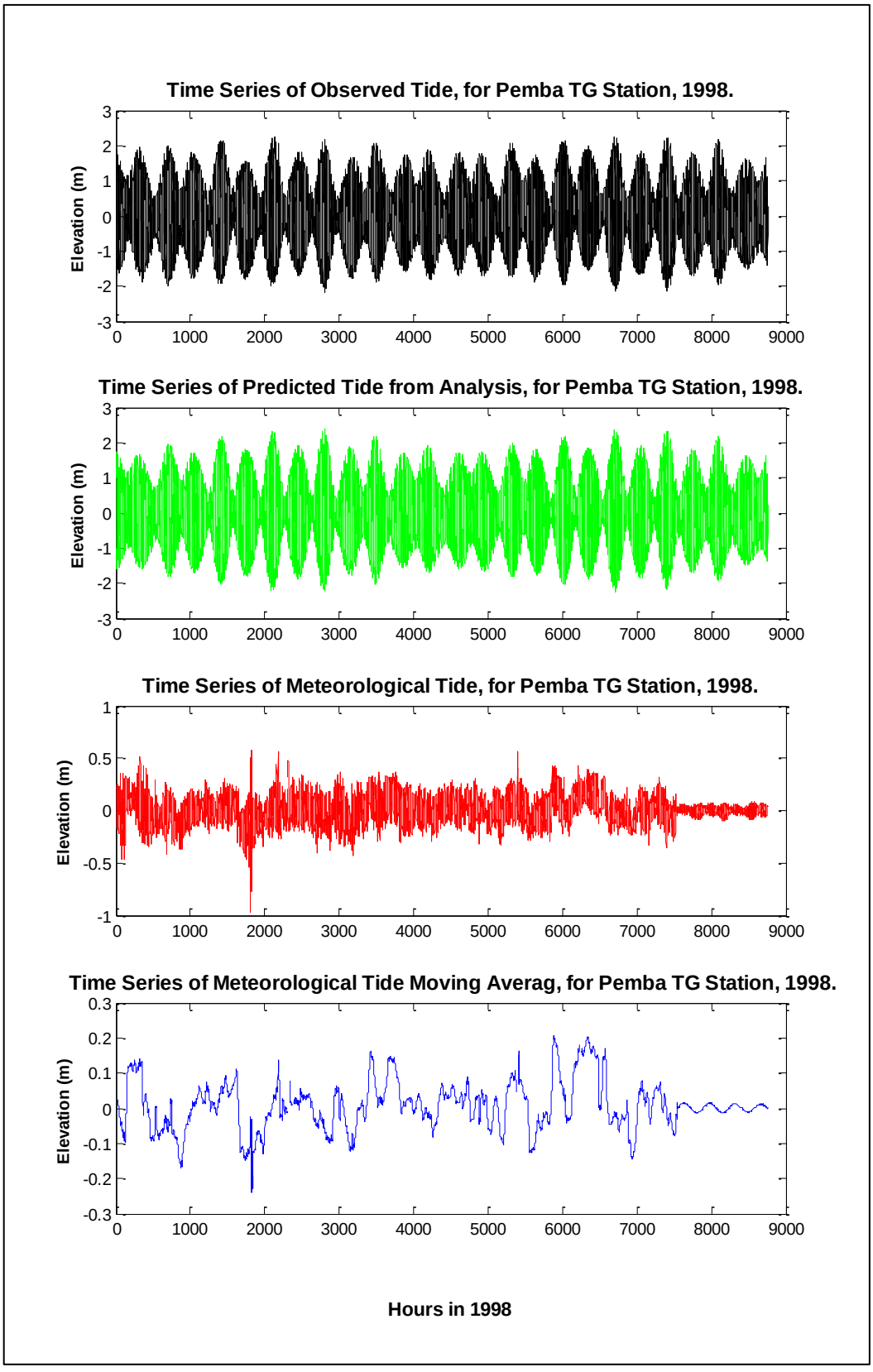

Figure 17. Same as Figure 15, but for Pemba Station.

For Beira station, the period of analysis coincides with the passage of an intense TC named Bonita, in January 1996 (Appendix G.3), in the north part of Beira, not far away from the TG station of Beira. Yet, the Beira TG station registered the changes in sea level due to the passage of this TC, which proved destructive in northern Mozambique, notably in the provinces of Cabo Delgado, Nampula and Zambezia. The storm extensively damaged about 400 houses in the city of Quelimane, which was left with severely impaired electric facilities. At the time no TG were operational in Quelimane. Appendix H presents a detailed list of TC landed in Mozambique where TC Bonita is included.

This is explained by looking at the calculated STS from TG for Beira for 1996 which has higher values, 0.83 m for the class of P99.9 and a maximum of 1.06 m if compared with Maputo and Pemba stations. The STS values obtained from observed meteorological data from NOAA also features the same, despite presenting relatively lower values (Figure 18), yet the values are close.

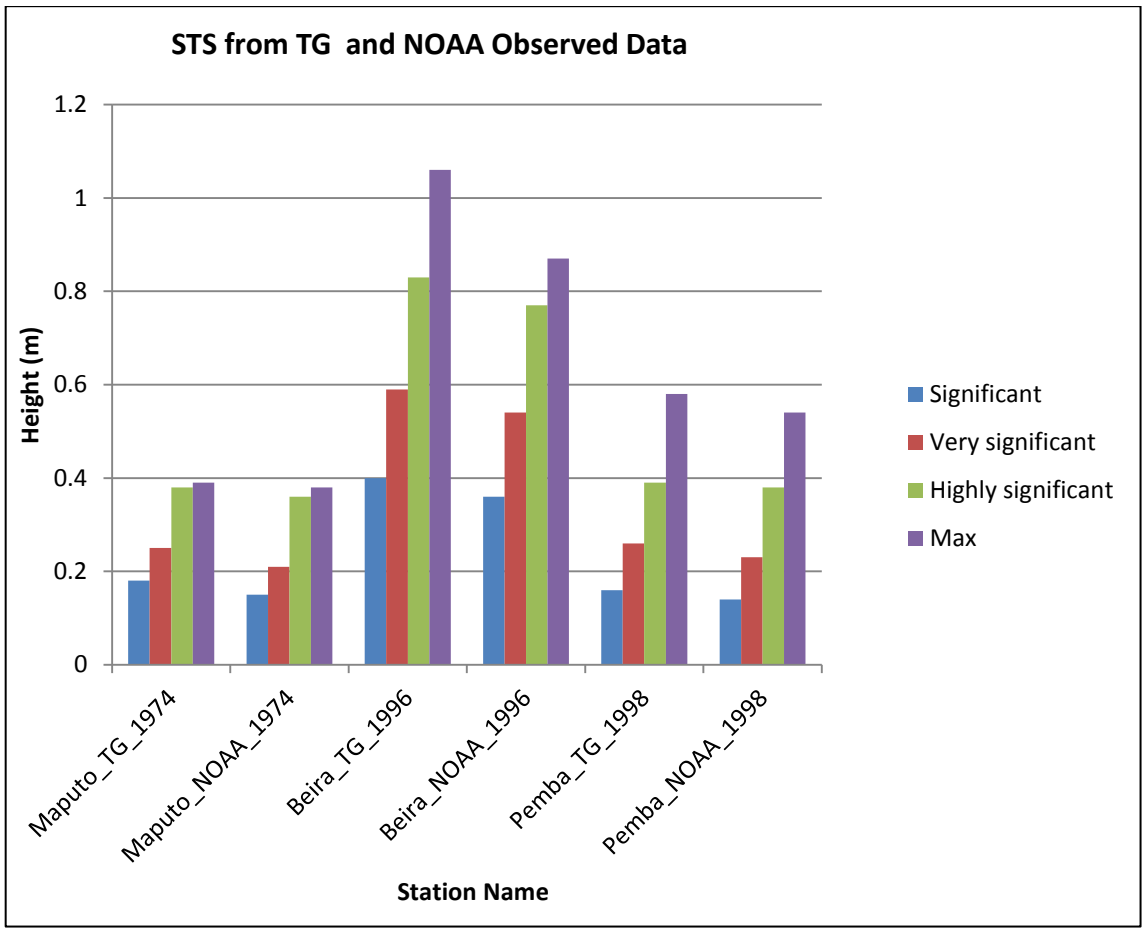

Figure 18. STS percentiles, P95 (significant), P99 (very significant) and) P99.9 (highly significant) as defined in section 3.2.3, for TG data and NOAA derived data.

From the analysis done, this fact took place because, while the TC was affecting the near province of Zambezia causing disturbance in the sea levels, the weather parameters at Beira station did not change much. This can be explained by considering the distance at which the TC eye made its landfall. Nevertheless, the propagation of sea level disturbance has reached Beira station TG, resulting in an observed maximum of 1.06 m storm surge. This category IV TC was characterized by sustained winds of 185 km/h and the SLP dropped to 920 hPa. The maximum storm surge height registered by this TG does not represent the maximum STS that a TC can cause for Beira station. Other TC track that crossed near the TG station are shown in Appendix G1, G2 and G4.

By analyzing and considering a normal behavior of sea level variation, for the stations of Maputo, Beira and Pemba, it can be seen that the STS calculated for Beira, from TG data for 1996, shows an abnormal variation of sea level which coincides with the passage of TC Bonita in this period. This fact is found also in STS calculated from observed data from NOAA, despite the value being relatively smaller. This STS comparison between TG and NOAA derived data is shown in Figure 18 using the percentile defined in section 3.2.3, namely P95 for significant, P99 for very significant and P99.9 for highly significant STS.

As mentioned before, at this stage we want to verify whether the observed atmospheric-derived meteorological tide using data from NOAA with the analytical model can reproduce the behavior of meteorological tide obtained from TG. The objective is to validate the analytical model to be used later with atmospheric data simulated by the MPI-ESM-LR model in climate change studies. After obtaining the results of meteorological tide from TG, the analytical model was used with atmospheric observed data, wind and sea level pressure, to obtain meteorological tide.

Figure 19 shows the PDFs of meteorological tide for Maputo, Beira and Pemba using both methods. It is clear that, for each local, there is a very good agreement between the PDFs of the meteorological tide calculated (NOAA derived) and observed (TG) .

Small differences between PDFs may be due to the fact that the analytical model only considers the influence of wind and atmospheric pressure whereas the observed meteorological tide from TG considers also other local factors such as batimetry and wave setup. Figure 20 shows the dispersion graphics and the respective linear fits of meteorological tide obtained from both methods. Again, the match is strong.

The correlation coefficients between the meteorological tides obtained from both methods are 0.98, 0.97 and 0.98 for Maputo, Beira and Pemba station, respectively. Those correlations are in line with the index of agreement between them with values equal to 0.98, 0.96 and 0.97, respectively. Both are highly statistical significant. Table 4 shows these measures together with the RMSE which is also very small confirming that the analytical method used with meteorological observed data from NOAA agree well with TG data.

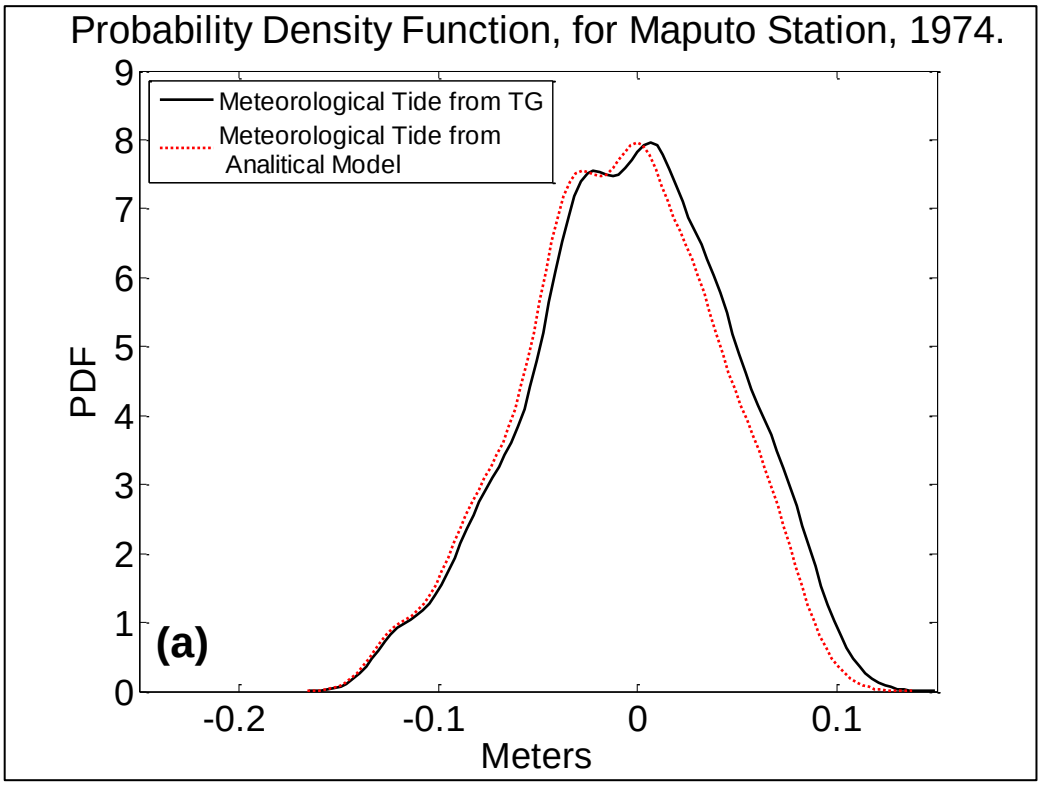

Figure 19 (Continued on next page, see caption)

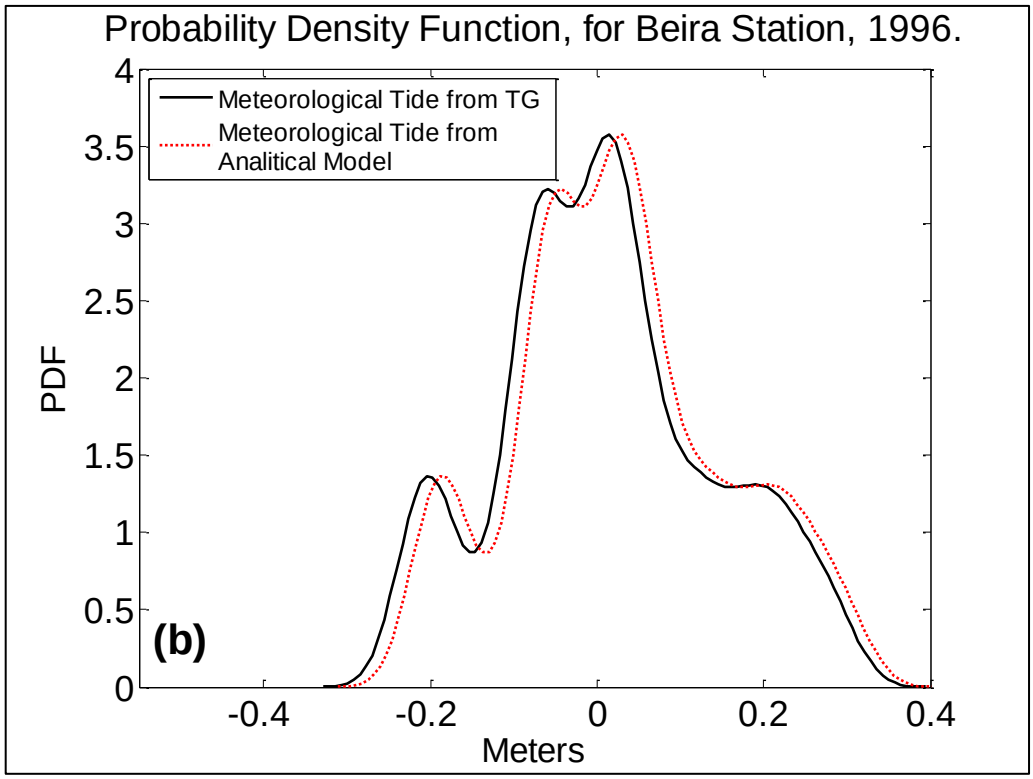

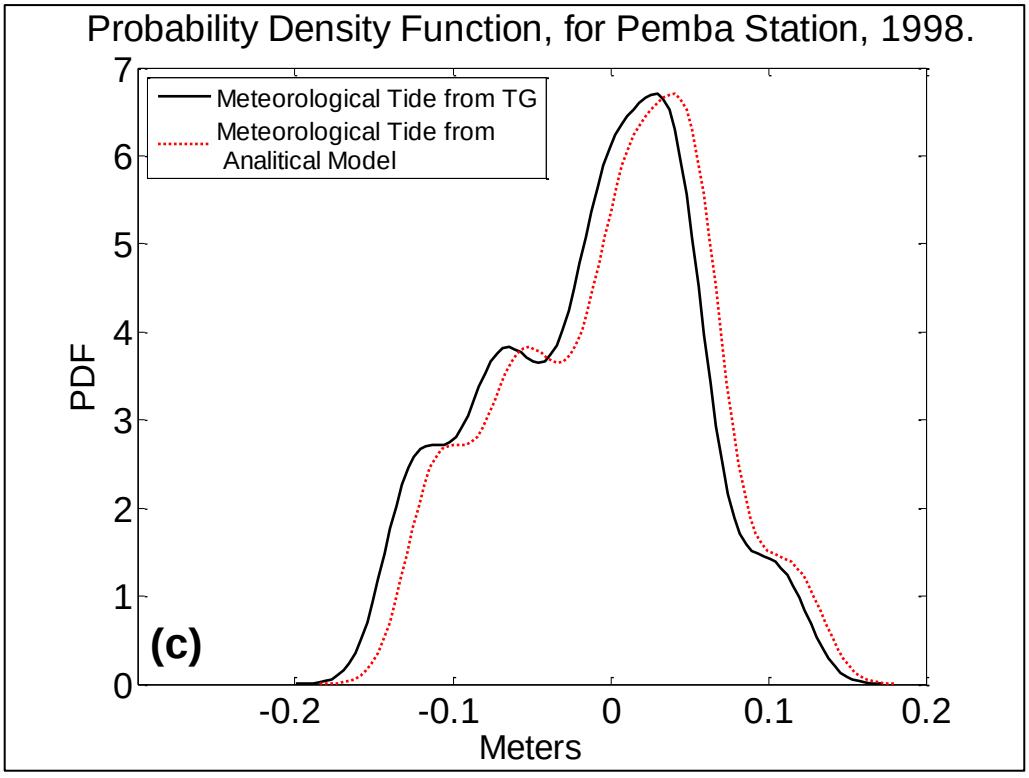

Figure 19. Probability density function (PDFs) of Meteorological tide from TG (red) and analytical model (black), for Maputo (a), Beira(b) and Pemba(c) Station.

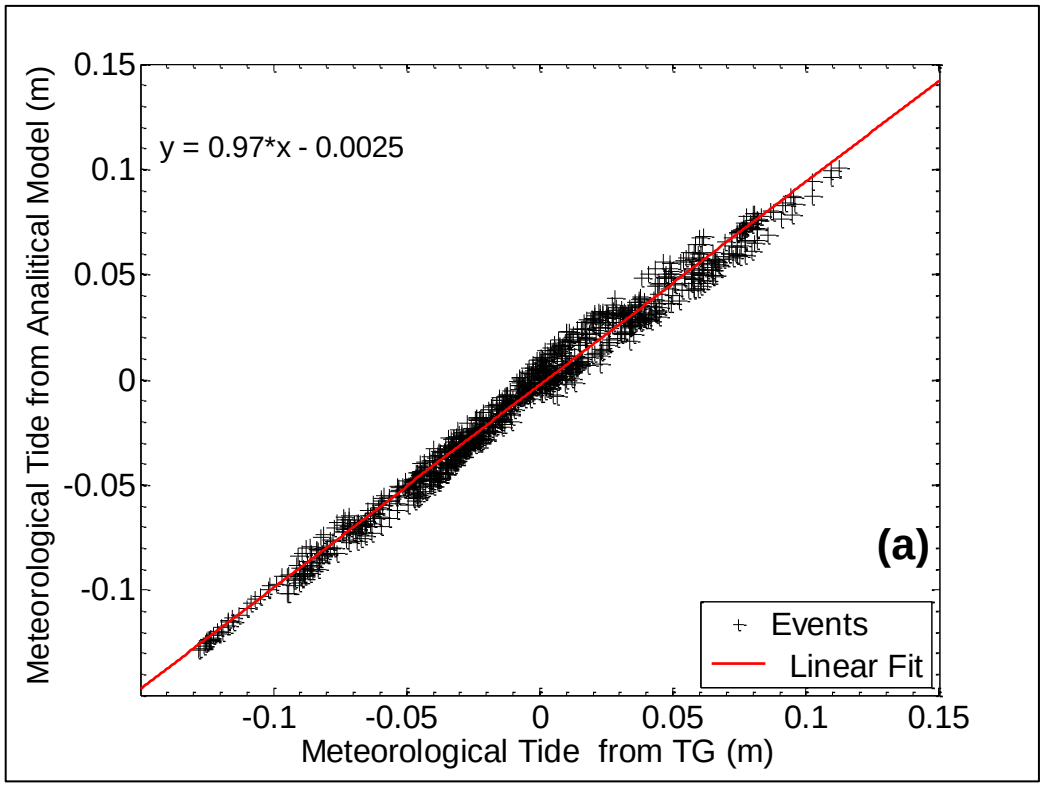

Figure 20 (Continued on next page, see caption)

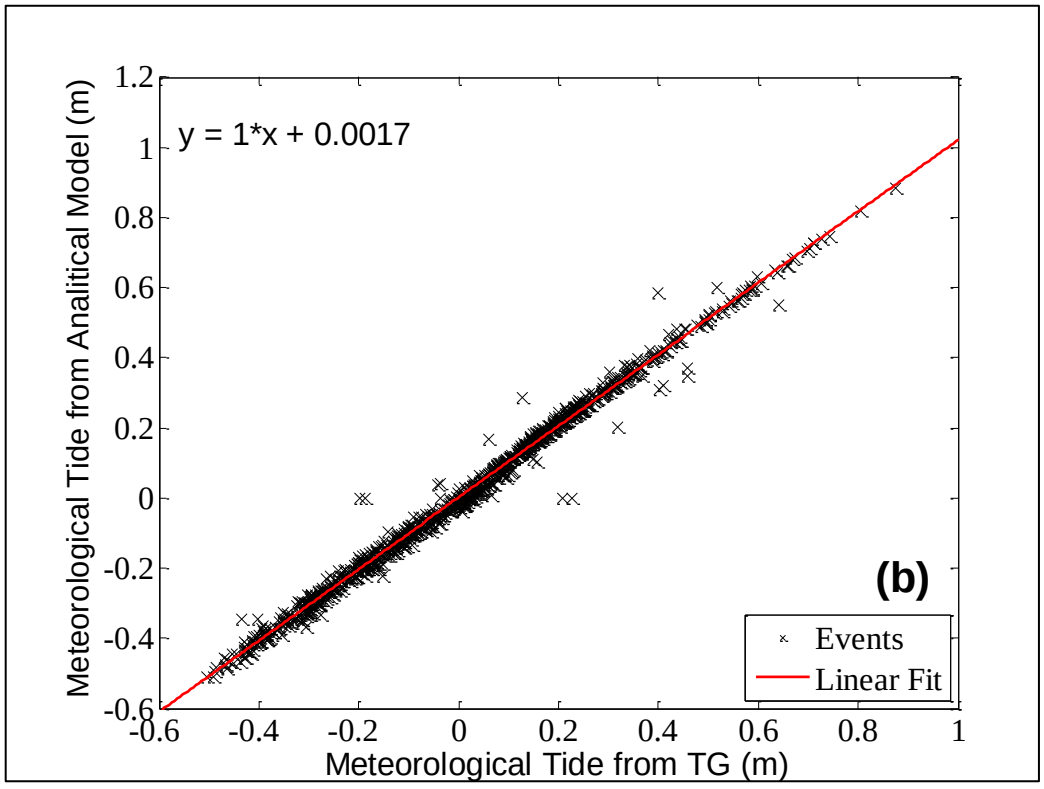

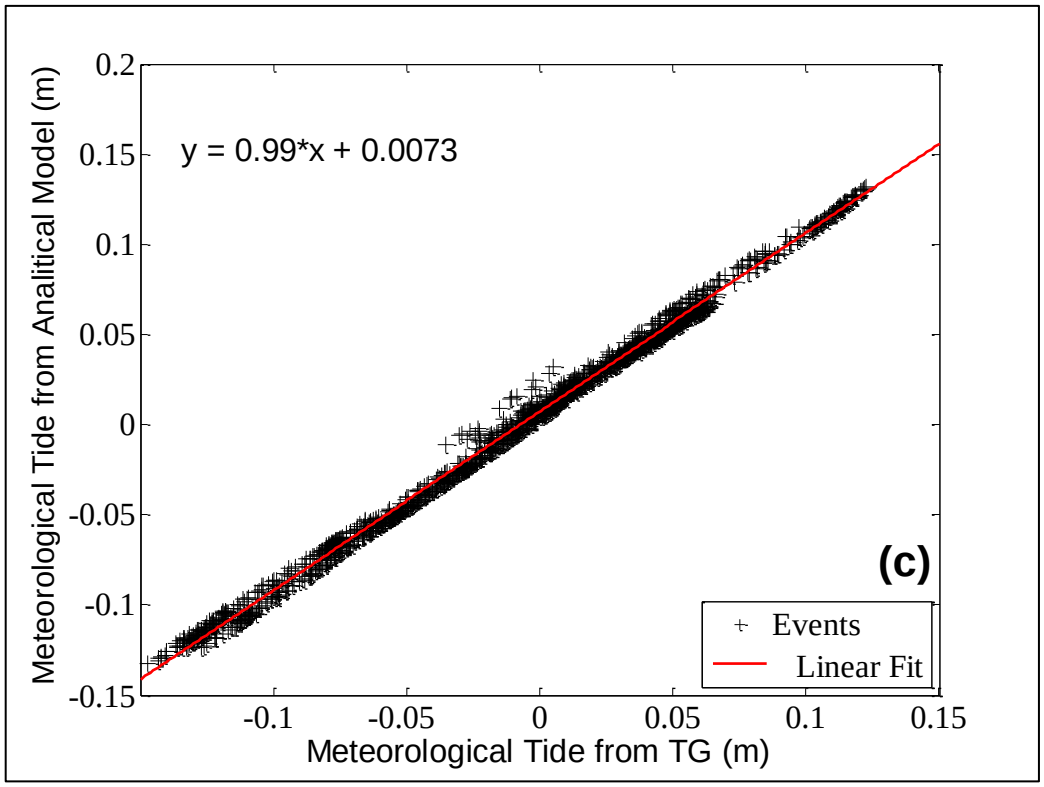

Figure 20. Dispersion graphics and respective linear fits of meteorological tides obtained from both methods, namely from TG and the analytical model, for Maputo 1974 (a), Beira 1996 (b) and Pemba 1998 (c) Station.

Table 4. Statistical analysis of Meteorological Tide from TG and NOAA for Maputo, Beira and Pemba stations.

	Stations		
	Maputo	**Beira**	**Pemba**
Correlation	0.98	0.97	0.98
RMSE	0.02	0.03	0.01
Index of Agreement	0.98	0.96	0.97

4.1.2 Storm Surge From Analytical Model, by Using Historical Wind and SLP Data from NOAA and MPI-ESM-LR

After the first validation stage, the next stage is to evaluate if the meteorological tide calculated using the analytical model, with the historical observed atmospheric data from NOAA and atmospheric data from the MPI-ESM-LR model, agree. If this second validation stage is passed, one may use the analytical model with future climate data scenarios simulated by the MPI-ESM-LR model.

The meteorological tide data for the historical period, from 1986-2005, were computed by applying the analytical model to near surface atmospheric pressure and winds simulated by the MPI-ESM-LR model. The calculations were performed for all seven stations, for which sea level pressure and winds are available from NOAA.

Figure 21 shows the STS for both datasets using the percentiles defined in section 3.3.3, for highly significant STS. The TC effect has not been considered here. The results obtained shows STS heights much higher for NOAA than for MPI-ESM-LR, despite the good agreement between the STS percentiles. However, except for Quelimane, the three SST percentiles are slightly underestimated by the MPI-ESM-LR when compared to NOAA.

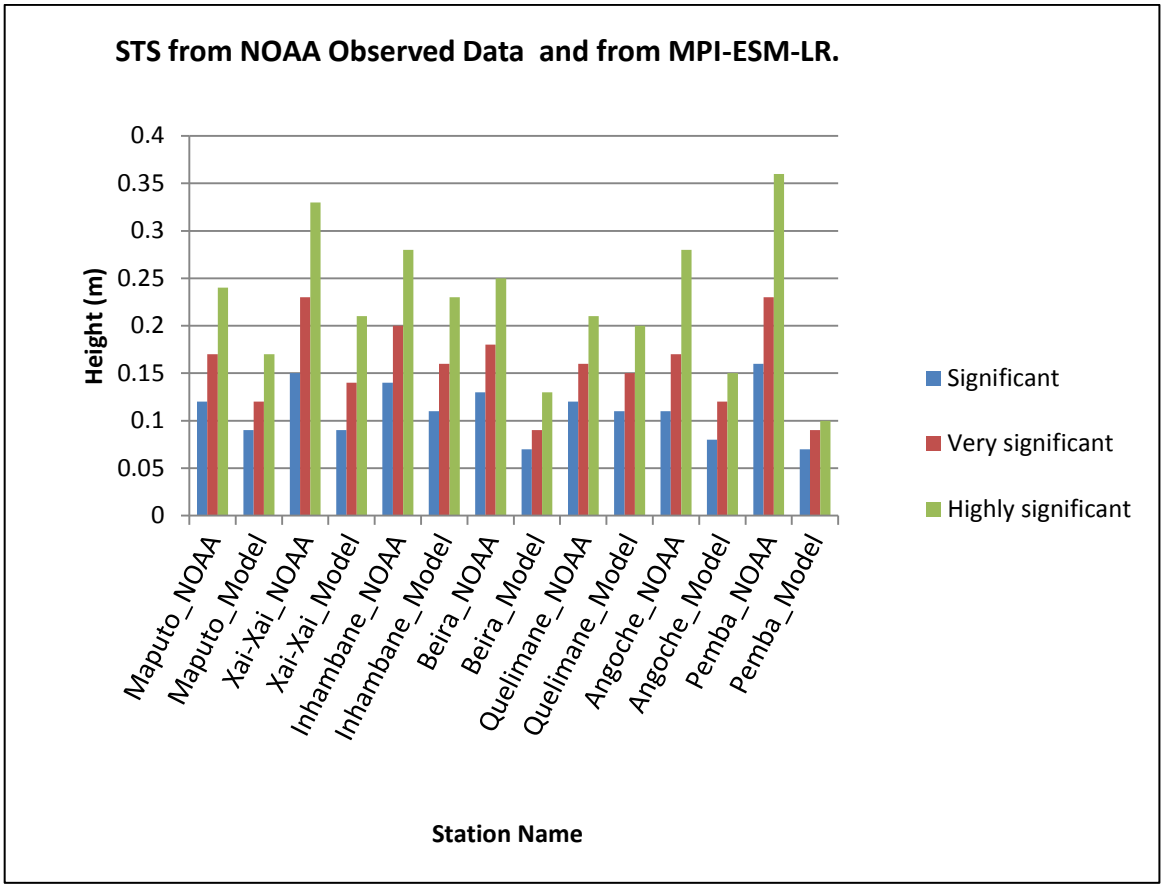

Figure 21. Significant (P95), very significant (P99) and highly significant (P99.9) storm surge for NOAA Observed and from MPI-ESM-LR, for the seven stations.

The reason for this is that the properties of TCs, in particular wind speed, pressure gradients and, consequently, the minimum pressure of TC are underestimated by climate models (Camargo and Wing, 2016) such as the MPI-ESM-LR due to their relatively low horizontal resolution to characterize these phenomena. If climate models, such as the MPI model did not capture the TC at all, one would consider an underestimation of about 10% in the simulation of its intensity. However, climate models simulate partially the TC and, as such, some of the underestimation of the STS simulated by the MPI-ESM-LR model, as seen in figure 21, may be attributed to this fact. Overall, we consider that STS are reasonably well simulated by the MPI-ESM-LR model when compared to NOAA derived STS which, in principle consider the effect of TC on STS.

4.1.3 Tropical Cyclone STS Estimation

The calculation of STS for future climate required the knowledge of the historical situation. The data used to study future climate scenarios are derived from the MPI-ESM-LR model simulations. As it has been said before, TCs are fairly small and dynamic atmospheric phenomena with relation to the spatial resolution of climate models. Therefore, the cyclone-generated STS are not well represented by the MPI-ESM-LR data.

Here, we try to estimate the missing TC information on STS as simulated by climate models.

An idealized radial wind profile, fitted to the analytical model output, were used to estimate maximum storm surge.

We have compiled historical data of tropical cyclone intensities from the annual tropical reports maintained by the Joint Typhoon Warning Centre, https://metoc.ndbc.noaa.gov/JTWC/.

These records typically contain storm center positions every six hours together with a single intensity estimate, maximum wind speed and central seal level pressure every time period.

As stated by Neumann et al. (2013), many wind risk assessment techniques rely directly on historical tropical cyclone track data to estimate the frequency of storms passing close to points of interest, and must assume that the intensity evolution is independent of the particular track taken by the storm. For this study we have calculated the average maximum sustained wind intensity and central SLP for the storm surge calculation for the 1985 to 2015 period that occurred in the SWIO basin (Appendix A). For these cyclones, no storm surge data were available. Extreme wind intensity and atmospheric pressure of these tropical cyclones were used to estimate, with the analytical model, the extreme cyclone generated STS.

A statistical analysis was performed for a better understanding of the frequency distribution of the maximum sustained wind of the TC events. Figure 22 shows a histogram of TC for four wind speed classes. Similar information is shown in Figure 23 for as TC distribution by category.

From an universe of 129 TC events used for this study, 10.9% are severe tropical storm with wind speed ranging from 80-117 km/h, 45% are TC with wind speed ranging from

118-165 km/h, 36.4% represents intense TC wind speed ranging from 166-212 km/h and 7.8% are very intense TC wind speed ranging from greeter than 212 km/h. Despite the low occurrence of very intense TC, if compared with tropical and intense TC, due to the wind category associated with them, the level of damage when it makes its landfall in the coast is very substantial.

The average historical wind intensity of SWIO tropical cyclone is 160 km/h and the center sea level pressure average is 940 hPa.

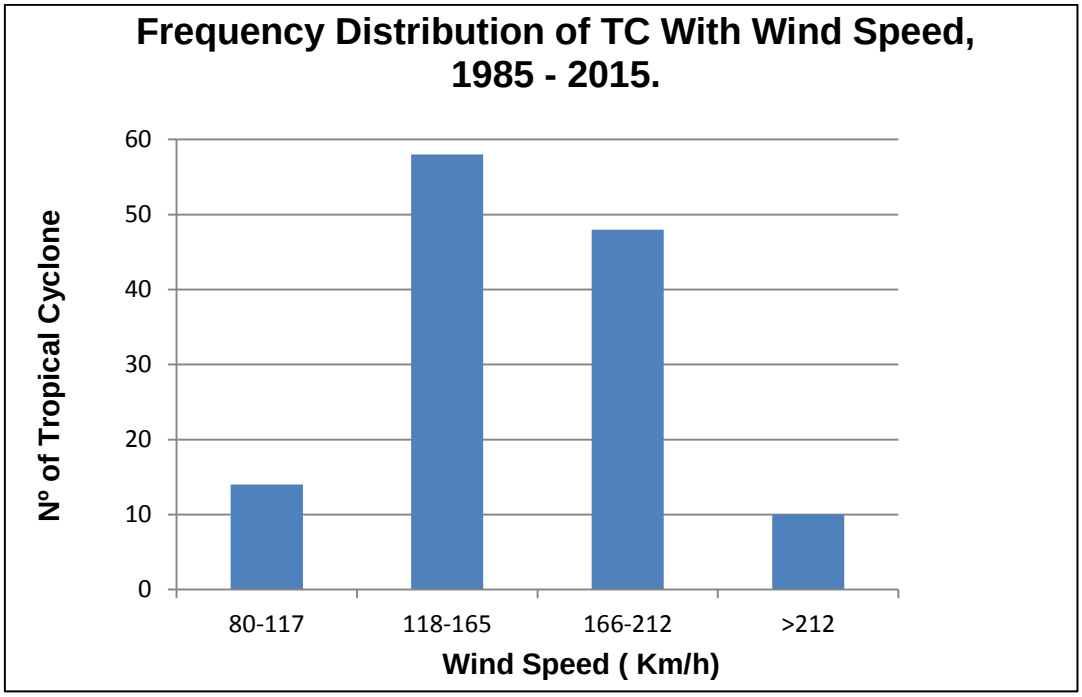

Figure 22. Frequency distribution of TC wind speed, 1985-2015, SWIO basin.

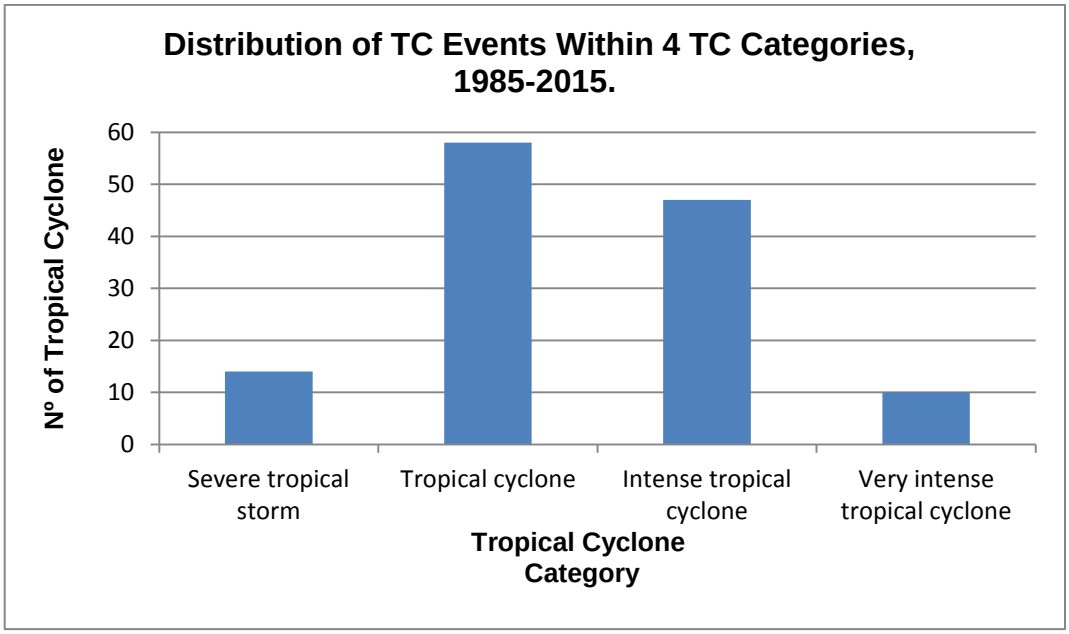

Figure 23. Distribution of TC events within 4 categories of TC, 1985-2015.

Using these climatological values with the analytical model results in STS equal to 0.8 meters for winds blowing from the east. This is, indeed, the most frequent wind direction associated with TC that reach the Mozambican coast. For the same wind speed but considering other wind directions, STS are maximum for southeast winds which is the second most frequent wind direction associated with TC in the region.

4.1.4 Results for Historical Period, Data from MPI-ESM-LR

Figure 23 shows STS for the historical period considering the TC correction of +0.8m as mentioned in section 4.1.3. The same procedure will be applied latter on for simulated future climate scenarios. We are aware that, by doing such, we may be overestimating the STS but, since our main goal is to evaluate differences between STS in the future and in the historical period, part of the introduced systematic error may be minimized.

The simulated historical STS, represented in the Figure 24, show that with the correction of TC intensity in the model, the STS increase considerably.

The difference in the magnitude of STS between the stations has to do mainly with the difference in the wind intensity determined by the TC preferable tracks and the location of the stations.

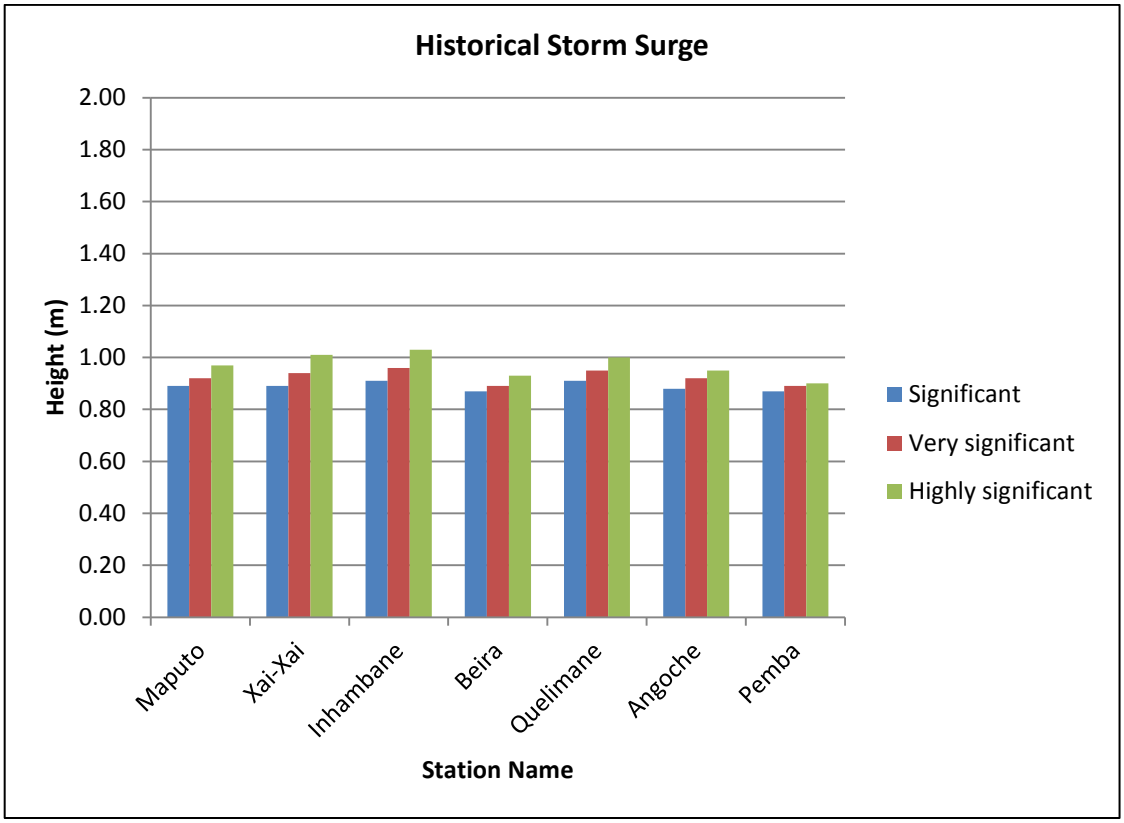

Figure 24. Significant (P95), very significant (P99) and highly significant (P99.9) storm surge for historical period (1986-2005). STS were corrected for the effect of TC-induced STS of +0.8 m.

Figure 25 shows the PDFs of the meteorological tide, using the analytical model, and meteorological data from NOAA and from the MPI-ESM-LP for the various locations. Here the TC-derived STS correction has not been applied. Of course, we are mainly concerned with STS, that is the right extreme of the distributions. Even so, the PDFs are generally in agreement, particularly their shapes. In some cases the position of the PDFs are not in phase (i.e. Maputo, Quelimane and Angoche). For Inhambane, Beira and Pemba the model PDFs overestimate the variance of the meteorological tide time series, whereas for Xai-Xai the match is nearly perfect. Also, the extreme right side of the PDFs are much better simulated than their left side counterparts. This is encouraging since STS are located on the extreme right side of the PDFs.

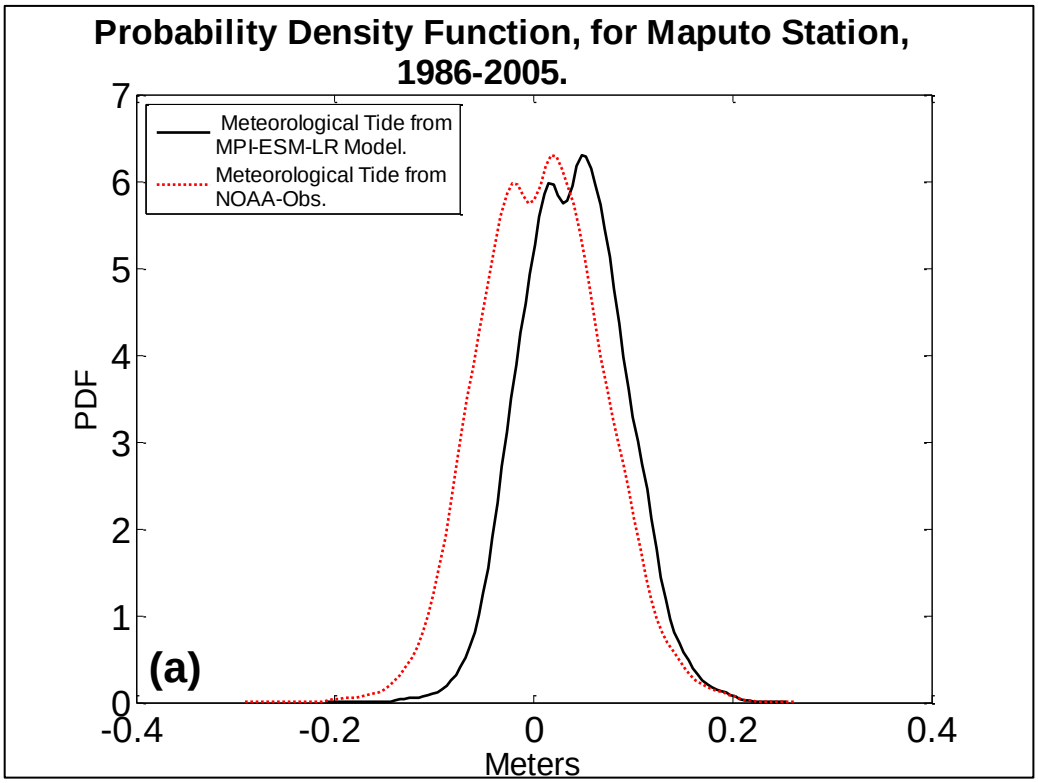

Figure 25 (Continued on next page, see caption)

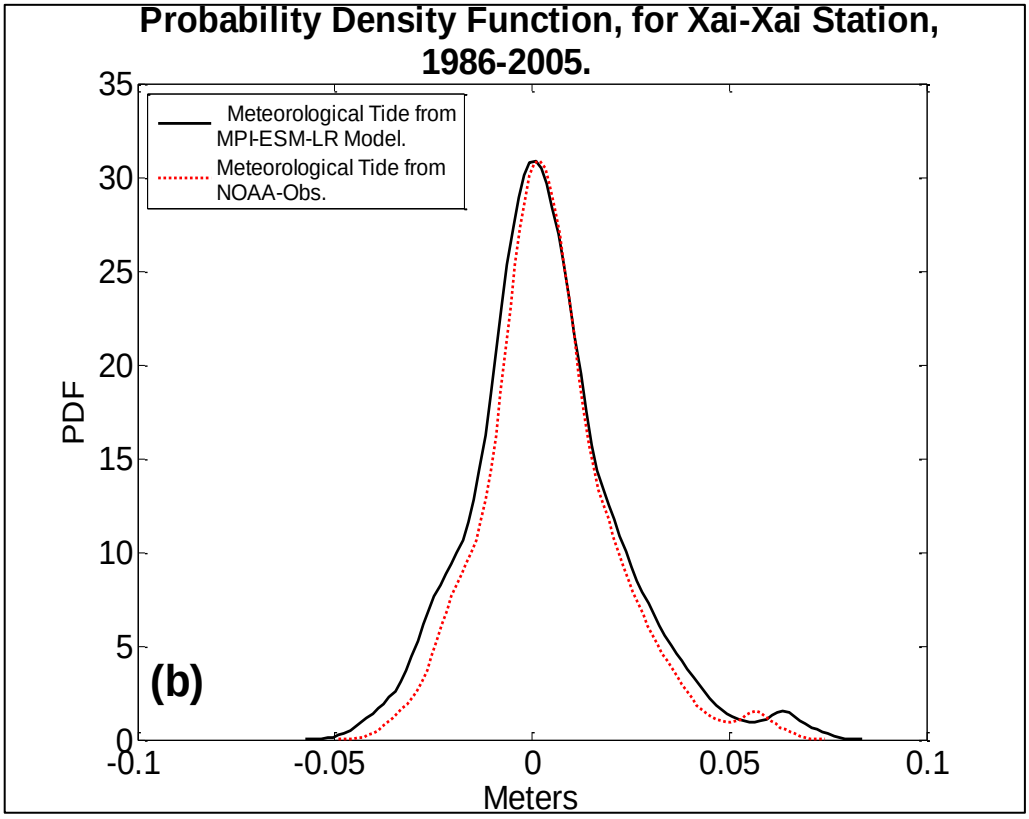

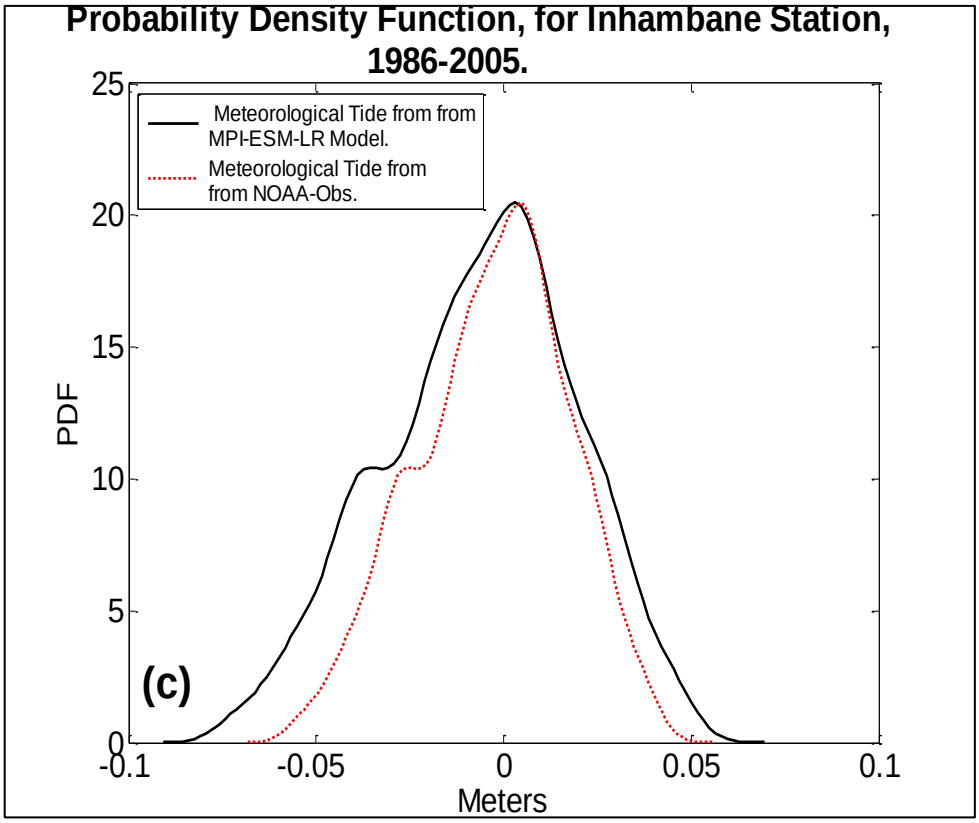

Figure 25 (Continued on next page, see caption)

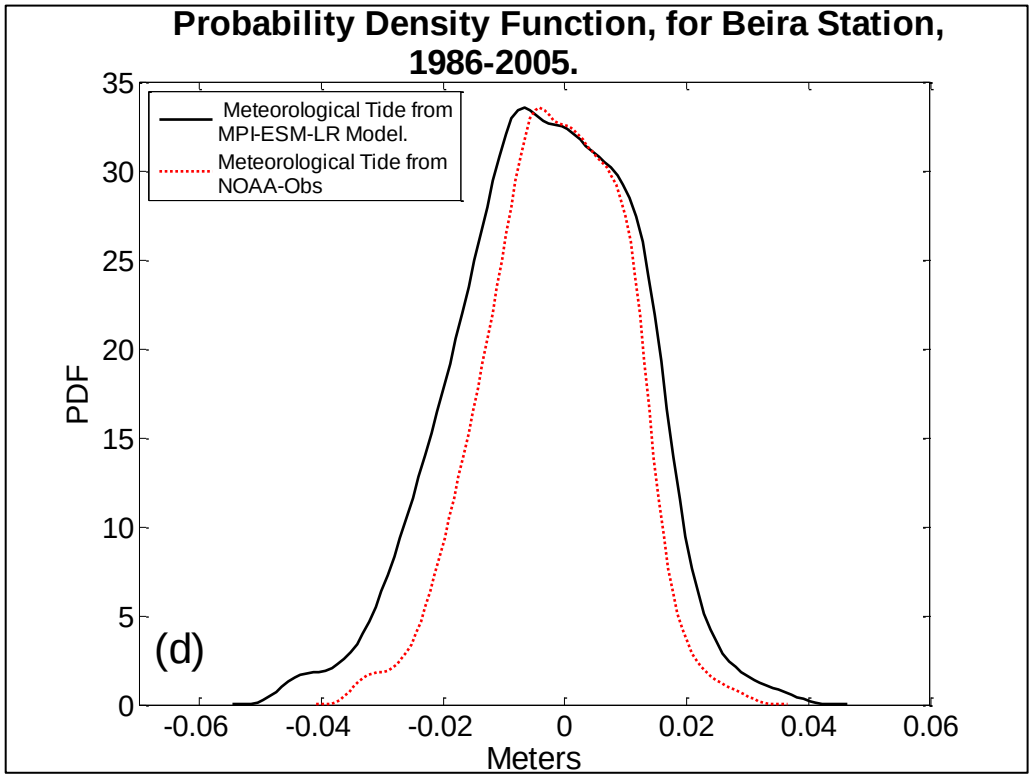

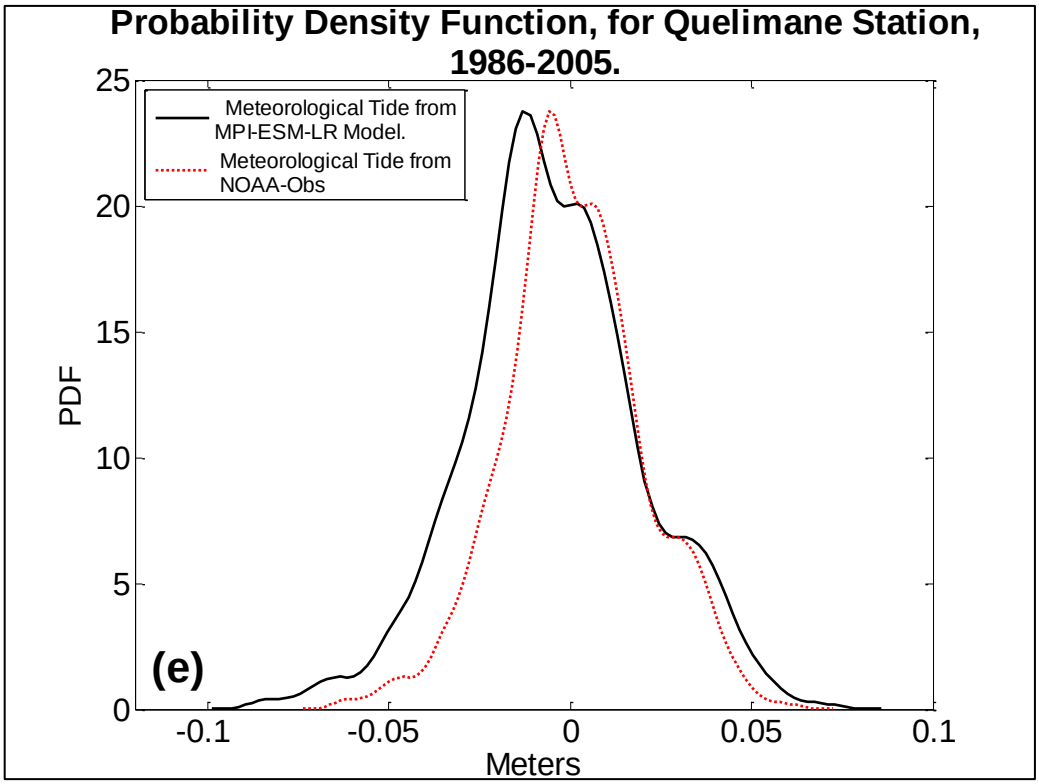

Figure 25 (Continued on next page, see caption)

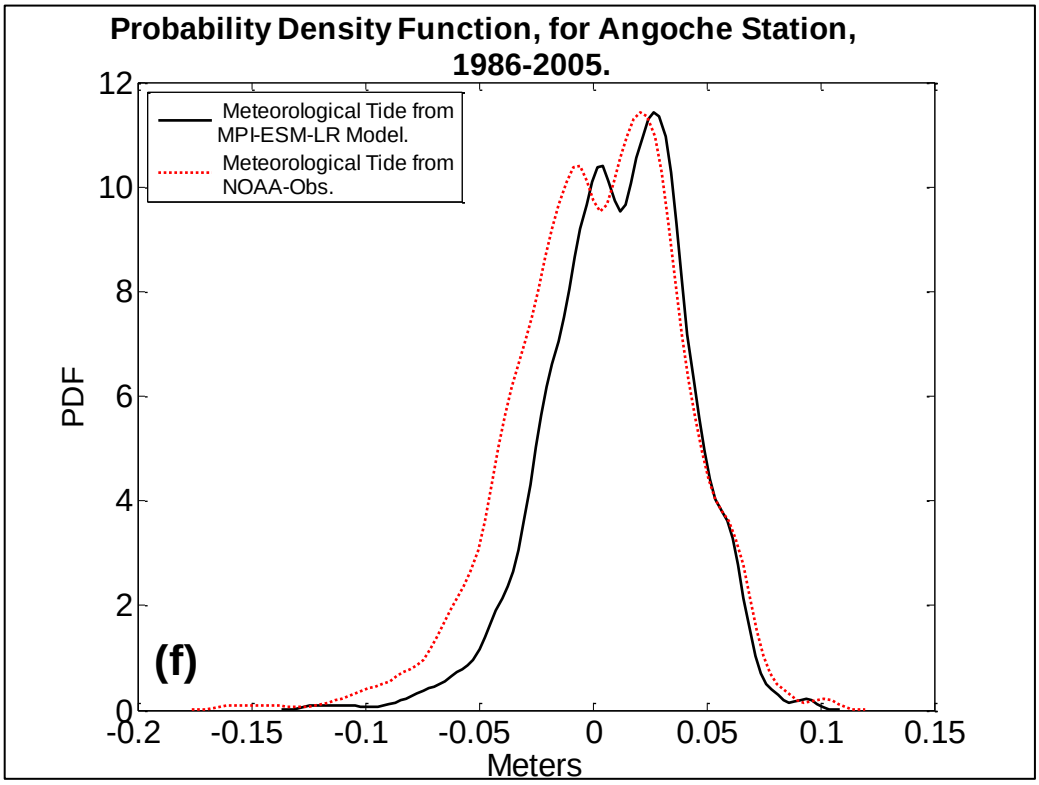

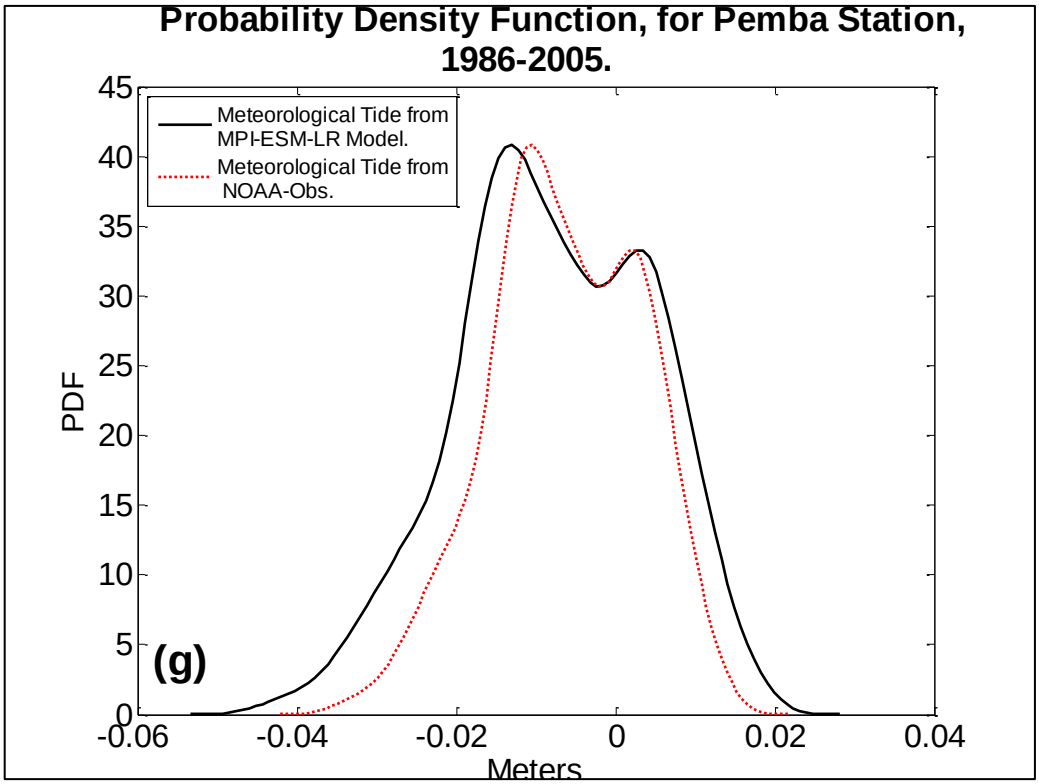

Figure 25. PDF graphical comparison between historical meteorological tide from NOAA (black) and MPI-ESM-LR (red) data series, for station of Maputo (a), Xai-Xai (b), Inhambane (c), Beira (d), Quelimane (e), Angoche (f) and Pemba (g). The TC correction as well as SLR were not applied.

The wind is the most important parameter for the storm surge generation because more than 85% of storm surge generation is due to wind and 5% to 10% due to sea level pressure. A strong wind blowing onshore induces sea level rise and, consequently, water heights higher than those blowing from any other direction with the same intensity. To gain a better insight on the prevailing winds we have calculated the wind roses for all locals, for the historical period, which are shown in Figure 26, 27 and in Appendix I, for NOAA and in for the MPI-ESM-LR model. The intensity and frequency scales are the same for each station but may differ amongst the stations since the objective here is to compare, for the same station the winds generated from NOAA and the MPI-ESM-LR model.

In general, the wind intensity and frequency properties are similar from both datasets. We note, however, that NOAA winds are recorded at meteorological stations whereas those simulated by the MPI-ESM-LR model are downloaded from the model grid to the nearest coordinates of each station. This introduced error may be amplified by the fact that all stations are located along the coast where horizontal gradients are stronger. The complex

configuration of the coastline at some locations may also contribute to the uncertainty of the downscaling process. But, clearly, the most frequent winds blow from the south/east quadrant. Cyclones reaching the coast come from the Indian Ocean and produce very strong winds also from south to the east. These are the directions which, for the same sea-level pressure, generate the most strong meteorological tides and, therefore, STS. For example, for a sea-level pressure of 940 hPa and a wind speed of 160 km/h (climatological values for TC reaching the coast of Mozambique) the meteorological tides for the most predominant directions are, 1.16 m, 1.18 m and 0.80 m, for winds blowing from south, southeast and east, respectively. For the other directions the meteorological tides are much inferior and eventually negative (i.e. wind blowing from north and west).

As it has been explained above, in the methods section, this is based on the effect of Coriolis force as well as the Ekman theory for the southern hemisphere. These wind roses are also in line with well-known synoptic processes occurring in the region.

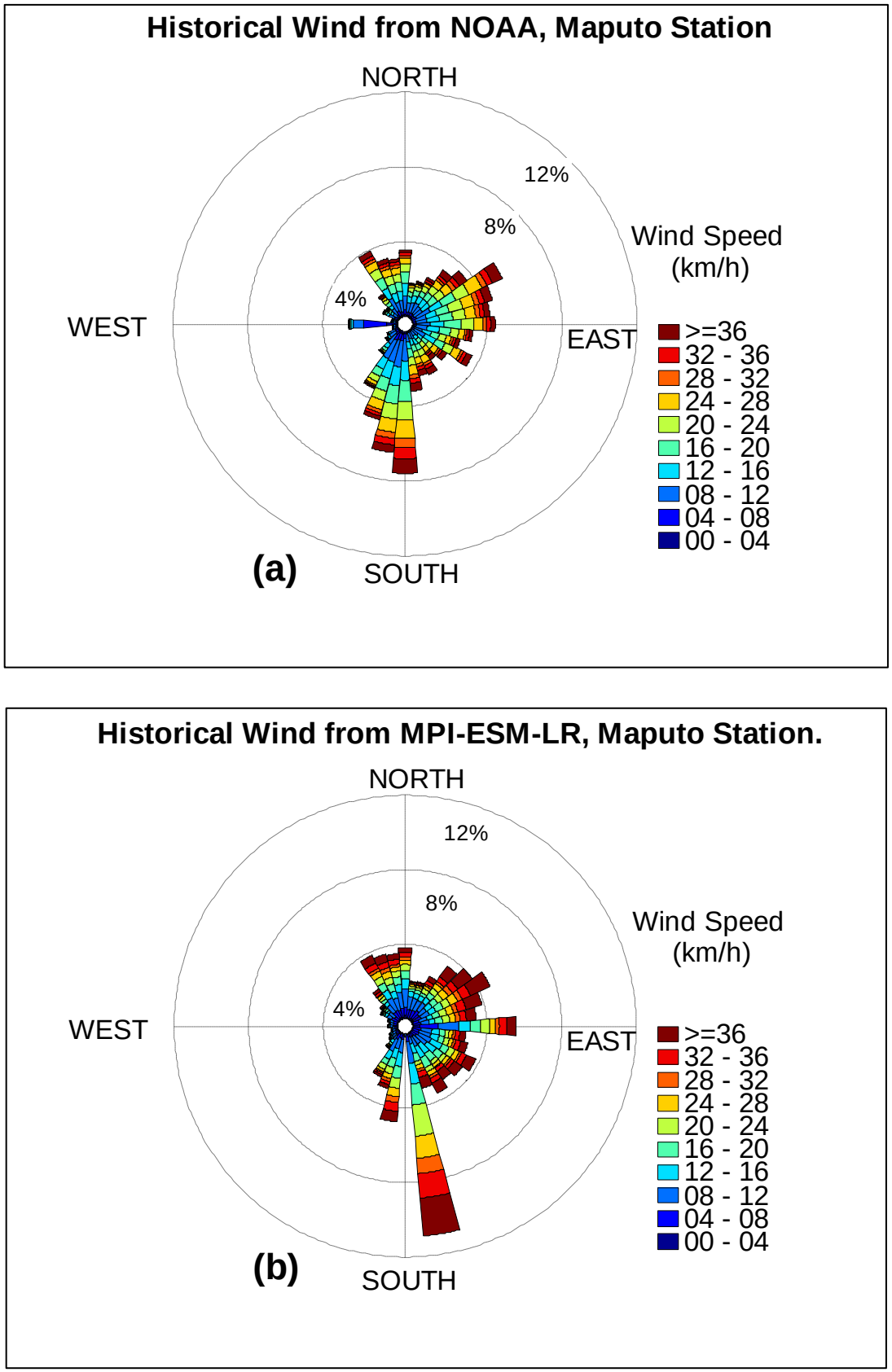

Figure 26. Wind speed and direction for historical data from NOAA (a) and MPI-ESM-LR (b), Maputo station.

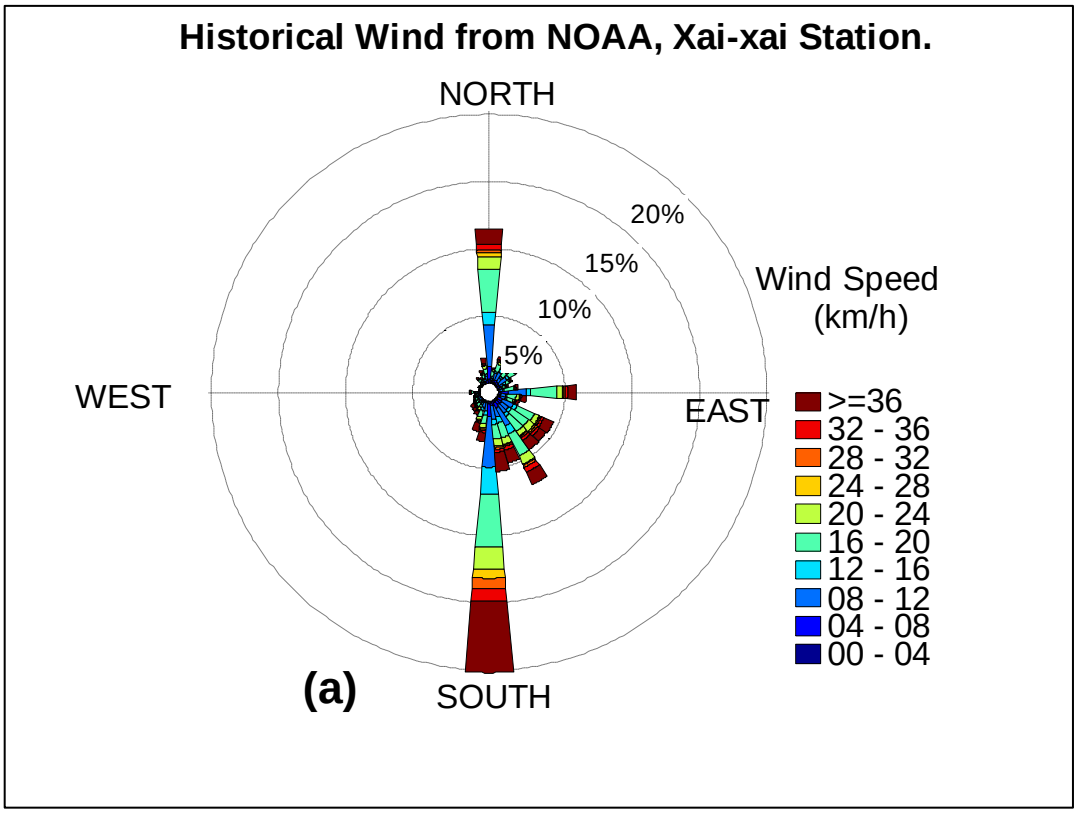

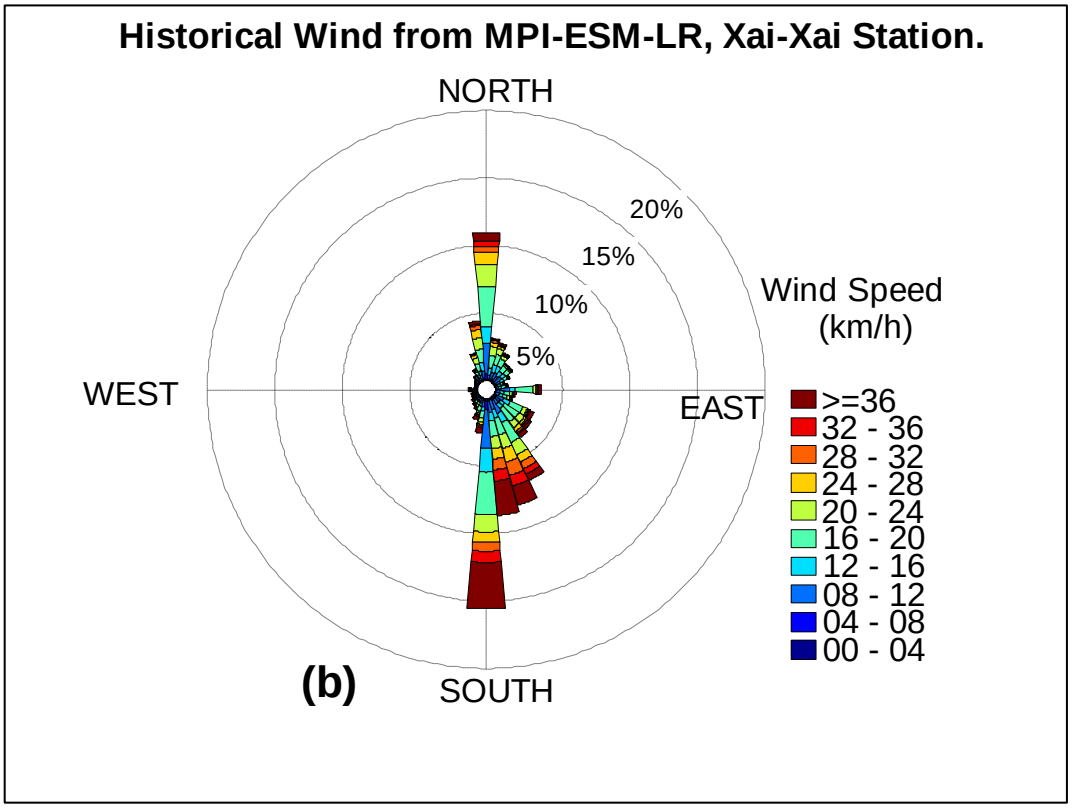

Figure 27. Wind speed and direction for historical data from NOAA (a) and MPI-ESM-LR (b), Xai-Xai station.

4.2 Results for Near Term Future Period

Is this section we evaluate the near-term future (2016-2035) changes of STS relative to the historical period, simulated by the MPI-ESM-LR model. As for the historical period, the STS identified in the meteorological tide time series for the near term period were corrected for the TC effect (see 4.1.3). As mentioned in the theoretical framework chapter of this study, the global mean sea level will continue to rise during the 21st century. Under all RCP scenarios, the rate of SLR will very likely exceed that observed during 1971 to 2010 due to increased ocean warming and increased loss of mass from glaciers and ice (IPCC, 2013). In this regard, aside from considering TC intensity, the SLR was also considered for the STS calculation. For the near term future, a SLR scenario of 0.12 meters was considered. This value was obtained by interpolation of Figure 9, for the RCP8.5. Also, we have considered an increase of TC intensity of +10 percent, relative to the historical scenario (Emanuel et al., 2008; Bender et al., 2010; Knutson et al., 2010, 2013; Yamada et al., 2010; Murakami et al.,2012). This corresponds to a wind speed of 176 km/h, compared to 160 km/h used for the historic period. We considered, as for the historic period the east wind direction. Such a wind of 176 km/h blowing from east generate a STS of 0.9 m. We maintained the sea level pressure of 940 hPa used for the historic period. By doing this, we might be underestimating the intensity of future TCs. The references cited above do not distinguish between the near term future, medium term future and long term future. Therefore, the same wind and sea level pressure were used for the three future periods. Also, as for the historic period, we considered the east wind direction in these corrections.

Figure 28 shows SL for the near term period and the respective changes relative to the historical period. The SL exceed 1.0 m at all locations. STS changes are positive for all locations and the respective changes increase from south to North up to Quelimane and then decrease. Also of note is a maximum increase for very significant SL (red bars) in the south (Maputo, Xai-Xai and Inhambane) and for extremely significant (green bars) in the north (Angoche and Pemba). The explanation for this behavior has to do with the natural characteristics and geographical orientation of the Mozambican coast, which is north-south oriented, as well as the latitude at which the stations are located. Also, the equation (3.28), to determine the displacement of water level from the mean due to alongshore wind, is directly proportional to the Coriolis parameter.

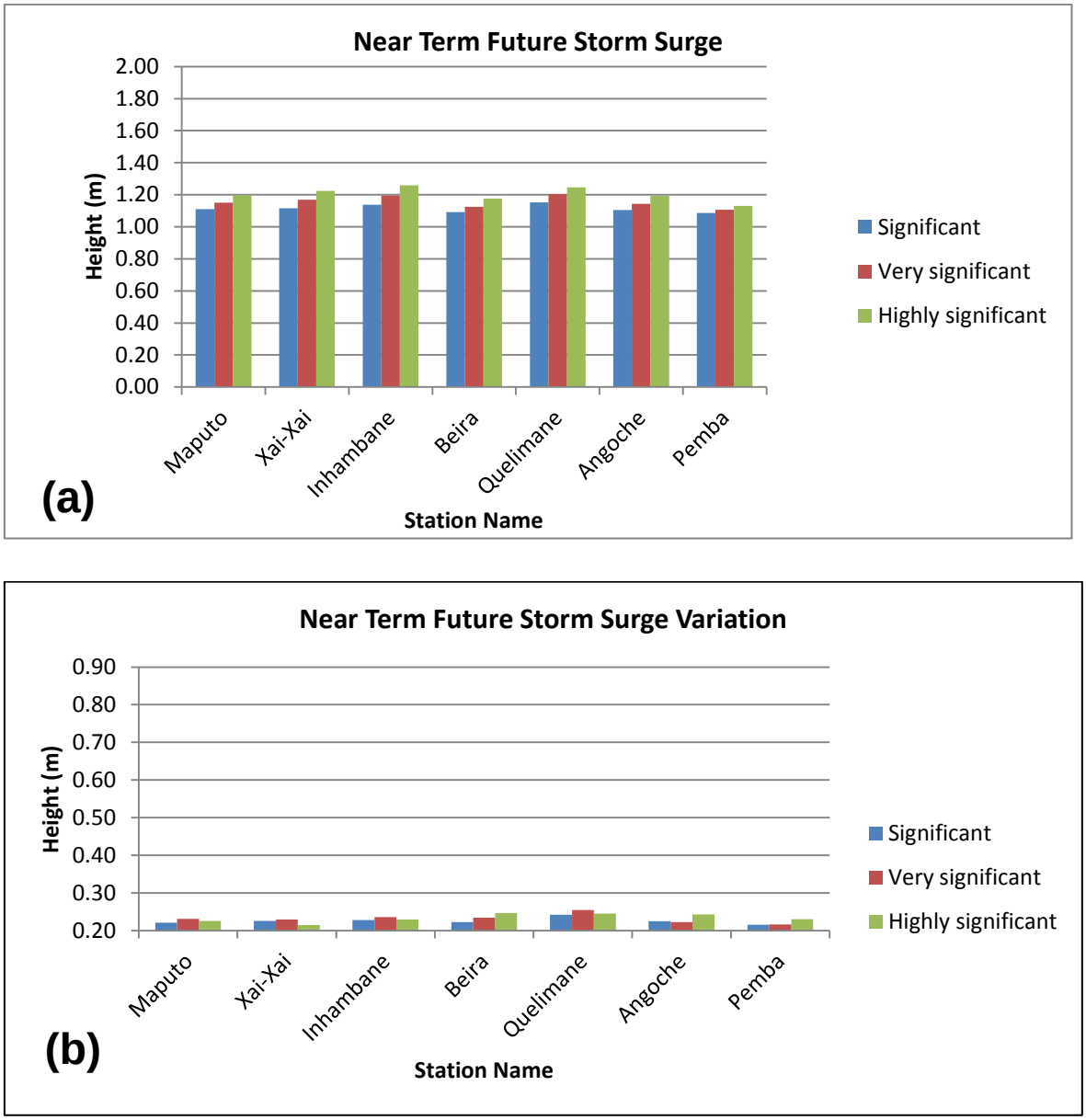

Figure 28. Significant (P95), very significant (P99) and highly significant (P99.9) for (a) SL and (b) SL variation (future minus historic), for the near future period (2016-2035). STS were corrected for the effect of TC correction by considering a +10% increase in intensity, which correspond to +0.9 m. A SLR of +0.12 m was added for the near term future period.

Climate change may alter the wind patterns in the future with an increase of wind intensity or the frequency of severe winds, which may have implications in storm surge generation. The wind characteristics projected for near term future, according to the MPI-ESM-LR (Figures 29, 30 and Appendix J), show prevailing winds from East to Southeast quadrant.

The wind from this quadrant is known to be favorable for the piling up the water in the coast, considering the Ekman theory when applied to the southern hemisphere.

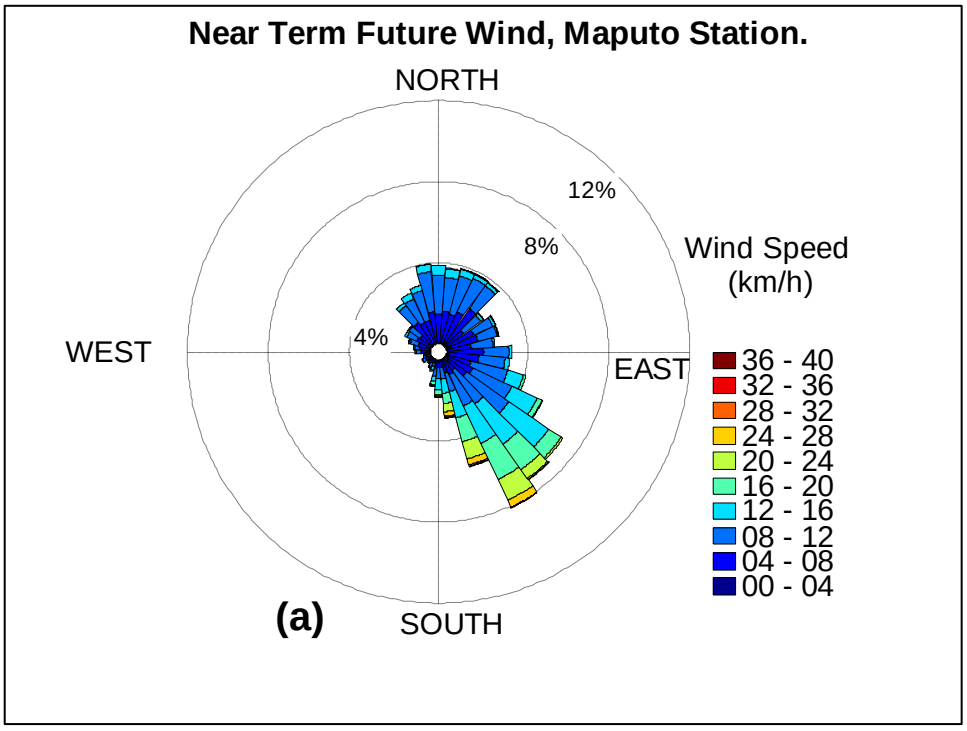

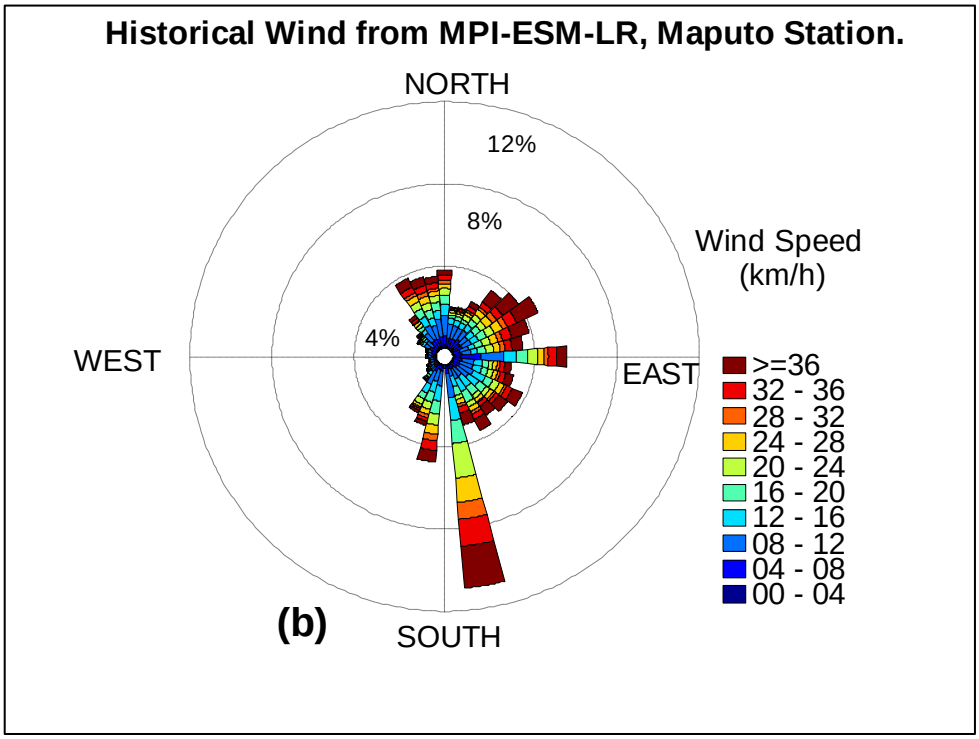

Figure 29. Wind speed and direction for near term future (a) and historical (b), from MPI-ESM-LR for Maputo station.

The wind roses shown consider all wind observations and not just those for extreme winds which generate STS. Since the wind effect on STS depends both on wind speed and direction, it is not clear which of these properties are responsible for the positive STS intensity changes shown in Figure 28. We also have to consider the contributions from SLR of +0.12 m that was added to P95, P99 and P99.9. Apart from TC and SLR changes, the residual STS changes which are also positive for all locations (not shown) may be related to changes in the synoptic setting in the future scenario. We anticipate more extreme southward excursions of the ITCZ position in summer which is expected to occur in a warmer world (Weller et al., 2014).

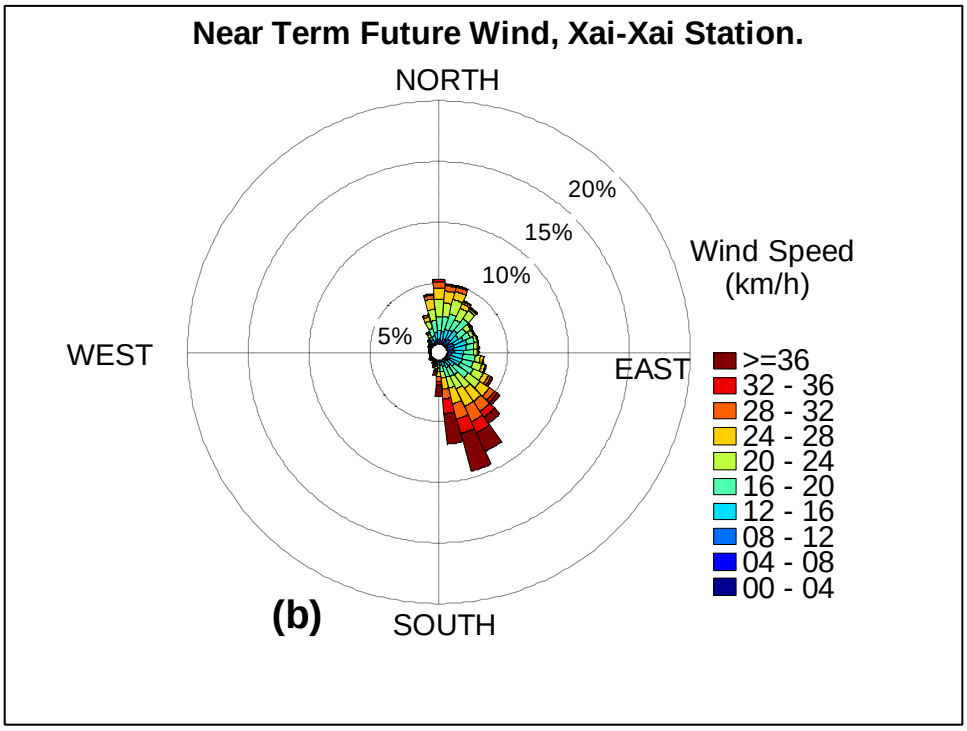

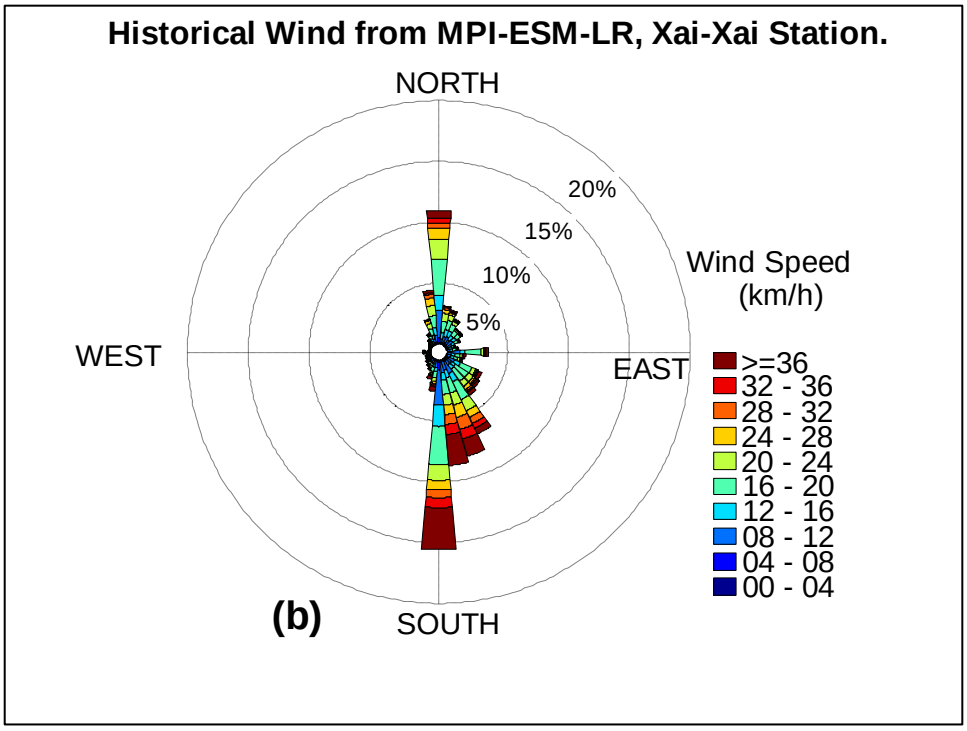

Figure 30. Wind speed and direction for near term future (a) and historical (b), from MPI-ESM-LR for Xai-Xai station.

4.3 Results for Medium Term Future Period

Is this section we evaluate the medium term future (2046-2065) changes of STS relative to the historical period, simulated by the MPI-ESM-LR model. As it was done for the near term period, the same wind and sea level pressure correction due to TC intensification was added to the STS. For the medium term future, a SLR scenario of 0.39 meters was considered. This value was, again, obtained by interpolation from Figure 12, for the RCP8.5 scenario.

Figure 31 shows SL for the medium term period and the respective changes relative to the historical period. The SL exceed 1.30 m at all locations. The structure of the changes are similar to those for the near-term, but of larger magnitude.

Neumann et al. (2013) combined a range of SLR scenarios for 2050 for Beira. Their study suggests that the potential maximum storm surge level for 100-year return storm in Beira, currently estimated to be 1.9 m may occur every 40 years in the medium term future (i.e. 2050). According to the same study, the results for Maputo show similar and even more dramatic changes. For a potential maximum storm surge of 1.1 m the return period of 100 may reduce to 20 years.

Our results in this study are in accordance with Neumann et al (2013), suggesting for Maputo and Beira STS of the order of 1.70 m (adding the P99.9 values from Figure 24 and the STS changes of P99.9 in Figure 31, for Maputo and Beira), for the 20-year period of this study.

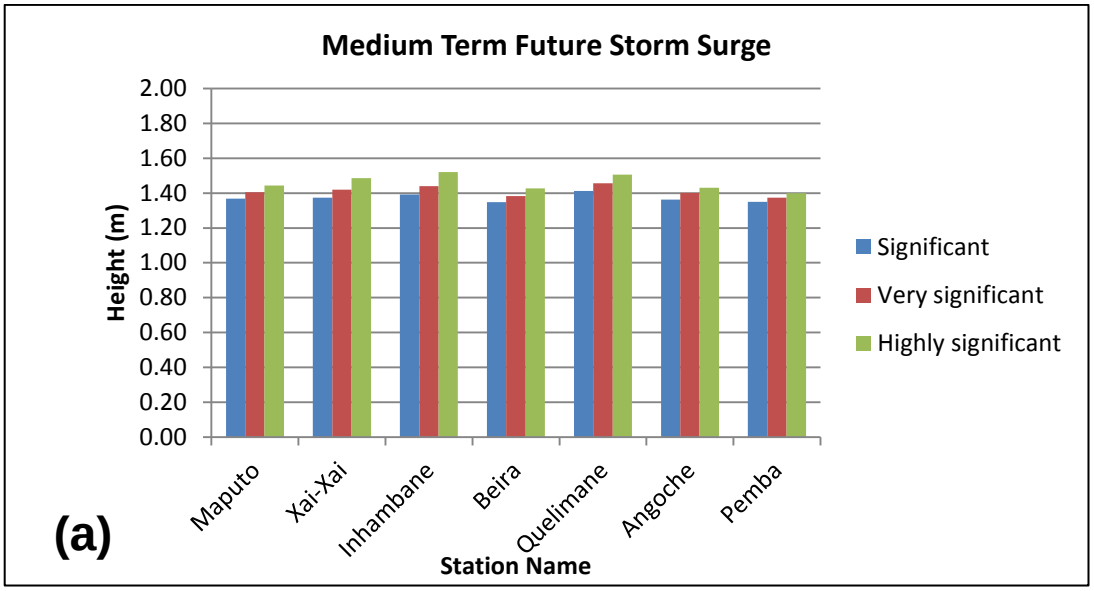

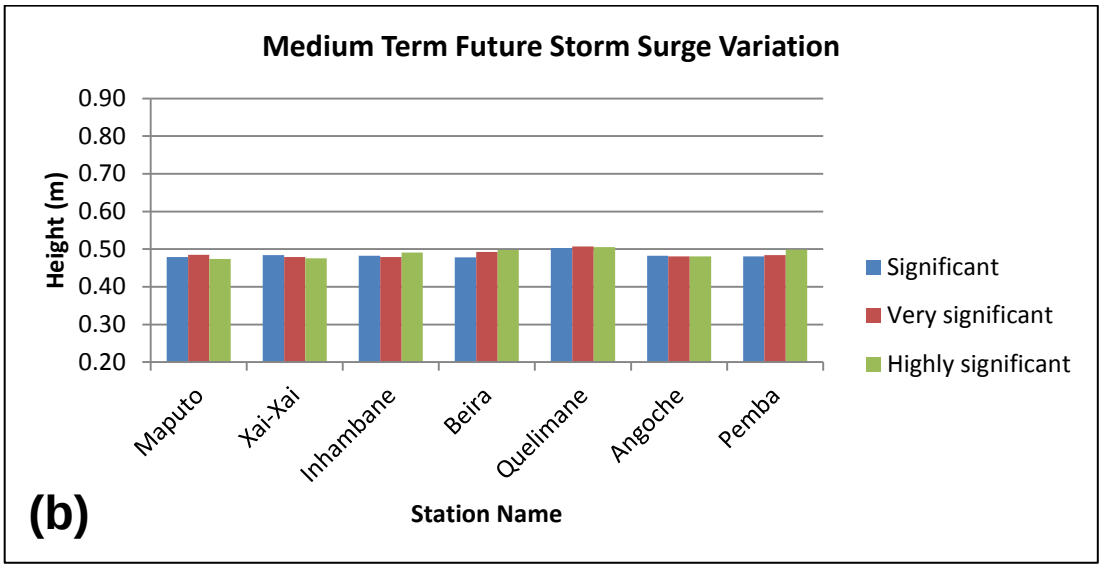

Figure 31. Significant (P95), very significant (P99) and highly significant (P99.9) for (a) SL and (b) SL variation (future minus historic), for medium term future period (2046-2065). STS were corrected for the effect of TC correction by considering a +10% increase in intensity, which correspond to +0.9 m. A SLR of +0.39 m, was added for the medium term future period.

Figures 32, 33 and Appendix K show the projected wind roses for the medium term future for the seven location. For sake of a quick comparison, the historical wind roses are shown again. In the seven stations the wind direction is projected for the quadrant Southeast, varying from East to South through Southeast. With the exception of Xai-Xai and Inhambane station, it is noted that the projection for all remain stations shows no substantial increase or decrease in wind speed, comparing to the near term future studs.

The Station of Xai-Xai have increased the amount of days with high magnitude wind while the Inhambane station did the opposite.

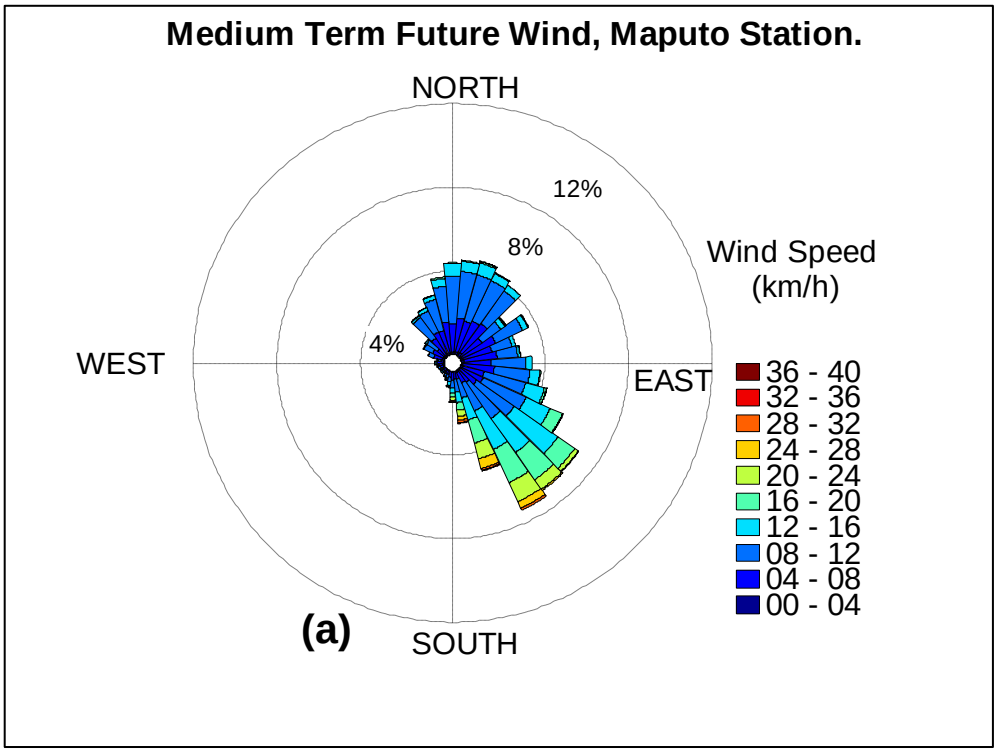

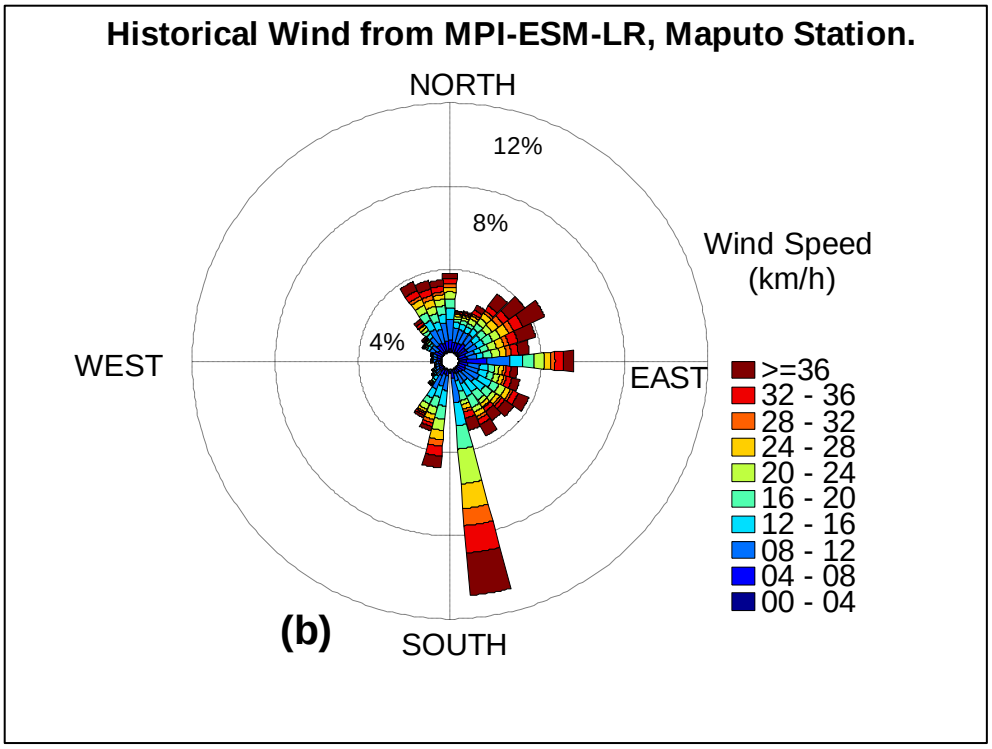

Figure 32. Wind speed and direction for medium term future (a) and historical (b), from MPI-ESM-LR for Maputo station.

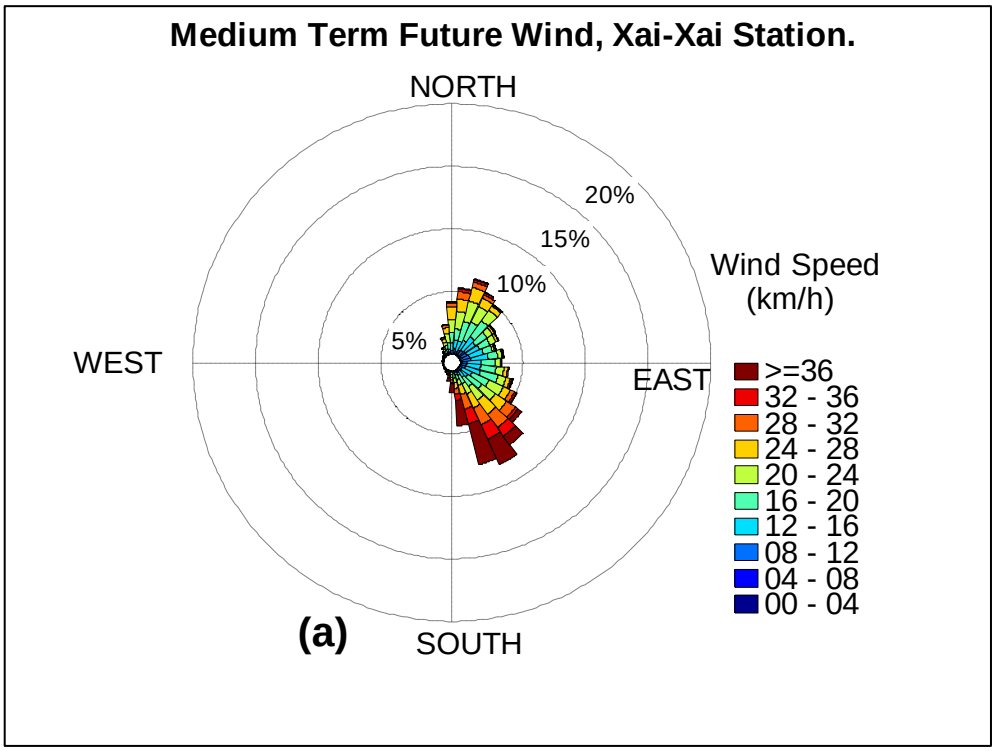

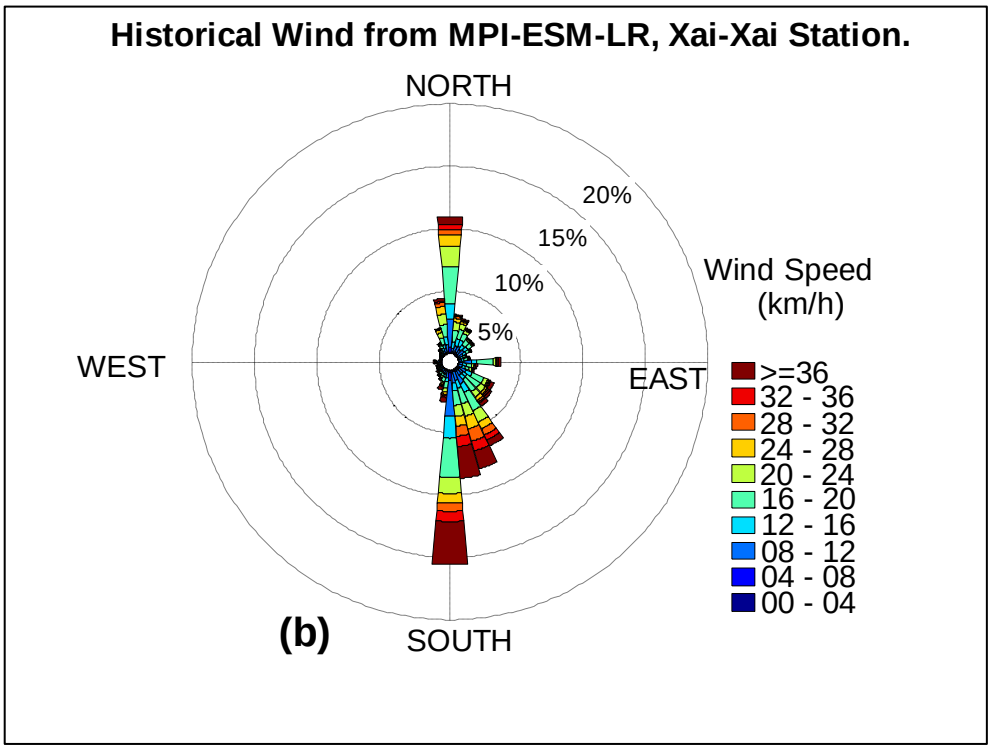

Figure 33. Wind speed and direction for medium term future (a) and historical (b), from MPI-ESM-LR for Xai-Xai station.

4.4 Results for Long Term Future Period

Following the same methodology applied for the near and medium term periods, a SLR of 0.72 meters was added to the STS of the long term period. Again, this value was obtained by interpolation of SLR for the RCP8.5 shown in Figure 9. The same TC corrections, corresponding to an intensification of +10%, were also applied, namely, a climatological wind of 176 km/h) and the climatological sea level pressure of 940 hPa.

Figure 34 shows the STS and the respective changes, relative to the historical period, for the long term period. As for the other periods, all changes are positive. Changes decrease from south to north and the magnitude of the changes are similar for the three types of STS, except for Maputo where the largest changes are simulated for highly significant STS.

In average, for long term future climate changes, all stations show SL heights of about greater than 1.6 meter. As for the other future periods, the high point by which the STS will be launched is mostly due to SLR. SL of this order clearly cause damages in coastal regions, mainly in low-lying land which occupies nearly the whole coastal region, even if the corresponding STS is of a small magnitude. The evaluation of our results are consistent with previous studies by Dasgupta et al (2009a) which suggested an increase of storm surge in 30% in the future due to climate change (Figure 3).

Figures 35, 36 and Appendix L, show that the wind properties do not change significantly relative to the medium term future. Clearly, changes in the STS appear to be mostly associated to the TC, however the SLR plays important role by increasing the height by which the STS starts its propagation.

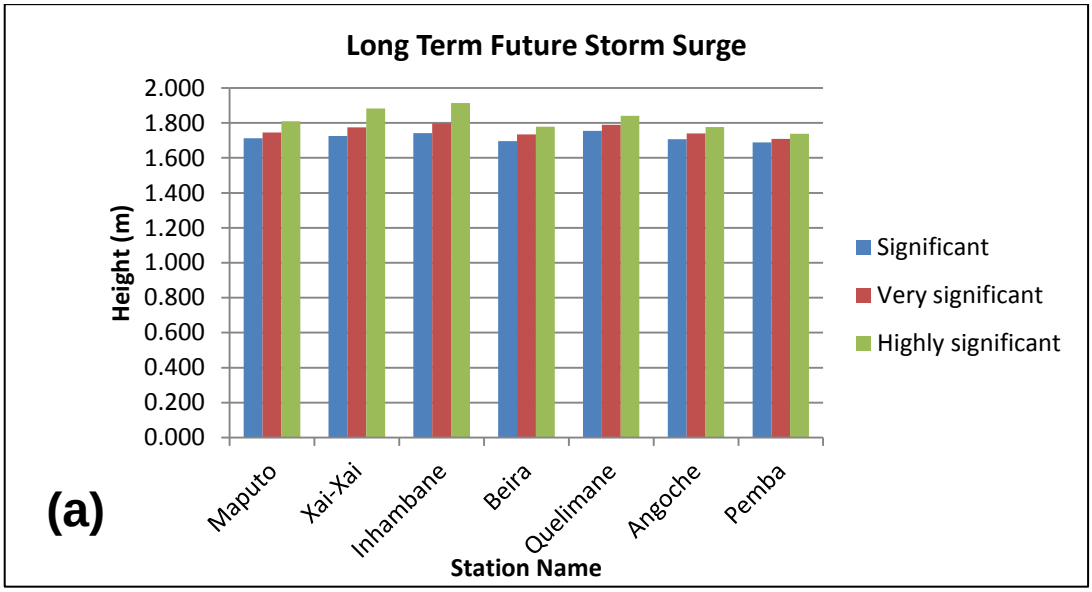

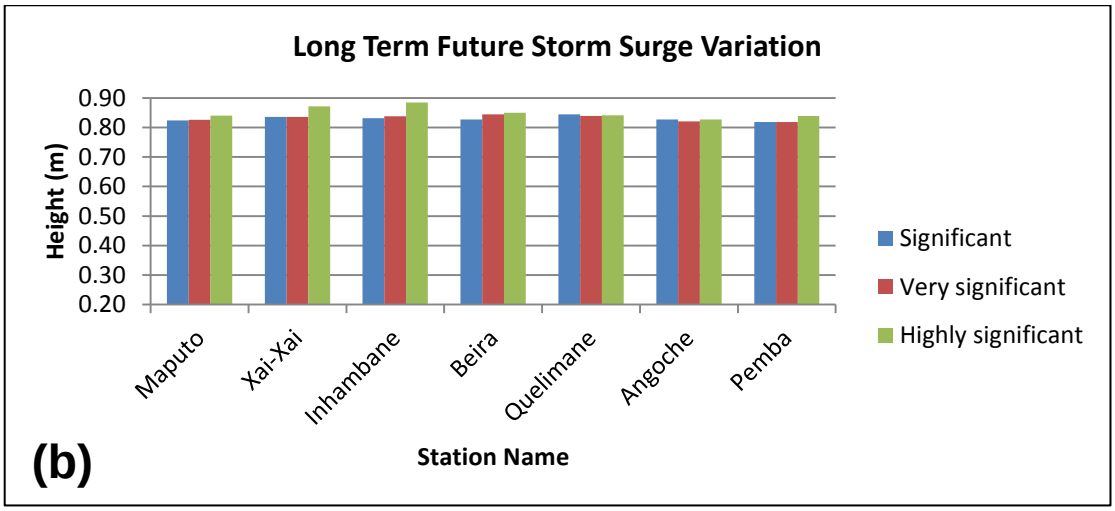

Figure 34. Significant (P95), very significant (P99) and highly significant (P99.9) for (a) SL and (b) SL variation (future minus historic), for Long term future period (2081-2100). STS were corrected for the effect of TC correction by considering a +10% increase in intensity, which correspond to +0.9 m. A SLR of +0.72 m was added for the long term future period.

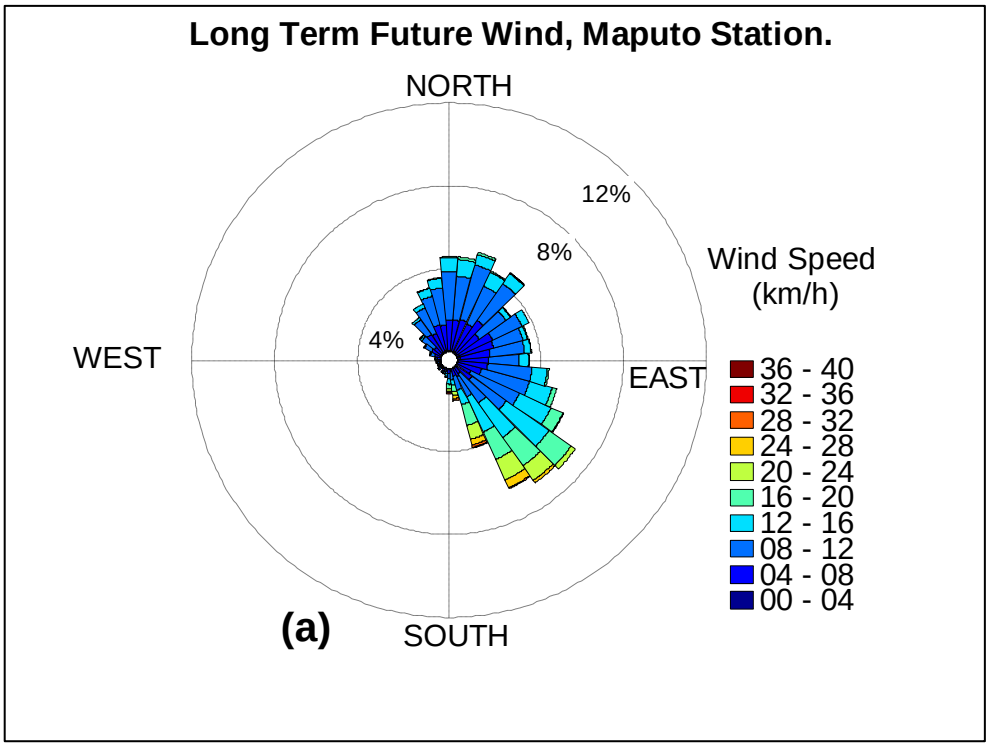

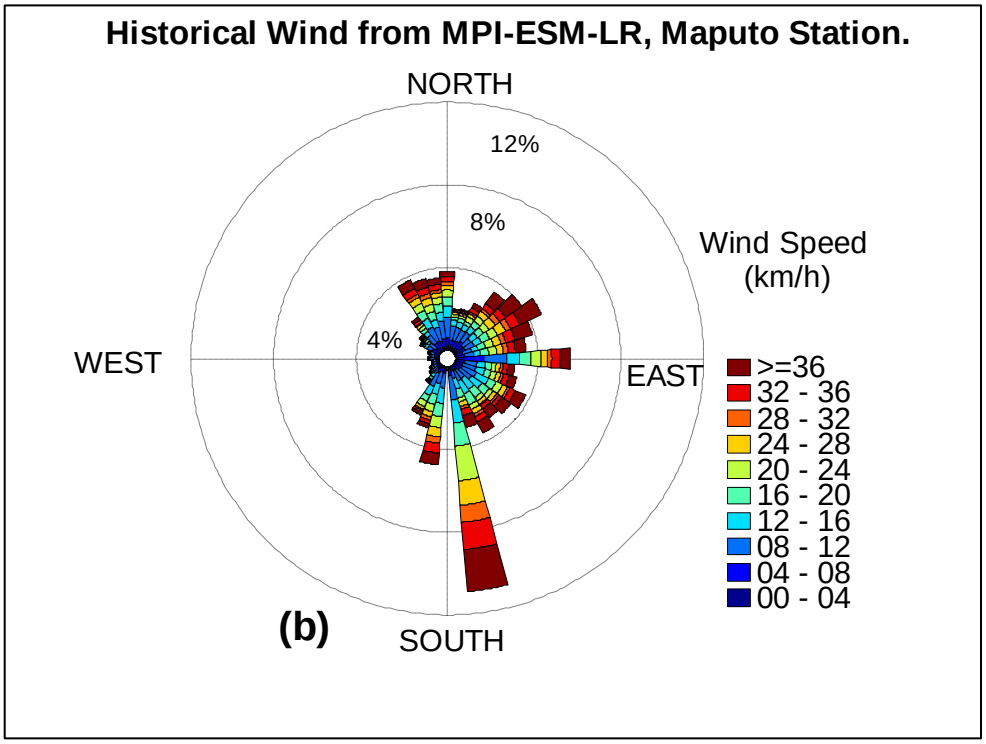

Figure 35. Wind speed and direction for long term future (a) and historical (b), from MPI-ESM-LR for Maputo station.

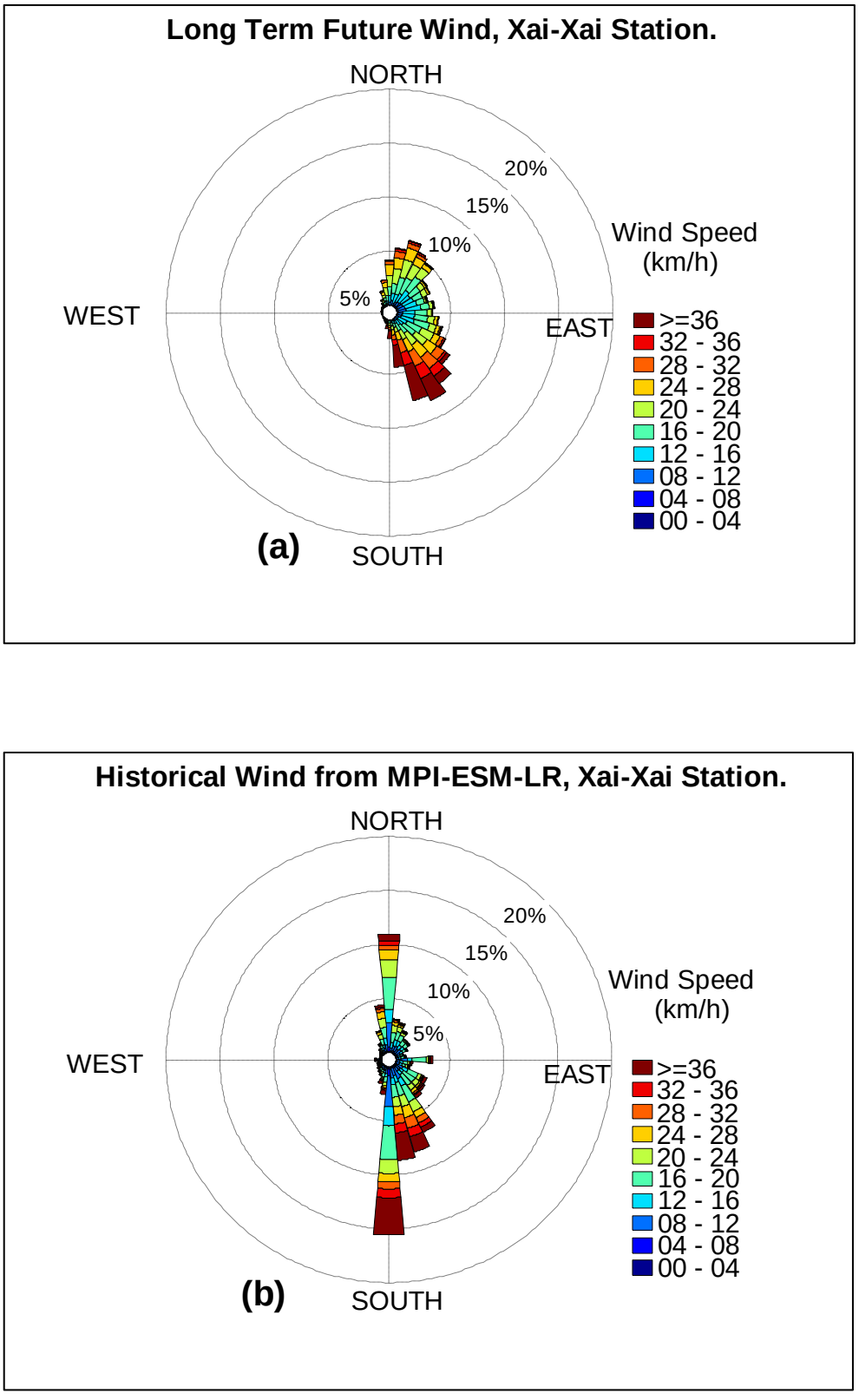

Figure 36. Wind speed and direction for long term future (a) and historical (b), from MPI-ESM-LR for Xai-Xai station.

Chapter V – Summary and Conclusion

The present study was mainly concerned with climate change on storm surges properties along the cost of Mozambique. This was done by using an analytical model which estimates the local meteorological tide based on sea level pressure and the cross and along shore wind components near the surface. The analytical model proposed here does not couple the mechanisms of hydrodynamics. It is a purely static method and, as such, it does not consider the cyclonic system dynamics itself. Everything else being equal, the meteorological tide and STS at the coast are different for fast-moving and slow-moving systems.

The meteorological data used by this model is generated by the MPI-ESM-LR model which is a global, low resolution model and, therefore, does not capture the full characteristics of extreme winds and pressure mainly associated with TCs (Hamilton, 2008; Flato et al., 2013). The global models used for recent climate assessments have exhibited tropical cyclone intensity statistics which were biasedly weak, since models cannot adequately resolve the dynamics of tropical cyclone. In particular, wind speed, pressure gradients and, consequently, the minimum pressure of TC are underestimated by climate models (Camargo and Wing, 2016).

To minimize this problem, we corrected extreme winds and sea level pressure associated with TCs by adding (subtracting) 10% to the winds (sea level pressure). Firstly, we calculated the climatological wind and minimum sea level pressure for all cyclones which occurred in the 1985-2015 period. The values of wind speed and sea level pressure are 160 km/h and 940 hPa, respectively. These values were used with the analytical model to obtain an estimation of the TC effect. Since most TC are associated to easterly winds along the coast of Mozambique, we only considered the cross shore sea level component. The obtained values were, then, added to the percentiles corresponding to the three categories of STS but not to the full meteorological tide time series. This was equally done for the seven locations and for the historical period.

For the future climate scenarios a further +10% TC correction was applied based on estimates of increased TC intensity in the future. This is a crude estimate since it is not referred to which regions and future periods this estimates correspond. Therefore, we

considered the same TC effect for the three periods and for all seven locations. On top of this, SLR estimates for the future scenarios were added to the same percentiles. These were obtained from global SLR projections shown in Figure 9. Local SLR for this region was not considered but it was shown to be similar, or even slightly higher, than global SLR.

Next, we validated the analytical model, using atmospheric NOAA-derived data, against TG observed data. The astronomical tide was removed from the TG data. Since TG data are scarce in Mozambique, the best data were chosen. The TG dataset comprised data for one full year recorded at three stations located along the coast of Mozambique. Small differences found between both approaches may be partly due to the fact that TG records inherently includes the local effects of the bathymetry and the instantaneous wave setup in sea level measurements. Overall, the analytical model simulated well the PDFs and the STS of meteorological tide data when compared to those calculated for TG derived data. In some cases, sea level extremes were not captured by the analytical model but we attribute this to the fact that, at that stage, we had not considered the effects of TC.

After, we performed the validation of the MPI-ESM-LR model by comparing the meteorological tide series derived using the analytical model with simulated meteorological data with similar time series using the analytical model with meteorological data observed and similar data obtained from NOAA. Results show that, except for Quelimane, the three STS percentiles are slightly underestimated by the MPI-ESM-LR when compared to NOAA but, overall, the MPI-ESM-LR estimated STS are in good agreement with those obtained using NOAA data.

Next, the analytical model was applied with meteorological data simulated by the MPI-ESM-LR model for three future climate periods, namely, near term (2016-2035), medium term (2046-2065) and long term (2081-2100), for the RCP8.5 scenario. This was performed for the seven locations for which there are meteorological observed data available (i.e. obtained from NOAA). At this moment, TC and SLR corrections were not applied. The meteorological tide and STS characteristics for the three future periods were compared to those for the historical period (1986-2005). The main conclusion is that there are no significant differences in the meteorological tides along the cost of Mozambique. This means that meteorological conditions, which are considered the forcing, do not change in the future when ignoring the TCs effects.

Next, after the calculation of P95, P99 and P99.9 of the meteorological series, which correspond to significant, very significant and highly significant STS, respectively, the TC (for historic and future periods) and SLR (only for future periods) corrections were applied.

This was equally done for the seven locations. For the three future periods the 10% TC intensity increase results in a wind speed of 176 km/h. The minimum sea level pressure was maintained at 940 hPa. As a result, similar sea level corrections of +0.9 m were added to all STS. By considering the same climatological TC correction for the future periods we may be underestimating TC effect.

For the RCP8.5, SLR is expected to be 0.12 m, 0.39 m and 0.72 m for near, medium and long-term future, respectively. This results from interpolation of SLR in Figure 9. The uncertainty range for these values are 0.09 m to 0.19 m for the near future, 0.29 m to 0.49 m for the medium term future and 0.51 m to 0.99 m for the long future.

Finally the STS changes were estimated for the three periods, relative to the historical period, and for the seven locations.

Results show that, considering the SLR scenarios, STS, which include the TC correction, increase in the three future periods. The degree of risk of STS occurring in the future are mainly due to SLR and not to the STS themselves. The second most important contribution is the estimated 10% intensity increase of TC that were added to STS. The remaining contributions are due to small changes in the synoptic future settings which are identified in this study by changes in the wind roses in the future.

This is clearly seen in Figure 37 which shows, for each location, the PDFs of meteorological tide for the historic and future periods considering also the SLR and its uncertainty range mentioned above. The dotted lines represent the uncertainty lower limits and the dashed-point lines the uncertainty upper limits for the respective future scenarios. There is a clear shift of all PDFs to the right and very little change in the format shape of the PDF. This means that changes in the impact of the STS are mainly due to systematic differences which arise from an intensification of TC and SLR and not due to the changes of wind and atmospheric forcing directly obtained from the MPI-ESM-LR model and that were used to generate the meteorological tide data.

In summary, STS, which inherently include the TC correction applied, for the historic period are slightly less than 1 m (see Figure 24). Considering the SL for the future periods, STS plus SLR, for the near term future the SL variation and SL is estimated in

0.26 and 1.19 m respectively (Figure 28). Estimated values for SL change and SL, also considering SLR rise, for the medium term future period is 0.49 m and 1.42 m (Figure 31), respectively. For the long term period, considering SLR, the respective values are 0.81 m and 1.74 m (Figure 34). Table 5 summarizes the final results considering also the uncertainty of SLR.

Table 5. Sea Level (SL) and its change due to each contributing factor for each climatic period.

SL Projections (m)							
	Historical	Near Term		Medium Term		Long Term	
		SL (m)	Δ SL (m)	SL (m)	Δ SL (m)	SL (m)	Δ SL (m)
STS (no TC)	0.13	0.17	0.04	0.13	0.00	0.12	-0.01
TC	0.80	0.90	0.10	0.90	0.10	0.90	0.10
STS (w/TC)	0.93	1.07	0.14	1.03	0.10	1.02	0.09
SLR		0.12		0.39		0.72	
STS w/TC+SLR	0.93	1.19	0.26	1.42	0.49	1.74	0.81
SL Uncertainty (m)							
	Historical	SL Near Term		SL Medium Term		SL Long Term	
		Lower	Upper	Lower	Upper	Lower	Upper
SLR		0.09	0.19	0.29	0.49	0.51	0.99
STS w/TC+SLR	0.93	1.16	1.26	1.32	1.52	1.53	2.01
SL Relative Contributions (%)							
	SL				ΔSL		
	Historical	Near Term	Medium Term	Long Term	Near Term	Medium Term	Long Term
STS (no TC)	14.0	14	9	7	15	0	-1
TC	86.0	76	63	52	38	20	12
SLR		10	27	41	46	80	89

The analytical model used here, corrected with TC and with added SLR estimates, can be expected to be a useful tool for generating and analyzing the impact of meteorological tide series and STS, since it is based on solid physical principles. The added value of this approach is that it can be applied to meteorological data rather than to be restricted to sea level data either obtained from TG or simulated by appropriate ocean models. We note

that TG records are much more scarce than meteorological data. This is, indeed, the case of Mozambique where few TG records are available and with a questionable quality.

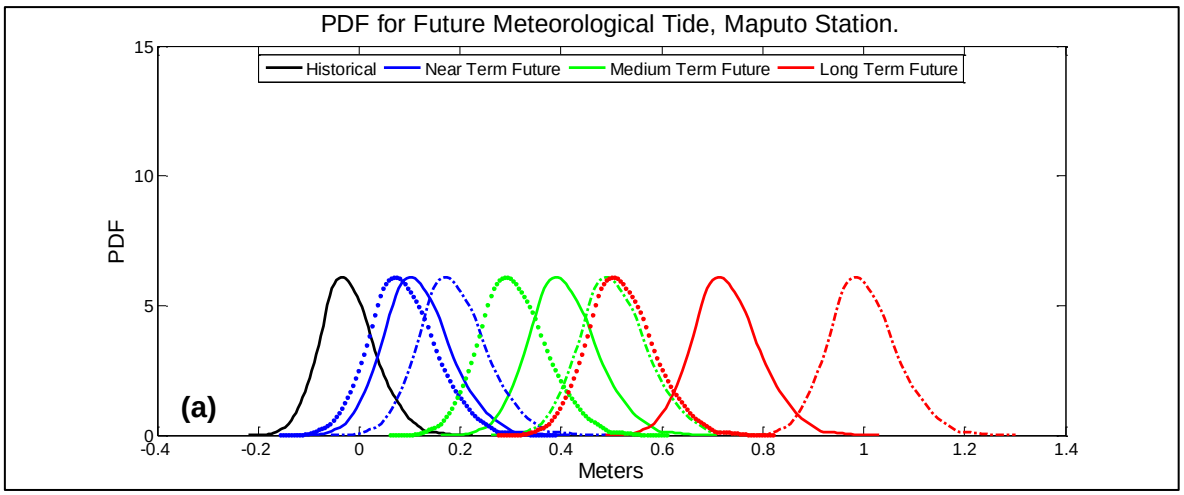

Figure 37. (Continued on next page, see caption)

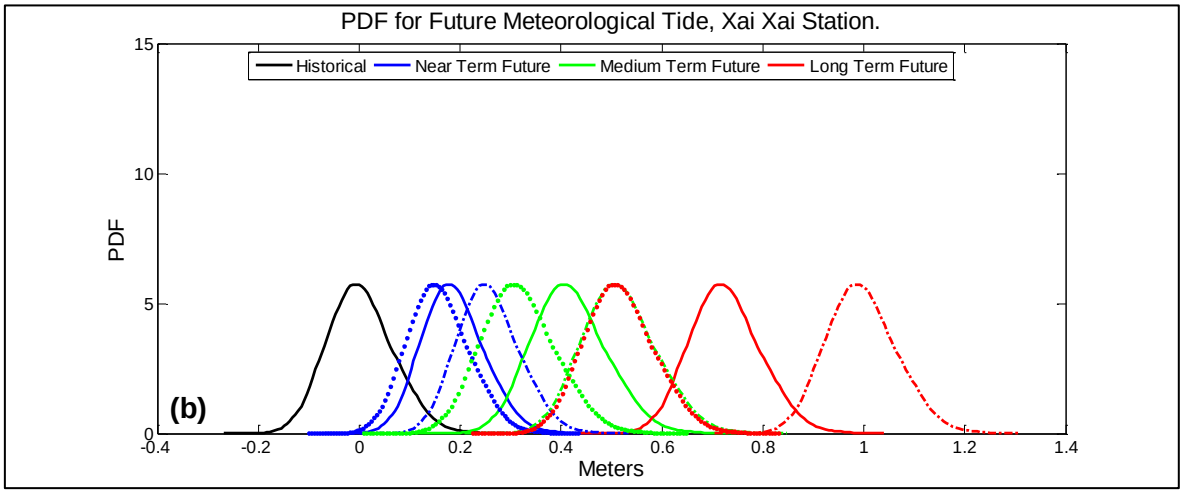

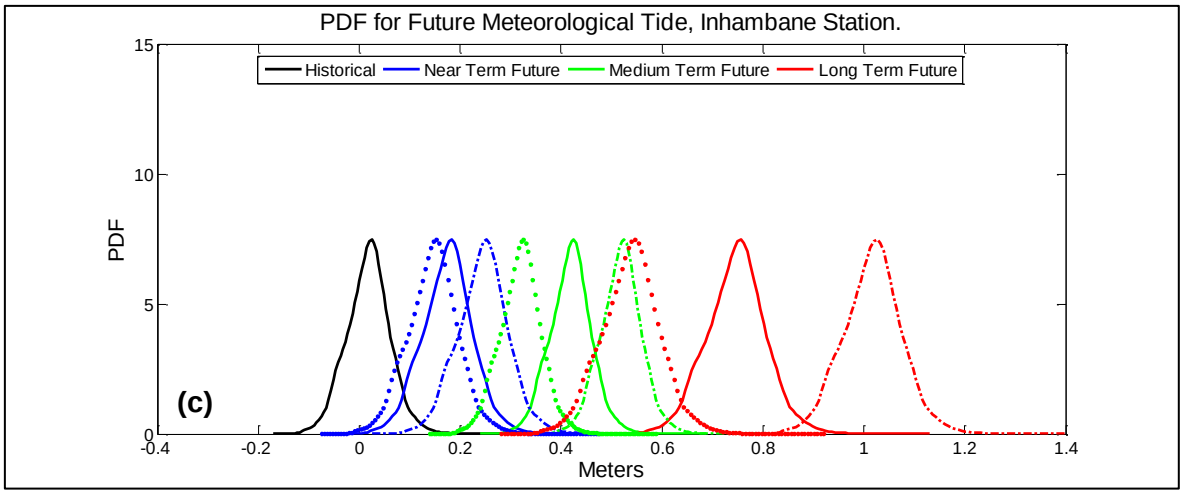

Figure 37. (Continued on next page, see caption)

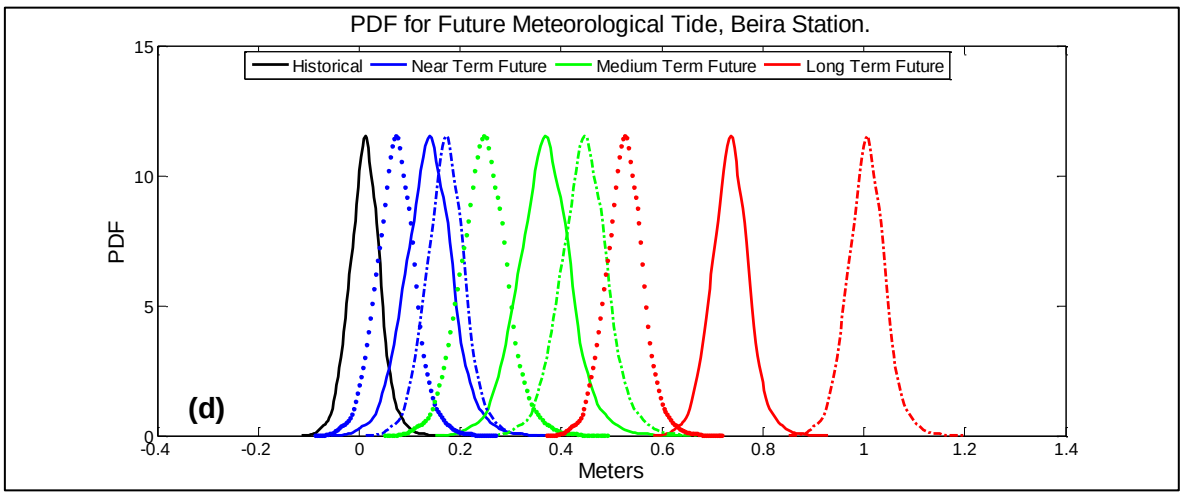

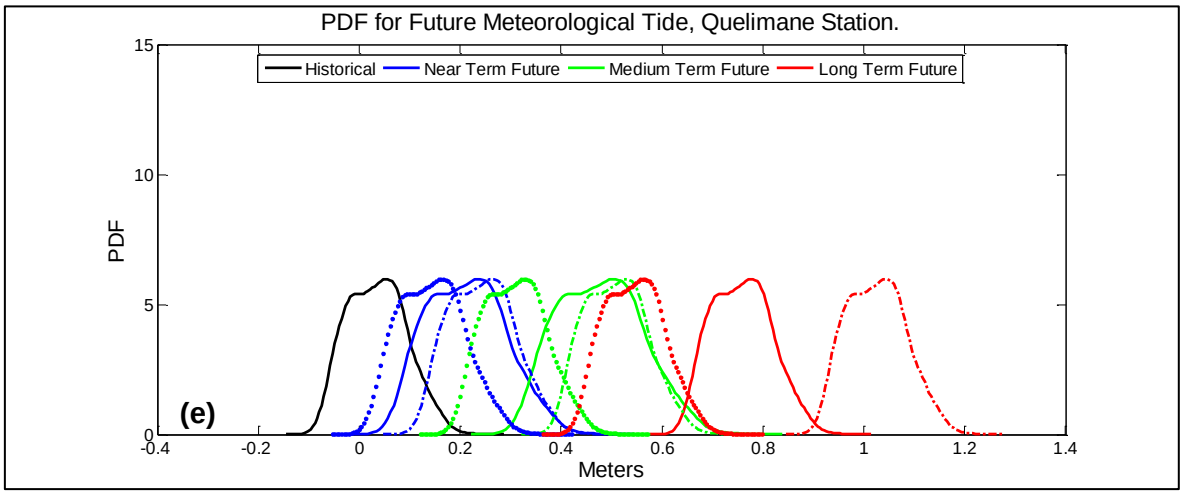

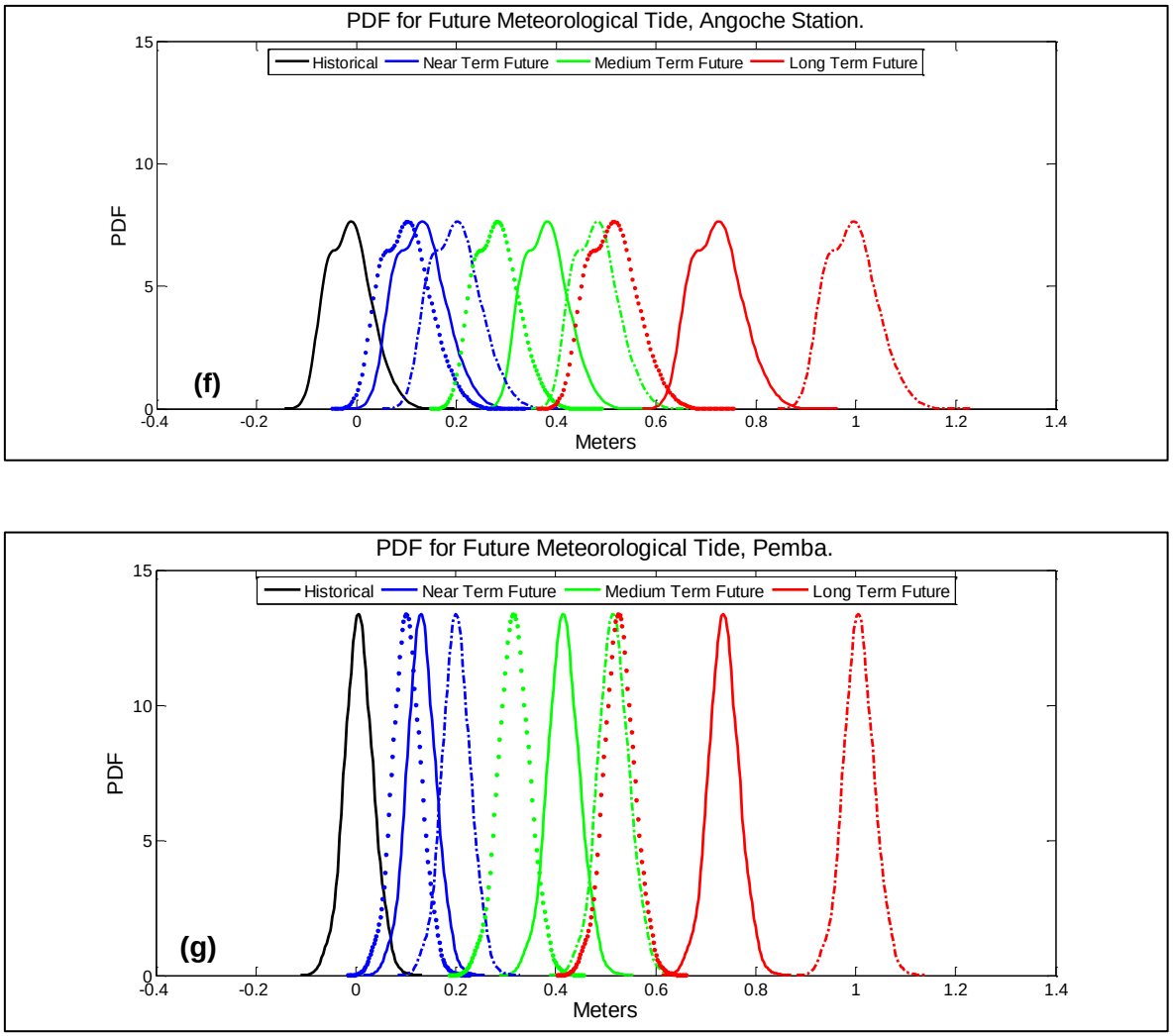

Figure 37. PDFs of meteorological tide (solid line) for the historic and future periods (with uncertainties) for (a) Maputo, (b) Xai-Xai, (c) Inhambane, (d) Beira, (e) Quelimane, (f) Angoche and (g) Pemba. The dotted lines and dash-dotted lines represent the lower and upper uncertainty limits. SLR of 0.12 m, 0.39 m and 0.72 m were considered for the near, medium and long term future, respectively.

Notwithstanding its great simplicity, the method of STS estimation from meteorological information data, allows to obtain useful results with a minimum calculation effort. The analytical model used in this study simulates well the storm surge events in the considered locations.

The results achieved in this study contain important conclusions of interest to flood risk managers, coastal engineers and other decision makers. It follows from this work that any risk analysis must recognize the dependence of tide and STS.

Dasgupta et al (2009b) studied climate change and the future impacts of storm-surge disasters in developing countries. They report that in Mozambique, the cities of Nacala,

Quelimane and Beira, are in a rank of top 10 cities of southern Africa region, with severe impacts of future storm surge on coastal areas, with rank of 1.0, 2.5 and 4.0, respectively. Despite the impacts in cities observed from their study, the study does not mention the heights that the storm surge will reach in the future climate, unlike our present study. Although the methodologies applied in both studies were different, there is an agreement with respect to the storm surge height obtained from the present study and the expected impacts in the study of Dasgupta et al (2009b). Neumann et al (2013) also suggest an enhancement of storm surge in the future. In summary, model results suggest that for the future climate change scenario, in the coast of Mozambique, the storm surges will be characterized by an enhancement of intensity.

This analysis demonstrates a proof of concept for storm surge and SLR risk analysis for seven stations along the coast of Mozambique. The method developed for this analysis has the advantage of being able to be applied in areas where tide gauge data are relatively sparse.

Considering the height of storm surge for future climate change scenarios along the coast can reach more than 1.0 m, the major impact to Mozambique would be a possible increase in frequency and scale of sea flooding from storm surges brought about by tropical cyclones, mainly if the STS arrive at the coast during spring tide. These events are of practical significance for flood risk, particularly at central region of Mozambique where low-lying land areas are frequent (see Figure 2).

This confirms the necessity to assess the socio-economic impacts of coastal floods based on the combination of SLR and storm surge projections, as the common effect is nonlinear.

5.1 Directions for Further Research

One of major uncertainties in the results of this study is related to the properties of TCs and their association with STS. Here, a correction was used to minimize two aspects: the low horizontal resolution of the MPI-ESM-LR model which underestimates those properties, and the future climate scenarios of TCs. A more realistic approach, which eliminates this problem consists of performing a dynamical downscaling simulations with the MPI-ESM-LR forcing a high-resolution regional model such as the WRF model.

Therefore, one could generate TC climate data which would allow to correctly identify the properties of TCs and their suggested increase of intensity for the future.

This study does not include an assessment on flood and inundation due to storm surge. The further research will consist on the assessment of the risk of inundation due to storm surge caused by extreme events like tropical cyclone.

5.2. Recommendation

Taking into account the difficulties we went through for the calculation, validation and work comparison with other authors studies, due to lack of TG data we recommend:

- A countrywide survey on high water mark collection for the storm surge due to tropical cyclones is required; The wind and pressure observations for TCs is required.
- A local storm surge database needed to be developed. A collection of Tide gauge records should be collected for all storm surge prone areas along the coast and the tide should be removed from these records, the residual must be very well organized in database.

Despite this study not include the inundation level, nevertheless, our recommendation goes to: the structural options, for adapting the areas to address the risks of inundation and episodic flooding. This includes constructing or reinforcing new and existing levees and, elevating vulnerable structures in low-lying areas subject to episodic flooding; the nonstructural approaches, include planning a managed retreat from the areas which probably face the most severe risks, and utilization of financial mechanisms, such as crop and property insurance programs.

This study gives a vision of likely changes in storm-surge return levels of coastal storm surges in the future. Depending on the location, these estimates may significantly alter risk assessment related to high water levels and should be considered a relevant result for stakeholders and policy makers involved in decisions about coastal infrastructure and environmental protection decisions.

References

Anthes, R. A., 1982. “Tropical cyclones, their evolution, structure and effects”. *Met Mon* 19, 41, 208 pp.

Bender, M. A., Knutson, T. R., Tuleya, R. E., Sirutis, J. J., Vecchi, G. A., Garner, S. T., and Held, I. M. 2010. “Modeled Impact of Anthropogenic Warming on the Frequency of Intense Atlantic Hurricanes”. *Science* Vol. 327 no. 5964 pp. 454-458. DOI: 10.1126/science.1180568.

Bowden, K.F., 1983. “Physical Oceanography of coastal water”. *Ellis Horwod Ldt*., Chichester, 302 pp.

Brands, S., Herrera, S., Fernandez , J., Guterrez, J.M., 2013. “How well do CMIP5 Earth System Models simulate present climate conditions in Europe and Africa? A performance comparison for the downscaling community”. Clim Dyn (2013) 41:803–817, DOI 10.1007/s00382-013-1742-8.

Camargo, S. and Wing, A. A., 2016. “Tropical cyclones in climate models*”. WIREs Clim Change 2016, 7:211–237. doi: 10.1002/wcc.373.*

Cazenave, A., Dominh, K., Guinehut, S., Berthier, X, Llovel, W., Ramillien, G., Ablain, M., Larnicol, G., 2008. “Sea level budget over 2003–2008: A reevaluation from GRACE space gravimetry, satellite altimetry and Argo, Glob”. *Planet Change*, DOI:10.1016/j.gloplacha.2008.10.004.

Cazenave, A., and Llovel, W., 2010. “Contemporary Sea Level Rise”. Annual Review of *Marine Science*”. Vol. 2: 145-173, 2010. DOI: 10.1146/annurev-marine-120308-081105.

Chang-Seng, D. S., and Jury, M. R., 2010. “Tropical cyclones in the SW Indian Ocean. Part 2: structure and impacts at the event scale”. *Meteorology and Atmospheric Physics*, 1–16.

Church, J.A., J.M. Gregory, N.J. White, S.M. Platten, and J.X. Mitrovica. 2011. “Understanding and projecting sea level change”. *Oceanography* 24(2):130–143, http://dx.doi.org/10.5670/oceanog.2011.33.

Colling, A. 2001. “Ocean Circulation”, *Open University Course Team*. Second Edition. 2001. ISBN 978-0-7506-5278-0.

Crimp, S. J., Lutjeharms, J. R. E. and Mason, S. J., 1998. “Sensitivity of a tropical-temperate trough to sea-surface temperature anomalies in the Agulhas retroflection region”. *Water S. A.,* 24, 93-101.

Csanady, G. T., 1982. “Circulation in the Coastal Ocean”. *Reidel,* 279 pp.

Dasgupta, S., Laplante, B., Murray, S., and Wheeler, D., 2009a. “Sea-Level Rise and Storm Surges: A Comparative Analysis of Impacts in Developing Countries”. Policy Research Working Paper 4901. The World Bank Development Research Group Environment and Energy Team. April 2009.

Dasgupta, S., Laplante, B., Murray, S., and Wheeler, D., 2009b. “Climate Change and the Future Impacts of Storm-Surge Disasters in Developing Countries”. *CGD Working Paper 182. Washington,* D.C.: Center for Global Development. September 2009.

Dean, R.G., and Dalrymple, R.A., 2002. “Coastal Processes with Engineering Application”. *Cambridge University Press*, pp. 475.

Dikolli, S. S., Evans, J. H., JHales, J., Matejka, M., Moser, D. V., Williamson, M. G., 2012. “Testing Analytical Models Using Archival or Experimental Methods”. Accounting Horizons Vol. 27, No. 1, 2013 pp. 129–139, DOI: 10.2308/acch-50287.

Donat, M. G., Renggli, D., Wild, S., Alexander, L. V., Leckebusch, G. C., and Ulbrich, U., 2011. “Reanalysis suggests long-term upward trends in European storminess since 1871”. *Geophys. Res. Lett.,* 38, L14703, DOI:10.1029/ 2011GL047995.

Doyle, J. D., 2002. “Coupled ocean wave/atmosphere mesoscale model simulations of cyclogenesis”. Tellus A Volume 47, Issue 5, pages 766–778, October 1995 DOI: 10.1034/j.1600-0870.1995.00119.x.

Du Plessis, L. A., 2002. “A review of effective flood forecasting, warning and response system for application in South Africa”, *Water SA*, 28, 129 – 137.

Elsberry, R.L. (Ed), 1995. “Global perspectives on tropical cyclones”, *WMO Report* TD-No. 693, Geneva, Switzerland, 289 pp.

Emanuel K. 2003. “Tropical Cyclones”. *Annual Review of Earth and Planetary Sciences* 31: 75-104.

Emanuel, K., 2008. “The Hurricane - Climate Connection”. *Bull. Amer. Meteor. Soc*., 89, ES10–ES20. doi: http://dx.doi.org/10.1175/BAMS-89-5-Emanuel.

Emanuel, K., Sundararajan, R., and William, J., 2008. “Hurricanes and global warming: Results from downscaling IPCC AR4 simulations”. *Journal of Climate*, 89, 347-367.

Emanuel, K. A., 2013. “Downscaling CMIP5 climate models shows increased tropical cyclone activity over the 21st century”. *Proc. Natl. Acad. Sci*. USA, 110, 12 219–12 224, doi:10.1073/pnas.1301293110.

Faggioni, O., Arena, G., Bencivenga, M., Bianco, G., Bozzano, R., Canepa, G., Lusiani, P., Nardone, G., Piangiamore, G., Soldani, M., Surace, L., and Venzano, G. , 2006. “The Newtonian approach in meteorological tide waves forecasting: Preliminary observations in the East Ligurian harbours”. *Annals of geophysics,* vol. 49, n.6, December 2006.

Flather, R.A., 2001. “Storm surges”. In: J.H. Steele, S.A. Thorpe, and K.K. Turekian (Editors), Encyclopedia of Ocean Sciences. Academic Press, San Diego, 2882-2892.

Flato, G., J. Marotzke, B. Abiodun, P. Braconnot, S.C. Chou, W. Collins, P. Cox, F. Driouech, S. Emori, V. Eyring, C. Forest, P. Gleckler, E. Guilyardi, C. Jakob, V. Kattsov, C. Reason and M. Rummukainen, 2013: Evaluation of Climate Models. In: Climate Change 2013: “The Physical Science Basis. Contribution of Working Group I to the Fifth Assessment Report of the Intergovernmental Panel on Climate Change”. [Stocker, T.F., D. Qin, G.-K. Plattner, M. Tignor, S.K. Allen, J. Boschung, A. Nauels, Y. Xia, V. Bex and P.M. Midgley (eds.)]. Cambridge University Press, Cambridge, United Kingdom and New York, NY, USA.

Fallet, U., Brummer, G. J., Zinke, J., Vogels, S., and Ridderinkhof, H., 2010. “Contrasting seasonal fluxes of planktonic foraminifera and impacts on paleothermometry in the Mozambique Channel upstream of the Agulhas Current”, *Paleoceanography*, 25, PA4223, doi:10.1029/2010PA001942.

Fitchett, J. M. and Grab, S. W., 2014. “A 66-year tropical cyclone record for south-east Africa: temporal trends in a global context”. *International journal of climatology*, DOI: 10.1002/joc.3932.

Gama, C., Dias, J., Ferreira, O., and Taborda, R., 1994. “Analysis of storm surge in Portugal between June 1986 and May 1988”. Proceeding Littoral'94, EUROCOAST, Lisboa, Portugal: 381-387.

Garrett, C. J. R., 1983. “Variable sea level and strait flows in the Mediterranean: Atmospheric pressure a theoretical study of the response to meteorological forcing”. *Oceanol. Acta, 1983*, Vol. 6, nº1, 79-87.

Gaslikova, L., Schwerzmann, A., Raible, C. C. and Stocker, T. F., 2011. “Storm surge insurable losses for future scenarios”. Nat. Hazards Earth Syst. Sci., 11, 1205–1216, doi:10.5194/nhess-11-1205-2011.

Gill, A.E., 1982. “Atmosphere-Ocean Dynamics”. Academic Press, 661pp.

Giorgetta, M. A., Jungclaus, J., Reick, C. H., Legutke, S., Bader, J., B□ottinger, M., Brovkin, V., Crueger, T., Esch, M., Fieg, K., et al., 2013. “Climate and carbon cycle changes from 1850 to 2100 in MPI-ESM simulations for the Coupled Model Intercomparison Project Phase 5”. *Journal of Advances in Modeling Earth Systems* 5, 572-597. DOI:10.1002/jame.20038.

Gornitz, V., 2005. “Storm Surge”. In: M.L. Schwartz (ed.), Encyclopedia of Coastal Science. Springer, 912-914.

Gray, W.M., 1968. "A global view of the origin of tropical disturbances and storms". *Mon. Wea. Rev*., 96, 669-700.

Hamilton, K., 2008. “Numerical resolution and modeling of the global atmospheric circulation: A review of our current understanding and outstanding issues, in High Resolution Numerical Modelling of the Atmosphere and Ocean”. Edited by K. Hamilton and W. Ohfuchi, pp. 7– 27, Springer, New York, doi:10.1007/978-0-387-49791-4_1.

Held, I.M., Soden, B.J., 2006. “Robust Responses of the Hydrological Cycle to Global Warming”. *Journal of Climate*, Vol. 19. DOI: 10.1175/2010JCLI4045.1

Henderson-Sellers, Zhang, H., Berz, G., Emanuel, K., Gray, W., Landsea, C., Holland, G., Lighthill, J., Shieh, S.-L., and Webster, P., 1998. “Tropical cyclones and global climate change: A post IPCC assessment”. *Bulletin of the American Meteorological Society*, 79, 19-38.

Hinton, C., Townend, I.H. and Nicholls, R.J., 2007. Coastal Processes. Chap. 9 in ‘’Future flooding and coastal erosion risks” ed. Thorne, C.R., Evans, E.P. and Penning Rowsell, E.C. Thomas Telford. 514pp. ISBN: 978-0-7277-3449-5.

Ho, C.-H., Kim, J.-H., Jeong, J.-H., Kim, H.-S., and Chen, D., 2006. “Variation of tropical cyclone activity in the South Indian Ocean: El Niño–Southern Oscillation and Madden-

Julian Oscillation effects". *Journal of Geophysical Research*, 111, D22101, DOI:10.1029/2006JD007289

Hoguane, A., 1999". Sea level measurements and analysis in the western Indian Ocean". *National report, Mozambique. IOC,UNESCO,* 6-7 21.

Hoguane, A.M. and Pereira, M.A.M., 2003. "*National Report*: Marine biodiversity in Mozambique - the known and the unknown". p. 138-155. In C. Decker, C. Griffiths, K. Prochazka, C. Ras and A. Whitefield Marine Biodiversity in Sub-Saharan Africa: the known and the unknown. Proceedings of the marine biodiversity in Sub-Saharan Africa: the known and the unknown Cape Town, South Africa 23-26 September 2003.

Holthuljsen, L.H., 2007. "Waves in oceanic and coastal waters". *Cambridge University Press,* The Edinburgh Building, Cambridge CB2 8RU, UK. ISBN-10 0-521-86028-8.

Hoozemans, F.M.J., Marchand, M., and Pennekamp, H.A., 1993. "A Global Vulnerability Analysis: *Vulnerability Assessment for Population, Coastal Wetlands and Rice Production on a Global Scale*". 2nd edition. Delft Hydraulics and Ministry of Transport, Public Works and Water Management, Delft and The Hague. 202p.

INGC (National Institute for Disaster Management), 2009. "*Main Report*: INGC Climate Change Report: Study on the impact of climate change on disaster risk in Mozambique". *(K. Asante, G. Brundrit, P. Epstein, A. Fernandes, M.R. Marques, A. Mavume, M. Metzger, A. Patt, A. Queface, R. Sanchez del Valle, M. Tadross, and R. Brito, eds.). Maputo, Mozambique: INGC.*

IPCC 2007. "Contribution of Working Group II to the Fourth Assessment Report of the Intergovernmental Panel on Climate Change, 2007". M.L. Parry, O.F. Canziani, J.P. Palutikof, P.J. van der Linden and C.E. Hanson (eds). Cambridge University Press, Cambridge, United Kingdom and New York, NY, USA, 976.

IPCC, 2013. "Climate Change 2013: The Physical Science Basis. Contribution of Working Group I to the Fifth Assessment Report of the Intergovernmental Panel on Climate Change", [Stocker, T.F., D. Qin, G.-K. Plattner, M. Tignor, S.K. Allen,J. Boschung, A. Nauels,Y. Xia, V. Bex and P.M. Midgley(eds.)]. *Cambridge University Press*, Cambridge, United Kingdom and New York, NY, USA, 1535 pp.

IPCC, 2014. "Summary for policymakers. In: Climate Change 2014: Impacts, Adaptation, and Vulnerability. Part A: Global and Sectoral Aspects. Contribution of Working Group

II to the Fifth Assessment Report of the Intergovernmental Panel on Climate Change", [Field, C.B., V.R. Barros, D.J. Dokken, K.J. Mach, M.D. Mastrandrea, T.E. Bilir, M. Chatterjee, K.L. Ebi, Y.O. Estrada, R.C. Genova, B. Girma, E.S. Kissel, A.N. Levy, S. MacCracken, P.R. Mastrandrea, and L.L. White (eds.)]. *Cambridge University Press*, Cambridge, United Kingdom and New York, NY, USA, pp. 1-32.

Jeffreys, H., 1916. "Causes contributory to the annual variation of latitude, *Mon. Not. R. Astron. Soc*., 76, 499-524, 1916.

Jelesnianski, C.P., 1972. SPLASH (Special Program To List Amplitudes of Surges From Hurricanes): 1. Landfall Storms. NOAA Technical Memorandum NWS TDL-46. NWS Systems Development Office, Silver Spring, MD, 56 pp.

Jury MR, Pathack B. 1991. "A study of climate and weather variability over the tropical Southwest Indian Ocean". *Meteorol. Atmos. Phys.* 47:37–48.

Jury, M. R., 1993. "A preliminary study of climatological associations and characteristics of tropical cyclones in the SW Indian Ocean". *Meteor. Atmos. Phys.,* 51, 101–115.

Jury M.R., Pathack, B., and Parker, B., 1999. "Climatic determinants and statistical prediction of tropical cyclone days in the Southwest Indian Ocean". *J. Climate* 12: 1738–46.

Kantha, L. H., Whitmer, K. R. and Born, G. H.,1994. "The Inverted Barometer Effect in Altimetry: A Study in the North Pacific", *TOPEX/POSEIDON Res. News*, 2, 18-23, March, 1994.

Knutson, T. R., McBride, J.L., Chan, J., Emanuel, K., Holland, G., Landsea, C., Held, I., Kossin, J. P., Srivastava, A. K. and Sugi, M., 2010. "Tropical cyclones and climate change". *Nature Geoscience* 3, 157 – 163 (2010). DOI:10.1038/ngeo779.

Knutson, T. R., Sirutis, J.J., Vecchi, G. A., Garner, S., Zhao, M., Kim, H., Bender, M., Tuleya, R. E., Held, I. M., and Villarini, G., 2013. "Dynamical Downscaling Projections of Twenty-First-Century Atlantic Hurricane Activity: CMIP3 and CMIP5 Model-Based Scenarios". *J. Climate,* 26, 6591–6617. DOI: http://dx.doi.org/10.1175/JCLI-D-12-00539.1

Klinman, C. J. and Reason C., 2008. "On the peculiar storm track of TC Favio during the 2006–2007 Southwest Indian Ocean tropical cyclone season and relationships to ENSO". *Meteorol Atmos Phys* 100, 233–242 (2008) DOI: 10.1007/s00703-008-0306-7.

Landsea, C. W., Pielke, R. A., Mestas-Nuñez, A. M. and Knaff, J .A. 1999. "Atlantic basin hurricanes. Indices of climatic changes". *Climate Change*, 42, 89-129.

Large, W.G. and Pond, S., 1981. "Open ocean momentum fluxes in moderate to strong winds". *Journal of Physical Oceanography* 11: 324-336.

Lee, C. J., Park, K. S., Kwon, J., and Kim, S., 2009. " Storm Surge Calculations Using Sea Level Data". *Marine Geodesy,* Volume 32, Issue 2, 2009, pages 108-117, DOI: 10.1080/01490410902869193.

Lutjeharms, J. R. E., Wedepohl, P. M. and Meeuwis, J. M., 2000b. "On the surface drift of the East Madagascar and the Mozambique Currents". *S. Afr. J. Sci.*, 96, 141-147.

Lutjeharms, J. R. E., de Ruijter, W. P. M., Ridderinkhof, H. , van Aken, H., Veth, C., Leeuwen, P. J.V, Drijfhout, S. S., Jansen, J. H. F. and Brummer, G.-J. A., 2000d. "MARE and ACSEX: new research programmes on the Agulhas Current system". *S. Afr. J. Sci.*, 96, 105-110.

Madden, R. A. and Julian, P. R. 1994. "Observations of the 40-50 day tropical oscillation - A review". *Monthly Weather Review*, 122, 814-837.

Manhique AJ, Reason CJC, Rydberg L, Fauchereau N. 2011. "ENSO and Indian Ocean sea surface temperatures and their relationships with tropical temperate troughs over Mozambique and the Southwest Indian Ocean". *Int. J. Climatol.* 31: 1–13, DOI: 10.1002/joc.2050.

Malherbe J., Engelbrecht, F.A., Landmanb, W.A. and Engelbrechta, C.J., 2012. "Tropical systems from the southwest Indian Ocean making landfall over the Limpopo River Basin, southern Africa: a historical perspective". *Int. J. Climatol.32*(7): 1018 – 1032 (2012). DOI: 10.1002/joc.2320.

Matyas, C. J. 2015. "Tropical cyclone formation and motion in the Mozambique Channel". *Int. J. Climatol.,* 35: 375–390. DOI: 10.1002/joc.3985.

Marcos, M., Jordà, G., Gomis, D. and Pérez, B., 2001. "Changes in storm surges in southern Europe from a regional model under climate change scenarios". Global and Planetary Change 77 (2011) 116–128.

Mavume AF, Rydberg L, Roualt M, Lutjeharms JRE. 2009. "Climatology and landfall of tropical cyclones in the southwest Indian Ocean". *West.Indian Ocean J. Mar. Sci.* 8: 15–36.

Menemenlis, D., Fukumori, I., and Lee, T., 2007. “Atlantic to Mediterranean Sea Level Difference Driven by Winds near Gibraltar Strait“. *American Meteorological Society* Vol.37, DOI: 10.1175/JPO3015.1

McBride, J. L., 1995. “Tropical cyclone formation”. In: Elsberry, R. L. (ed.), *Global perspectives on tropical cyclones*. World Meteorological Organization, Geneva.

Miles J. W., 1960. “On the generation of surface waves by turbulent shear flows”. *J. Fluid Mech*. 7, 469-478.

Moon, Il-J., 2005. “Impact of a coupled ocean wave–tide– circulation system on coastal modeling”, Ocean Modelling, 8, 203–236.

Moss, R. H., Edmonds, J. A., Hibbard, K.A. Martin R. Manning, Steven K. Rose, Detlef P. van Vuuren, Timothy R. Carter, Seita Emori, Mikiko Kainuma, Tom Kram, Gerald A. Meehl, John F. B. Mitchell, Nebojsa Nakicenovic, Keywan Riahi, Steven J. Smith, Ronald J. Stouffer, Allison M. Thomson, John P. Weyant, Thomas J. Wilbanks, 2010. “The next generation of scenarios for climate change research and assessment”. Nature 463, 747-756. doi:10.1038/nature08823.

Muchangos, A., 1999. “Moçambique paisagens e regiões naturais”. *Tipografia Globo,Lda*. República de Moçambique, 01048/FBM/93, 163pp.

Mucke, P., Lars Jeschonnek, Matthias Garschagen, Almuth Schauber, Thomas Seibert, Torsten Welle, Jörn Birkmann, Jakob Rhyner, Stefan Kohler, Thomas Loster, Dirk Reinhard, Ira Matuschke, 2014. *WorldRiskReport 2014*: “The city as a risk area”. Bündnis Entwicklung Hilft. ISBN 978-3-9814495-4-9.

Murty,T.S., 1984. “Storm surges - meteorological ocean tides”. National Research Council of Canada, *Canadian Bulletin of Fisheries and Aquatic Sciences*, Vol.212, 897 pp.

Murakami, H., Wang, Y., Yoshimura, H., Mizuta, R., Sugi, M., Shindo, E., Adachi, Y., Yukimoto, S., Hosaka, M., Kusunoki, S., Ose, T., and Kitoh, A., 2012. “Future Changes in Tropical Cyclone Activity Projected by the New High-Resolution MRI-AGCM”. *J. Climate,* 25, 3237–3260. DOI: http://dx.doi.org/10.1175/JCLI-D-11-00415.1.

New, A. L., Alderson, S. G., Smeed, D. A. and Stansfield, K. L., 2006. “On the circulation of water masses across the Mascarene Plateau in the South Indian Ocean”, *Deep Sea Res*., Part I, 54, 42–74.

Nicholls, R.J. and Tol, R.S.J., 2006." Impacts and responses to sea-level rise: a global analysis of the SRES scenarios over the twenty-first century". *Phil. Trans. R. Soc*. A 364, 1073–1095 (23 February 2006) (doi:10.1098/rsta. 2006.1754).

Nicholls, R.J. and Cazenave, A., 2010. Sea-Level Rise and Its Impact on Coastal Zones. *Science*, Vol. 328, 2010.

Neumann, J. E., Emanuel, K. A., Ravela, S., Ludwig, L. C., Verly, C., 2013. "Assessing the risk of cyclone-induced storm surge and sea level rise in Mozambique", *WIDER Working Paper*, No. 2013/036, ISBN 978-92-9230-613-7.

Nkono, N., 2012. "An Introduction to Storm Surge Prediction". Preliminary reference for the 8th JCOMM/TCP Workshop on Storm Surge and Wave Forecasting (SSW-8). Nairobi, Kenya 19 – 23 November 2012. JCOMM Technical Report Nº 68. https://www.wmo.int/pages/prog/amp/mmop/jcomm_reports.html

Padgett, G. 2007. "Monthly Global Tropical Cyclone Summary: February 2007. http://www.maybagyo.com/garyp mgtcs/feb07sum.htm..

Pawlowicza, R., Beardsleyb, B., and Lentzb, S., 2002. "Classical tidal harmonic analysis including error estimates in MATLAB using T TIDE$", *Computers & Geosciences* 28 (2002) 929–937. PII: S 0098-3004(02)00013-4.

Peixoto, J. P. and Oort, A., 1992. "Physics of Climate". *1. ed. New York: American Institute of Physics,* 1992, 520 pp.

Palmén, E., 1948. "On the formation and structure of tropical hurricanes". *Geophysica*, 3, 26-38.

Pielke, R. A. and Landsea, C. W., 1999. "La Niña, El Niño, and Atlantic hurricane damages in the United States". *Bulletin of the American Meteorological Society*, 80, 2027-2033.

Powell, M.D., Vickery, P.J., and Reinhold, T. A., 2003. "Reduced drag coefficient for high wind speeds in tropical cyclones". *Nature 422: 278-283.*

Pradhan, D., Mitra, A., De, U. K., 2012. "Estimation of pressure drop and storm surge height associated to tropical cyclone using Doppler velocity". Indian Journal of Radio & Space Physics. Vol 41, June 2012, 348-358.

Proudman, J., 1953. "Dynamical Oceanography". *1. ed. London,Methuen and* Co., 1953.

Pugh, D. T., 1987. “Tides, Surges and Mean Sea Level”. *GreatBritain: John Wiley & Sons,* 1987, 472 pp.

Pugh, D. T., 2004. “Changing sea levels: Effects of tides, weather and climate*”*. Cambridge University Press.

Pugh, D., and Woodworth,P., 2014. “Sea-Level Science: Understanding Tides, Surges, Tsunamis and Mean Sea-Level Changes”. *Science,* Cambridge University Press, 2014. ISDN 978-1-107-02819-7.

Rahmstorf, S., 2007. “A Semi-Empirical Approach to Projecting Future Sea-Level Rise”. *Science* Vol. 315 nº 5810 pp. 368-370.

Reason C. J. C. and Keibel, A., 2004. “Tropical Cyclone Eline and Its Unusual Penetration and Impacts over the Southern African Mainland”. *Wea. Forecasti*ng, **19**, 789–805. doi: http://dx.doi.org/10.1175/1520-0434(2004)019<0789:TCEAIU>2.0.CO;2

Reason, C. J. C., 2007. “Tropical cyclone Dera, the unusual 2000/01 tropical cyclone season in the southwest Indian Ocean and associated rainfall anomalies over Southern Africa”. *Meteorol Atmos Phys 97*, 181–188 (2007) DOI 10.1007/s00703-006-0251-2

Riahi, K., Rao, S., Krey, V., Cho, C., Chirkov, V., Fischer, G., Kindermann, G., Nakicenovic, N., Rafaj, P., 2011. “RCP8.5 – A scenario of comparatively high greenhouse gas emissions”. *Climatic Change* (2011). 109:33–57 DOI 10.1007/s10584-011-0149-y.

Saetre, R. and Silva, R. P., 1979. “The Marine Fish Resources of Mozambique. *Reports on Surveys with the R/V*” Dr. Fridtjof Nansen, Serviço de Investigação Pesqueira. Maputo. Institute of Marine Research, Bergen, 134p.

Saetre, R. and Silva, R., 1982. “Water masses and circulation on the Mozambique channel”. *Rev. Inv. Pesq*: 3-38.

Saetre, R., 1985. “Surface currents in the Mozambique Channel”. *Deep-Sea Res.*, 32, 1457-1467.

Santos, F. D. and Miranda, P., (eds), 2006. “Alterações climáticas em Portugal, cenários, impactos e medidas de adaptação”. *Projecto SIAM II, Gradiva, Lisboa* 2006, 506p.

Seneviratne, S.I., Nicholls, N., Easterling, D., Goodess, C.M., Kanae, S., Kossin, J., Luo, Y., Marengo, J., McInnes, K., Rahimi, M., Reichstein, M., Sorteberg, A., Vera, C., and

Zhang, X., 2012. “Changes in climate extremes and their impacts on the natural physical environment”. In: Managing the Risks of Extreme Events and Disasters to Advance Climate Change Adaptation [Field, C.B., V. Barros, T.F. Stocker, D. Qin, D.J. Dokken, K.L. Ebi, M.D. Mastrandrea, K.J. Mach, G.-K. Plattner, S.K. Allen, M. Tignor, and P.M. Midgley (eds.)]. *A Special Report of Working Groups I* and II of the Intergovernmental Panel on Climate Change (IPCC). Cambridge University Press, Cambridge, UK, and New York, NY, USA, pp. 109-230.

Shen, J., and Gong, W., 2009. “Influence of model domain size, wind directions and Ekman transport on storm surge development inside the Chesapeake Bay”: a case study of extratropical cyclone Ernesto. *J. Mar. Sys.* 75, 198-215.

Silverman, B. W., 1986. “*Density estimation for statistics and data analysis”*. Chapman and Hall, 175pp.

Simpson, R.H., and Riehl, H., 1981. “The Hurricane and Its Impact. Louisiana State” University Press, Baton Rouge, LA, 398pp.

Smith, S. D., 1980. “Wind stress and heat flux over the ocean in gale force winds”. *J. Phys. Oceanogr.,* 10, 709-726.

Stammer, D., Cazenave, A., Ponte, R. M., and Tamisiea, M. E., 2013. “Causes for Contemporary Regional Sea Level Changes”. *Annu. Rev. Marine. Sci*. 2013.5:21-46.

Suzuki, M., Igarashi, R., Sekiya M., Utsugi T., Morishita S., Yukawa M. and Ohya Y., 2004. “Dynactin is involved in a checkpoint to monitor cell wall synthesis in Saccharomyces cerevisiae”. *Nat Cell Biol* 6(9):861-71.

Taylor, K. E., Stouffer, R. J. and Meehl, G. A. 2012. “An Overview of CMIP5 and the Experiment Design”. *Bull. Amer. Meteor. Soc.*, **93**, 485–498. doi: http://dx.doi.org/10.1175/BAMS-D-11-00094.1

Tang, Y.M., Holloway, P., and Grimshaw, R., 1997. “A numerical study of the storm surge generated by Tropical Cyclone Jane”. *J. Phys. Oceanogr.* 27, 963-976.

Terry, J. P., 2007. “Tropical cyclones: Climatology and impacts in the South Pacific” (pp. 210). New York: Springer.

Tinley, K., 1971. “Determinants of coastal conservation: dynamics and diversity of the environment as exemplified by the Moçambique coast". *Proc. Symp: Nature*

Conservation as a form of land use Gorongosa National Parks – 13-17 September 1971. Sarcus 125-153*).*

Turner, R.K., Subak, S. and Adger, W.N., 1996. "Pressures, Trends, and Impacts in Coastal Zones: Interaction between socio-economic and natural systems". *Environmental Management*, 20, 159-173.

Van Vuuren, D. P., Edmonds, J., Kainuma, M., Riahi, K., Thomson, A., Hibbard, K., Hurtt, G.H., Tom Kram., Volker K., Lamarque, J., Masui, T., Meinshausen, M., Nakicenovic, N.,Smith, S.J., Rose,S.K. 2011. "The representative concentration pathways: an overview". Climatic Change (2011) 109:5–31 DOI 10.1007/s10584-011-0148-z.

Valdiya, K.S., 2004. "Coping with Natural Hazards: Indian Context". Orient Blackswan; January 2004 edition, ISBN-10: 8125027351, 282p.

Vitart, F., Anderson, D.L.T., Stockdale, T., 2003. " Seasonal forecasting of tropical cyclone landfall over Mozambique". *J Climate* 16: 3932–45.

Walker, N. D., 1990. "Links between South African summer rainfall and temperature variability of the Agulhas and Benguela Current Systems". *J. Geophys. Res.*, 95, 3297-3319.

Weisberg, R.H., and Zheng, L., 2006b. "A simulation of the hurricane Charley storm surge and its breach of North Captiva Island". *Florida Scientist* 69, 152-165.

Willmott, C. J., Robesonb, S. M., and Matsuuraa, K., 2012. "Short Communication: A refined index of model performance". *Int. J. Climatol*. 32: 2088–2094 (2012). DOI: 10.1002/joc.2419.

WMO-No. 1076, 2011. "Guide to Storm Surge Forecasting". SPA_ETWS_general_02. Word Meteorological Organization.

Wannawong, W. and Ekkawatpanit, C., 2012. "Tropical Cyclone Wind-Wave, Storm Surge and Current in Meteorological Prediction". Natural Disasters, Dr. Sorin Cheval (Ed.), ISBN:978-953-51-0188-8,InTech,availablefrom: http://www.intechopen.com/books/natural-disasters/tropical-cyclone-wind-wave-stormsurge-and-current-in-meteorological-prediction.

Web Site: Reliefweb.int (2008 June 30). "Topographic Map of Mozambique as of June 2008". Retrieved on April 12, 2016. http://reliefweb.int/map/mozambique/topographic-map-mozambique-jun-2008

Weller, E., C. Wenju, M. Seung-Ki, W. Lixin, A. Karumuri and Y. Toshio. 2014. “More-frequent extreme northward shifts of eastern Indian Ocean tropical convergence under greenhouse warming.” Sci. Rep. 4, 6087; DOI:10.1038/srep06087.

Wunsch C. and Stammer, D., 1997. “Atmospheric loading and the oceanic inverted barometer effect”. Reviews of Geophysics, 35, 1 /February 1997. pages 79-107.

Xie, B., Zhang, Q. and Wang, Y., 2008. “Trends in hail in China during 1960–2005”, Geophys. Res. Lett., 35, L13801, doi:10.1029/2008GL034067.

Yamada, Y., Oouchi, K., Satoh, M., Tomita, H. and Yanase, W., 2010. “Projection of changes in tropical cyclone activity and cloud height due to greenhouse warming: Global cloud-system-resolving approach”. *Geophysical Research Letters*, Vol. 37, L07709, DOI:10.1029/2010GL042518, 2010.

Yin, J., 2012. “Century to multi-century sea level rise projections from CMIP5 models”. *Geophys. Res. Lett*., 39, L17709, doi:10.1029/2012GL052947.

Appendix A – The predominant tropical cyclone trajectories before making landfall on Madagascar and Mozambique.

Source: Fitchett and Grab (2014).

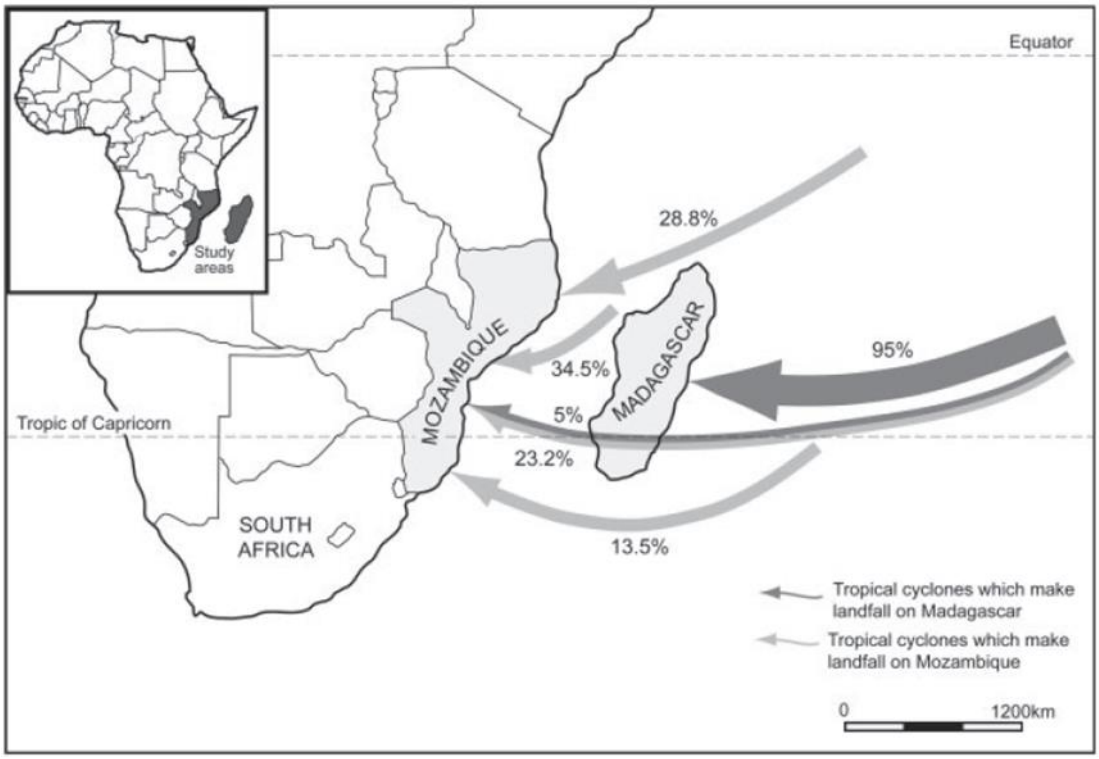

Appendix B - Available Observed data from TG, NOAA and MPI-ESM-LR for the study stations.

Station Name	Tide Gauge Data From INAHINA (Hourly)		Atmospheric Data from NOAA (Hourly)		Atmospheric Data from MPI-ESM-LR (Daily)	
	Period Range	Missing Data(%)	Period Range	Amount of data	Period Range	Amount of data
Maputo	1974, 1980-1986, 1995-2002	33	1973-2011 1986-2005	148,230 89,106	1986 - 2005 2016 - 2035 2045 - 2065 2081 - 2100	7,300 7,300 7,300 7,300
Xai-Xai	No data	100	1973-2011 1986-2005	46,289 29,208	1986 - 2005 2016 - 2035 2045 - 2065 2081 - 2100	7,300 7,300 7,300 7,300
Inhambane	1994-1995	71	1973-2011 1986-2005	60,143 25,617	1986 - 2005 2016 - 2035 2045 - 2065 2081 - 2100	7,300 7,300 7,300 7,300
Beira	1996-2000, 2002	29	1973-2011 1986-2005	97,388 53,813	1986 - 2005 2016 - 2035 2045 - 2065 2081 - 2100	7,300 7,300 7,300 7,300
Quelimane	1995	25	1973-2011 1986-2005	92,484 42,398	1986 - 2005 2016 - 2035 2045 - 2065 2081 - 2100	7,300 7,300 7,300 7,300
Angoche	No data	100	1973-2011 1986-2005	19,545 7,683	1986 - 2005 2016 - 2035 2045 - 2065 2081 - 2100	7,300 7,300 7,300 7,300
Pemba	1984, 1996-2004, 2007-2010	39	1973-2011 1986-2005	77,392 38,735	1986 - 2005 2016 - 2035 2045 - 2065 2081 - 2100	7,300 7,300 7,300 7,300

Appendix C - Major Tropical Cyclone in Indian Ocean Basin, 1985-2014.

Period	Nº of Events	Event name	Date	Maximum 10 minute sustained wind (Km/h)	SLP (hPa)
1985/1986	4	Deleninina	Jan 10-19	135	954
		Erinesta	Jan 29-Feb4	170	927
		Honorinina	Mar 7-23	170	927
		Jefotra	Mar 27-April 5	135	954
1986/1987	2	Clotilda	Feb 9-22	110	970
		Daoda	Mar 2-18	135	954
1987/1988	4	Doaza	Jan 31- Feb 1	135	954
		Gwenda	Feb 12-18	150	914
		Filão	Fev26-Mar 1	135	954
		Gasitão	Mar 19-25	170	927
1988/1989	6	Barisoana	Nov 12-23	135	954
		Galasanjy	Jan 6-15	135	955
		Edme	Jan 20-27	115	966
		Firinga	Jan 24-Feb 1	135	954
		Leon	Feb 19-Mar 1	150	940
		Krissy	Mar28-Apr 11	150	940
1989/1990	6	Alibera	Dec 16-Jan 5	140	954
		Baomavo	Jan 2-9	150	940
		Dety	Feb 2-11	135	954
		Edisoana	Mar 1-8	135	954
		Walter-Gre	Mar 13-27	170	927
1990/1991	3	Cynthia	Fev 16 - 19	125	970
		Fatima	Fev22-Mar 02	135	954
		Bella	Jan 18-Feb 4	155	936
1991/1992	3	Farida	Feb 23-Mar 4	150	941
		Harriet	Mar 1-7	165	930
		Jane-Irra	April 14-19	140	950
1992/1993	4	Colina	Jan 13-20	135	970
		Edwina	Jan 19-29	170	925
		Jourdace	April 2-10	165	930
		Konita	May 2-7	130	955
1993/1994	5	Geralda	Jan 26-Feb 8	205	905
		Hollanda	Feb 6-14	155	940
		Litane	Mar 7-19	195	910
		Nadia	Ma 16-19	175	925
		Odile	Mar29-Apr4	175	925
1994/1995	6	Albertine	Nov22- Dec 3	175	925
		Dorina	Jan 18- Feb1	175	925
		Fadah	January 24-29	100	920
		Gail	Jan 31-Feb 11	120	970
		Ingrid	Feb 22-Mar 3	150	945
		Marlene	Mar29-Apr 11	185	920
1995/1996	6	Daryl-Agniel	Nov 19-27	175	925

		Bonita	Jan 3-15	185	920
		Edwige	Feb 19-29	150	945
		Flossy	Feb 25-Mar 6	150	945
		Hansella	April 2-10	120	962
		Itelle	April 6-19	175	925
1996/1997	6	Melanie	Nov 1-11	175	925
		Daniala	Dec 2-10	185	915
		Gretelle	Jan 19-31	140	950
		Pancho-Hel	Jan 23-31	185	915
		Josie	Feb 5-16	140	950
		Liset	Feb 28-Mar3	95	950
1997/1998	2	A1	Jan 6-13	-	950
		Anacelle	Feb 6-13	140	950
		Elsie	Marc 9-18	100	975
1998/1999	3	Alda	Jan 14 - 18	95	975
		Davina	Marc 2-19	165	930
		Frederic	April 1-10	175	925
1999/2000	5	Babiola	Jan 3-12	155	950
		Connie	Jan 25-Feb1	185	930
		Eline	Feb 8-29	185	930
		Felicia	Feb 18-24	110	975
		Hudah	Mar 25-Apr 9	220	905
2000/2001	5	Ando	Dec 31- Jan 9	195	925
		Bindo	Jan 3-17	150	955
		Charty	Jan 17-31	185	930
		Dera	Marc4-12	150	955
		Evarist	April 2-8	110	973
2001/2002	7	Bessi-Bako	Nov 30- Jan 3	120	968
		Dina	Jan 16-25	215	910
		Eddy	Jan 22-25	130	965
		Francesa	Jan 22-30	195	925
		Guillaume	Feb 14-23	205	920
		Hary	Mar 3-13	220	905
		Ikala	Mar 21-29	165	945
2002/2003	6	Delfina	Dec14-Jan 8	100	985
		Boura	Nov 14-27	130	965
		Gerry	Feb 5-15	165	940
		Japhet	Fev 25-Mar 5	175	935
		Kalunde	Mar 3-14	215	910
		Manou	May 1-13	155	950
2003/2004	5	Beni	Nov9-25	175	935
		Cela	Dec 4-20	120	975
		Elita	Jan 24-Feb 4	120	970
		Frank	Jan 26-Mar 6	185	930
		Gafilo c	Mar 8-9	120	970
2004/2005	4	Bento	Nov19 –Dec 4	220	915
		Chambo	Dec 22-28	155	950
		Ernest	Jan 16-23	165	950
		Adeline	April 12	220	905
2005/2006	3	Boloetse	Jan 30-Fev 04	155	950

		Diwa	Marc3- Mar 9	110	980
		Carine	Feb 23- Mar 3	205	915
2006/2007	6	Bondo	Dec 15 – 28	205	930
		Dora	Jan 26- Feb 8	195	925
		Favio	Fev 19 - 23	195	925
		Gamede	Feb 19- Mar 1	165	935
		Ndlala	Mar 9-19	175	935
		Jaya	Mar 26-Apr 8	185	935
2007/2008	5	Fame	Jan 22- Feb 1	130	972
		Gula	Jan 25-Feb 1	155	950
		Hondo	Feb 2-29	215	915
		Ivan	Feb 5-27	185	930
		Jokwe	Mar 6 – 15	105	930
		Kamba	Marc 5-14	185	930
2008/2009	4	Fanele	Jan 16-22	185	930
		Izilda	Mar 22-27	110	978
		Gael	Feb 1-9	185	930
		Jade	April 3-10	110	975
2009/2010	4	Joel	May 25-26	100	990
		Cleo	Dec 6-14	195	925
		Gelane	Feb 1-3	205	930
		Edzani	Jan 15	220	910
2010/2011	2	Abele	Nov29- Dec 3	130	973
		Bingiza	Feb 8-18	155	958
2011/2012	4	Dando	Jan 15-17	85	992
		Funso	Jan 19 – 28	205	925
		Giovanna	Feb 7-22	195	935
		Irina	Feb25-Mar 12	95	978
2012/2013	4	Anais	Oct 12-19	185	945
		Claudia	Dec 6 – 13	165	950
		Falleng	Jan26 – Febr3	165	950
		Haruna	Feb 18-25	150	965
2013/2014	4	Amara	Dec 14 – 27	205	933
		Basija	Dec27 – Jan 4	175	950
		Coling	Jan 9-14	185	930
		Hellen	Mar 27- Apr 1	150	965
2014/2015	4	Kate	Dec30 – 31	175	947
		Bansi	Jan 10-18	220	923
		Chedza	Jan 10-18	100	975
		Eunice	Jan 26- Feb 1	240	900

Appendix D - Tidal Constituents for Maputo Station, 1974.

Tidal amplitude and phase with 95% of confidence interval estimates, for Maputo 1974. Tidal constituents (tide), frequency of oscillation (freq), amplitude (amp), error of amplitude calculation (amp_err), phase lag (pha), error of phase lag calculation (pha_err) and the signal to noise ratio (snr).

tide	freq	amp	amp_err	pha	pha_err	snr
SSA	0.000228	0.0036	0.019	183.06	306.72	0.035
MSM	0.00131	0.007	0.019	73.23	156.64	0.13
MM	0.001512	0.0181	0.019	272.27	60.32	0.9
*MSF	0.002822	0.0213	0.019	273.23	51.27	1.2
MF	0.00305	0.0083	0.019	39.84	131.62	0.19
ALP1	0.034397	0.0016	0.004	138.52	149.6	0.15
2Q1	0.035706	0.0031	0.004	99.45	78.37	0.55
SIG1	0.035909	0.0019	0.004	124.07	128.28	0.21
*Q1	0.037219	0.0075	0.004	118.58	32.26	3.3
RHO1	0.037421	0.0014	0.004	266.25	169.58	0.11
*O1	0.038731	0.0229	0.004	167.83	10.53	31
*TAU1	0.038959	0.0059	0.004	21.02	37.88	2
BET1	0.04004	0.004	0.004	25.04	60.94	0.92
NO1	0.040269	0.0029	0.004	230.86	75.18	0.49
*CHI1	0.040471	0.0044	0.004	36.25	54.2	1.1
P1	0.041553	0.0037	0.004	40.18	63.7	0.81
*P1	0.041553	0.0101	0.004	339.46	23.4	6
*K1	0.041781	0.0306	0.004	332.39	7.83	55
*PHI1	0.042009	0.0065	0.004	86.39	36.91	2.4
THE1	0.043091	0.0024	0.004	155.74	96.29	0.34
J1	0.043293	0.0022	0.004	26.05	107.1	0.29
*SO1	0.044603	0.0049	0.004	38.96	49.19	1.4
OO1	0.044831	0.004	0.004	42.9	61.15	0.94
UPS1	0.046343	0.0008	0.004	126.51	296.46	0.04
OQ2	0.075975	0.0032	0.008	43.18	124.36	0.17
*EPS2	0.076177	0.0147	0.008	125.82	28.97	3.6
*2N2	0.077487	0.0263	0.008	61.66	15.89	12
*MU2	0.07769	0.0614	0.008	135.41	7.11	63
*N2	0.078999	0.1413	0.008	66.4	3.11	3.30E+02
*NU2	0.079202	0.0344	0.008	34.43	12.81	20
*M2	0.080511	0.9402	0.008	74.42	0.47	1.50E+04
*MKS2	0.08074	0.0324	0.008	216.35	14.2	18
*LDA2	0.081821	0.0194	0.008	62.53	22.67	6.3
*L2	0.082024	0.0423	0.008	69.95	10.35	30

*S2	0.083333	0.5528	0.008	104.18	0.8	5.10E+03
*K2	0.083562	0.1511	0.008	99.89	3.07	3.80E+02
*K2	0.083562	0.1504	0.008	126.58	3.08	3.80E+02
MSN2	0.084846	0.0074	0.008	235.62	59.29	0.91
*ETA2	0.085074	0.0081	0.008	100.65	52.95	1.1
*MO3	0.119242	0.0039	0.001	301.24	20.94	7.6
*M3	0.120767	0.0052	0.001	347.77	15.29	14
*SO3	0.122064	0.0031	0.001	57.98	26.71	4.8
MK3	0.122292	0.0012	0.001	349.39	65.74	0.76
*SK3	0.125114	0.004	0.001	76.97	20.52	7.9
*MN4	0.159511	0.0031	0.001	308.92	21.45	6.9
*M4	0.161023	0.0058	0.001	72.89	11.32	25
SN4	0.162333	0.001	0.001	246.94	67.47	0.71
*MS4	0.163845	0.0123	0.001	177.19	5.36	1.10E+02
*MK4	0.164073	0.0037	0.001	197.39	18.48	10
*S4	0.166667	0.0014	0.001	82.68	47.24	1.5
SK4	0.166895	0.0002	0.001	4.28	430.44	0.019
*2MK5	0.202804	0.0008	0.001	201.02	50.74	1.3
*2SK5	0.208447	0.0008	0.001	250.03	51.13	1.3
*2MN6	0.240022	0.0045	0.001	273.7	17.73	10
*M6	0.241534	0.0101	0.001	288.77	7.92	50
*2MS6	0.244356	0.0209	0.001	304.41	3.87	2.10E+02
*2MK6	0.244584	0.0035	0.001	334.52	24.35	5.9
*2SM6	0.247178	0.009	0.001	335.09	9.1	39
*MSK6	0.247406	0.0046	0.001	345.93	18.37	10
*3MK7	0.283315	0.0005	0	76.86	50.79	1.2
*M8	0.322046	0.0024	0.001	169.53	11.93	22
*M10	0.402557	0.0006	0.001	44.83	49.42	1.2

Appendix E - Tidal Constituents for Beira Station, 1996.

Tidal amplitude and phase with 95% of confidence interval estimates, for Beira 1996. Tidal constituents (tide), frequency of oscillation (freq), amplitude (amp), error of amplitude calculation (amp_err), phase lag (pha), error of phase lag calculation (pha_err) and the signal to noise ratio (snr).

tide	freq	amp	amp_err	pha	pha_err	snr
*SA	0.000114	0.1277	0.024	29.61	10.72	29
*SSA	0.000228	0.0298	0.024	269.64	45.95	1.6
MSM	0.00131	0.0155	0.024	281.79	88.52	0.42
*MM	0.001512	0.0377	0.024	266.07	36.33	2.5
MSF	0.002822	0.0231	0.024	18.05	59.37	0.93
MF	0.00305	0.0152	0.024	10.74	89.99	0.41
ALP1	0.034397	0.0036	0.004	112.34	72.45	0.91
2Q1	0.035706	0.0021	0.004	279	121.47	0.32
*SIG1	0.035909	0.005	0.004	293.02	52.93	1.7
*Q1	0.037219	0.0141	0.004	15.51	18.59	14
*RHO1	0.037421	0.0098	0.004	324.26	26.07	6.8
*O1	0.038731	0.0461	0.004	17.26	5.75	1.50E+02
*TAU1	0.038959	0.0045	0.004	324.17	39.94	1.5
*BET1	0.04004	0.0041	0.004	222.98	67.25	1.2
*NO1	0.040269	0.0164	0.004	298.34	18.53	19
CHI1	0.040471	0.0035	0.004	127.31	74.47	0.89
PI1	0.041439	0.0017	0.004	117.95	124.76	0.21
*P1	0.041553	0.012	0.004	351.3	17.73	10
P1	0.041553	0.0015	0.004	49.31	143.06	0.16
*S1	0.041667	0.065	0.004	323.34	4.58	3.00E+02
*K1	0.041781	0.0045	0.004	42.24	54.15	1.4
*PSI1	0.041895	0.0059	0.004	114.18	37.41	2.4
PHI1	0.042009	0.0037	0.004	162.74	58.42	0.97
*THE1	0.043091	0.0146	0.004	310.31	17.36	15
J1	0.043293	0.0026	0.004	123.15	98.02	0.46
*SO1	0.044603	0.0071	0.004	311.04	37.54	3.5
*OO1	0.044831	0.0116	0.004	52.97	39.91	9.6
*UPS1	0.046343	0.0078	0.004	79.66	56.48	4.3
OQ2	0.075975	0.0067	0.015	115.15	128.77	0.21
*EPS2	0.076177	0.0382	0.015	158.28	21.6	6.9
*2N2	0.077487	0.0497	0.015	90.72	16.78	12
*MU2	0.07769	0.1327	0.015	177.42	6.1	83
*N2	0.078999	0.2741	0.015	109.49	2.93	3.50E+02
*NU2	0.079202	0.0697	0.015	82.5	11.64	23

*H1	0.080397	0.0186	0.015	92.01	45.8	1.6
*M2	0.080511	1.7502	0.015	124.56	0.46	1.40E+04
H2	0.080626	0.0138	0.015	171.66	59.39	0.89
*MKS2	0.08074	0.0184	0.015	325.2	58.18	1.6
*LDA2	0.081821	0.0421	0.015	116.48	19.01	8.3
*L2	0.082024	0.0754	0.015	145.81	9.99	27
*T2	0.083219	0.0626	0.015	157.35	13.33	18
*S2	0.083333	1.0216	0.015	171.86	0.82	4.90E+03
*R2	0.083447	0.017	0.015	94.36	39.26	1.4
*K2	0.083562	0.3026	0.015	167.55	3.65	4.30E+02
*K2	0.083562	0.278	0.015	194.26	3.98	3.60E+02
*MSN2	0.084846	0.0245	0.015	331.16	31.69	2.8
*ETA2	0.085074	0.0201	0.015	125.64	67.28	1.9
*MO3	0.119242	0.0115	0.008	88.78	45.54	2.2
*M3	0.120767	0.0698	0.008	296.53	6	82
SO3	0.122064	0.0061	0.008	175.01	89.11	0.63
*MK3	0.122292	0.009	0.008	349.7	53.75	1.4
*SK3	0.125114	0.0586	0.008	82.21	8.53	58
*MN4	0.159511	0.0497	0.005	190.93	5.56	91
*M4	0.161023	0.1001	0.005	210.46	2.77	3.70E+02
*SN4	0.162333	0.0148	0.005	210.51	19.36	8.1
*MS4	0.163845	0.1005	0.005	213.28	2.87	3.70E+02
*MK4	0.164073	0.0235	0.005	225.23	16.22	20
*S4	0.166667	0.0486	0.005	272.77	6.17	87
*SK4	0.166895	0.026	0.005	284.84	15.25	25
*2MK5	0.202804	0.0031	0.003	42.79	50.52	1.4
*2SK5	0.208447	0.0029	0.003	196.69	58.17	1.2
*2MN6	0.240022	0.0058	0.002	55.35	19.81	6.7
*M6	0.241534	0.0172	0.002	72.67	6.65	60
*2MS6	0.244356	0.0361	0.002	126.57	3.29	2.60E+02
*2MK6	0.244584	0.0082	0.002	138.45	19.19	14
*2SM6	0.247178	0.0221	0.002	183.19	5.58	99
*MSK6	0.247406	0.0126	0.002	182.92	12.95	32
*3MK7	0.283315	0.0022	0.001	28.22	29.86	3.8
*M8	0.322046	0.0042	0.001	126.18	11.42	19
M10	0.402557	0.0005	0.001	35.54	101.6	0.22

Appendix F - Tidal Constituents for Pemba Station, 1998.

Tidal amplitude and phase with 95% of confidence interval estimates, for Pemba 1998. Tidal constituents (tide), frequency of oscillation (freq), amplitude (amp), error of amplitude calculation (amp_err), phase lag (pha), error of phase lag calculation (pha_err) and the signal to noise ratio (snr).

tide	freq	amp	amp_err	pha	pha_err	snr
*SSA	0.000228	0.0238	0.02	351.87	47.8	1.4
*MSM	0.00131	0.0235	0.02	180.67	48.3	1.4
*MM	0.001512	0.0389	0.02	7.95	29.23	3.8
MSF	0.002822	0.0091	0.02	253.31	125.12	0.21
MF	0.00305	0.0054	0.02	353.59	209.34	0.075
ALP1	0.034397	0.0015	0.004	219.29	181.32	0.15
*2Q1	0.035706	0.0063	0.004	314.77	43.27	2.6
*SIG1	0.035909	0.0055	0.004	8.19	49.72	2
*Q1	0.037219	0.0224	0.004	17.09	12.22	32
*RHO1	0.037421	0.0058	0.004	74.37	49.13	2.2
*O1	0.038731	0.0916	0.004	34.61	2.98	540
*TAU1	0.038959	0.0053	0.004	19.37	33.94	1.8
*BET1	0.04004	0.0042	0.004	67.64	66.64	1.1
*NO1	0.040269	0.0075	0.004	42.65	24.87	3.6
CHI1	0.040471	0.0023	0.004	162.12	115.97	0.35
*P1	0.041553	0.0462	0.004	37.94	4.84	140
*P1	0.041553	0.0444	0.004	34.87	5.04	130
*K1	0.041781	0.1342	0.004	27.8	1.88	1200
PHI1	0.042009	0.0036	0.004	201.86	61.63	0.82
THE1	0.043091	0.0034	0.004	339.65	77.67	0.76
*J1	0.043293	0.0098	0.004	32.52	27.92	6.1
SO1	0.044603	0.0037	0.004	83.33	73.82	0.88
*OO1	0.044831	0.0054	0.004	75.34	63.51	1.9
UPS1	0.046343	0.0025	0.004	169.98	151.34	0.4
OQ2	0.075975	0.0006	0.008	17.6	699.61	0.006
EPS2	0.076177	0.003	0.008	17.85	152.16	0.13
*2N2	0.077487	0.0172	0.008	23.01	26.07	4.4
*MU2	0.07769	0.0262	0.008	77.28	17.34	10
*N2	0.078999	0.1811	0.008	65.38	2.51	490
*NU2	0.079202	0.0438	0.008	70.55	10.32	29
*M2	0.080511	1.1245	0.008	85.46	0.4	19000
*MKS2	0.08074	0.014	0.008	214.7	42.05	2.9
*LDA2	0.081821	0.0191	0.008	97.61	23.67	5.4
*L2	0.082024	0.0222	0.008	78.6	23.59	7.4
*S2	0.083333	0.573	0.008	125.88	0.82	4900

*K2	0.083562	0.1892	0.008	125.17	3.22	530
*K2	0.083562	0.1559	0.008	148.28	3.9	360
MSN2	0.084846	0.0012	0.008	249	360.52	0.022
ETA2	0.085074	0.0078	0.008	228.46	88.68	0.91
MO3	0.119242	0.0025	0.003	257.09	77.97	0.74
*M3	0.120767	0.0102	0.003	223.81	15.61	12
*SO3	0.122064	0.0084	0.003	340.5	24.22	8.2
*MK3	0.122292	0.0073	0.003	317.18	24.68	6.3
*SK3	0.125114	0.0073	0.003	26.23	25.75	6.2
*MN4	0.159511	0.0023	0.002	157.04	37.72	2
*M4	0.161023	0.0026	0.002	213.94	33.83	2.5
SN4	0.162333	0.0015	0.002	98.8	58.02	0.92
*MS4	0.163845	0.0033	0.002	183.52	27.45	4.1
*MK4	0.164073	0.0041	0.002	333.43	28.55	6.3
S4	0.166667	0.0005	0.002	273.77	205.9	0.078
SK4	0.166895	0.0007	0.002	97.63	173.68	0.18
2MK5	0.202804	0.0005	0.001	308.83	138.42	0.19
*2SK5	0.208447	0.0017	0.001	200.9	42.05	2.3
*2MN6	0.240022	0.0011	0.001	262.69	50.75	1
*M6	0.241534	0.0016	0.001	316.38	34.89	2.2
2MS6	0.244356	0.001	0.001	46.12	56.53	0.9
2MK6	0.244584	0.001	0.001	320.28	71.8	0.94
*2SM6	0.247178	0.0035	0.001	234.08	17.16	10
*MSK6	0.247406	0.005	0.001	12.98	15.27	22
3MK7	0.283315	0.0004	0.001	328.9	93.82	0.38
*M8	0.322046	0.0009	0.001	6.74	36.32	1.9
M10	0.402557	0.0003	0.001	94.09	110.64	0.19

Appendix G – The tropical cyclone affected Mozambique from 1986 to 2005 (historical period in study). Source: JTWC – Adapted

Appendix G. 1: Tropical Cyclone Filão, February/March of 1988.

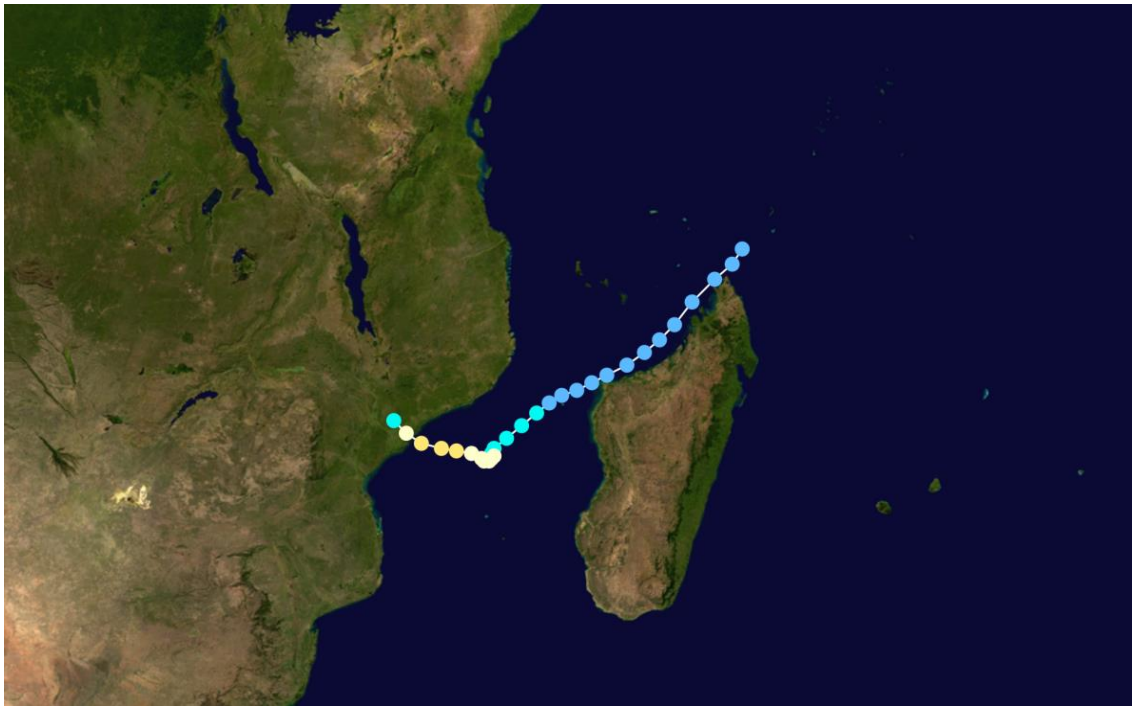

Appendix G. 2 : Tropical Cyclone Bonita, January of 1996.

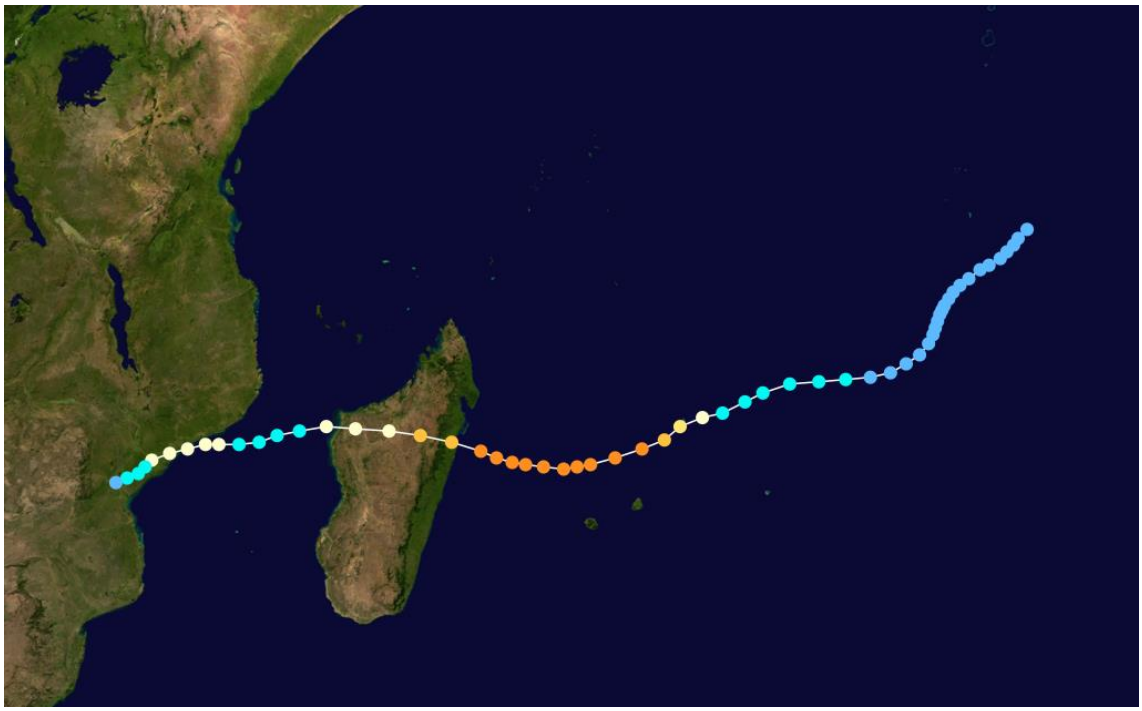

Appendix G. 3: Tropical Cyclone Nadia, January of 1994.

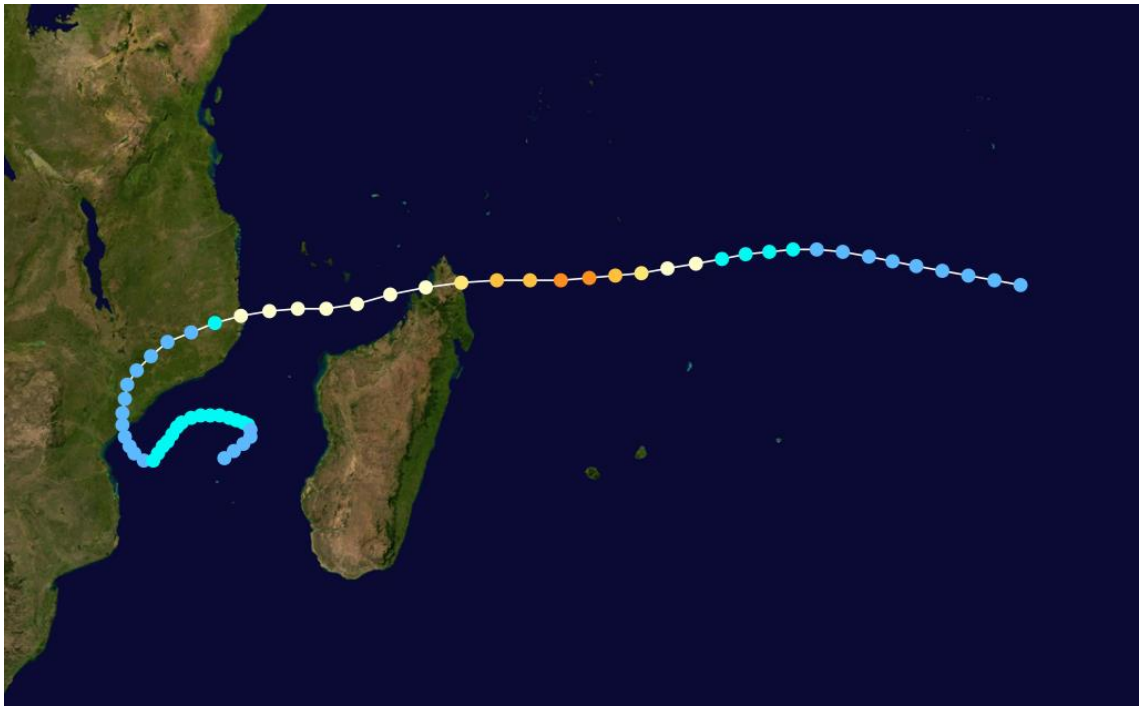

Appendix G. 4: Tropical Cyclone Leon - Eline, February of 2000.

Appendix H – The tropical cyclone that made landfall in Mozambique, from 1986 to 2005 (historical period in study).

Period	Nº of Events	Event name	Date	Affected region (Land fall)	Wind	SLP
1987/1988	2	Doaza	Jan 31- Feb 1	Sofala, Zambezia and Cabo Delgado	135	954
		Filão	Fev26-Mar 1	Quelimane	135	954
1990/1991	1	Cynthia	Fev 16 - 19	Between Beira and Quelimane	125	970
1993/1994	1	Nadia	Marc 16-19	Nampula Angoche	175	925
1994/1995	1	Fadah	Mar29-Apr 11	Nampula		920
1995/1996	1	Bonita	Jan 3-15	Quelimane Pebane	185	920
1996/1997	1	Liset	Feb 5-16	Beira	95	950
1997/1998	1	A1	Jan 6-13	Angoche and Quelimane	....	950
1999/2000	2	Eline	Feb 8-29	Between Beira and Vilanculo	185	930
		Hudah	Mar 25-Apr 9	Pemba	220	905
2000/2001	1	Dera	Marc4-12	Angoche		925
2002/2003	2	Delfina	Nov 14-27	Angoche Pemba	150	965
		Japhet	Fev 25-Mar 5	Zambezia	175	935
2004/2005	1	Ernest	Jan 16-23	Zambezia	165	950

Appendix I - Wind speed and direction for historical data from NOAA (a) and MPI-ESM-LR (b).

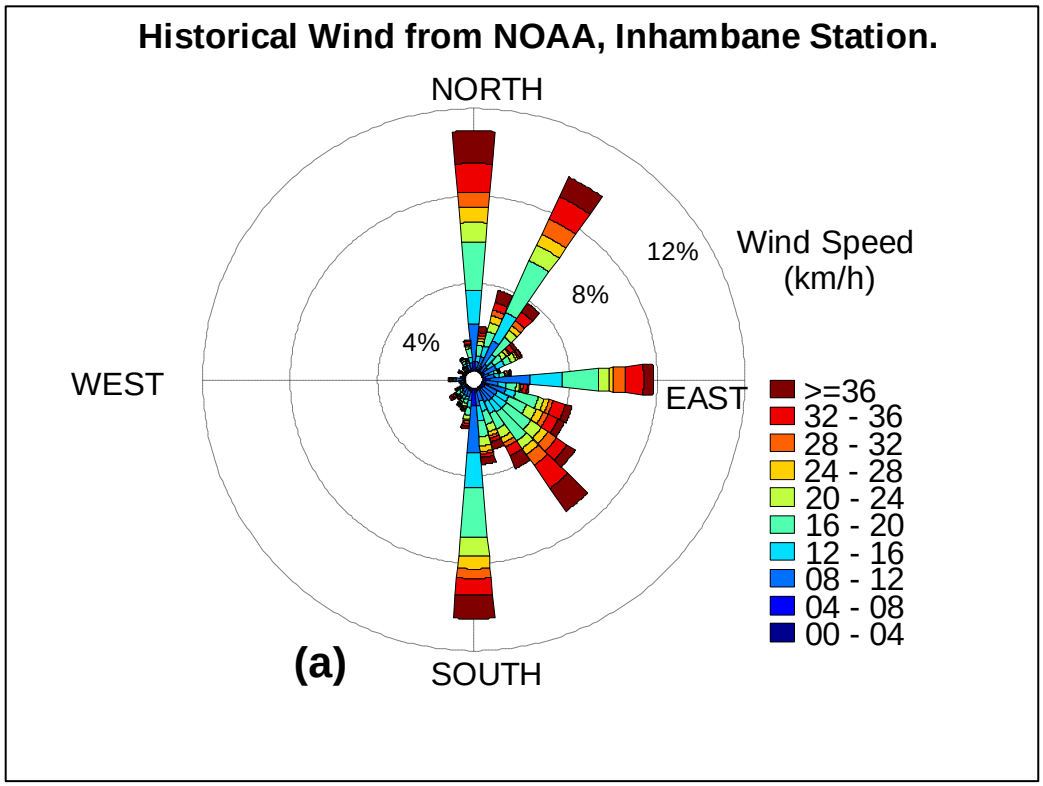

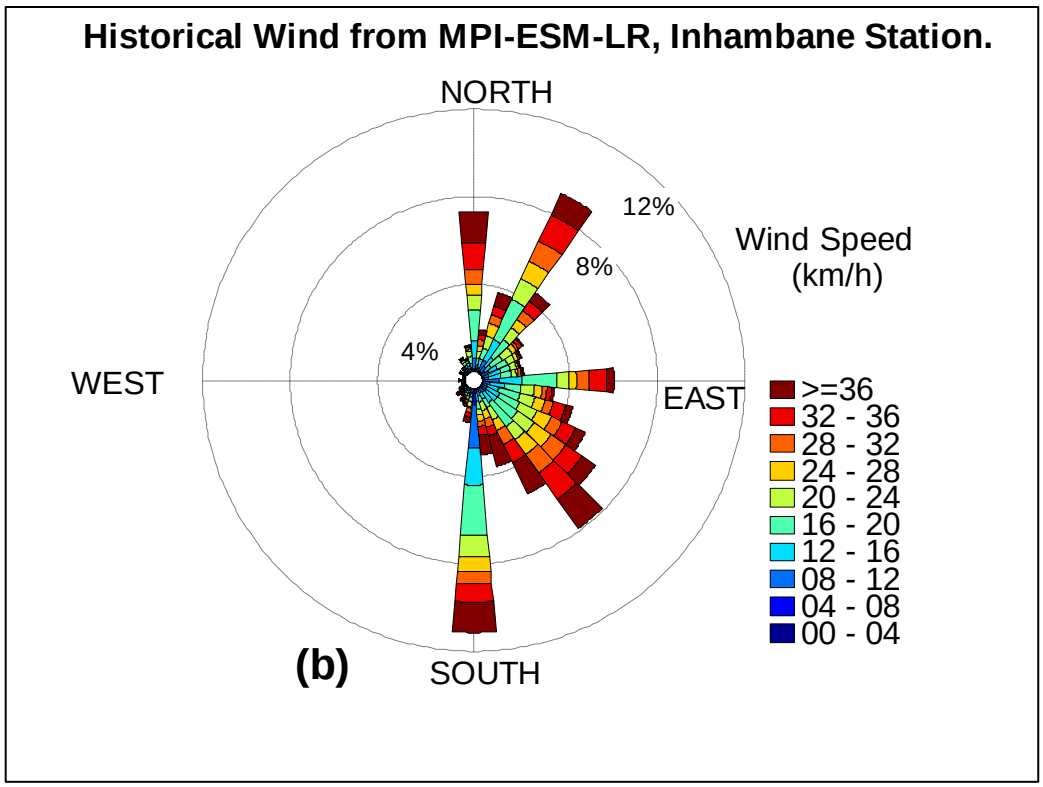

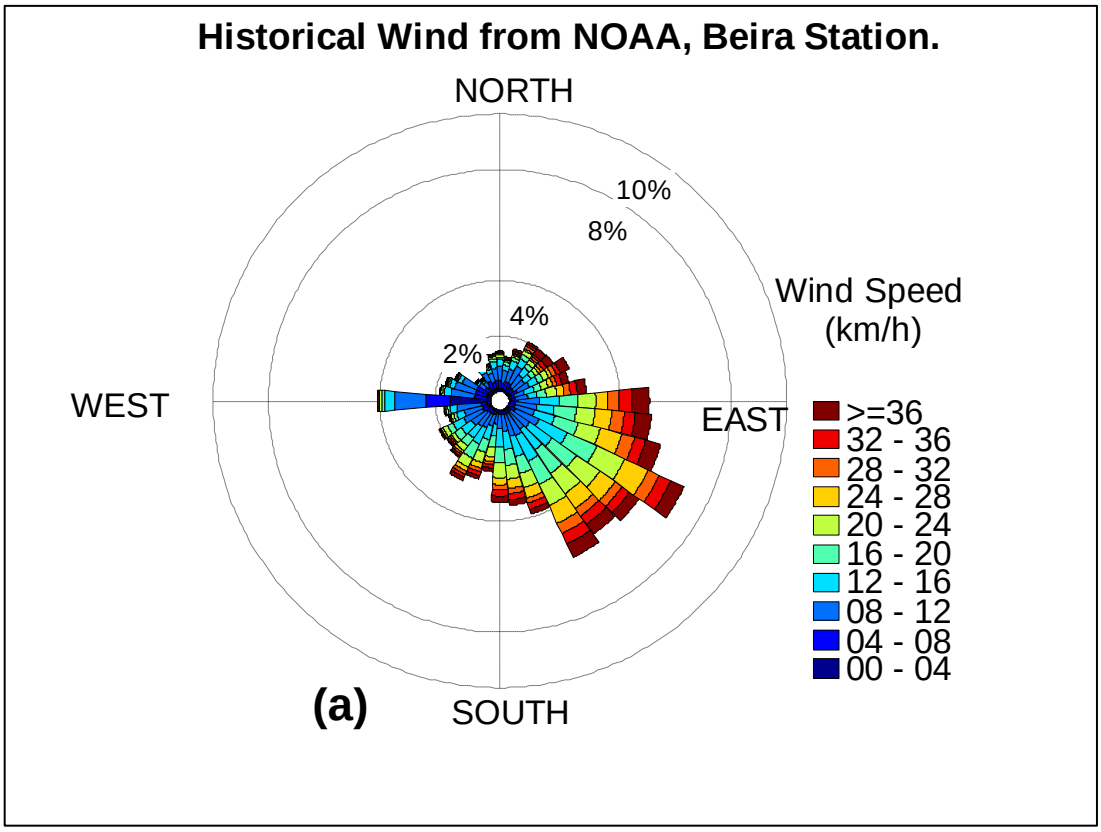
Historical Wind from NOAA, Beira Station.
NORTH
10%
8%
4%
2%
WEST
EAST
SOUTH
Wind Speed
(km/h)
>=36
32 - 36
28 - 32
24 - 28
20 - 24
16 - 20
12 - 16
08 - 12
04 - 08
00 - 04
(a)

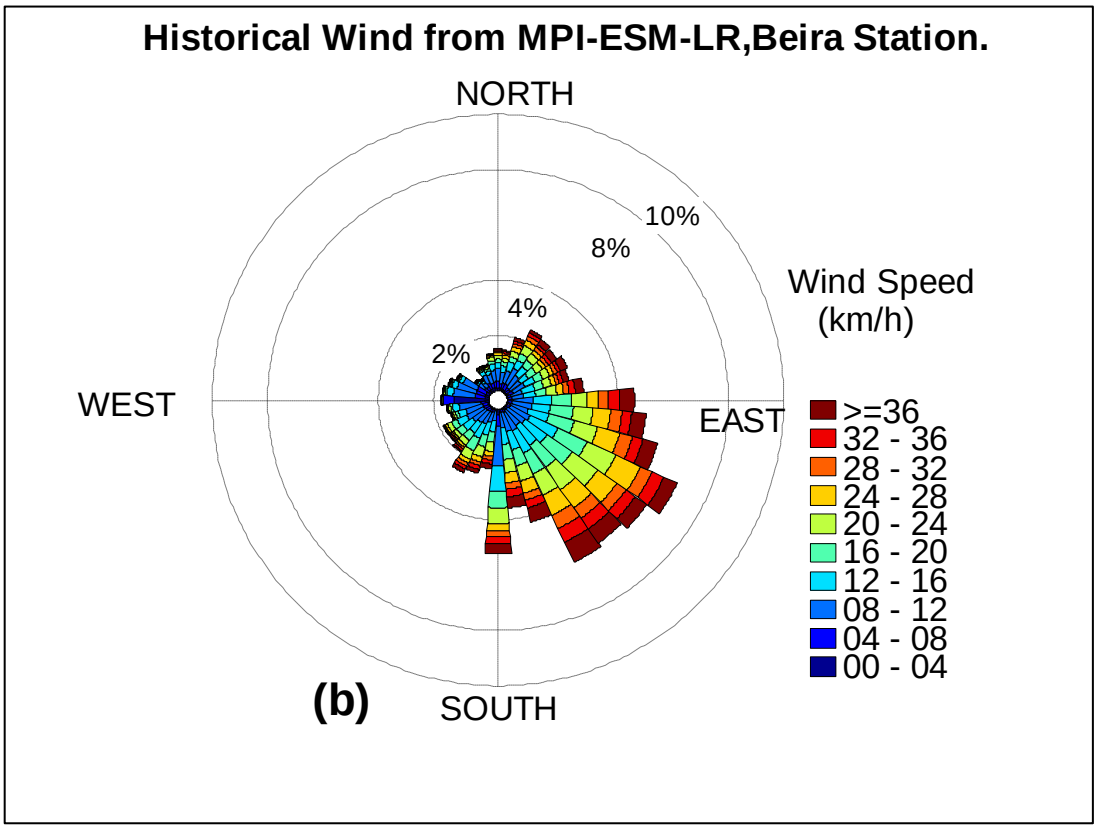
Historical Wind from MPI-ESM-LR,Beira Station.
NORTH
10%
8%
4%
2%
WEST
EAST
SOUTH
Wind Speed
(km/h)
>=36
32 - 36
28 - 32
24 - 28
20 - 24
16 - 20
12 - 16
08 - 12
04 - 08
00 - 04
(b)

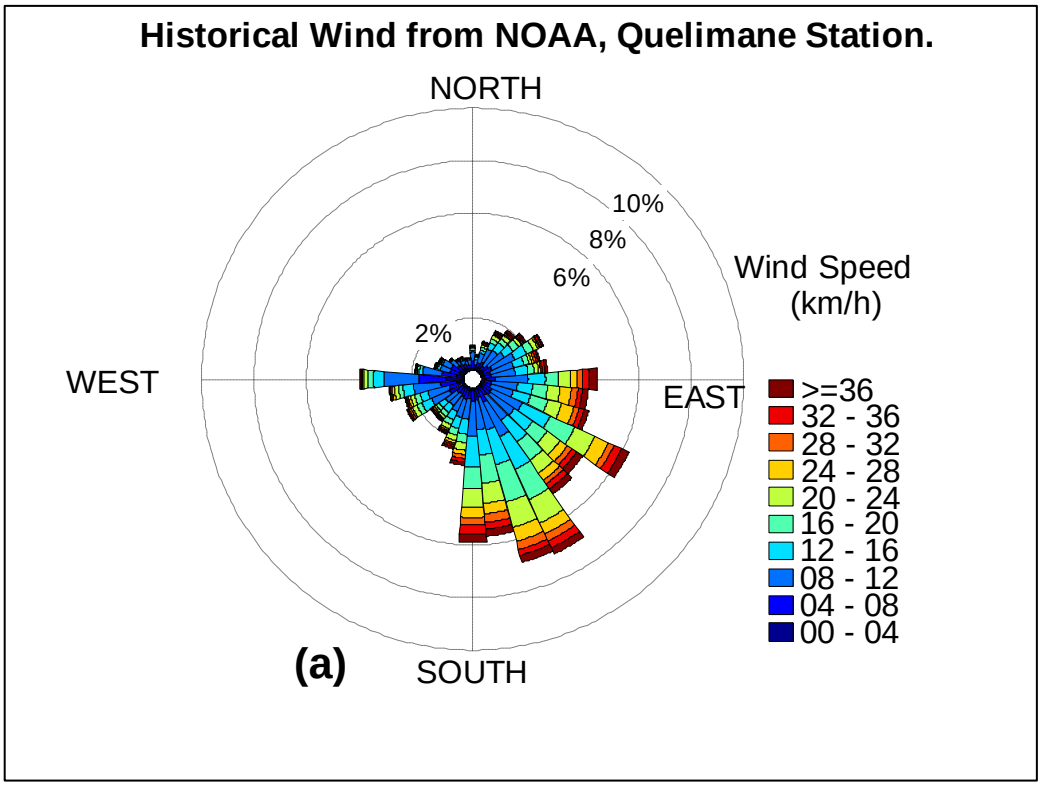
Historical Wind from NOAA, Quelimane Station.
NORTH
10%
8%
6%
2%
Wind Speed
(km/h)
WEST
EAST
>=36
32 - 36
28 - 32
24 - 28
20 - 24
16 - 20
12 - 16
08 - 12
04 - 08
00 - 04
(a)
SOUTH

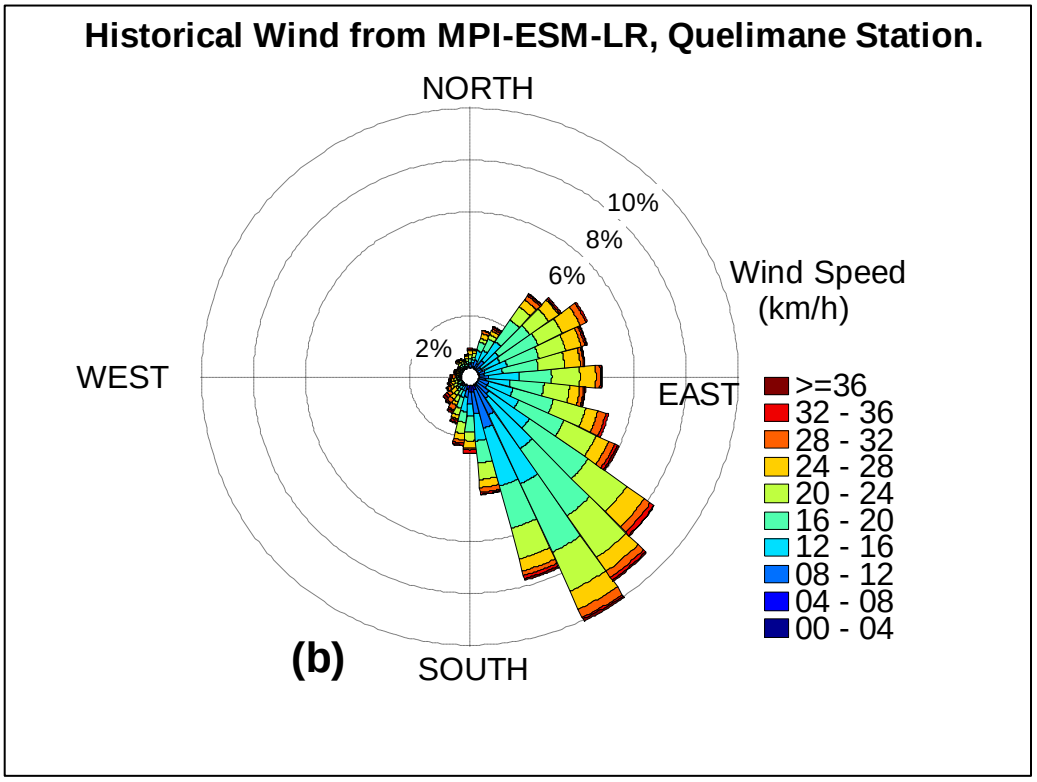
Historical Wind from MPI-ESM-LR, Quelimane Station.
NORTH
10%
8%
6%
2%
Wind Speed
(km/h)
WEST
EAST
>=36
32 - 36
28 - 32
24 - 28
20 - 24
16 - 20
12 - 16
08 - 12
04 - 08
00 - 04
(b)
SOUTH

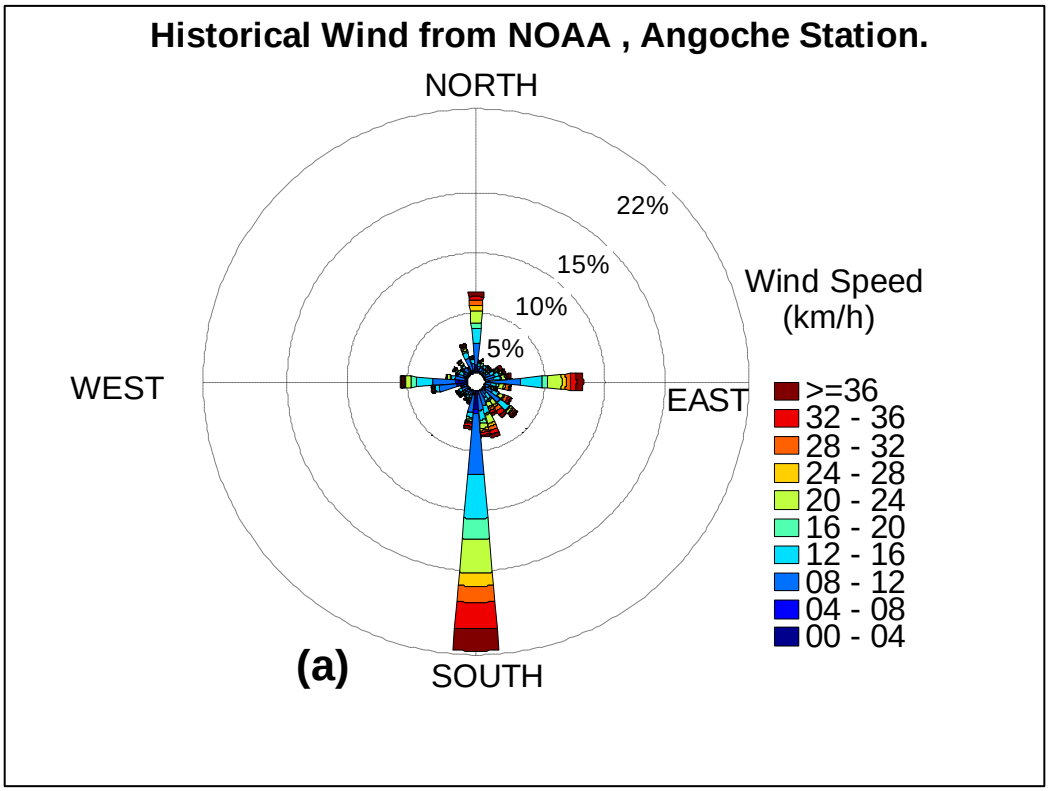
Historical Wind from NOAA , Angoche Station.
NORTH
22%
15%
10%
5%
Wind Speed
(km/h)
WEST
EAST
>=36
32 - 36
28 - 32
24 - 28
20 - 24
16 - 20
12 - 16
08 - 12
04 - 08
00 - 04
(a)
SOUTH

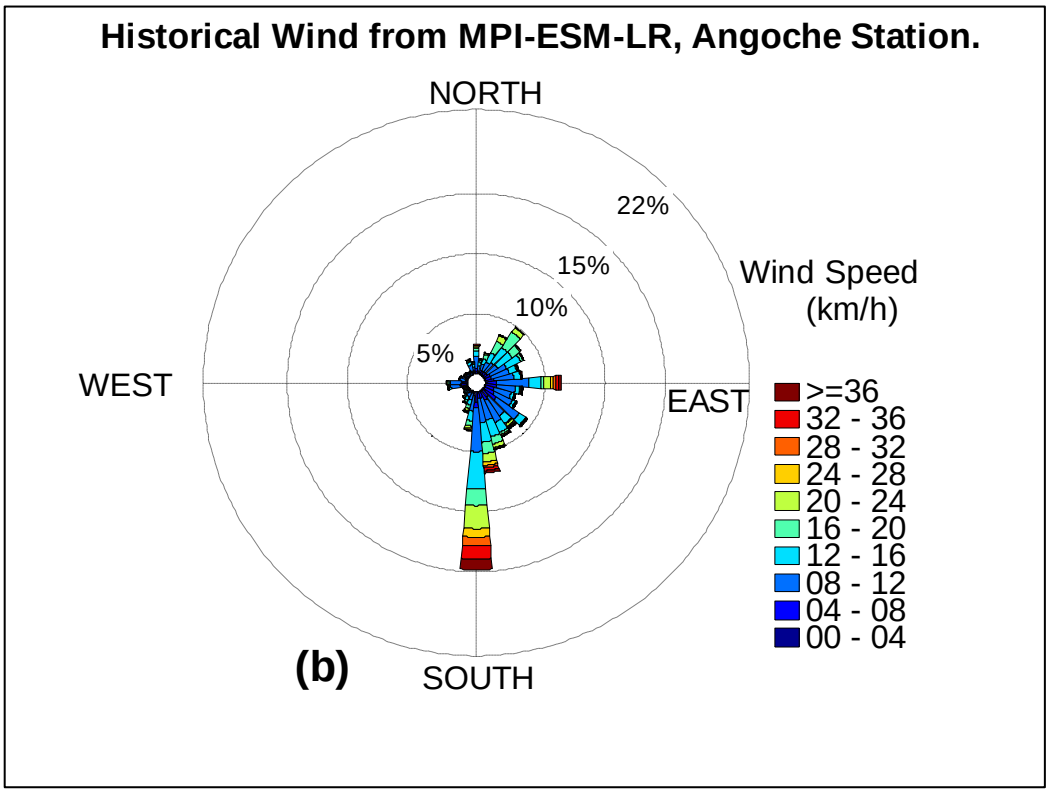
Historical Wind from MPI-ESM-LR, Angoche Station.
NORTH
22%
15%
10%
5%
Wind Speed
(km/h)
WEST
EAST
>=36
32 - 36
28 - 32
24 - 28
20 - 24
16 - 20
12 - 16
08 - 12
04 - 08
00 - 04
(b)
SOUTH

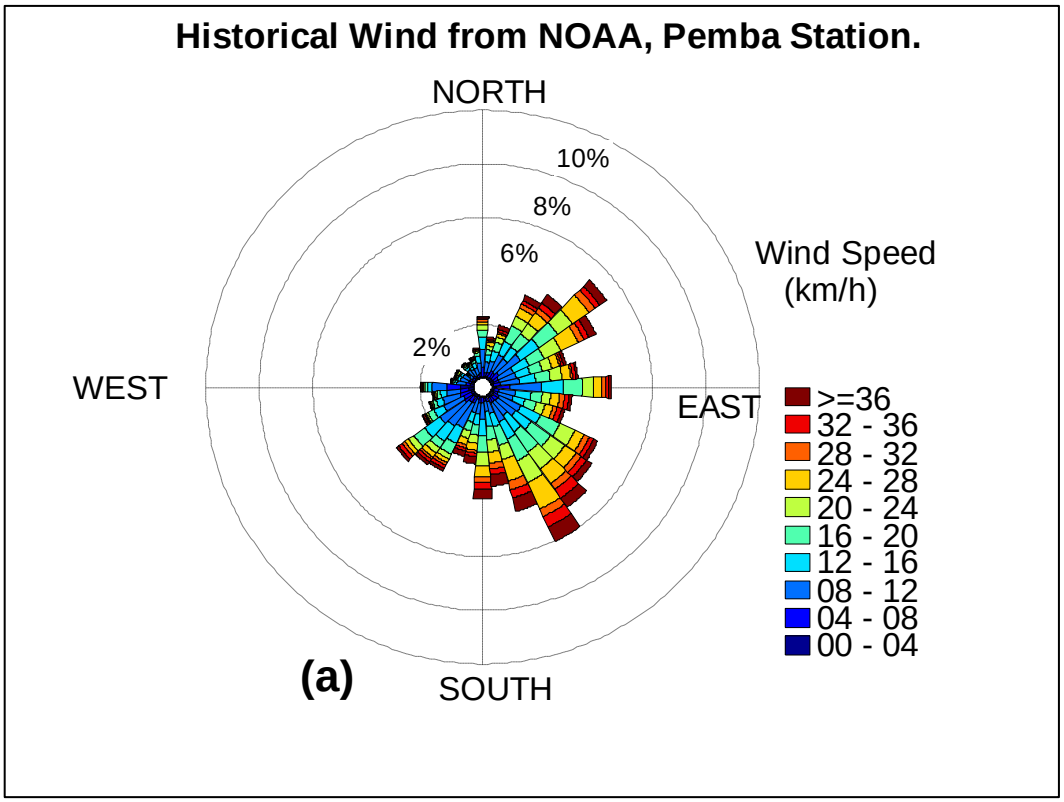
Historical Wind from NOAA, Pemba Station.
NORTH
10%
8%
6%
2%
WEST
EAST
SOUTH
Wind Speed
(km/h)
>=36
32 - 36
28 - 32
24 - 28
20 - 24
16 - 20
12 - 16
08 - 12
04 - 08
00 - 04
(a)

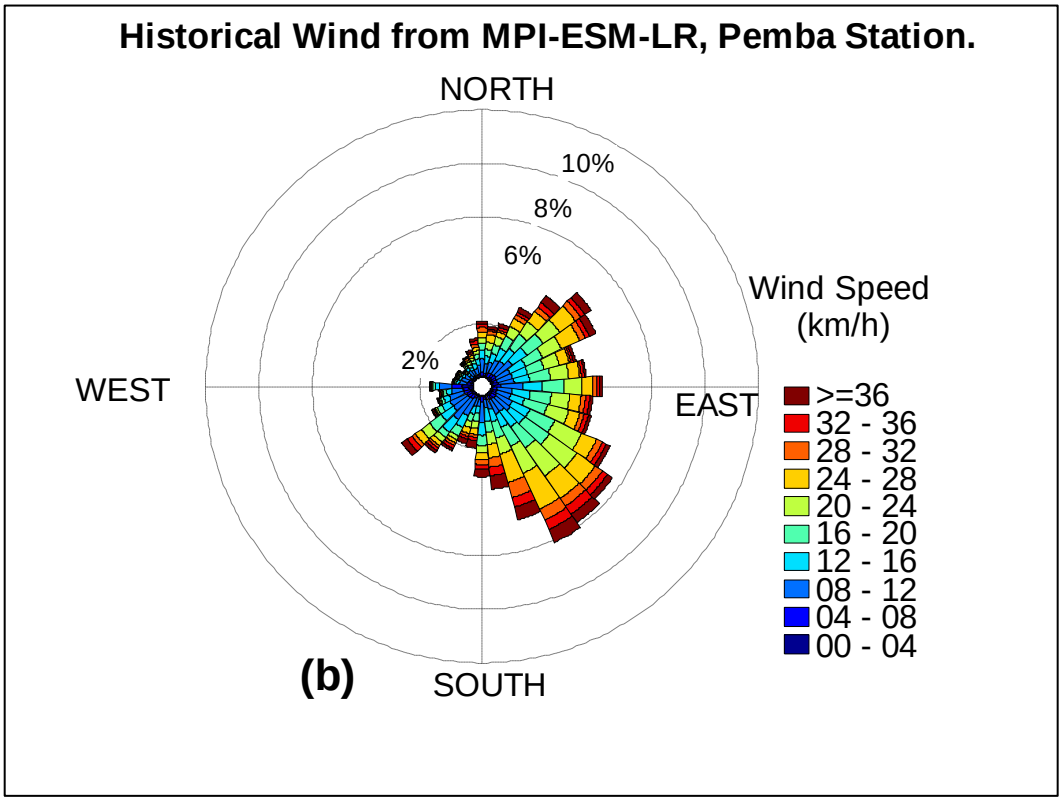
Historical Wind from MPI-ESM-LR, Pemba Station.
NORTH
10%
8%
6%
2%
WEST
EAST
SOUTH
Wind Speed
(km/h)
>=36
32 - 36
28 - 32
24 - 28
20 - 24
16 - 20
12 - 16
08 - 12
04 - 08
00 - 04
(b)

Appendix J - Wind speed and direction for Near Term Future and historical from MPI-ESM-LR

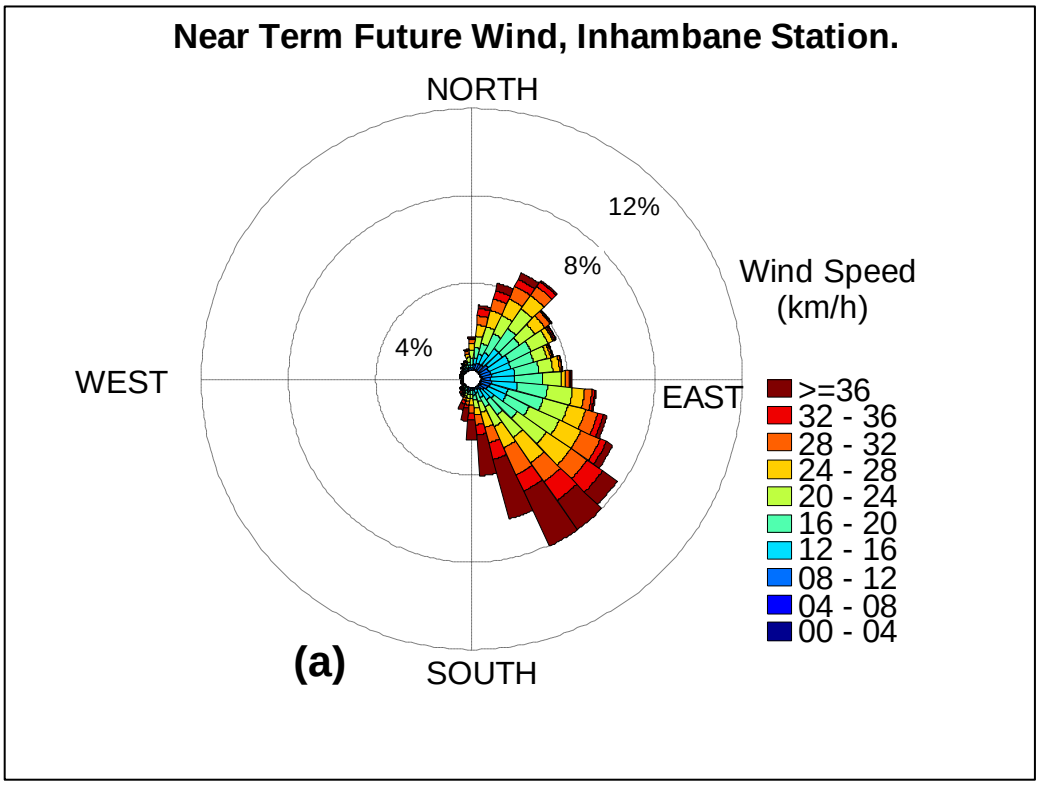

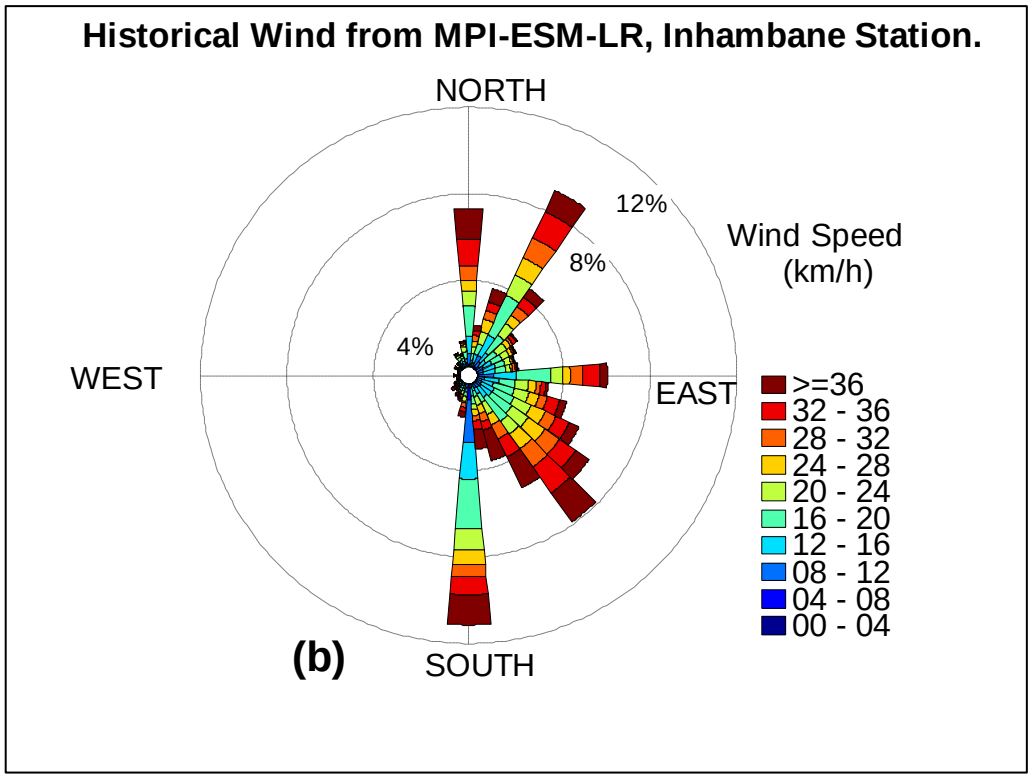

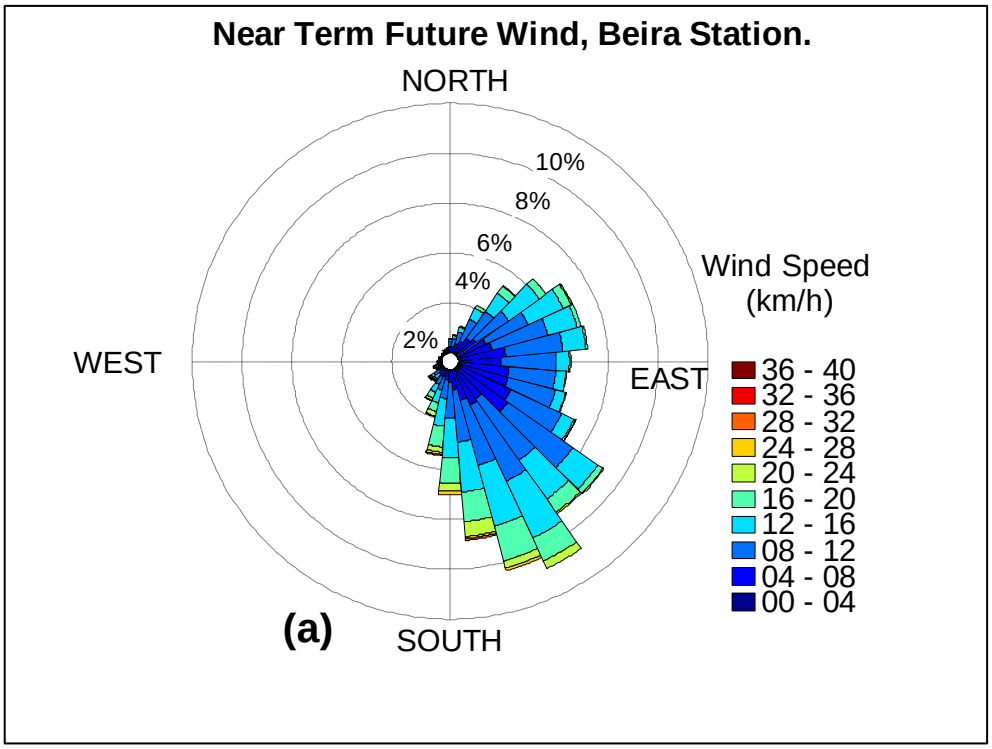
Near Term Future Wind, Beira Station.
NORTH
10%
8%
6%
4%
2%
WEST
EAST
SOUTH
(a)
Wind Speed
(km/h)
36 - 40
32 - 36
28 - 32
24 - 28
20 - 24
16 - 20
12 - 16
08 - 12
04 - 08
00 - 04

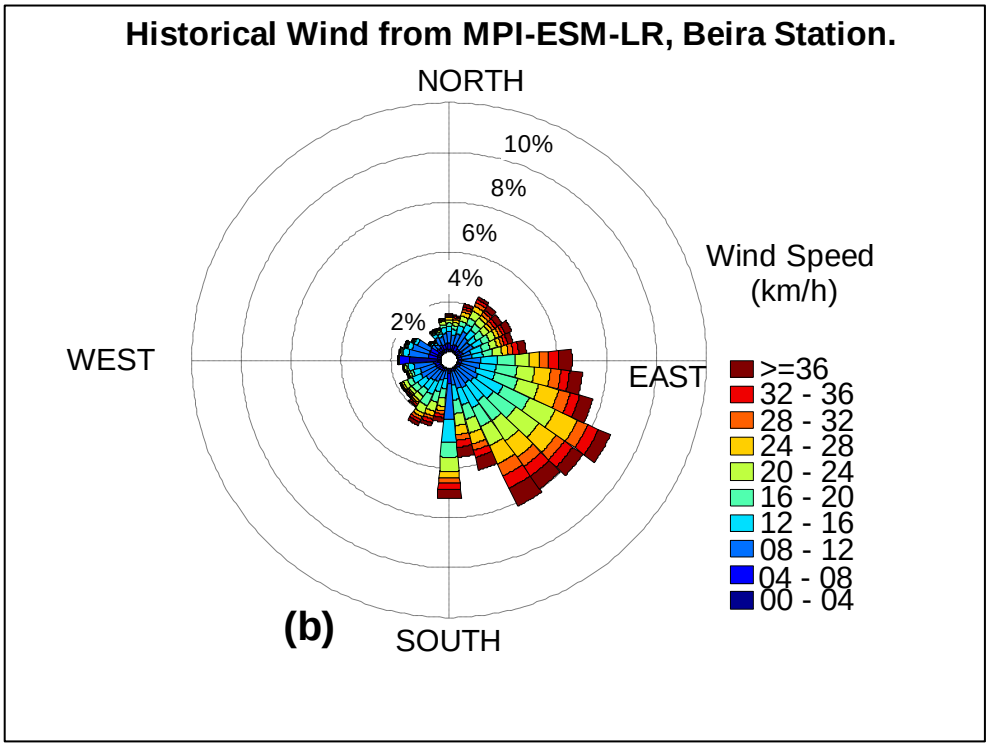
Historical Wind from MPI-ESM-LR, Beira Station.
NORTH
10%
8%
6%
4%
2%
WEST
EAST
SOUTH
(b)
Wind Speed
(km/h)
>=36
32 - 36
28 - 32
24 - 28
20 - 24
16 - 20
12 - 16
08 - 12
04 - 08
00 - 04

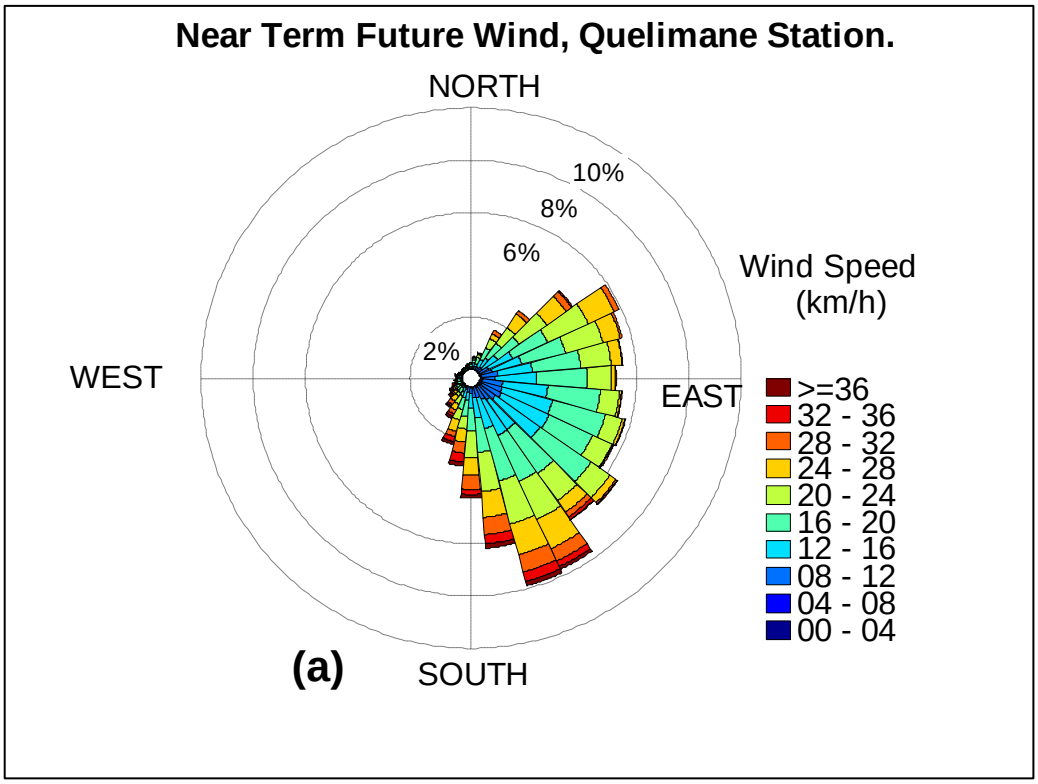
Near Term Future Wind, Quelimane Station.
NORTH
10%
8%
6%
2%
WEST
EAST
SOUTH
(a)
Wind Speed
(km/h)
>=36
32 - 36
28 - 32
24 - 28
20 - 24
16 - 20
12 - 16
08 - 12
04 - 08
00 - 04

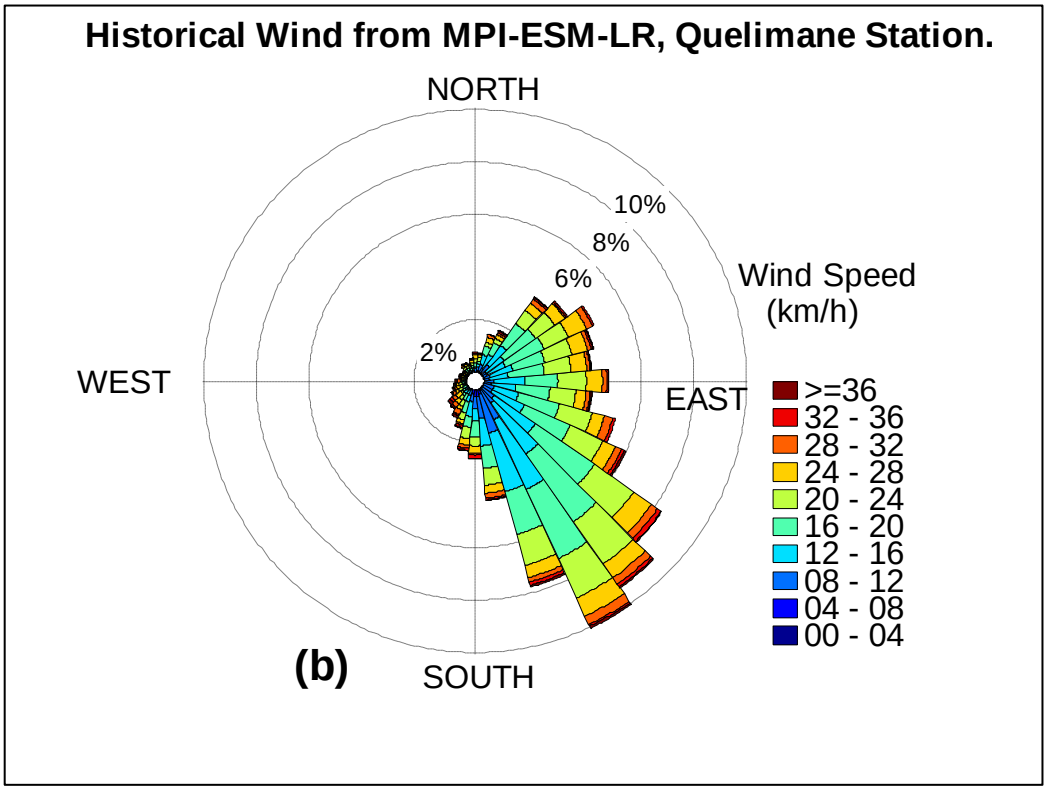
Historical Wind from MPI-ESM-LR, Quelimane Station.
NORTH
10%
8%
6%
2%
WEST
EAST
SOUTH
(b)
Wind Speed
(km/h)
>=36
32 - 36
28 - 32
24 - 28
20 - 24
16 - 20
12 - 16
08 - 12
04 - 08
00 - 04

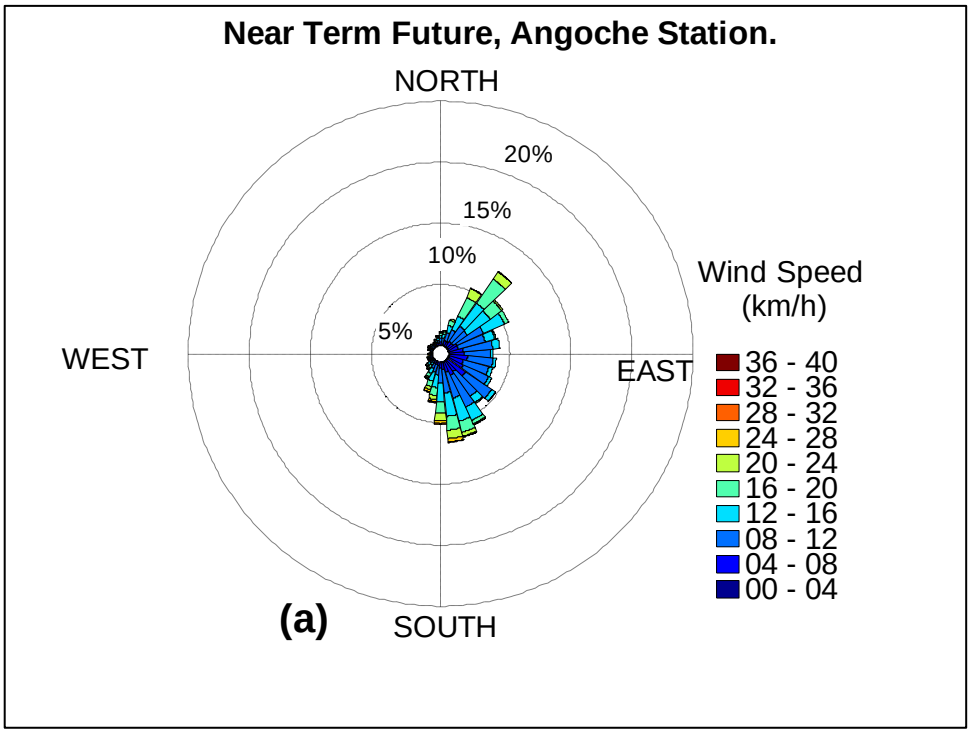
Near Term Future, Angoche Station.
NORTH
20%
15%
10%
5%
WEST
EAST
SOUTH
(a)
Wind Speed
(km/h)
36 - 40
32 - 36
28 - 32
24 - 28
20 - 24
16 - 20
12 - 16
08 - 12
04 - 08
00 - 04

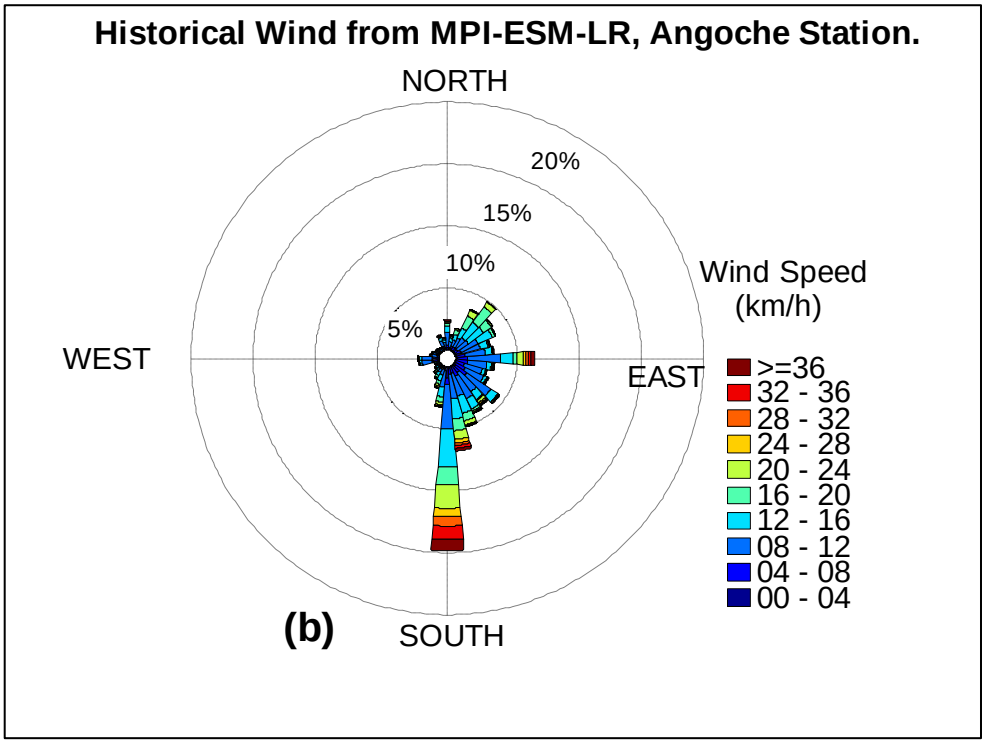
Historical Wind from MPI-ESM-LR, Angoche Station.
NORTH
20%
15%
10%
5%
WEST
EAST
SOUTH
(b)
Wind Speed
(km/h)
>=36
32 - 36
28 - 32
24 - 28
20 - 24
16 - 20
12 - 16
08 - 12
04 - 08
00 - 04

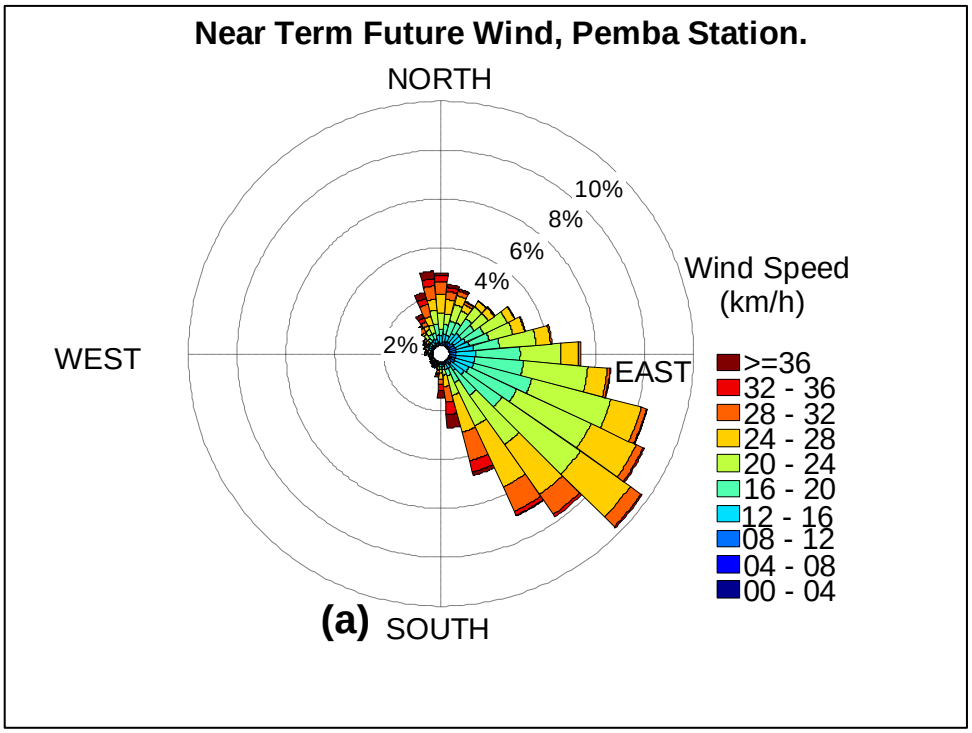
Near Term Future Wind, Pemba Station.
NORTH
10%
8%
6%
4%
2%
WEST
EAST
SOUTH
Wind Speed
(km/h)
>=36
32 - 36
28 - 32
24 - 28
20 - 24
16 - 20
12 - 16
08 - 12
04 - 08
00 - 04
(a)

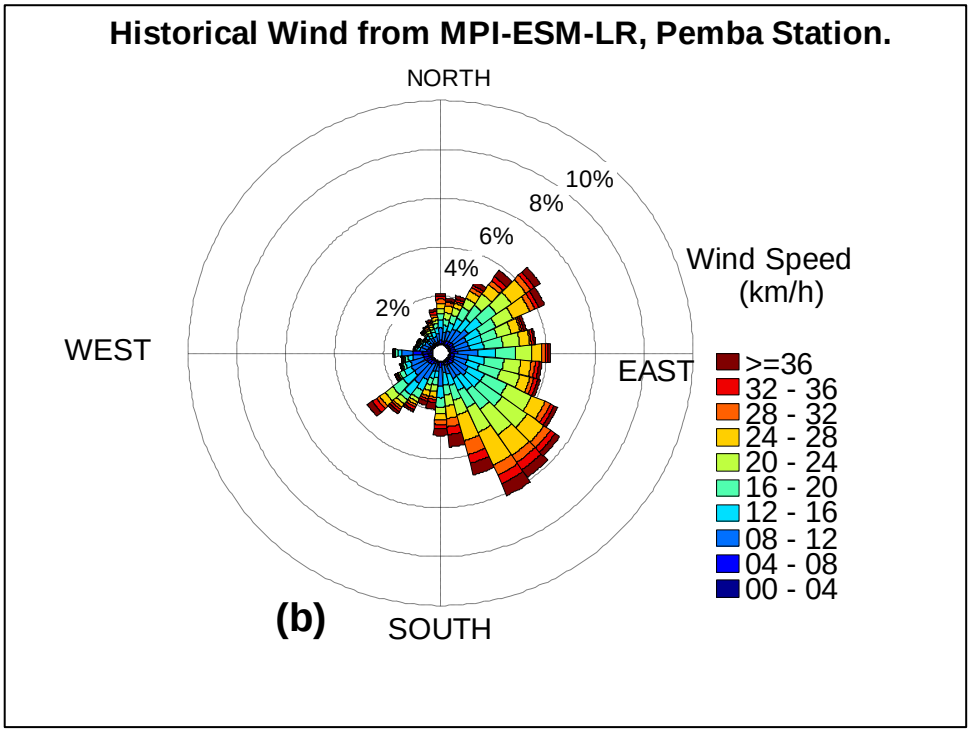
Historical Wind from MPI-ESM-LR, Pemba Station.
NORTH
10%
8%
6%
4%
2%
WEST
EAST
SOUTH
Wind Speed
(km/h)
>=36
32 - 36
28 - 32
24 - 28
20 - 24
16 - 20
12 - 16
08 - 12
04 - 08
00 - 04
(b)

Appendix K - Wind speed and direction for Medium Term Future and historical from MPI-ESM-LR

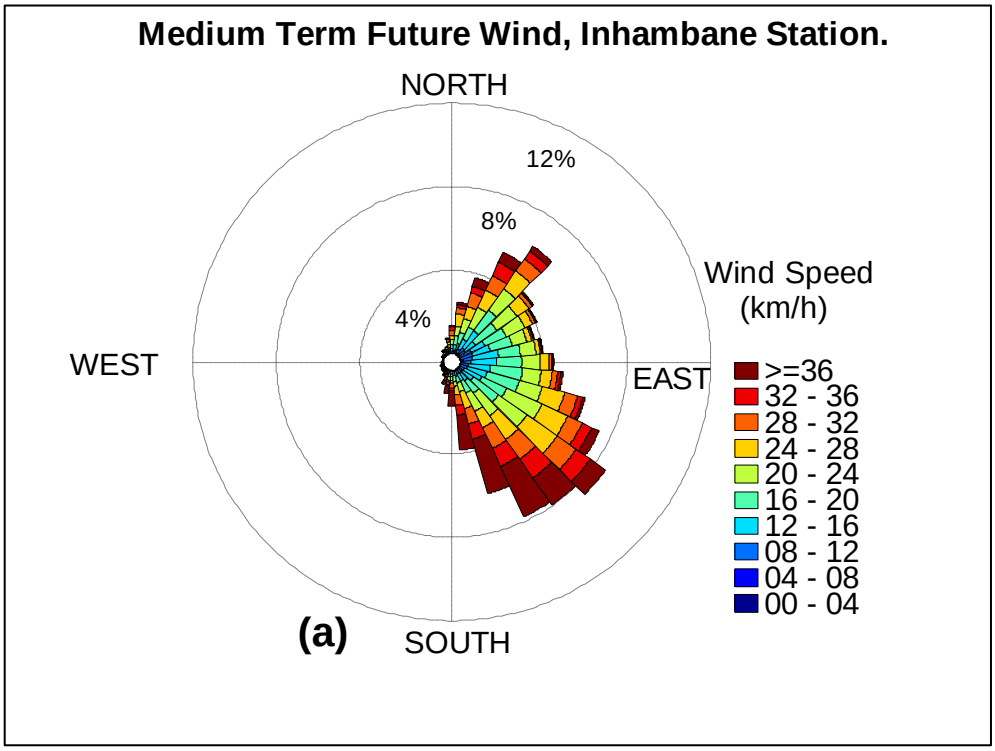

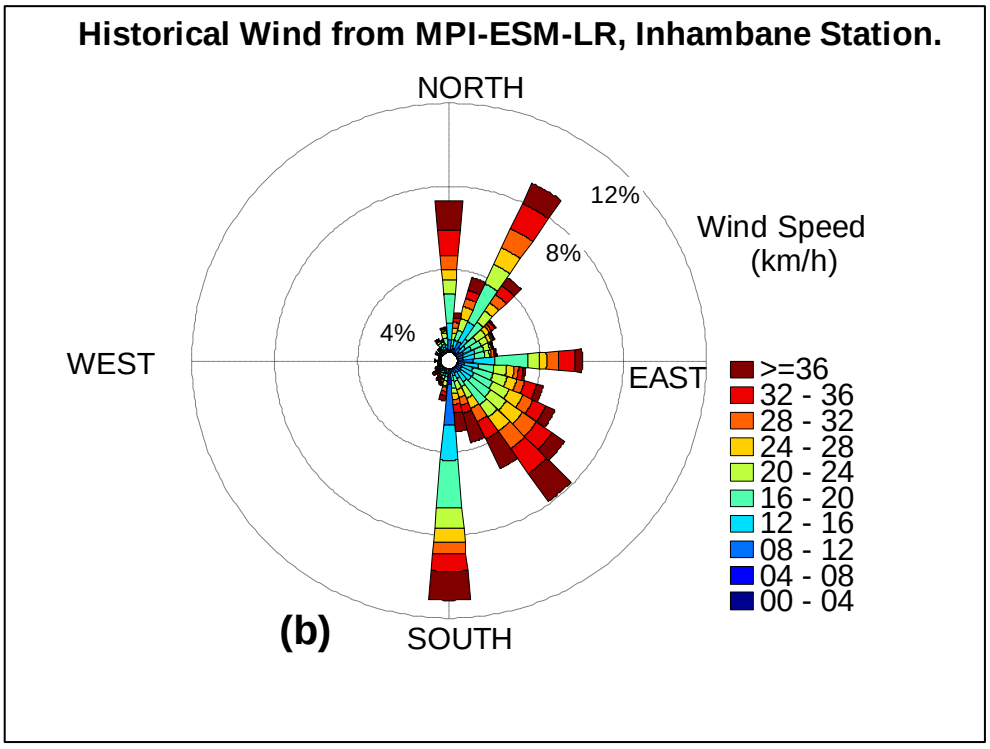

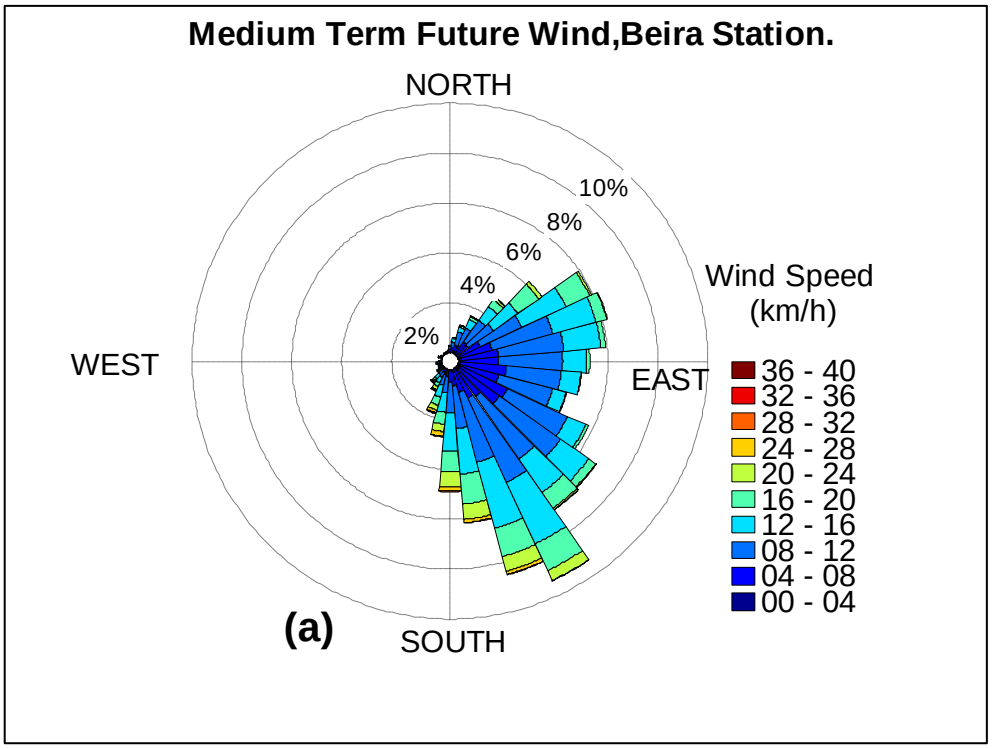
Medium Term Future Wind,Beira Station.
NORTH
10%
8%
6%
4%
2%
WEST
EAST
SOUTH
Wind Speed
(km/h)
36 - 40
32 - 36
28 - 32
24 - 28
20 - 24
16 - 20
12 - 16
08 - 12
04 - 08
00 - 04
(a)

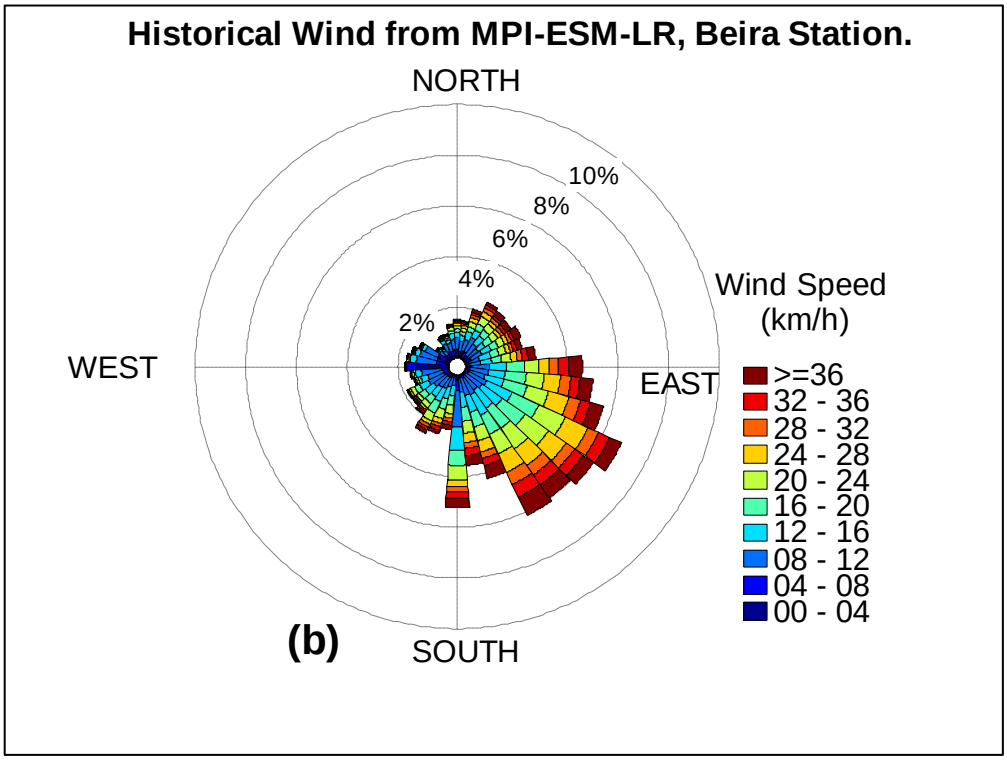
Historical Wind from MPI-ESM-LR, Beira Station.
NORTH
10%
8%
6%
4%
2%
WEST
EAST
SOUTH
Wind Speed
(km/h)
>=36
32 - 36
28 - 32
24 - 28
20 - 24
16 - 20
12 - 16
08 - 12
04 - 08
00 - 04
(b)

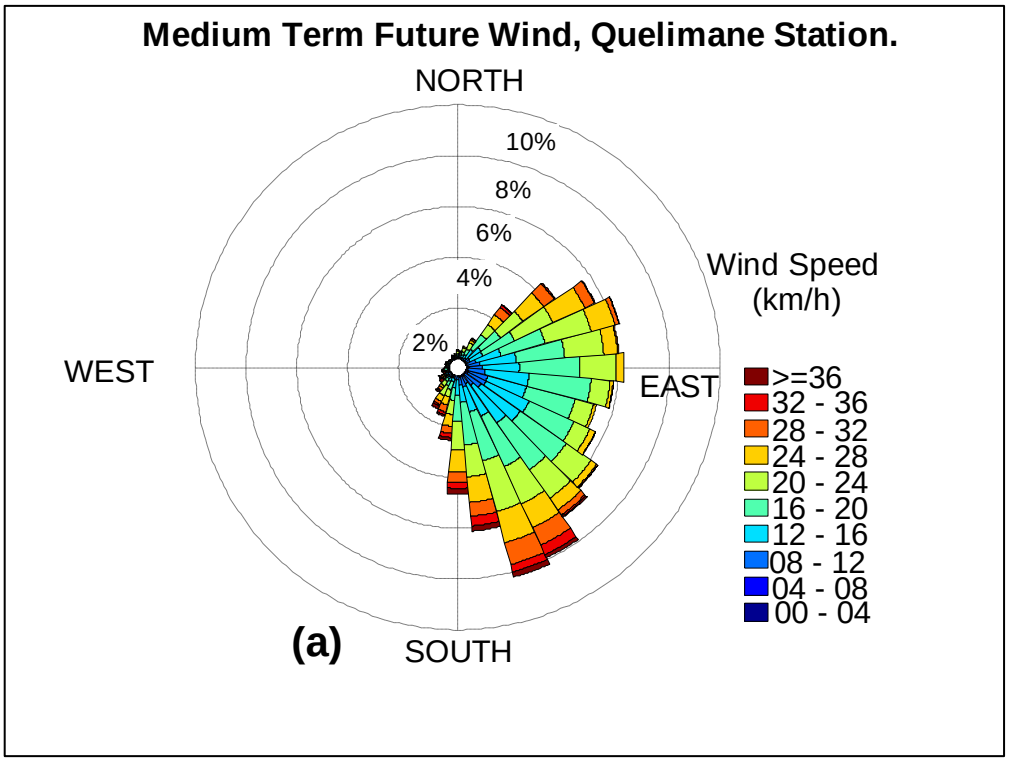
Medium Term Future Wind, Quelimane Station.
NORTH
10%
8%
6%
4%
2%
WEST
EAST
SOUTH
Wind Speed
(km/h)
>=36
32 - 36
28 - 32
24 - 28
20 - 24
16 - 20
12 - 16
08 - 12
04 - 08
00 - 04
(a)

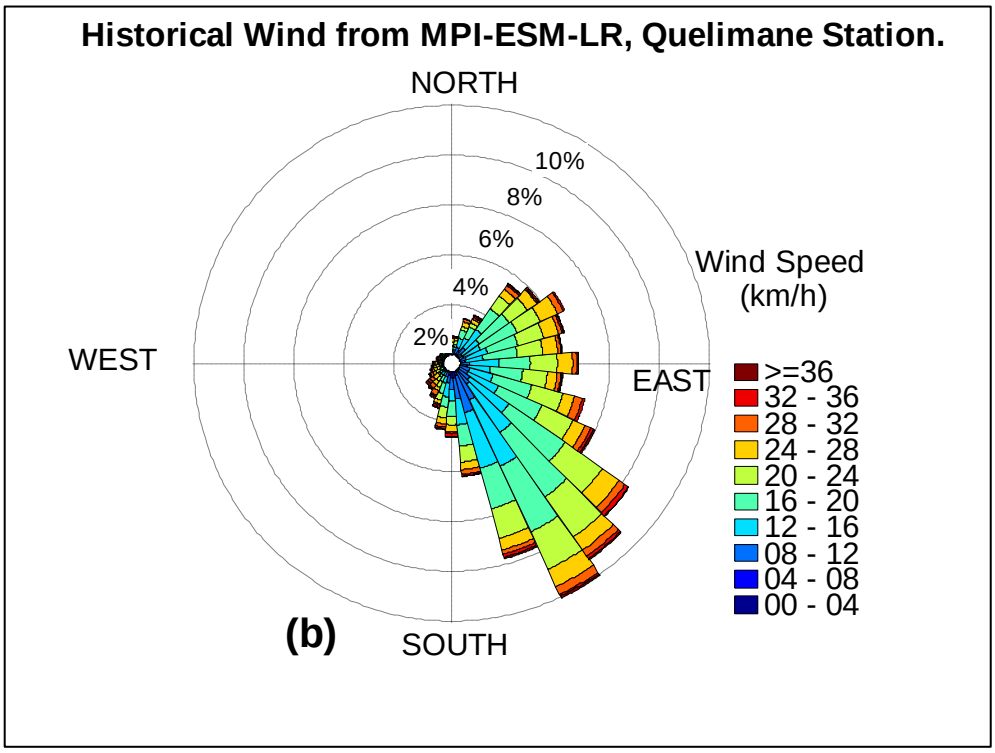
Historical Wind from MPI-ESM-LR, Quelimane Station.
NORTH
10%
8%
6%
4%
2%
WEST
EAST
SOUTH
Wind Speed
(km/h)
>=36
32 - 36
28 - 32
24 - 28
20 - 24
16 - 20
12 - 16
08 - 12
04 - 08
00 - 04
(b)

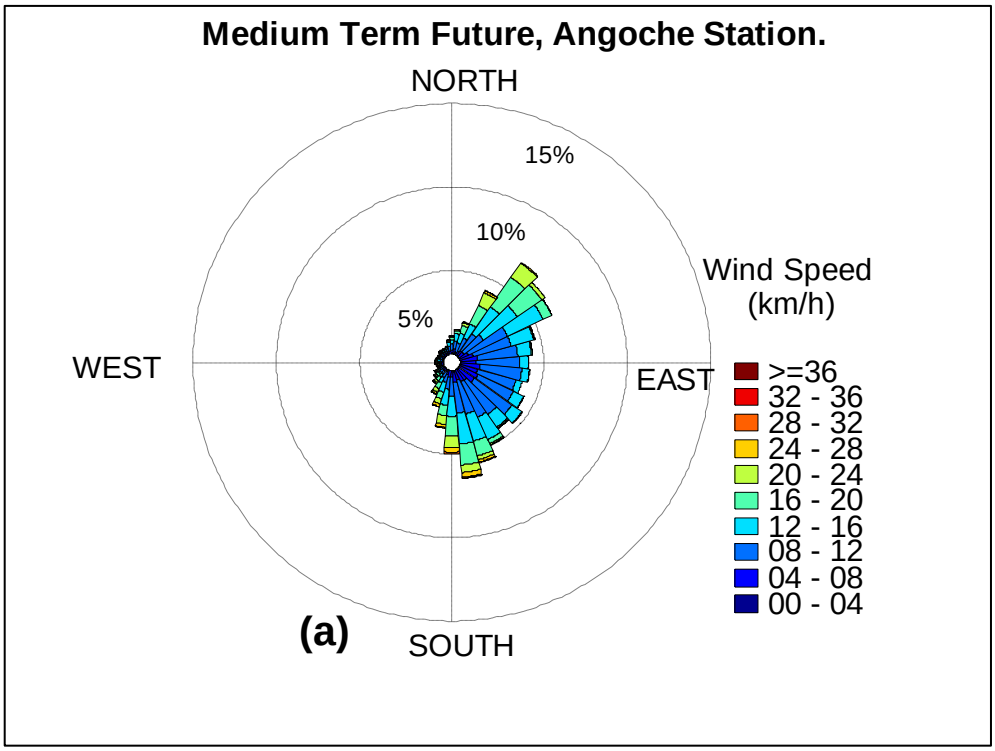
Medium Term Future, Angoche Station.
NORTH
15%
10%
5%
WEST
EAST
SOUTH
(a)
Wind Speed
(km/h)
>=36
32 - 36
28 - 32
24 - 28
20 - 24
16 - 20
12 - 16
08 - 12
04 - 08
00 - 04

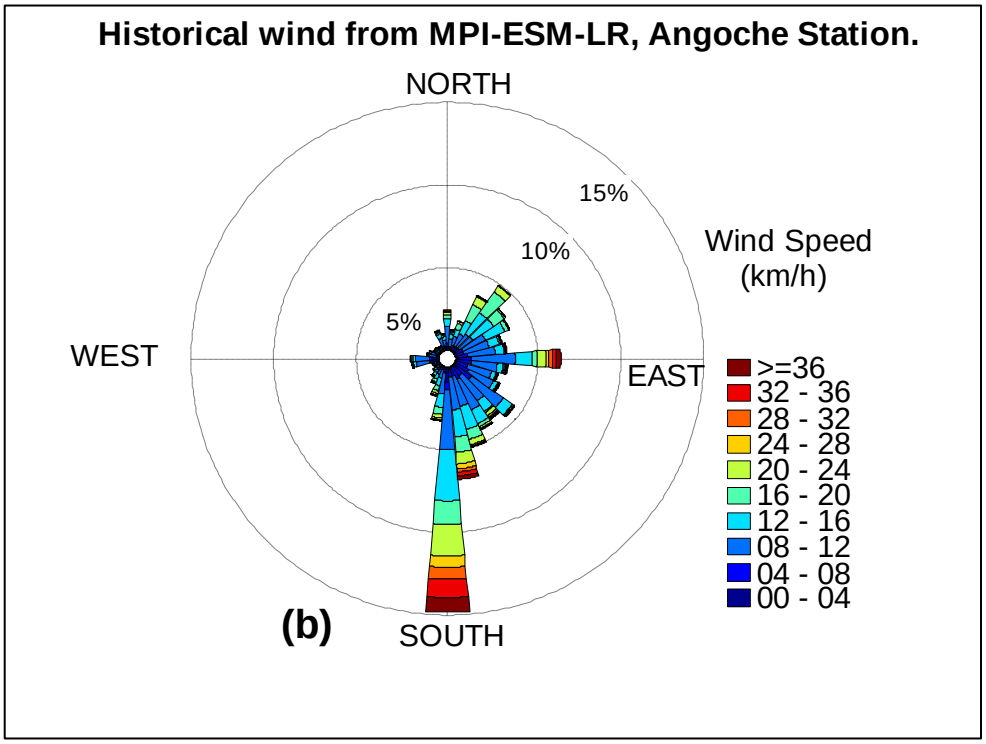
Historical wind from MPI-ESM-LR, Angoche Station.
NORTH
15%
10%
5%
WEST
EAST
SOUTH
(b)
Wind Speed
(km/h)
>=36
32 - 36
28 - 32
24 - 28
20 - 24
16 - 20
12 - 16
08 - 12
04 - 08
00 - 04

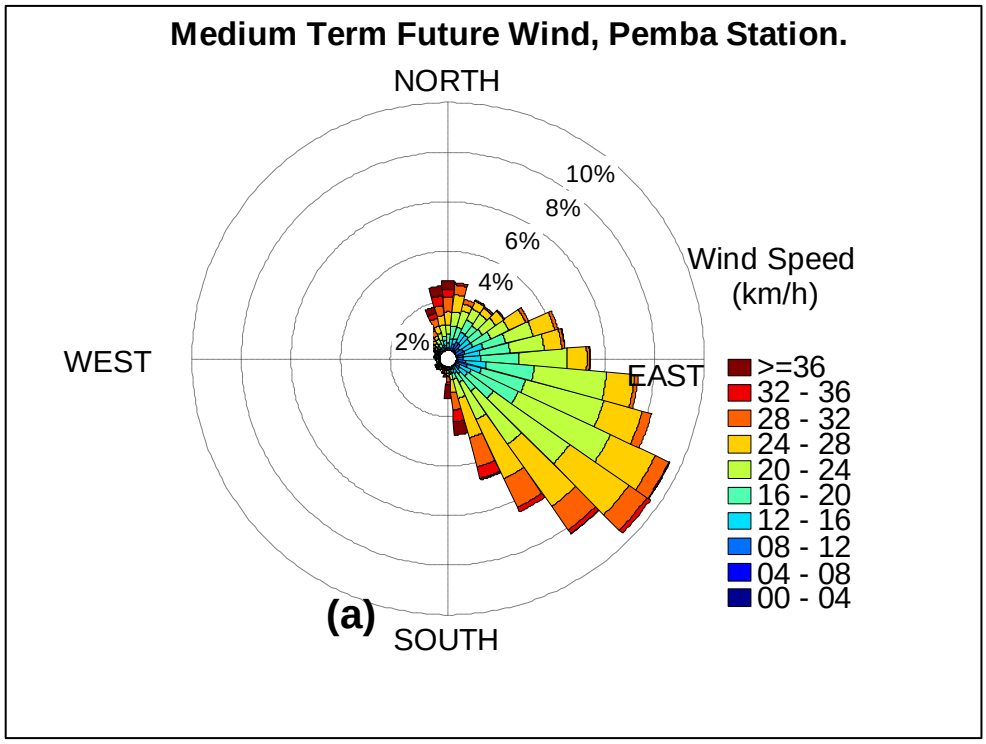
Medium Term Future Wind, Pemba Station.
NORTH
10%
8%
6%
4%
2%
WEST
EAST
SOUTH
(a)
Wind Speed
(km/h)
>=36
32 - 36
28 - 32
24 - 28
20 - 24
16 - 20
12 - 16
08 - 12
04 - 08
00 - 04

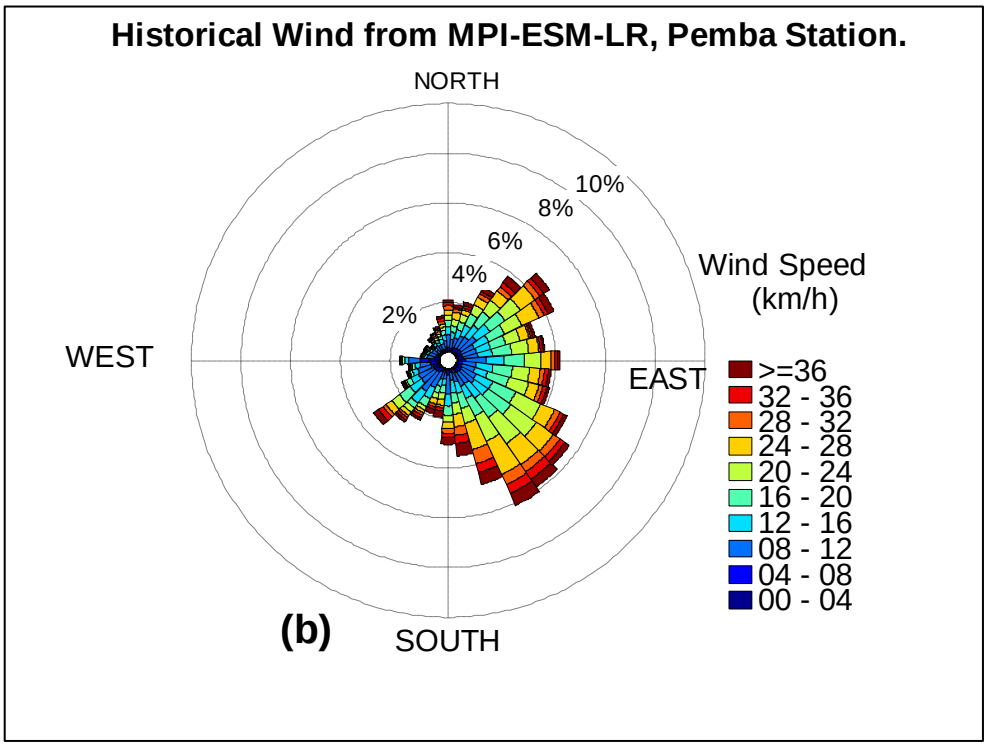
Historical Wind from MPI-ESM-LR, Pemba Station.
NORTH
10%
8%
6%
4%
2%
WEST
EAST
SOUTH
(b)
Wind Speed
(km/h)
>=36
32 - 36
28 - 32
24 - 28
20 - 24
16 - 20
12 - 16
08 - 12
04 - 08
00 - 04

Appendix L - Wind speed and direction for Long Term Future and historical from MPI-ESM-LR

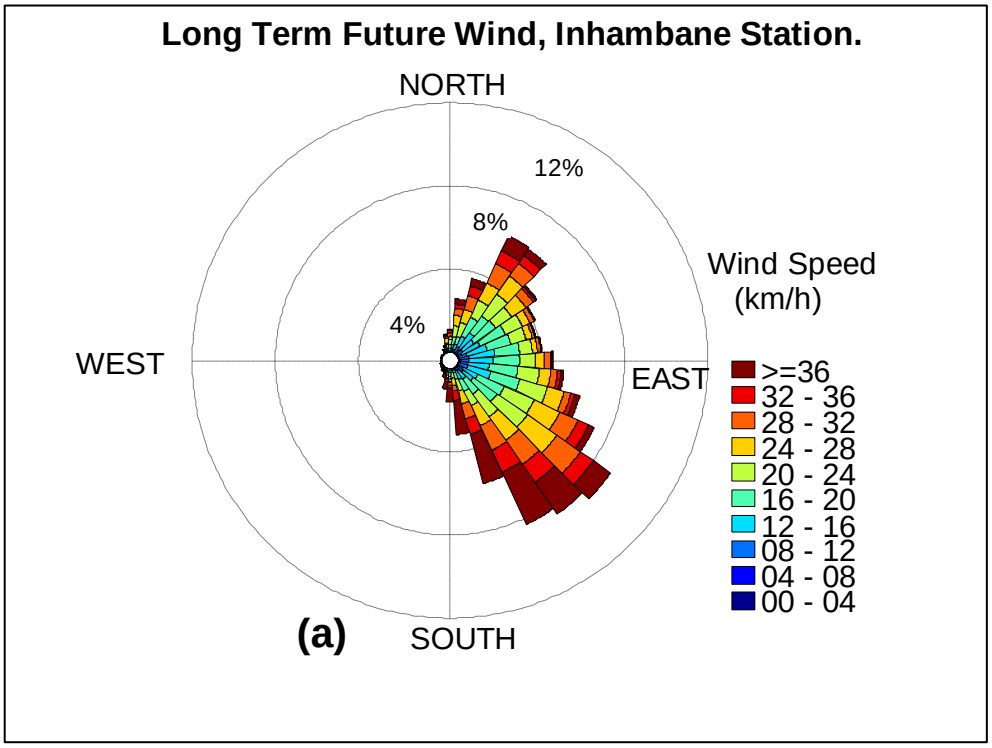

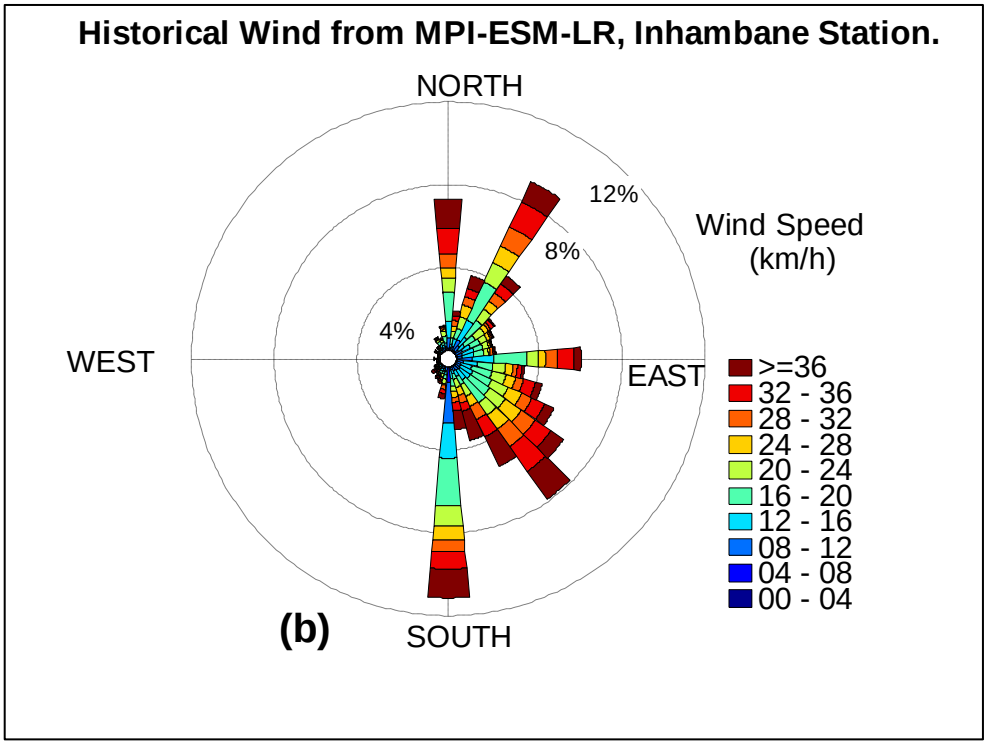

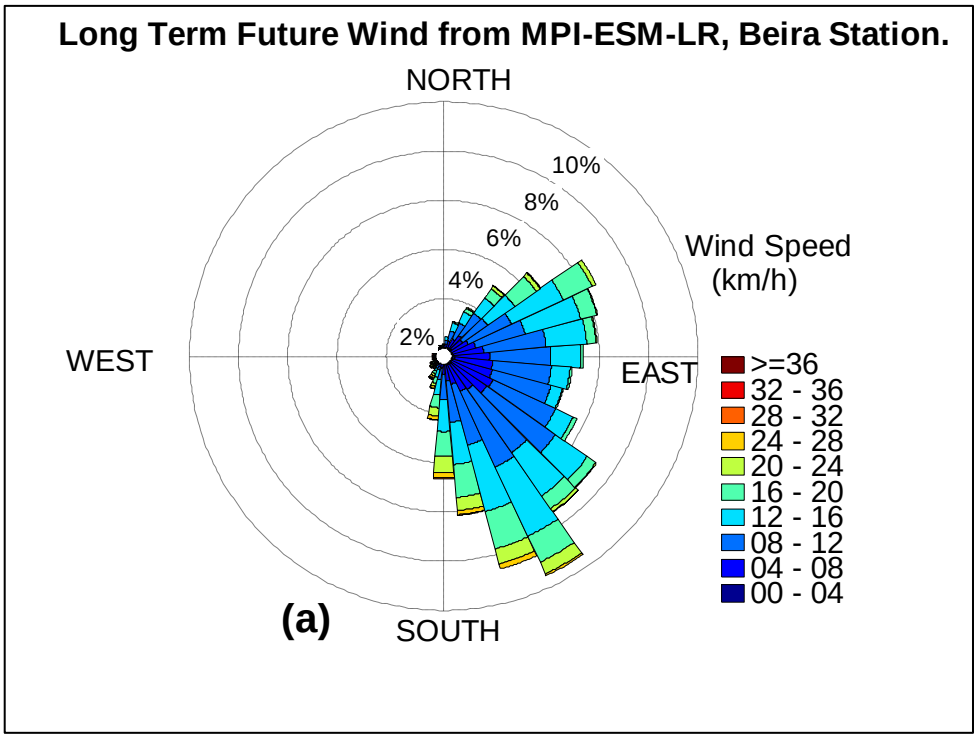
Long Term Future Wind from MPI-ESM-LR, Beira Station.
NORTH
10%
8%
6%
4%
2%
Wind Speed
(km/h)
WEST
EAST
>=36
32 - 36
28 - 32
24 - 28
20 - 24
16 - 20
12 - 16
08 - 12
04 - 08
00 - 04
(a)
SOUTH

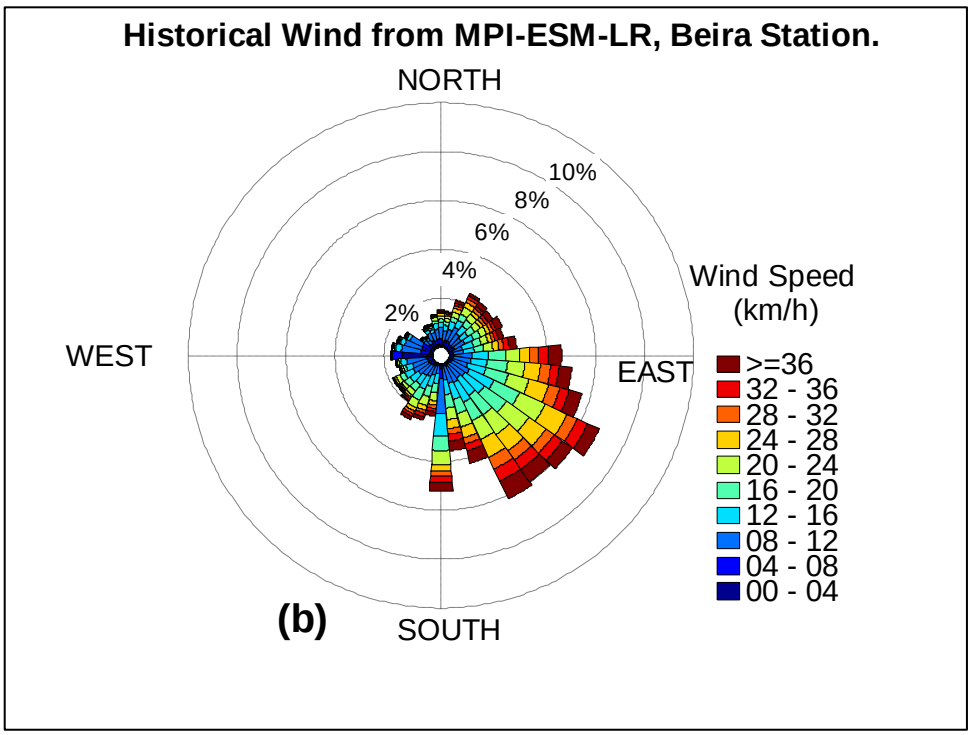
Historical Wind from MPI-ESM-LR, Beira Station.
NORTH
10%
8%
6%
4%
2%
Wind Speed
(km/h)
WEST
EAST
>=36
32 - 36
28 - 32
24 - 28
20 - 24
16 - 20
12 - 16
08 - 12
04 - 08
00 - 04
(b)
SOUTH

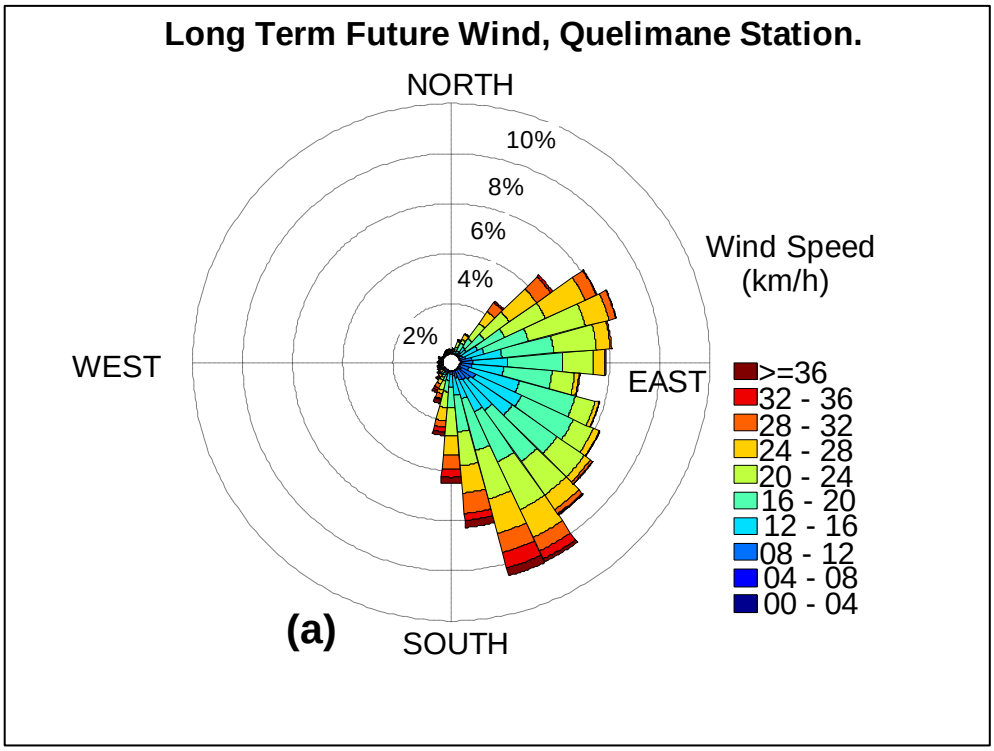
Long Term Future Wind, Quelimane Station.
NORTH
10%
8%
6%
4%
2%
WEST
EAST
SOUTH
Wind Speed
(km/h)
>=36
32 - 36
28 - 32
24 - 28
20 - 24
16 - 20
12 - 16
08 - 12
04 - 08
00 - 04
(a)

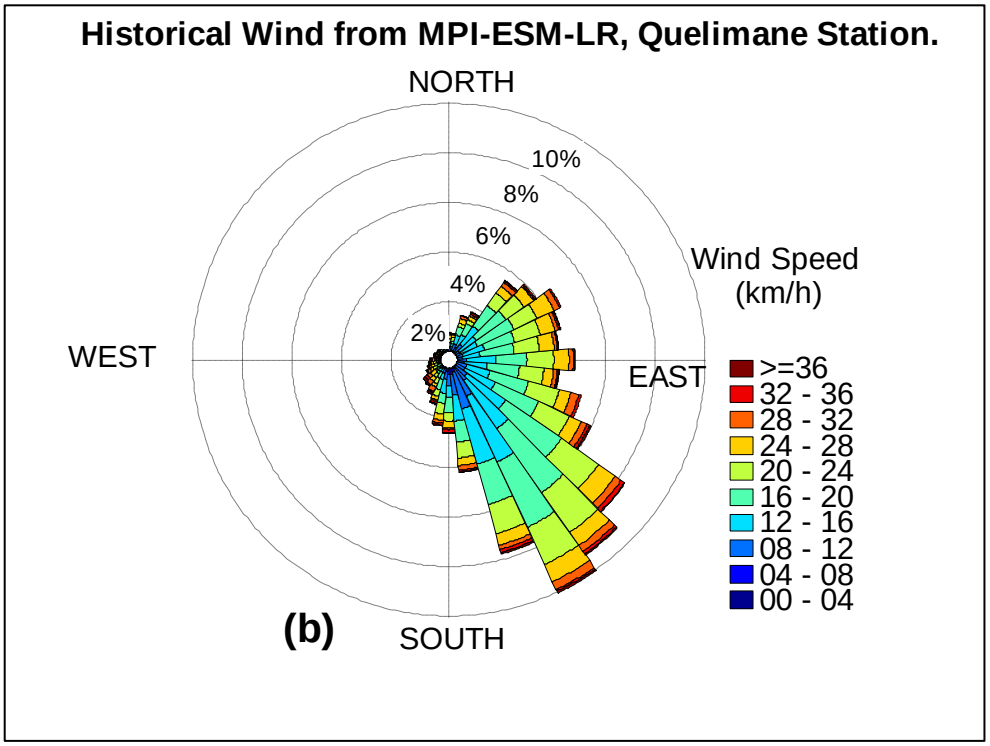
Historical Wind from MPI-ESM-LR, Quelimane Station.
NORTH
10%
8%
6%
4%
2%
WEST
EAST
SOUTH
Wind Speed
(km/h)
>=36
32 - 36
28 - 32
24 - 28
20 - 24
16 - 20
12 - 16
08 - 12
04 - 08
00 - 04
(b)

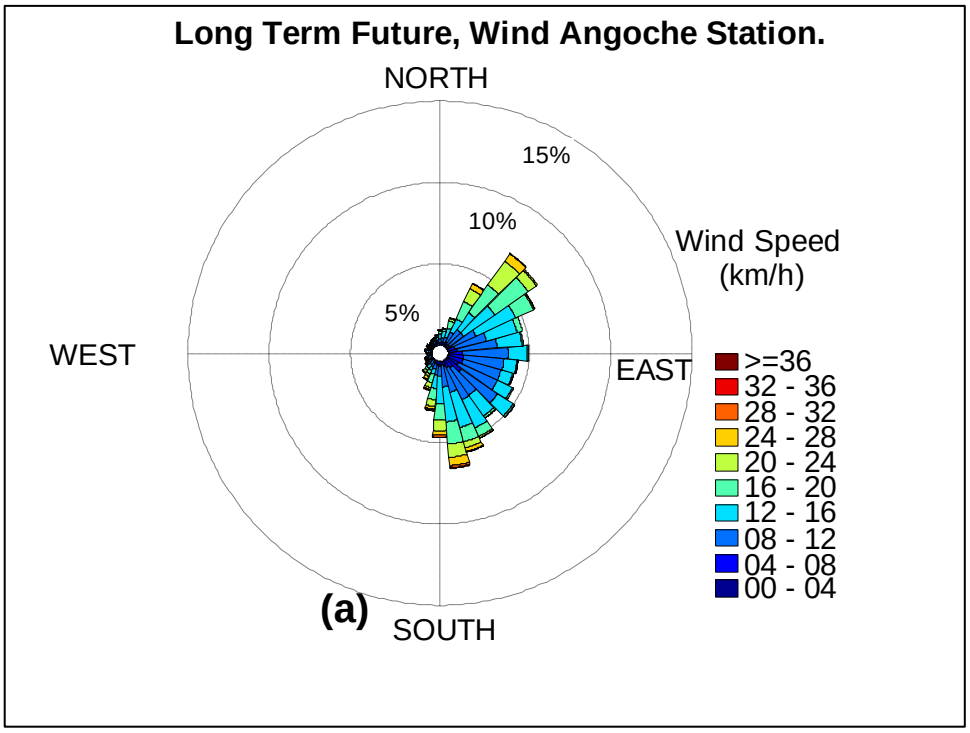
Long Term Future, Wind Angoche Station.
NORTH
15%
10%
5%
Wind Speed
(km/h)
WEST
EAST
>=36
32 - 36
28 - 32
24 - 28
20 - 24
16 - 20
12 - 16
08 - 12
04 - 08
00 - 04
(a)
SOUTH

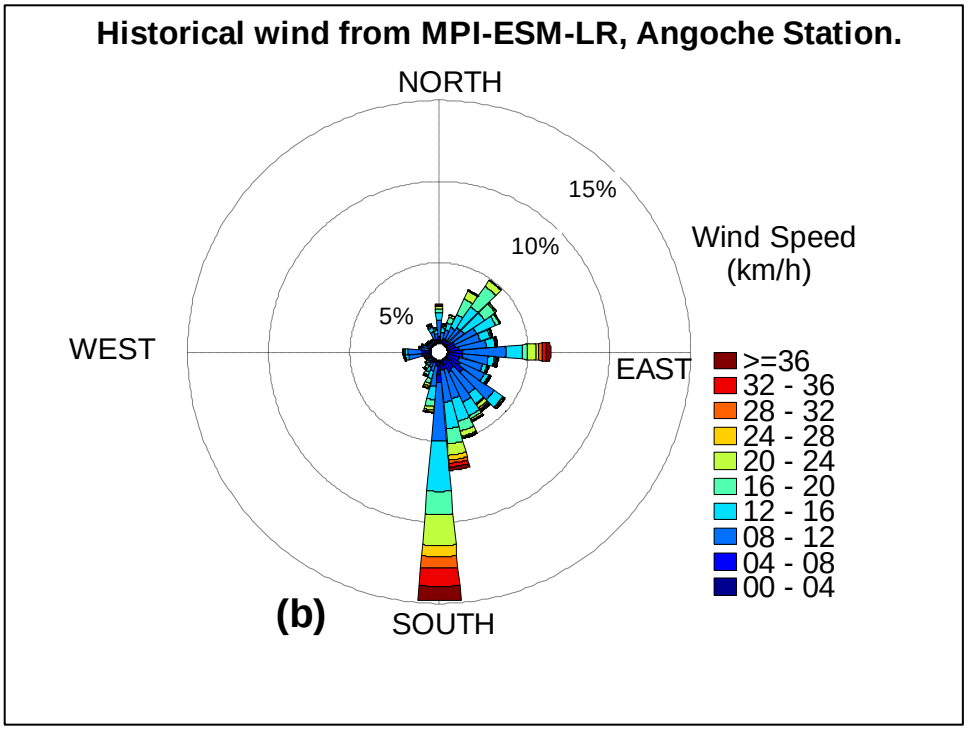
Historical wind from MPI-ESM-LR, Angoche Station.
NORTH
15%
10%
5%
Wind Speed
(km/h)
WEST
EAST
>=36
32 - 36
28 - 32
24 - 28
20 - 24
16 - 20
12 - 16
08 - 12
04 - 08
00 - 04
(b)
SOUTH

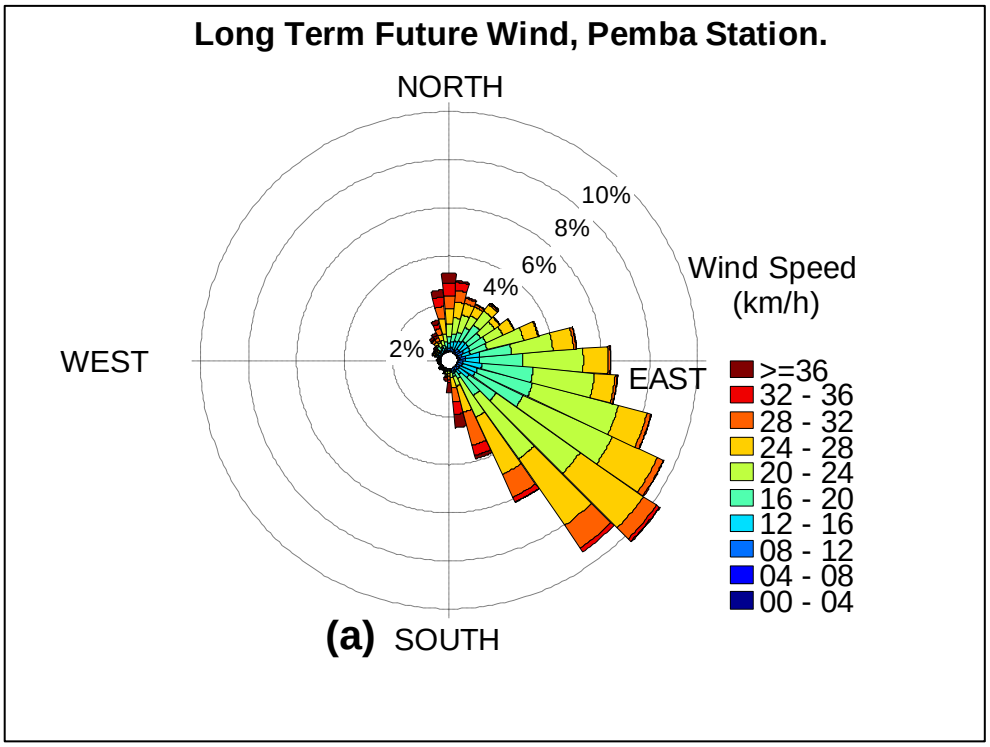
Long Term Future Wind, Pemba Station.
NORTH
10%
8%
6%
4%
2%
Wind Speed
(km/h)
WEST
EAST
>=36
32 - 36
28 - 32
24 - 28
20 - 24
16 - 20
12 - 16
08 - 12
04 - 08
00 - 04
(a)
SOUTH

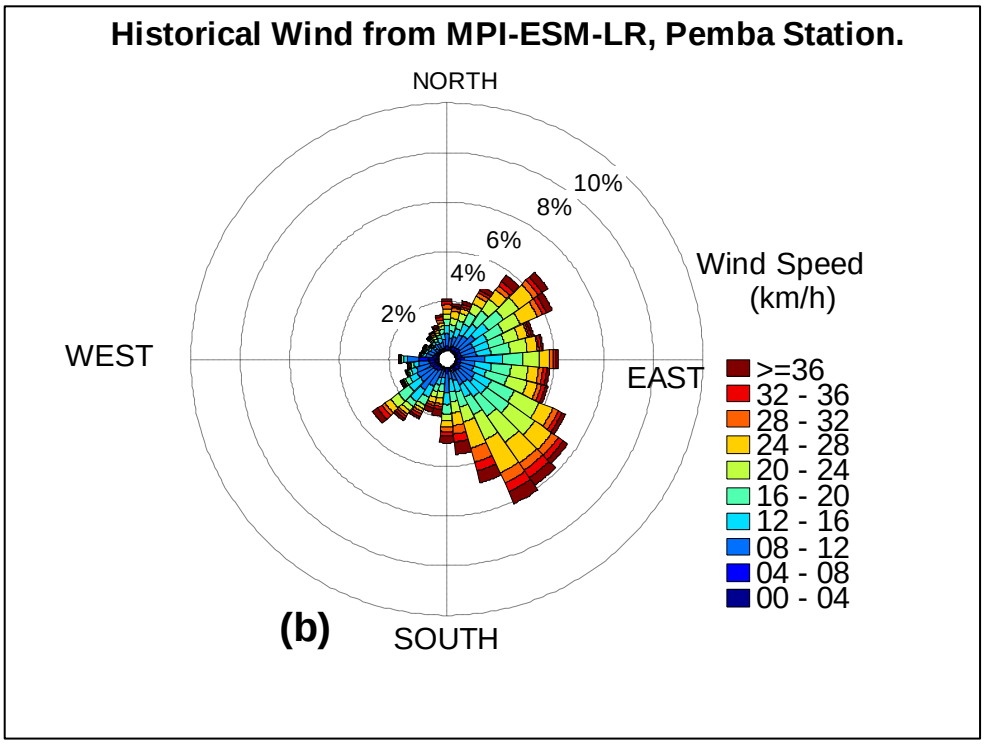
Historical Wind from MPI-ESM-LR, Pemba Station.
NORTH
10%
8%
6%
4%
2%
Wind Speed
(km/h)
WEST
EAST
>=36
32 - 36
28 - 32
24 - 28
20 - 24
16 - 20
12 - 16
08 - 12
04 - 08
00 - 04
(b)
SOUTH